Tampere University

VIGNESHKUMAR RANGASAMI

Immuno-engineering of Cells and Biomaterials for Biomedical Applications

Tampere University Dissertations 673

Tampere University Dissertations 673

VIGNESHKUMAR RANGASAMI

Immuno-engineering of Cells and Biomaterials for Biomedical Applications

ACADEMIC DISSERTATION
To be presented, with the permission of
the Faculty of Medicine and Health Technology
of Tampere University,
for public discussion in the F114
of the Arvo Building, Arvo Ylpönkatu 34, Tampere,
on October 28th, at 12 o'clock.

ACADEMIC DISSERTATION
Tampere University, Faculty of Medicine and Health Technology
Finland

Responsible supervisor and Custos	Associate Professor Oommen Podiyan Oommen Tampere University Finland	
Pre-examiners	Professor Micheal Raghunath ZHAW School of Life sciences Switzerland	Associate Professor Shukry Habib University of Lausanne Switzerland
Opponent	Professor Arto Urtti University of Helsinki Finland	

The originality of this thesis has been checked using the Turnitin Originality Check service.

Cover design: Roihu Inc.

ISBN 978-952-03-2572-5 (print)
ISBN 978-952-03-2573-2 (pdf)
ISSN 2489-9860 (print)
ISSN 2490-0028 (pdf)
http://urn.fi/URN:ISBN:978-952-03-2573-2

Carbon dioxide emissions from printing Tampere University dissertations have been compensated.

PunaMusta Oy – Yliopistopaino
Joensuu 2022

தொட்டனைத் தூறும் மணற்கேணி மாந்தர்க்குக்

கற்றனைத் தூறும் அறிவு.

ACKNOWLEDGEMENTS

Two countries, three cities, and four labs. That's what I have seen and where I have worked in the last five years to compile this thesis. It has been a journey with a lot of downs as well as ups (a few, but noteworthy ones). From my current perspective, a Ph.D. is a journey where the most important aspect is the relationship between the Ph.D. student and their supervisor. In this regard, I have been fortunate to have a great supervisor in Professor Oommen P Oommen to guide me. Oommen (O.P), I would like to thank you for all the support and the words of encouragement, without which I would have found it hard to have completed this piece of work. I have always enjoyed the endless discussions on science and other things that I have had with you. Over the years, I have learned a lot from you and feel that you have been more of a mentor and a friend, than a supervisor. I hope to see the lab grow and hope I could keep discussing science (along with other things) with you well into the future too.

I would also like to thank Professors Jöns Hilborn and Oommen Varghese (O.V) from Uppsala University, both of whom have been instrumental in this journey of mine. Jöns, it was a lecture given by you (back in 2013) that introduced me to the potential of biomaterials and the polymer kemi group. I have always admired the way you look at things and how you deal with situations. I would like to thank you for accepting me into then polymer kemi group and the now macromolecular chemistry group. OV, you were my first supervisor when I entered this field and I have to say that without the experience working with you, I wouldn't be where I am today. I have always enjoyed discussing science with you, especially when OP is also involved as I always got to see two different perspectives of looking at things. More recently, I would like to thank you for allowing me to work in your lab and for the questions you bring up during the internal paper reviews. I have learned to enjoy those questions now more so than ever, as they help in making the paper air tight.

I would also like to thank my thesis committee members Professors Susanna Miettinen and Minna Kellomäki. Susanna, thank you for the encouragement you have given me and for the valuable questions and suggestions you brought up during committee meetings, and for providing me access to your lab. Professor Minna, you and your lab members have taught me some of the most valuable lessons during my time in Tampere, which has undoubtedly helped me grow as a person.

I would also like to thank the current members of the Bioengineering and nanomedicine laboratory. Sumanta, you have been a real support and it was a great time working together with you on most of the projects. I think our disagreements on how to take a project forward has made us better scientists as we understand each other's perspective better now. I wish you the very best and hope to see you defend your thesis soon! You and Mousumi have been great friends and I have always enjoyed the time with you guys. Austin, I have enjoyed the talks we have had over time and wish you the very best for your Ph.D. I would also like to thank the previous members of the lab. Hanna Kemppi, thank you for all the wonderful times we had together, I will always cherish your friendship and hope to see you as a doctor soon. Jay Samal, thank you for the hard work you put in towards our publications and also for the fun moments discussing photography or even testing out the big screen in the office. I wish you the very best for your Ph.D. Ana, I had a good time teaching you and enjoyed all the 'like this?' moments while working. Wish you all the very best. Vijay *sahib,* thank you for all the good moments we have shared in and out of the lab.

I would also like to thank the current and past members of the Varghese lab at Uppsala University. Special thanks to Nithiyanandan Krishnan for all the discussions we have had on a lot of things and for the food and for inspiring me to cook. Rohith, thank you for all the fun moments in the office and outside. I hope to see you publish one paper every month soon and wish you the best of luck with your Ph.D. I would also like to thank Francesca Spagnuolo for being a wonderful friend and accompanying me while doing FACS and also for endless discussion on a wide variety of things. Francesca, I wish you the very best for your Ph.D. (show the organoids and the printers who is the capo!) and in life. I would also like to thank Shima Tavakoli, Partha Laskar, Hamid Reza, Christos Leliopoulos, and Adriana Saldivor for providing nice moments in the lab. Special thanks should also be mentioned to the people from my previous stint in the Varghese lab. Maruthibabu Paidikondala, Hongji Yan, Shujiang Wang, Deepanjali Gaurav, and Rekha Tripathi (*Rekha ji*), thank you guys for all the nice moments in the lab. I would also like to thank Sandeep Kadekar and Ganesh Nawale for being an instrumental part of this thesis. Sandeep, thank you for all the tips on how to make things work and for the various other discussions we have had. Ganesh, thank you for all the nucleic acids and for being patient and answering all my questions about chemistry and calculations. I would also like to thank all the current and past members of the polymer chemistry group/ macromolecular chemistry group at Uppsala University for providing a wonderful environment in the lab. I would also like to thank my

friends from Uppsala; Saravanan, Oviya, Bertin, Lavy, Rashmi, Sandesh, Pooja, Mihir, and Prashant for the wonderful times shared and for making my time in Uppsala a memorable one.

I would also like to thank all my co-authors of my publications. This would not have been possible if you had not worked hard. So, thank you all for that! Special thanks to Professor Robert Harris of Karolinska Institute for allowing me to work with immune cells and learn a lot about them. I must also thank the members of his lab, especially Keying Zhu and Heela Sarlus for being such wonderful collaborators. I must also thank Professor Yuji Teramura and Kenta Asawa for being wonderful collaborators.

I would like to thank Dr. Srujan Marepally, for trusting me and allowing me to work on his projects at the Center for stem cell research which resulted in my first publication. I would like to thank Priya Dharmalingam, Brijesh Lochania, Abisha Crystal, Harish, Tulaj, and Deepika for all the good times in CSCR. Special thanks to Sowmya Ramesh for the wonderful time spent during lunches and getting lost in metro stations in Stockholm and also for being my go-to person for solving my scientific problems.

I would also like to thank my friends Athul Alex, Karthik Kesavan, and Micheal John. Guys, you have been there since 2004/5 and it has always been nonstop comic relief since then. I would also like to thank my college friends, Koushik, Suresh, Poorani, Robin, Dr. Ninja, and Shravan. Guys, thank you for being there and for always being a source of stress relief. I would also like to thank Sreenithya Ravindran for being one of my closest friends and for providing always providing motivation and support. I would also like to thank Sanya Bhushan for being a constant source of support and motivation during the last five years. San, I wish you the very best in your career. I would also like to thank the doctoral school of Tampere University and the faculty of medicine and health technology for providing me with this opportunity as well as timely support during the Ph.D.

Finally, I would like to thank my family. Mom and dad, thank you for always being a source of inspiration and support. I wouldn't be where I am today if it were not for you both. I would also like to thank my sister, Dipika, for being a constant source of support and motivation.

ABSTRACT

Immune cells that constitute our immune system keep the human body safe and help in warding off infections mediated by different pathogens and also play a key role in regulating homeostasis, wound healing, and regeneration of tissues. Implantation or infusion of foreign agents such as biomaterials, nanoparticles, small molecule drugs, or living cells needs to navigate the complex immune landscape for successful therapeutic outcomes. Thus, devising new engineering tools or immune-responsive biomaterials that can safely traverse/modulate the aggressive immune system or harness the 'cell-killing' or 'wound healing' properties of the immune system as a potent tool for treating human diseases are of paramount importance for developing new therapies. In this context, this dissertation has developed new bioengineering strategies adopting nanomedicine or tissue engineering approaches for modulating our immune system which was successfully demonstrated for anti-cancer studies, stem cell delivery, and tissue regeneration applications.

Here in this thesis, hyaluronic acid (HA), one of the key polymers of our extracellular matrix (ECM) has been used as a major building block for engineering nanocarriers and a hydrogel scaffold. The HA-derived nanoparticles were designed for anti-cancer applications and immunosuppressive HA-based hydrogel scaffolds were designed for tissue engineering applications. The HA nanoparticles were designed following a novel self-assembly strategy where hydrophobic immunosuppressive drug, dexamethasone was conjugated to the HA backbone to induce amphiphilicity, which was subsequently loaded with a well-known chemotherapy drug, doxorubicin. These drug-loaded HA-nanoparticles formed an ideal nanocarrier for combination therapy and the delivery system was tested for its anticancer activity, macrophage polarization potential, and its capability to modulate thromboinflammation in human whole blood. Gratifyingly, the novel HA-based nanocarrier was found to suppress platelet aggregation and thrombin generation that are trigged by doxorubicin. The HA-based nanocarrier also triggered the repolarization of tumor-associated macrophages to M1 macrophages as evidenced by the increase in expression of proinflammatory genes like TNF.

Delivering therapeutic cells such as mesenchymal stem cells (MSCs) is another key objective of this thesis. The thrombotic activity induced by MSCs after

allotransplantation is a major obstacle in the field of cell-based therapies as these cells trigger the activation of coagulation and complement cascade, after intravenous infusion leading to poor in-vivo survival. To circumvent this challenge, we adopted two independent approaches, namely nanoparticle-mediated tissue factor gene silencing and layer-by-layer polyelectrolyte coating. We designed a novel pluronic-based nanomicelles conjugated with siRNA bearing a reducible disulfide linker that displayed efficient gene silencing (~70%) in MSCs. The effective silencing of the tissue factor gene in MSCs significantly enhanced the hemocompatibility in human whole blood as they did not activate the complement and coagulation pathways. Surprisingly, the silencing of tissue factor resulted in enhanced paracrine signaling and differentiation potential through some unknown molecular pathway. In the second strategy, we coated the MSCs with two polyelectrolytes namely, heparin and gelatin (H/G) in a layer by layer (LbL) manner. These coated cells were found to enhance hemocompatible when studied in human whole blood. The proliferation, paracrine signaling aspects and differentiation aspects of these coated cells were also studied. These studies revealed that the H/G coating did not hinder the paracrine signaling and differentiation capabilities of the cells.

Finally, we engineered an immunoresponsive HA hydrogel by conjugating gallic acid, a polyphenol that is known to display antioxidant properties and are found in green tea, and other medicinal plants. The addition of gallol to HA hydrogel enhanced the adhesive and antioxidant properties while also providing a shear thinning/self-healing property to the hydrogel. Surprisingly, gallic acid functionalization provided immunosuppressive characteristics as verified by culturing primary murine M1 macrophages. Subcutaneous implantation of gallol-functionalized HA gels in healthy mice displayed infiltration of immunosuppressive myeloid cells within these gels, while higher numbers of pro-inflammatory myeloid cells were observed in the control HA gels.

In conclusion, this dissertation formulates a wide range of engineering strategies for regulating our immune system that supported enhanced survival of stem cells after transplantation, provided safer delivery of chemotherapeutic agents using biomimetic HA-based nanocarriers, and identified gallic acid as an immunomodulatory molecule that can be exploited to design immunosuppressive 3D scaffolds for tissue engineering applications.

TIIVISTELMÄ

Immuunijärjestelmän muodostavat immuunisolut, jotka pitävät kehomme turvassa ja auttavat torjumaan eri taudinaiheuttajien välittämiä infektioita sekä ovat keskeisessä roolissa homeostaasin säätelyssä, haavan paranemisessa ja kudosten uusiutumisessa. Onnistuneen hoidon saavuttamiseksi on potilaan kehoon lisätyn implantin tai muiden vieraiden aineiden, kuten biomateriaalien, nanopartikkeleiden, pienimolekyylisten lääkkeiden tai elävien solujen selviydyttävä monimutkaisessa immuuniympäristössä. Tämän vuoksi on ensiarvoisen tärkeää kehittää uusia teknisiä ratkaisuja tai immuunivasteisia biomateriaaleja, jotka pystyvät turvallisesti muuttamaan aggressiivista immuunijärjestelmää tai hyödyntämään immuunijärjestelmän "soluja tappavia" tai "haavoja parantavia" ominaisuuksia potilaiden sairauksien hoidossa. Tähän ongelmaan liittyen tässä väitöskirjassa kehitettiin uusia biotekniikan strategioita, jotka hyödyntävät nanolääketieteen tai kudosteknologian lähestymistapoja immuunijärjestelmän muuttamiseksi.

Tässä väitöskirjassa on käytetty nanokantajien ja hydrogeelitukirakenteiden suunnittelussa hyaluronihappoa (eng. hyaluronic acid, HA). HA-pohjaiset nanopartikkelit suunniteltiin syövän vastaisiin sovelluksiin, kun taas immunosuppressiiviset HA-pohjaiset hydrogeelitukirankenteet suunniteltiin kudosteknologian sovelluksiin. HA-nanopartikkelit suunniteltiin käyttäen uutta itsekokoontumisstrategiaa, jossa vettä hylkivä immunosuppressiivinen lääke, deksametasoni, yhdistettiin HA-runkoon amfifiilisyyden luomiseksi. Tämän jälkeen tunnettu kemoterapialääke, doksorubisiini, lastattiin nanopartikkeliin. Nämä lääkettä sisältävät HA-nanopartikkelit muodostivat ihanteellisen nanokantajan yhdistelmähoitoon ja lääkkeenkuljetusjärjestelmää tutkittiin sen syövänvastaisen aktiivisuuden, makrofagien polarisaatiopotentiaalin ja sen kyvyn muuttaa trombiintulehdusta ihmisen kokoveressä. Havaittiin, että uusi HA-pohjainen nanokantaja esti verihiutaleiden yhteen kasautumista ja trombiinin muodostumista, mitä doksorubisiini yleensä aiheuttaa. HA-pohjainen nanokantaja aiheutti myös kasvaimeen liittyvien makrofagien repolarisaation M1-makrofageiksi, mikä on osoituksena tulehdusta edistävien geenien, kuten TNF:n, ilmentymisen lisääntymisestä.

Toinen väistökirjan keskeinen tavoite on terapeuttisten solujen, kuten mesenkymaalisten kantasolujen (eng. mesenchymal stem cells, MSC) toimittaminen kohteeseen. MSC-solujen aiheuttama trombioottinen aktiivisuus allotransplantaation jälkeen on suuri haaste solupohjaisissa hoidoissa, koska nämä solut laukaisevat veren hyytymisen ja komplementtijärjestelmän aktivoitumisen suonensisäisen infuusion jälkeen. Tämä johtaa solujen huonoon *in vivo* eloonjäämiseen. Haasteen välttämiseksi hyödynsimme kahta riippumatonta strategiaa. Suunnittelimme uudet pluronic-pohjaiset nanomisellit, jotka oli yhdistetty pelkistävää disulfidilinkkeria sisältävään siRNA:han. Tämä yhdistelmä osoittautui tehokkaaksi geenin vaimentamisessa (~ 70 %) MSC-soluissa. Kudostekijägeenin tehokas vaimentaminen MSC-soluissa paransi merkittävästi veriyhteensopivuutta ihmisen kokoveressä, koska ne eivät aktivoineet komplementti- ja hyytymisreittejä. Yllättäen kudostekijän vaimentaminen johti parakriinisen signaalin ja erilaistumispotentiaalin parantumiseen ennestään tuntemattoman molekyylireitin kautta. Toisessa strategiassa pinnoitimme MSC-solut käyttäen kahta polyelektrolyytiä layer-by-layer (LbL)-tekniikalla: hepariinia ja gelatiinia (H/G). Näiden päällystettyjen solujen havaittiin parantavan veriyhteensopivuutta, kun niitä tutkittiin ihmisen kokoveressä. Myös näiden päällystettyjen solujen lisääntyminen, parakriininen signalointi ja erilaistuminen tutkittiin. Tutkimuksista paljastui, että H/G-pinnoite ei estänyt solujen parakriinisia signalointi- ja erilaistumiskykyjä.

Lopuksi kehitimme immuunivasteisen HA-hydrogeelin konjugoimalla gallushappoa. Gallolin lisääminen HA-hydrogeeliin paransi adhesiivisia sekä antioksidanttisia ominaisuuksia, samalla kun se tarjosi hydrogeelille pseudoplastiset/itseparantuvat ominaisuudet. Yllättäen gallushapon funktionalisointi tarjosi immunosuppressiivisia ominaisuuksia, mikä varmistettiin viljelemällä primäärisiä hiiren M1-makrofageja. Gallolifunktionalisoitujen HA-geelien ihonalainen implantointi terveisiin hiiriin osoitti immunosuppressiivisten myeloidisolujen tunkeutumista näissä hydrogeeleissä. Kun taas kontrolli-HA-geeleissä havaittiin suurempi määrä tulehdusta edistäviä myeloidisoluja.

Yhteenvetona voidaan todeta, että tämä väitöskirja esittelee laajan valikoiman teknisiä strategioita immuunijärjestelmän säätelyyn. Strategiat tukivat kantasolujen parempaa eloonjäämistä transplantaation jälkeen, tarjosivat kemoterapeuttisten aineiden turvallisemman kuljettamisen käyttämällä biomimeettisiä HA-pohjaisia nanokantajia ja tunnistivat gallushapon immunomodulatoriseksi molekyyliksi, jota voidaan hyödyntään immunosuppressiivisten 3D tukirakenteiden suunnittelussa kudosteknologian sovelluksiin.

CONTENTS

ABBREVIATIONS

ALP	Alkaline phosphatase
BGLAP	Bone gamma-carboxyglutamate protein
BMDM	Bone marrow derived macrophages
C3	Complement component 3
C5	Complement component 5
CCL2	C-C motif ligand 2
CCL4	C-C motif ligand 4
CDH	Carbodihydrazide
c-MSC	Coated mesenchymal stem cells
CRL2429	Human fibroblast cells
CXCL8	C-X-C motif ligand 8
DC	Dendritic cells
DEX	Dexamethasone
DLS	Dynamic light scattering
DLX5	Distal less homeobox 5
DMSO	Dimethyl sulfoxide
DNA	Deoxyribonucleic acid
DOX	Doxorubicin
ECM	Extracellular matrix
ELISA	Enzyme linked immunosorbent assay
FBGC	Foreign body giant cells
FBR	Foreign body response
GA	Gallic acid
GAG	Glycosaminoglycans
HA	Hyaluronic acid
HA-ALD	Hyaluronic acid functionalized with aldehyde
HA-CDH	Hyaluronic acid functionalized with carbodihydrazide
HA-DEX	Hyaluronic acid dexamethasone conjugate
HA-DEX-DOX	Hyaluronic acid dexamethasone doxorubicin particle
HA-GA	Hyaluronic acid functionalized with gallol moiety

HCT116	Colorectal cancer cell lines
H/G	Heparin gelatin coating
HIF1	Hypoxia inducible factor 1
IBMIR	Instant blood mediated inflammatory reactions
IFN	Interferon
IL	Interleukin
LPL	Lipoprotein lipase
LPS	Lipopolysaccharides
MCF7	Breast adenocarcinoma cell line
MG63	Osteosarcoma cell line
MHC	Major histocompatibility complex
MMP	Matrix metalloproteinases
mRNA	Messenger ribonucleic acid
MSCs	Mesenchymal stem cells
NET	Neutrophil extracellular traps
NK	Natural Killer cells
OCT4	Octamer binding transcription factor 4
PAGE	Polyacrylamide gel electrophoresis
PBS	Phosphate buffer saline
PCL	Polycaprolactone
PEG	Polyethylene glycol
PET	Polyethylene terephthalate
PMA	Phorbol 12-myristate 13-acetate
PPARG	Peroxisome proliferator activated receptor gamma
Plu-SS	Pluronic with pyridyl disulfide
Plu-SS-TF	Pluronic with pyridyl disulfide conjugated to tissue factor siRNA
PVA	Polyvinyl alcohol
RGD	Arginine-glycine-aspartic acid
RNA	Ribonucleic acid
ROS	Reactive oxygen species
siRNA	Small interfering ribonucleic acid
TAM	Tumor associated macrophages
TAT	Thrombin anti-thrombin complex
TF	Tissue factor
TF-KD	Tissue factor knockdown
TGF	Transforming growth factor

THP1	Human monocyte cell line
TLR	Toll like receptors
TME	Tumor microenvironment
TNBS	Trinitrobenzene sulfonic acid
TNF	Tumor necrosis factor
TRegs	T-Regulatory cells
UV	Ultraviolet spectrum
VEGF	Vascular endothelia growth factor

ORIGINAL PUBLICATIONS

This thesis is composed of and based on the following publications identified as Publications I-IV. Publications I, II and IV have been published. Publication III will be submitted and therefore is listed under Unpublished manuscripts. The published articles are all reprinted here with the kind permission of the publishers.

Publication I **V.K. Rangasami**, S. Samanta, V.S. Parihar, K. Asawa, K. Zhu, O.P. Varghese, Y. Teramura, B. Nilsson, J. Hilborn, R.A. Harris, O.P. Oommen, Harnessing hyaluronic acid-based nanoparticles for combination therapy: A novel approach for suppressing systemic inflammation and to promote antitumor macrophage polarization, Carbohydrate Polymers. 254 (2021) 117291. DOI: 10.1016/j.carbpol.2020.117291.

Publication II **V.K. Rangasami**, G. Nawale, K. Asawa, S. Kadekar, S. Samanta, B. Nilsson, K.N. Ekdahl, S. Miettinen, J. Hilborn, Y. Teramura, O.P. Varghese, O.P. Oommen, Pluronic micelle-mediated tissue factor silencing enhances hemocompatibility, stemness, differentiation potential, and paracrine signaling of mesenchymal stem cells, Biomacromolecules. 22 (2021) 1980–1989. DOI: 10.1021/acs.biomac.1c00070.

Publication IV S. Samanta ±, **V.K. Rangasami** ±, H. Sarlus, J.R.K. Samal, A.D. Evans, V.S. Parihar, O.P. Varghese, R.A. Harris, O.P. Oommen, Interpenetrating gallol functionalized tissue adhesive hyaluronic acid hydrogel polarizes macrophages to an immunosuppressive phenotype, Acta Biomaterialia. (2022). DOI: 10.1016/j.actbio.2022.01.048.

± These authors contributed equally.

Unpublished Manuscript

Publication III **V.K. Rangasami**, K. Asawa, L. Davies, J. Hilborn, K. LeBlanc, Y. Teramura, B. Nilsson, O.P. Varghese, O.P. Oommen, Immuno-isolation of mesenchymal stem cells via layer by layer polyelectrolyte coating enhances its survival in human blood and retains its immunomodulatory properties. Unpublished.

Author's Contributions

The author of this thesis contributed to the publications as follows.

Publication I As the first author of Publication I, M.Sc. Vigneshkumar Rangasami was involved in all the experiments involving the use of cells. V.K. Rangasami performed the experiments which included the cytotoxicity studies, uptake and blocking studies, extraction of primary bone marrow macrophages from mice, studies the effected of nanoparticle on the polarized macrophages. Rangasami also was also involved in the analysis and interpretation of data from the hematological studies and release studies while also contributing to the writing of the manuscript and preparing the figures. The experimental designs and the manuscript were revised together and under guidance from Associate professor Oommen P. Oommen.

Publication II As the first author of Publication II, M.Sc. Vigneshkumar Rangasami was involved in all the experiments involving the use of cells along with performing the size and zeta measurements, gel electrophoresis and SEM. V.K. Rangasami also performed and analyzed data from the transfection studies, immunomodulatory studies and the differentiation experiments. V.K. Rangasami also contributed to the writing of the manuscript. The experimental designs and the manuscript were revised together and under guidance from Associate professor Oommen P. Oommen.

Publication III As the first author of Publication III, M.Sc. Vigneshkumar Rangasami was involved in all the experiments. V.K. Rangasami performed and analyzed data from the coating procedure, cell viability studies, the TEM, preparing the cells for hematological studies, secretome analysis by ELISA and PCR, immunomodulatory studies and the differentiation studies. V.K. Rangasami also contributed to the writing of the manuscript. The experimental designs and the manuscript were revised together and under guidance from Associate professor Oommen P. Oommen.

Publication IV As the shared first author of publication IV, M.Sc. Vigneshkumar Rangasami was involved in all the experiments involving the use of cells. V.K. Rangasami was involved in the cell viability studies, stress test with cells, immunomodulatory studies with bone marrow derived mice macrophages, while also contributing to the in-vivo studies. V.K. Rangasami also contributed to the writing. The experimental designs and the manuscript were revised together and under guidance from Associate professor Oommen P. Oommen.

1 INTRODUCTION

Over the last few decades, the role of biomaterials in healthcare has drastically increased. The application of biomaterials has greatly improved the fields of tissue engineering, immunotherapies, drug delivery and medical implants. [1–3] The capability of the current generation of biomaterials to be easily modified with respect to their chemical and physiochemical properties, to protect biologically active products (cells, peptides, nucleic acids) and to be used as biocompatible supports; in the form of scaffolds and medical devices; has made them more potent for use in a wide range of applications. [4–6] The term biomaterial has been broadened in recent years to include a range of substances that could differ structurally and functionally, originating naturally or being completely synthetic.

While a great deal of progress has been made in the field of biomaterial research, there has been comparatively slower progress in translating this research into clinical application.[7] This clinical translation of the biomaterials has been slowed down due to the effort required to complete the process by the participating research organizations, industries and regulatory bodies in different countries. However, apart from these bureaucratic problems, there have also been issues where the induction of the biomaterials creates adverse immune responses.[8] Though there have been a few commercially available biomaterials products that have not been known to create an adverse immune response, there are still several biomaterials that could create excessive inflammation, hinder the healing processes, destroy the surrounding tissue, and even be rejected by the body. This has brought the spotlight on favorable biomaterial-immune cell interactions for successful clinical translation of new devices and implants for various biomedical needs.

The immune system is key to our sustenance and survival as it provides the defense of the body against infections and harmful substances, and protect us against tumor formations by eliminating aberrant cells while also stimulating wound healing and tissue regeneration after injury. Here in this thesis, we focus on the macrophages as they are some of the first cells to be on the site of injury or inflammation and are present in all tissues in the form of resident macrophages.[9,10] The ability to manipulate these cells of the immune system has brought about a new generation of

therapies wherein the design of the biomaterials are focused on reorienting and exploiting the potential of the immune cells.[11–13] The design of these immunomodulatory biomaterials requires the combined knowledge in immunology, materials science and bioengineering for the biomaterials to harness the healing or destructive capabilities of the immune system are needed for different therapies (e.g., anti-cancer therapies and tissue regeneration).

2 REVIEW OF LITERATURE

2.1 Immune system and its responses to foreign bodies

Every biomaterial that is used for therapeutic purposes is targeted by the host immune system. Traditionally, when a biomaterial is injected or implanted into the body, there is an immediate aggressive response towards it from the immune system. This response when uncontrolled, results in the encapsulation of the biomaterial as a fibrous capsule or triggers chronic inflammation, leading to the failure of the implant. This process is called the foreign body response (FBR). The main strategy before the advent of immunomodulatory biomaterials was to design bioinert materials that evade the detection of the materials by the immune cells. However, with the advent of immunomodulatory biomaterials, the host immune response to the biomaterials could be exploited to our advantage to enhance the survival of therapeutic cells in living scaffolds after implantation and ameliorate biomaterial-tissue integration to stimulate tissue regeneration.[14] The nature of the immunomodulatory biomaterials can be used to fine-tune the response of the immune system and ensure the proper functionality of the implanted material. In the following sections, the immune system-biomaterials interactions and the different cells involved in regulating these processes are discussed in detail.

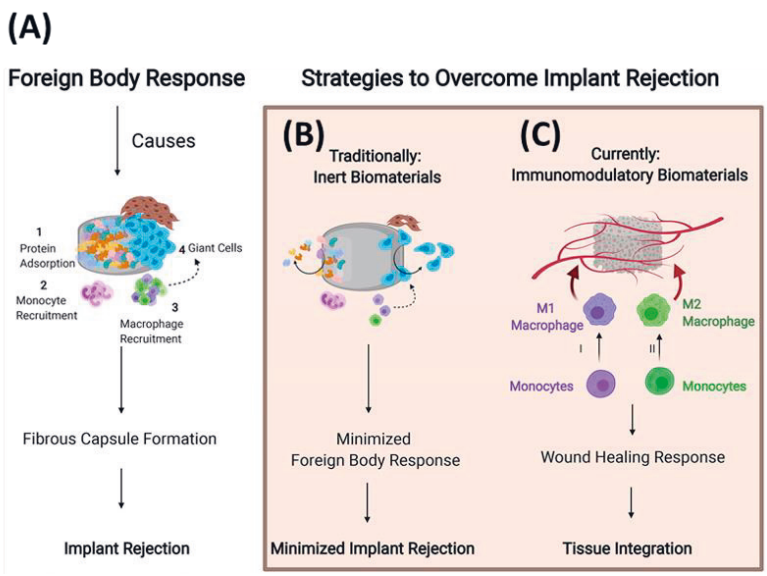

Figure 1. (A) Schematic description of foreign body response when a biomaterial is implanted into the body. (B)&(C) Two different strategies that could be employed to overcome biomaterial failure. Figure Adapted and modified with permission from Whitaker et al. 2021.[14]

2.1.1 Foreign Body Response

The immune system in the human body can broadly be classified into two types based on how they respond and the types of cells involved in the responses. The innate immune system is responsible for the immediate and non-specific inflammatory response following the recognition of foreign material or pathogens in the body. The innate immune system being the first responders, consists of a wide range of immune cells from polymorphonuclear cells, mononuclear cells consisting of the dendritic cells, monocytes and macrophages and the lymphocytes which include the natural killer cells (NK cells), gamma delta T-cells, and the innate lymphoid cells.[15] The adaptive immune system or the acquired immune system is the more specialized arm of the immune system where specific antigen responses are effectuated. This adaptive immune system is also responsible for the development of long-term memory, which enable long-term protection against specific pathogens or antigens.[16]

As mentioned above, the introduction of the biomaterials to the human body triggers a reaction to the biomaterial that determines the outcome and the biological performance of the biomaterial. The immune system is also activated by the

degradation products released by the biomaterial.[17] This release of the products caused by the degradation leads to an uncontrolled inflammatory reaction (a process called FBR) which ends with the fibrotic encapsulation of the implanted biomaterial and ultimately leading to the failure of the implant.[18] The foreign body reaction (FBR) being the first response of the immune system towards the biomaterial comprises the cells of the innate immune system like the neutrophils, monocytes and macrophages. The macrophages involved in the FBR tend to fuse into foreign body giant cells (FBGCs) which then recruit fibroblasts and ultimately lead to the formation of the fibrous capsule around the implanted biomaterials. Generally, when the FBR happens, it is considered to be detrimental to the function and performance of the biomaterial. Over the years there have been many strategies to overcome the FBR or decrease the impact the FBR has on the outcome and functionality of the biomaterial. However, it is also believed that FBR will happen to every biomaterial and in cases like wound healing and tissue repair, the FBR can be manipulated for the proper functioning of the biomaterial.[14] Therefore, the successful application of most biomaterials depends on how the biomaterial can modulate the FBR to enhance or perform its function.

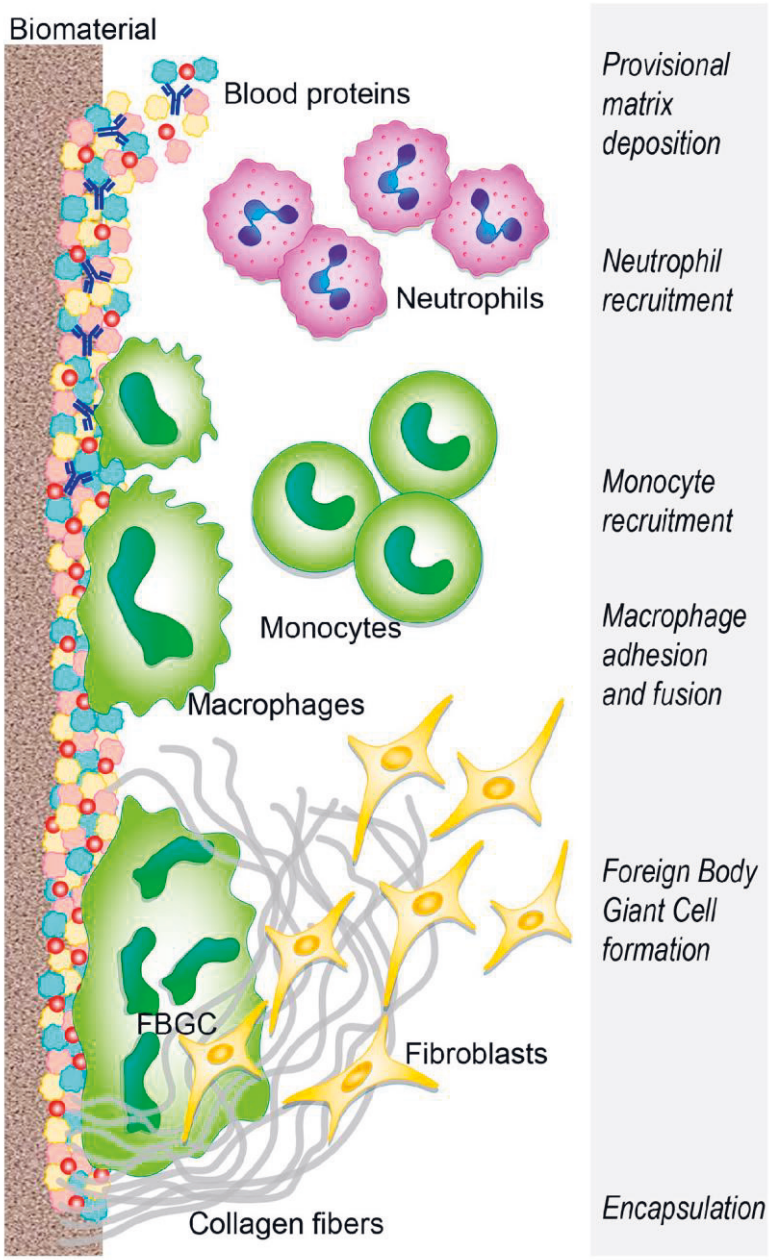

Figure 2. The figure depicts the different events that combine to form the process of FBR that forms the part of the innate immune response against the biomaterial. As soon as the biomaterials are implanted proteins are adsorbed on the surface which leads to the recruitment of immune cells that leads to the formation of fibrous capsules. Illustration adapted with permission from Mariani et al. 2019.[8]

2.1.2 Protein adsorption on the biomaterial surface

Immediately after a biomaterial is implanted in the body, the blood from the surrounding damaged blood vessels comes in contact with the biomaterial and the first step of the FBR is initiated. Within minutes of the FBR initiation, a wide range of serum proteins are adsorbed onto the surface of the biomaterial. This adsorption of proteins onto the surface, a process called opsonization, creates a gradient that acts as a chemoattractant for the neutrophils, monocytes and macrophages. Many components in the plasma such as proteins, lipids, sugars and ions are rapidly adsorbed onto the surface of the biomaterial. [19] This adsorption process or the opsonization can be influenced by the different characteristics of the biomaterial surface. The energy, charge, chemistry, topography, and roughness of the surface can play a vital role in determining the amount, composition, and conformational changes of proteins adsorbed on the surface.[8]Furthermore these changes, over time, also influence the recruitment and adhesion of the different inflammatory and stromal cells that come in contact with the biomaterial.[20,21]

All the proteins (albumin, globulins, fibronectin, vitronectin, and fibrinogen) that are adsorbed on the surface of the biomaterials are capable of signaling the immune cells towards the biomaterial. However, the complement class of proteins, particularly C3 and C5, are the most potent signaling agents. These proteins are known to fragment and coat the biomaterials which in turn makes the biomaterial an easier target for the circulating immune cells.[22] After coating the biomaterial, the complement proteins activate the circulating platelets [23] and become conducive to platelet adhesion which leads to activation of other factors of the coagulation cascade and culminates in the formation of a clot.[24] Among the other signaling proteins, fibronectin and vitronectin are requisite for modulating the inflammatory response and the fibrinogen is involved in activating the cellular components of the immune response along with the complement proteins.[8]

In the paragraph above, a brief account of protein adsorption when biomaterials are implanted into the human body is given. It has also been mentioned how these adsorbed proteins can trigger the platelets leading to the activation of the complement and coagulation system triggering the instant blood mediated immune response. It has to be mentioned that a competitive protein exchange happens on the surfaces where these proteins are adsorbed. This phenomenon was first observed by Vroman and Adams when they studied the interaction of artificial surface with blood plasma proteins.[25] The different proteins adsorbed on the surfaces of the biomaterials form layers called protein adsorption layers (PALs). The PALs are

formed through a dynamic process and can be made of different proteins at different times. The initial PALs are formed by the proteins in the blood with high concentrations and lower molecular weights. The proteins in the initial PALs are gradually replaced by the proteins with higher affinity to the surface of the biomaterials, thereby changing the composition of the PALs. This phenomenon of competitive protein exchange is known as the Vroman effect.[26] The protein adsorption is affected by structural stability and isoelectric points of the proteins. The properties of the materials like the wettability, morphology, size and surface charge can influence the adsorption of the proteins on the surface of the biomaterials.[26]

For the most part, the higher the levels of protein adsorption, the higher the cell adhesion and increased fibrotic encapsulation which increases the risk of biomaterial failure. As a result, there have been quite a number of studies where the authors have tried to reduce the levels of proteins adsorbed on the surface of the biomaterial. The most common strategy has been to coat the biomaterial with non-fouling polymers, thereby reducing the amount of proteins adsorbed. One prime example of this kind of polymer are the zwitterionic polymers that have shown promise of reducing the effect of FBR. These studies like Zhang *et al.* and Liu *et al.* have shown that the addition of zwitterionic moieties to hydrogel components showed lower adsorption of proteins as well as lower cell adhesion even when tested in animal models.[27,28] However, lowering the protein adsorption on biomaterials is not always good. Keselowski *et al.* observed that the discs made of polyethylene terephthalate (PET) when implanted in fibronectin deficient mice had increased fibrous encapsulation.[29] Another study observed that polyethylene glycol (PEG) hydrogels grafted with arginine-glycine-aspartic acid (RGD), a cell adhesion motif, displayed thinner fibrotic encapsulation when compared to the hydrogels without RGD in-vivo even though they had similar amounts of cells adhered and proteins adsorbed..[30] They theorized that the early recruited cells, mostly macrophages, sense the underlying RGD peptide which is known to mitigate FBR These studies also showed that the ability to modulate the amount of proteins adsorbed lessens the severity of the FBR. Further studies are required to understand the intricacies of this process.

2.1.3 Neutrophils recruitment

Neutrophils, the most abundant of the immune cells in the blood, are phagocytic cells and degrade any foreign objects to a certain extent.[31] After the formation of a provisional matrix by the platelets, the neutrophils are activated and recruited by the chemoattractant released by the platelets and the other immune cells surrounding the biomaterial. There have also been reports that neutrophils are present for longer durations at the site of biomaterial implantation when compared to regular wound sites.[32] The neutrophils adhere to the biomaterial site through the β2 integrins and start degradation of the biomaterial through phagocytosis and other enzymes released through the cell's cytoplasmic granules.[33] The neutrophils also release a sticky network of elastase, chromatin DNA, histones, and granular proteins. This network also called the neutrophils extracellular traps (NETs) helps in trapping the pathogens and mitigates the spread of infection.[34,35] The neutrophil released NETs also hinder the healing and tissue regeneration capability by sustaining an environment that is conducive to increased fibrotic encapsulation of the biomaterials.[36] There have been studies where the process of the formation of NETs can be modified by modulating the biomaterial. Fetz *et al.* have observed that their electron spun polydioxanone (PDO) and polydioxanone-collagen I (PDO-COL) templates could attenuate the NET formations. The PDO templates with larger fiber diameters reduced the NET process and the blended PDO-COL templates attenuated the NET formation irrespective of the fiber diameters in both in-vitro and in-vivo studies.[37] It is also reported that neutrophils are not key to the formation of fibrosis as Daniel. G Anderson and colleagues had observed that the lack of neutrophils did not cause a complete absence of fibrosis.[38] They observed that their alginate particles clumped more, an indication of heightened immunity, in a rodent model where they depleted the neutrophil population (using Ly6g neutralizing antibody) comparable with what they had observed with smaller diameter implants.[39]

The activated neutrophils also release a variety of immunoregulatory signals like CXCL8 (C-X-C Motif ligand 8), CCL2 (C-C motif chemokine ligand2), and CCL4 (C-C motif chemokine ligand 4). The CXCL8 released by these neutrophils helps in recruiting more neutrophils while the CCL2 and the CCL4 act as a chemoattractant for recruiting the monocytes, macrophages, and dendritic cells (DCs) and the lymphocytes.[40] The consistent release of these factors is of interest to the monocytes that infiltrate the implant site, thereby suppressing the neutrophils which diminish progressively due to the lack of activating signals.[17]

2.1.4 Macrophages and foreign body giant cells (FBGCs)

As the activated neutrophils release the CCL2 and CCL4 cytokines, the monocytes circulating in the blood get attracted to the inflamed tissue. As the monocytes arrive at the implant site, they differentiate into macrophages and release inflammatory cytokines and accelerate the FBR progression. The monocytes and macrophages exhibit high plasticity and are known to exist in various distinct phenotypes. The plasticity and the distinct phenotypes of the macrophages depend on the cues given by the biomaterials and the proteins adhered on the surface of the biomaterials.[41] The macrophage phenotypes can broadly be referred to as either classically activated or pro-inflammatory 'M1' and alternatively activated or anti-inflammatory 'M2' macrophages. These macrophages being adherent, secrete more chemokines and help in the recruitment of additional immune cells.[42] The macrophages, at the site of biomaterial implantation, also attempt to disintegrate the biomaterial through the degrading enzymes and reactive oxygen species (ROS). The macrophages being smaller than the implanted biomaterial, ultimately fail to complete phagocytosis, thereby undergoing a process called frustrated phagocytosis. During this process, these macrophages start to release anti-inflammatory cytokines like IL10 and shift towards the M2 phenotype. This shift in the macrophage phenotype triggers the tissue regenerative mode and attracts fibroblasts to the biomaterial site.[43] The frustrated phagocytosis and the resulting switch of the macrophages from the M1 to the M2 phenotypes creates a process where the macrophages fuse to each other and form FBGC. These FBGCs, being a distinctive feature of the chronic inflammation in the biomaterial site, can adhere to the biomaterials and form a barrier between the tissue and the biomaterials thereby leading to the failure of the biomaterial.[44] The formation of the FBGCs also signifies that the biomaterial-mediated FBR has commenced and the biomaterial is most likely to fail.

The importance of the role played by the macrophages has been depicted in several studies where the macrophages or monocytes are depleted due to treatment with clodronate liposomes. In these mice models, the authors observed that the fibrous encapsulation of their biomaterials was largely inhibited.[45,46] Other strategies involve disrupting the different macrophage signaling pathways such as the Nlpr3 (NOD-like receptor pyrin domain 3) and Asc (apoptosis-associated speck-like protein 1, monocyte chemoattractant protein- 1α; MCP1), which modulated the efficacy of FBR.[47,48] Kyriakides and colleagues reported that mice implanted with where poly-vinyl alcohol (PVA) sponges that were deficient in CCL2 displayed lower FBGCs formation even though the number of monocytes and macrophages in these

mice were not affected. Despite this, the deposition of other materials (like collagen) on the PVA implants were comparable to the control groups.[49] The rate of degradation of these implants was however much slower in the CCL2 deficient mice when compared to the control mice suggesting that macrophages do mediate the formation of fibrous capsules but there might also be additional processes that mediate the formation of capsules even without the help of the macrophages. Taking all this together, it is evident that macrophages are indispensable for the FBR but their exact role in this process is still being studied.

2.1.5 Instant blood mediated immune response

In sections above, we have seen in detail how the immune system reacts to the biomaterial when a biomaterial is implanted in the body. Nanomaterials used for different therapies and transplanted cells also encounter a similar treatment from the immune system. When the nanomaterials or cells are injected into the blood, they induce a thrombotic reaction called instant blood mediated immune response (IBMIR). The IBMIR is generally characterized by the activation of the complement and the coagulation systems, recruitment of leukocytes and activation of platelets.[50] The complement system is made up of at least 30 soluble and membrane-bound proteins. These proteins allow the complement system to act in different situations like host defense, inflammatory, homeostatic, and immune reactions. There are three main pathways of complement activation are the classical, the lectin, and the alternative pathways. Briefly, the classical pathway is activated by the antigen-antibody complexes. The lectin pathway is triggered by the binding of mannose-binding lectin (MBL) to pathogen surfaces and the involvement of MBL-associated serine proteases MASP-1 and MASP-2. The alternate pathway is triggered by the spontaneous hydrolysis of C3 to C3(H_2O). In all three pathways, the generation of C3b by C3 cleavage helps in the cleavage of C5 to C5a anaphylatoxin and C5b. C5b is involved in the recruitment of components C6, C7, C8, and C9 to form the membrane attack complex (MAC). The main function of the MAC is to mediate the lysis of pathogens of targeted cells.[51]

Apart from the complement system, the coagulation cascade is involved in the reaction toward the nanomaterials and cells that are injected into the body. Tissue factor is reported to be the central player of coagulation in the extrinsic cascade and is known to be involved in thrombotic pathologies and biomaterial-associated processes.[51] Briefly, a stimulus from the cells or the nanomaterials results in the

activation of the extrinsic Xase complex which is comprised of the tissue factor and the factor VII.[52] This complex then triggers the activation of the factor X which along with the activated factor V forms the prothrombinase complex that mediates the conversion of prothrombin to thrombin. This generation of thrombin then activates the platelets resulting in the formation of a clot. There have been reports suggesting the mutual regulation between the complement and coagulation systems.[53]

There have been attempts to attenuate the IBMIR when cells are transplanted in to the body. In the case of nanoparticles, the surface of the nanoparticles can be treated/coated with hydrophilic polymers like polyvinylpyrrolidone (PVP)[54] and poly(hydroxyethyl methacrylate) (PHEMA)[55] and poly (2-methacryloyloxyethyl phosphorylcholine (MPC)-co-2-vinylnapthalene (vN)) (PMvN)[56] to make their surface less adhesive to proteins and platelets, which would help in reducing the effect of IBMIR. Biomacromolecules or bioactive molecules like heparin, hirudin, prostaglandins have been added to surfaces of nanoparticles and have made them less prone to induce thrombosis.[57] When the cells are transplanted into the body, they are known to trigger the IBMIR. It is well known that the expression of CD142 or tissue factor on the cell surface has been a major cause for the cells induced thrombosis. This activation of the coagulation and the complement systems by the cells results in the low engraftment and cellular destruction. Johansson *et al.* have reported a solution wherein they observed that low molecular weight dextran sulfate blocked the activation of IBMIR when islet cells were exposed to blood in an in-vitro model [58] and in-vivo models.[59] Based on these reports, there has been an ongoing clinical trial with a low molecular weight dextran sulfate based therapy in diabetic patients to study if it causes any adverse events.[60] Surface modification cells with IBMIR inhibiting biomacromolecules have also been reported. Cabric *et al.* have reported that engraftment of heparin with biotin/avidin interactions on islet cells surface had reduced the IBMIR induced by these cells in-vitro models[61] as well as in in-vivo models.[62] Lipid coatings, more specifically maleimide modified PEG was used to coat the surface of the islet cells isolated from pancreas of Syrian hamsters. The addition of this PEG coating on the cells suppressed IBMIR, reduced cell damage and increased graft survival when these PEG modified cells were transplanted in diabetic mice.[63] Some of the more recent strategies used to suppress IBMIR triggered by cells are mentioned in section 2.3.

2.2 Role of the immune system in cancer and tissue regeneration

2.2.1 Tumor microenvironment and immune system

One of the major ways through which our immune system is programmed to recognize harmful pathogens is through antigens. The human body is also capable of producing its own antigens, however, the immune system in most cases is programmed not to respond towards these particular antigens.[64] As the tumor cells increase in number, they acquire a large number of mutations that allow them to produce antigens that can be recognized by the immune system. This recognition of the tumor cells by the immune system helps in destroying the tumor and preventing metastasis.[65] Briefly, there is a cancer immunity cycle that Chen *et al.* have described in their review. They state that the cycle begins when the neoantigens from the tumor formation or oncogenesis are detected by the DCs for it to be processed to later steps. For these antigens to elicit a response from the T-cells, proinflammatory cytokines or factors released by dying cancer cells are necessary. (Step1) These DCs then present these antigens through the MHCI and MHCII to the T-cells (Step 2), which results in the priming and the activation of the effector T-cells against these specific cancer antigens (Step 3). Step 4 begins when these effector T-cells are taken to the tumor and culminates with step 5 which is when these T-cells start to infiltrate the tumor. The T-cells then bind to the tumor cells through the interaction between the T-cell receptors (Step 6) and proceed to kill the cancer cell (Step 7).[65] The tumor-specific antigens released by the death of these tumor cells begin the cycle again (Step 1). The development of cancer in cancer patients begins when this cycle does not ensue accurately. In many instances, in these patients, the tumor microenvironment (TME) is chiefly responsible for the suppression of the anti-tumor effector cells.

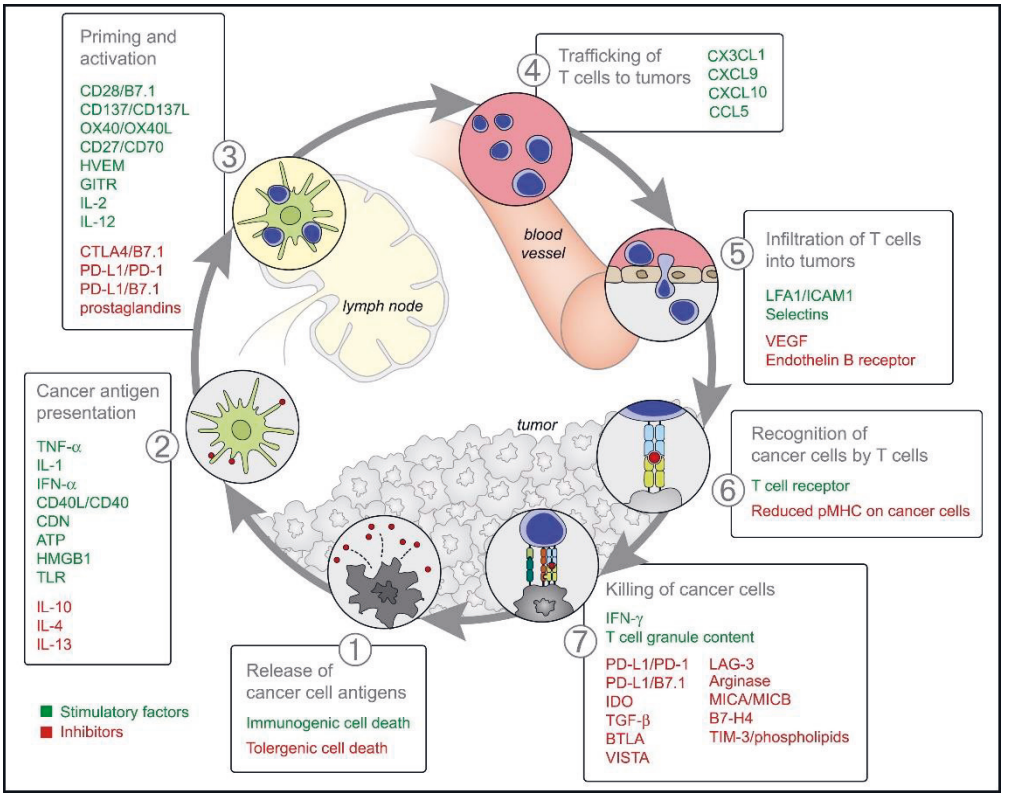

Figure 3. The cancer table of the cancer immunity cycle. The description in the cycle also shows the stimulatory and inhibitory factors for each step in the cycle that could be used in cancer therapy. The illustration is adapted with permission from Chen et al. 2013.[65]

The TME is one of the most complex tissues in the body that continues to evolve. The TME mainly consists of the fibroblasts, the immune cells, and the stromal cells. With time, knowledge of the TME has drastically expanded, and it is now indisputable that the innate immune cells sculpt the TME while also indirectly controlling the TME by influencing the T-cell fate. The cytokines released by the tumor cells manipulate the immune cells such that the immune responses are muted and are influenced towards tumor progression. This cross-talk between the tumor cells and the immune cells fosters tumor growth and ultimately promotes tumor metastasis.[66] Among the immune cells, the monocyte-derived macrophages are the ones that have been studied the most in this context. This is due to the fact that these cells can be polarized into the M1 phenotype, which are the proinflammatory or the tumor killer type, and the M2 phenotype which are the ones involved in

wound healing and tissue regeneration. In the cancer context, the TME polarizes the macrophages into the M2 phenotype and these cells grow to make up almost 50% of the tumor mass.[67] The M2 macrophages are also known to regulate the epithelial cell movement during tissue remodeling. This function of the M2 macrophages and the release of M2 factors like (epidermal growth factor, EGF)[68] is used by the tumor cells within the TME to promote the movement and invasion of cancer cells.[69,70] In most cancers, the tumor growth, proliferation, angiogenesis, and the epithelial-mesenchymal transition are enabled by the wound healing properties of the M2 macrophages.[71] There have been reports suggesting that the polarization of the macrophages to the M2 phenotype is influenced by the hypoxic conditions and the cytokines released by the tumor cells.[72] The IL4 present in the TME also influence the macrophages to polarize to the M2 phenotypes by activating the STAT6 pathway, which triggers the alternate polarization of the macrophages M2 or in the context of cancer, tumor-associated macrophages (TAMs).[66] Hanna and colleagues have also reported that the tumor cells are known to influence the polarization of the macrophages through hedgehog signaling ligands that help in sustaining the M2 polarization of the macrophages in the TME.[73] The inhibition of this cross-talk was observed to be beneficial as it reduced the metastasis and also was observed to re-educate the TME.

Among the other immune cells involved in the cancers, DCs, when taken in the context of cancer can be broadly referred to as the tumor-infiltrating dendritic cells (TIDC). As with the macrophages, the DCs can also help in the formation of the tumor as evidenced by the $CD5^{hi}$ DCs that help in the suppression of the immune response.[74] The TME manipulates the DCs into a tolerogenic phenotype by secreting cytokines that promote the immune suppression in DCs by activating the IDO, Arg1, and STAT3 metabolic pathways.[75] The activation of these pathways ensures that the DCs ability to secrete inflammatory cytokines and then activate the effector T-cells is hindered. The immunosuppressive cytokines like the TGFβ, IL10, VEGF, and prostaglandin E2 (PGE2) in the TME are also known to inhibit the maturation of DCs into immunogenic cells and promote their development into tolerogenic cells that promote the growth and formation of the tumor.[76] The response of the DCs in different cancers is not known to be uniform. For example, the DCs are not known to support the tumor formation in breast cancer, whereas the presence of TIDCs is a positive prognosis in endometrial cancer.[77,78] The plasticity of the DCs in the TME is attributed to the tumor, its subtype, and the unique TME of each of the tumors.

As with the macrophages and the DCs, the circulating neutrophils also react to different tumor types in different ways. Even though the neutrophils do not stay

long at the tumor site, they are known to exhibit a tumor-associated neutrophil (TAN) phenotype. The neutrophils can be broadly classified into N1 (tumor-suppressive) and N2 (tumor-promoting) phenotypes. It is also reported that the N2 neutrophil phenotypes are present at the later stage of tumor development.[79] The neutrophils are known to modulate the immune responses via the reactive oxygen species (ROS) or the reactive nitrogen species (RNS) and reconfigure the extracellular matrix in the TME through matrix metalloproteinases (MMP8/9). This is known to promote angiogenesis, tumor progression, and metastasis through the release of Oncostatin-M, PGE2, neutrophil esterase (NE), and MMP-9.[80,81] In patients with cancers, the neutrophils are categorized as high-density neutrophils, which corresponds to N1 phenotype and low-density neutrophils, that corresponds to N2 phenotypes of the neutrophils. The low-density neutrophils are known to exhibit an immature phenotype and are involved in the tumor progression and metastasis.[82]

The NK cells, which are recognized for their cytotoxic effector cells role, are also influenced by the TME. The NK cells can broadly be classified as the $CD56^{hi}$ $CD16^{lo}$ which secrete inflammatory cytokines and the $CD56^{lo}$ $CD16^{hi}$ which function as the cytotoxic cells that eliminate the tumor.[83] In normal circumstances, these NK cells are very efficient in eliminating the malignant cells and limiting the metastasis of the cancer cells. However, low NK cell activity has been associated in most patients with cancer.[84] Though the NK cells are efficient in capturing and eliminating the circulating tumor cells through the perforin/granzyme mediated pathway, they are much less efficient in eliminating the tumor cells in the TME.[85] In the TME, both the subtypes of the NK cells are known to have reduced inflammatory cytokines and reduced cytotoxic ability. This is due to the factors present in the TME and the TME cells communicating with the NK cells. As with the macrophages and the DCs, the NK cells also get influenced by the cytokines released by the tumor cells in the TME. These cytokines hinder the cytotoxic nature of the NK cells and ensure that these cells enhance the immunosuppressive nature of the TME by arresting the growth and expansion of the T-cells. The ability of the TME to manipulate these immune cells, and make them assist in the growth and proliferation of the tumor, shows the importance of direct cell to cell communication that impacts the tumor fate. However, there are also reports that other components such as the extracellular matrix (ECM) can indirectly impact the tumor fate. The ECM can impact the tumor in two ways, it can provide pathways to allow T-cell infiltrations and also inhibit the T-cell proliferation.[86] The TME also consists of the stromal cells, which become influenced by the tumor cells and become cancer-associated fibroblasts (CAF). The

CAF are reported to contribute to the growth, proliferation and invasiveness of the tumor. The CAFs are also known to influence the polarization of the macrophages to the M2 phenotype in the TME and also help in the reduction of the T-cell population in the TME.[87]

Immunotherapies are treatments that help the immune system or cells fight cancer. Traditionally, immunotherapies involve the use of either immune checkpoint inhibitors, T-cell transfer therapy. The most common treatment targets for the immune checkpoint inhibitors are the PD-1 or PD-L1 and the CTLA-4/B7-1/B7-2 proteins.[88] The checkpoint inhibitors block these proteins and allow the T-cells to kill the tumor cells. Some of the recent advancements in this area are discussed in the forthcoming sections. In the T-cell transfer therapy, tumor infiltrating lymphocytes or CAR T-cell cells are injected into the patients to fight against the tumor cells. The other major immunotherapy option is the monoclonal antibody treatment where antibodies targeting specific proteins on the T-cells to make them more responsive towards the cancer cells. There are also treatments where interferons or interleukins are used to activate the NK-cells and the T-cells and aid the immune system in fighting the cancer cells. More recently, reprogramming the myeloid cells in TME by engineering strategies like targeting prostaglandin E2 receptor 4,[89] increasing the ROS generation using copper based nanoparticles,[90] delivering mRNAs of proinflammatory markers,[91] using microRNA 155 [92], using exosomes to deliver antisense oligonucleotides targeting STAT6[93] have been included in the umbrella of immunotherapy. The reprogramming of the myeloid cells from the pro-tumor phenotype makes these myeloid cells more aggressive towards cancers. The observations of how the immune cells behave in the TME indicate an intricate set of interactions that takes place in the TME that leads to tumor proliferation, invasion, and metastasis. These observations also indicate that the TME should be a target in any future cancer therapies.

2.2.2 Immune system and tissue regeneration

As seen in the sections above, the immune system plays a huge role in the development and progression of a tumor. Similarly, there are a lot of studies that indicate that the immune system is crucial for tissue repair and the restoration of the functionality of the original tissue. The role of the immune system in tissue repair and regeneration can at best be described as complex, as their role depends on

various other factors like tissue type, organ, and the stage of life (neonatal or adult).[94] As with anything that enters the human body, an injury or tissue damage is followed by an immune response. The innate immune system is triggered by the hazardous signals that are emitted by the damaged tissues. This triggering of the immune system in the absence of pathogens or foreign objects creates a situation that is termed as sterile inflammation.[95] The adaptive immune system then follows the innate immune system and responds to these signals from the activated innate immune system. It has always been thought that the response of the innate was the critical factor in tissue repair, however, it is now thought that the adaptive immune system also plays a crucial role in the tissue repair and regeneration.[96]

During pathogen attacks or during cancer, the immune system is activated or triggered by certain signals released by the pathogens or the cancer cells. In the case of wound healing or tissue repair, there are certain signals released from the tissue damage area by necrotic and stressed cells.[97] In the wound healing and tissue repair context, these signals are known as danger signals or damage-associated molecular patterns (DAMPs). Heat shock proteins, high mobility group box protein, nucleic acids, inflammatory cytokines like IL1, IL33, and certain ECM proteins like collagen, elastin, and hyaluronic acid (HA) can all stimulate inflammation by acting as DAMPs.[98] The inflammation is triggered when the toll-like receptors (TLRs) recognize the DAMPs and activate the NF-ϰB pathway. The activation of the TLRs also triggers the tissue-resident macrophages. These cells then release factors that act as chemoattractants for the neutrophils, monocytes, and the macrophages, which in turn release the inflammatory factors like tumor necrosis factor-α (TNF-α), IL-1β, and IL-6.[99] The activation of the TLRs and the sustained release of pro-inflammatory signals seem to cause a detrimental effect in most cases of tissue repairs [100,101] but there are some studies that report that the TLRs are beneficial to wound healing in skin.[96] It has also been reported that the role of the TLRs can either be beneficial or detrimental depending on when, where, and how the TLRs and the inflammatory signals are activated.[102] In summary, the danger signals given out after the infliction of the wound can significantly influence the healing process at the early stages.

Neutrophils, being the first among the immune cells to arrive at the site of tissue damage, are known to enhance the host defense while also removing foreign objects.[96] As mentioned above, the tissue-resident macrophages, activated by the DAMPs and TLRs, release CXCL8 which triggers the cascade that attracts the neutrophils to the tissue damage site. The infiltration of the injury site by the neutrophils and the release of cytokines like IL17 and vascular endothelial growth factor (VEGF) leads to the recruitment of more neutrophils and promotion of

angiogenesis, and proliferation of other cells such as the fibroblasts and epithelial cells.[103] In the context of tissue repair and wound healing, neutrophils are also known to exhibit anti-inflammatory phenotypes. These kinds of neutrophils help in the attraction of monocytes and macrophages that help in the elimination of dying cells and other debris in the injury site. The monocytes and macrophages also help in the removal of dying neutrophils which assists in the resolution of inflammation.[104] Therefore, controlling the mobilization of the neutrophils could be a good strategy to promote tissue healing and regeneration.[105]

Among the immune cells involved in the tissue repair/regeneration process, macrophages are known to have a critical role. The macrophages also play an active role in the tissue healing/repair process by eliminating the neutrophils, the cellular debris, and other dying cells by phagocytosis. The tissue-resident macrophages that are activated by the neutrophils, actively recruit a large number of circulating monocytes and macrophages. The tissue microenvironment plays an important role in determining the role, phenotype, and functions of these macrophages.[96] In normal circumstances, in 1-3 days the circulating monocytes differentiate into macrophages and their presence in the tissue damage site can last up to 21 days.[106] The monocytes are usually recruited from the blood, bone marrow, and the spleen. CCL2/CCR2 and CX3CL1/CX3CR1 are the main receptors involved in the recruitment of these cells. The fibroblasts, epithelial and endothelial cells in the tissue damage area, and the surrounding areas produce CCL2 in response to the DAMPs and other inflammatory cytokines produced by the damaged cells or the necrotic cells. In the context of wound healing and tissue repair, the M2 or the anti-inflammatory macrophages are the cells that are considered to be more beneficial. These M2 macrophages express factors like arginase, VEGF, platelet-derived growth factor (PDGF), and insulin-like growth factor (IGF) which help in the successful tissue repair process.[107] As seen above, the cytokines play a major part in the polarization of the macrophages. However, there have also been reports suggesting that microRNAs (miRNAs) like miR-9, miR-127, miR-125b, miR-21, miR-223, and miR-146a are crucial in helping the polarization of macrophages.[108] The M2 macrophages, though beneficial in wound healing, due to their sustained activation, can contribute to the formation of pathological fibrosis. The M2 cells are known to promote fibrosis due to the significant amount of matrix metalloproteinases (MMPs) they produce during the tissue repair process.[96]

Among the different cytokines produced by the M2 macrophages, IL-10 is known to be a critical cytokine for the tissue repair process. The production of the IL-10 by these macrophages modulates the TRegs, which contribute towards the resolution

of inflammation and help in tissue repair and regeneration. Even though there has been enough evidence of the role of the macrophages in the tissue repair/regeneration process, there remains doubt about the plasticity of these cells. It is still unclear whether individual macrophages residing in the tissues can change their phenotypes at any given time or if there are particle subsets of macrophages that can only perform certain roles.[107] In all, the successful tissue repair or regeneration requires the active contribution of immunosuppressive M2 macrophages.

The other main immune cells, the DCs, and the T-cells also play an important role in the tissue repair and wound healing processes. The DCs, similar in function to the macrophages, are known to be beneficial in wound healing as animal models that are deficient in DCs display poor wound healing after burn injuries.[109] The DCs also promote wound healing through their interactions with the TLRs and type 1 interferons.[110] It has also been reported that the role of DCs during wound healing is of an immunoregulator that control the macrophage homeostasis. The T-cells, on the other hand, are also shown to help in the tissue repair and wound healing, however, the exact mechanism of action is largely unknown due to the large variety of T-cells found in the injury sites. In the different subsets of T-cell, the alpha-beta T-cells (αβT-cells) are known to have both pro and anti-inflammatory populations, while the gamma-delta T-cells (γδT-cells) have been reported to have beneficial effects on regeneration. $CD4^+$ T-cells (TRegs) are also known to play a crucial role in the repair and regeneration of several tissues like skin, bone, lungs, and kidneys.[111–114] There have been significant studies done to prove that the T-reg cells and γδT-cells are crucial in tissue healing especially in muscular and skin injuries.

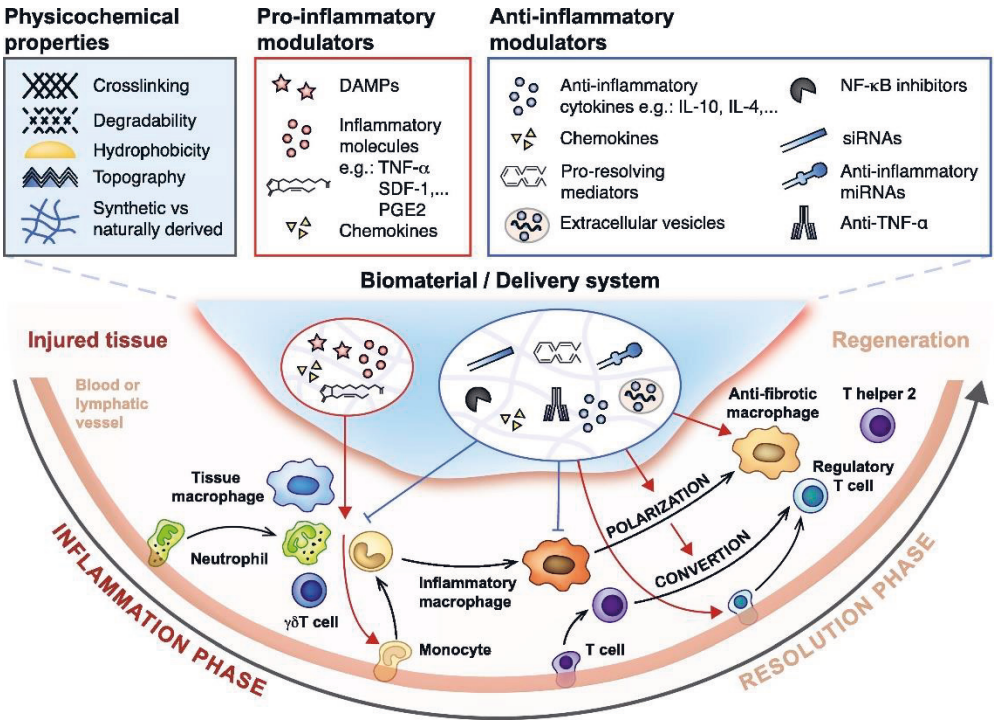

Figure 4. The figure depicts the different strategies through which the immune cells can be modulated using biomaterials and other factors like anti-inflammatory and pro-inflammatory factors. Differentiation factors are depicted by black arrows, induction is indicated by red arrows and blue arrows show inhibition. Figure adapted with permission from Julier et al. 2017. [96]

2.3 Engineering strategies for modulating the immune system

In the above sections, the role of the immune cells in tissue regeneration and cancer progression has been discussed at great length. Therefore, modulating the immune system using biomaterials has become an attractive course of action in the fields of cancer therapy and regenerative medicine. It is also generally accepted that in the context of cancer therapy where the TME is immunosuppressive in nature, there is a need for cancer immunotherapies which actively boost the immunity whereas in the case of tissue engineering the need is to suppress overactive inflammation and create an immunosuppressive environment. Through the previous sections, it has been established that manipulating the immune system can have enormous potential in regenerative medicine as well as cancer therapy. In the coming segments, some of the recent biomaterials that manipulate the immune system, developed for regenerative medicine and anti-cancer therapies will be discussed.

2.3.1 Evading the complement and coagulation system

It has been long reported, that the coagulation and complement systems get activated by based liposomal nanoparticles.[115] However, Moghimi *et al.* reported that the methylation of the phosphate oxygen moiety of phospholipid methoxy(polyethylene glycol) (mPEG) conjugates prevented the complement activation. They observed that liposomes with mPEG held their anionic charge and therefore activated the complement system and the liposomes made with the methylated mPEG removed the anionic charge and did not activate the complement system. The authors thus say that this method could be used to make safer liposomes.[116] In a similar manner, Adler and colleagues reported an alternate solution to PEGylation to avoid the activation of the complement system. When they synthesized the liposomes and coated them with different mol% of poly(2-methacyloyloxyethyl phosphorylcholine (PMPC) lipids, they observed lower complement activation. They observed that when the mol% of the PMPC lipids on the coating was between 1-10%, there was comparatively lower adsorption of proteins post-incubation in human plasma. The authors also observed a correlation between the PMPC molecular weight and the C3 binding. The higher polymerization degree on the PMPC were able to better suppress the total protein adsorption as well as the C3 binding. With their results, these authors show that the modification of liposomes with PMPC lipids can be a viable strategy to complement activation.[117] In another study, chondroitin sulphate (CS) polymer-coated nanoparticles were used to suppress the thromboinflammation caused by doxorubicin. To make the CS-coated gold nanoparticles, the authors first functionalized the CS with a disulfide group and free hydrazide units. This modified CS was then used as a surface capping agent for the preparation of the gold nanoparticle. Doxorubicin was then conjugated through an acid liable hydrazone linkage to make the complete nanoparticle (CS-Au-Dox). The authors exposed the doxorubicin conjugated to whole human blood and observed that the CS-Au-Dox nanoparticles did not cause clotting. The CS-Au-Dox nanoparticles also did not activate the thrombin anti-thrombin complex (TAT) suggesting that these nanoparticles could evade the systemic immune system.[118]

Like the strategies used in making the nanoparticles stealthier, the cells used for transplantation are also modified to avoid triggering the immune system. It has been reported that most of the cells are lost due to IBMIR.[119] To make the cells used for transplantation stealthier, Asawa and colleagues functionalized the cell surface with heparin conjugated lipids. The authors used fragmented heparin (fHep) and modified this to carry an aldehyde group at one end. The modified fHeps were then conjugated to oligo lysine bound polyoxyethylene (POE) chain lipids via Schiff base

reaction to produce the fHep-lipid. Briefly, they coated these fHep-lipids MSCs and evaluated the functionality of these fHep coating in whole blood. The cells coated with these lipids displayed significantly lower platelet generation and lower generation to TAT when compared to the uncoated cells. The authors thus show that engineering the surface of the cells with modified lipids can be used as a strategy to protect the cells from the attack of the immune cells.[120] Similarly, Nilsson *et al.* combined different strategies to create one method to coat the cells and prevent them from activating the complement system. Briefly, the authors conjugated a factor H binding peptide (5C6), an ADP degrading enzyme (Apyrase) with PEG linkers to cellular surfaces. Both the 5C6 peptide as well as the apyrase are known to regulate the platelet and complementation activation by recruiting factor H and ADP depletion. When the cells coated with these materials were exposed to whole human blood, it was observed that the coated cells did not cause coagulation and generated less TAT, and did not activate the complement system. These results clearly showed that the factor H clearly inhibited the complement system, while the activation of platelets and coagulation was attenuated by the ADP. These authors show that inhibiting thromboinflammation using a combined approach can potentially reduce IBMIR that are triggered when the cells are transplanted.[121]

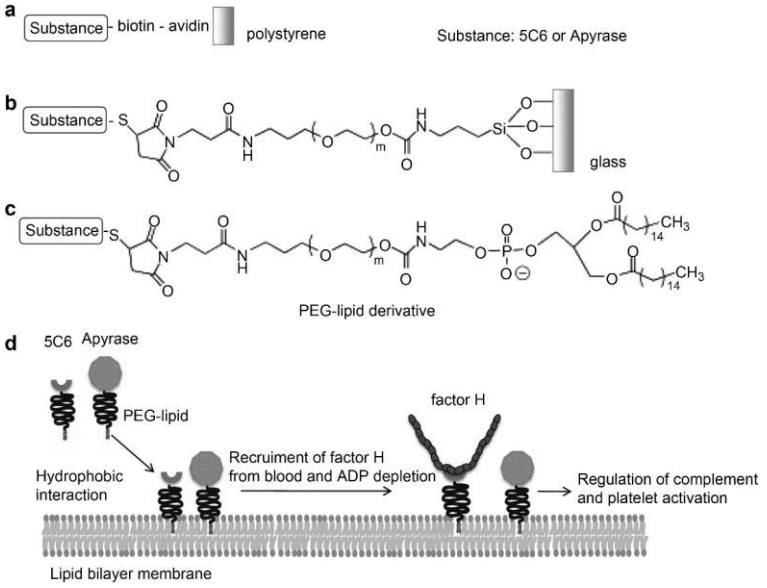

Figure 5. Surface modification of substrate and cell surfaces with 5C6 and apyrase. (a) Immobilization of biotinylated peptide onto polystyrene surfaces via avidin. (b) Immobilization of thiolated peptide and apyrase onto glass surfaces via maleimide-conjugated PEG. Thiolated factor H-binding peptide 5C6 and apyrase are conjugated to the end of PEG chains via a thiol-

maleimide reaction. (c) Chemical structure of 5C6-conjugated PEG-lipid for surface modification of cells (erythrocytes, endothelial cells). (d) Schematic representation of a cell surface modified with 5C6 and apyrase, which are co-immobilized on cell surfaces by incorporation into the lipid bilayer membrane. Factor H is recruited to the surface by 5C6 from human blood to impair complement activation, and apyrase degrades ADP to suppress platelet and coagulation activation. Adapted with permission from Nilsson et al .[121]

2.3.2 Immunomodulatory biomaterials in anti-cancer therapy

The practice of targeting the immune system as a means of anti-cancer treatment has been called cancer immunotherapy. Immunotherapeutic agents are designed to evoke an anti-tumor response from the immune cells that have been influenced by the tumor cells, thereby inhibiting the tumor growth and metastasis.[122] Since the approval of cytokine interferon-α (IFN-α) by the food and drug administration (FDA) in 1986,[122] there have been many other immunotherapeutic agents that have been developed and approved for clinical use. However, these agents have also known to have safety and efficacy problems that have yet to be solved. Most of the immunotherapeutic agents or drugs are usually systemically administered and thus a majority of dosage is rapidly excreted and lost due to poor targeting abilities. Due to these limitations, the drugs or immunotherapeutic agents are administered in large doses repeatedly leading to significant toxic side effects. The need to alleviate the toxic side effects and reduce the activation of systemic immune reactions has led to the advent of delivery systems using biomaterials. These biomaterial-based delivery systems are known to be target-specific with the added advantage of being highly efficient, non-toxic, and even having an anti-tumor stimulating effect on the immune cells.[123,124] Different biomaterials like liposomes, natural and synthetic polymers, and a few metals can be used as delivery vehicles. For the anti-tumor effect to reach its maximum, the material for the delivery vehicle can possess anti-tumor properties of its own as well as deliver the immunopharmaceuticals. In the paragraphs below, some of the most recent biomaterial-based cancer immunotherapeutics will be discussed.

Liposomes are nanoparticles that are made of lipids, mainly phospholipid bilayers. These liposomes have been extensively studied for their potential to carry and deliver drugs to specific targets. There have also been liposomes developed as vaccines for diseases like influenza (Inflexal), malaria (Mosquirix), and Hepatitis A (Epaxal). Liposomal delivery systems were also used as vaccines carrying mRNA for the currently ongoing coronavirus disease (COVID-19; Spikevax and Comirnaty)

and are also being developed as vaccines for human immunodeficiency virus (HIV).[125]

In the context of cancer immunotherapy, recently a liposome has been developed to target the DCs to stimulate them to create an anti-tumor response. Lai *et al.* incorporated DCs targeting mannose, vaccine adjuvant CpG oligodeoxynucleotides (CPG-ODNs) onto the surface of their liposome and loaded the liposomes with $TRP2_{180\text{-}188}$ peptide as a therapy for melanoma. The mannose on the surface of the liposome helps in the site-specific delivery while the CPG-ODNs help in stimulating the targeted DCs to produce proinflammatory cytokines. The $TRP2_{180\text{-}188}$ was used as an agent to make the DCs recognize the melanoma. When these liposomes (M/CPG-ODN-TRP2-Lipo) were tested in a B16 melanoma mice model, it was found that after 17 days the tumor size in the liposome treated group was much smaller when compared to the untreated groups (Figure 6). This was also correlated with the survival times of the mice where the liposome-treated mice survived the longest when compared to other groups. The dissection of the mice at the end of the experiments also revealed that the activated DCs were not infiltrating any of the other tissues and were present only at the tumor site. Further analysis revealed that this treatment reduced the number of myeloid-derived suppressor cells and TRegs and increased the number of anti-tumor cytotoxic T-cells and interferon-gamma-producing cells.[126]

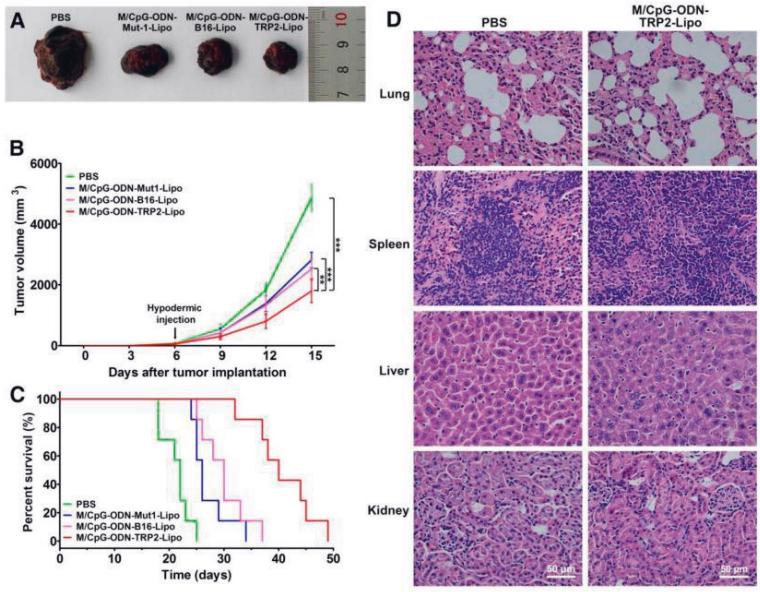

Figure 6. The figure depicts the effects of the M/CPG-ODN-TRP2-Lipo particle treatment on B16 tumor-bearing mice. (A) depicts the tumors from each tumor group (B) Depicts the tumor volume from each treatment group (C) Survival analysis on treatments with the particles and control (D) Safety evaluation of the nanoparticles evaluated in the different tissue samples. Figure adapted with permission from Lai et al.[126]

As mentioned earlier, one of the main requirements for a delivery vehicle is to evade the immune system while circulating in the blood and to reach and accumulate in good numbers at the tumor site to trigger an anti-tumor immune response. Zhang and colleagues did develop a nanoparticle that delivered anti-tumor payloads without systemic toxicity. The authors first chose to deliver the combination of the anti-CD137 antibody and the IL-2-Fc to B16F10 melanoma-bearing mice. When the combination of these drugs was administered intravenously, it was found to be highly toxic. The treatment activated a dose-dependent cytokine storm. They observed a significant increase in the levels of proinflammatory cytokines and vascular leak syndrome in these mice. Further analysis confirmed the role of NK cells and circulating T-cells in the activation of the cytokine storm as a direct effect of the IL-2 that stimulates the NK cells and anti-CD137 which co-stimulated the T-cells. Significant toxicity was also observed in the liver and the kidney with elevated levels of alanine transaminase and serum creatinine kinase. When the IL-2-Fc/anti-CD137 were conjugated to the surface of a PEGylated liposome, enhanced accumulation in the tumor was observed along with significantly delayed tumor outgrowth and no evidence of systemic toxicity or the activation of a cytokine storm. The liposome-treated mice were also found to exhibit intratumoral immune responses which they suggested could be due to the effect of the drug delivered by the liposomal constructs. The work by Zhang and colleagues elicits the importance of targeted delivery of the drugs to avoid systemic toxicity.[127]

Similar levels of target specificity and anti-tumor responses have been observed when delivery vehicles have been made only of specific polymers. As mentioned in the sections above, the TAMs compose of almost 50% of the tumor mass. The large presence of the TAMs in the tumors and the plastic ability of the macrophages motivated Lanlan Liu *et al.* to repolarize the TAMs to anti-tumor macrophages. They used the indirect ability of zinc protoporphyrin to generate ROS which is a known activator of proinflammatory macrophages. The zinc protoporphyrin (ZnPP) was grafted onto galactose functionalized poly (ethylene glycol)-b-poly(L-lysine) (PLL) block polymer. On grafting, a micelle is formed (ZnPP PM) with the block polymer being the outer surface of the micelles and ZnPP forming the core of the micelles. To further aid with the repolarization of the TAMs to M1 macrophages, a TLR antagonist poly I:C (PIC) was added to the ZnPP. The negatively charged PIC was

encapsulated by the ZnPP PM through electrostatic adsorption to form ZnPP PM/PIC. Further analysis in mice B16F10 tumor models revealed that the ZnPP PM/PIC particles successfully targeted the TAMs (through the galactose moiety) and encouraged the repolarization of the TAMs to M1 macrophages. The authors also observed the increased activity of the NK cells and T-cells and prompt tumor regression in the animal models that were treated with the ZnPP PM/PIC particles. The biosafety evaluation of the ZnPP PM/PIC revealed that these particles were not toxic as evidenced by no toxicity in the liver, kidneys, and other major organs. Altogether, these authors developed a non-toxic nanoparticle to target the TAMs and repolarized them towards M1 macrophages to activate enhanced anti-tumor responses in mice models.[128]

Another class of polymers called glycosaminoglycans (GAGs), which are commonly found in the ECM, are known to have great potential for delivering drugs and small molecules. Hyaluronic acid (HA) is a natural GAG, that is widely used as a component for drug delivery vehicles due to its ability to target the CD44 receptors, which are often overexpressed in cancers. In one of the studies, the authors used this ability of HA to co-deliver an anti-tumor immune stimulator resiquimod (R848) and the chemotherapeutic drug doxorubicin (Dox) in a 4T1 breast cancer models.[129] The R848 was combined with poly(L-histidine) (PHIS) to make PHIS/R848 nanocores. The Dox on the other hand was conjugated to the HA through the acid cleavable hydrazone chemistry to form HA-Dox. This HA-Dox was then used as a coating agent to coating the PHIS/R848 nanocores to assemble the HA-Dox/PHIS/R848 nanoparticle. The interaction between the PHIS and R848 and the bond between HA-Dox could be broken by the acid environment of the TME to release the R848 and the Dox. When the HA-Dox/PHIS/R848 nanoparticle was analyzed in the mice models with 4T1 breast cancer, it was observed that the nanoparticles were accumulating more at the tumor site when compared to controls. Further analysis revealed that the nanoparticle treatment was found to be non-toxic to other organs and was able to significantly reduce the tumor size when compared to the groups administered with free R848 and free Dox. The analysis of the tumors also revealed that there was a greater number of CD3+ and CD8+ T-cells present in the tumors when compared to the non-treated group. This work successfully exploited the properties of a natural polymer to develop a safe and non-toxic treatment for breast cancer.

i)

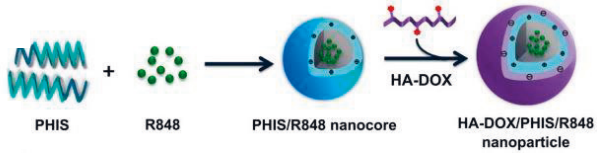
PHIS
R848
PHIS/R848 nanocore
HA-DOX
HA-DOX/PHIS/R848
nanoparticle

ii)

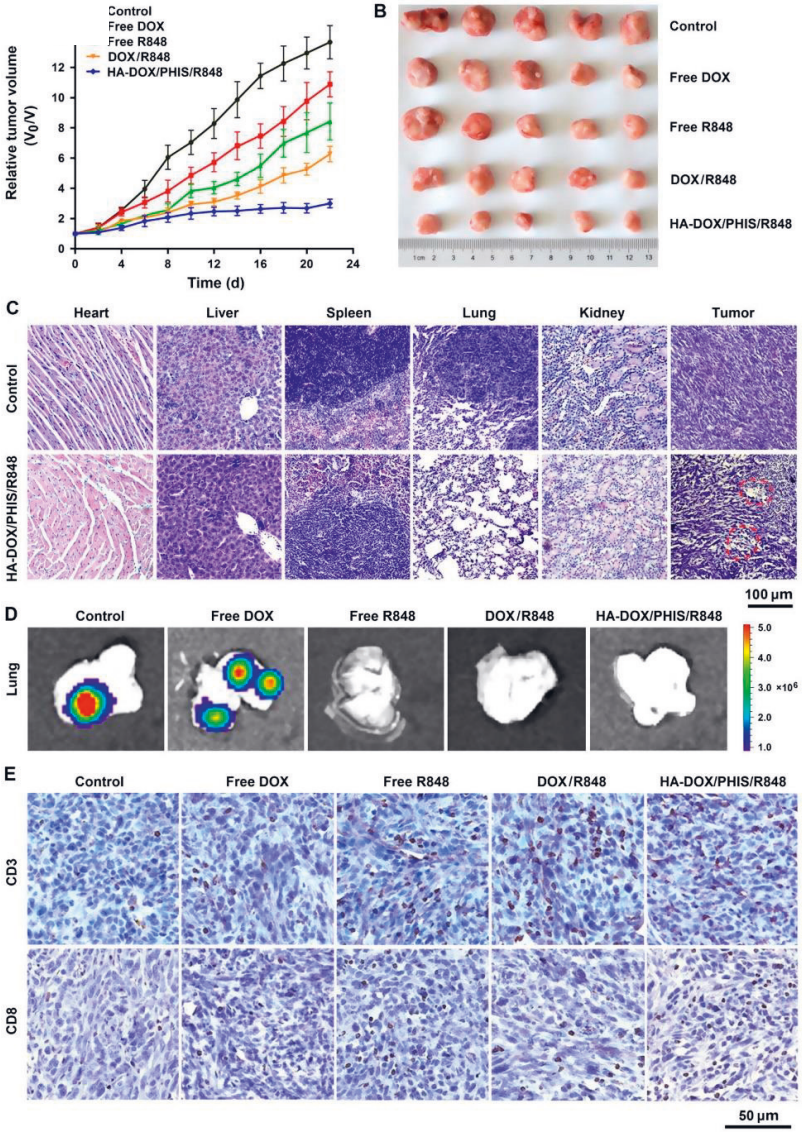
Control
Free DOX
Free R848
DOX/R848
HA-DOX/PHIS/R848
Relative tumor volume (V0/V)
Time (d)
B
Control
Free DOX
Free R848
DOX/R848
HA-DOX/PHIS/R848
C
Heart
Liver
Spleen
Lung
Kidney
Tumor
Control
HA-DOX/PHIS/R848
100 μm
D
Control
Free DOX
Free R848
DOX/R848
HA-DOX/PHIS/R848
Lung
E
Control
Free DOX
Free R848
DOX/R848
HA-DOX/PHIS/R848
CD3
CD8
50 μm

Figure 7. i) Schematic representation of HA-DOX/PHIS/R848 ii)The effect of HA-DOX/PHIS/R848 nanoparticles in 4T1 tumor model mice. (A) The volume of the tumor after treatment with the different groups and HA-DOX/PHIS/R848 (B) The tumor size after removal and treatments with different groups (C) H&E stained images of the main organs in the control and HA-DOX/PHIS/R848 treated groups. The necrotic areas are marked by red lines. (D) The bioluminescence images of lungs removed from the 4T1-LUC tumor-bearing mice after treatment and injected with D-luciferin. (E) Images depicting histochemical staining of CD3+ cells and CD8+ cells. Brown color represents the positive staining. Image adapted with permission from Liu et al. 2018.[129]

Similarly, HA was used in combination with extracellular vesicles (EVs), 3-(diethylamino) propylamine (DEAP), monophosphoryl lipid A (MPLA), and mucin 1 peptide (MUC1) to create a nanoparticle that could be potentially used as vaccines for cancer. Lee et al. synthesized these nanoparticles and designated them as HDEA@EVAT. These particles were evaluated on the different cell lines to test their functionality. It was observed that the particle was targeted to the DCs with the help of the MPLA and the HA which interacted with the TLRs and the CD44 receptors on the DCs. The DEAP helps the particle in escaping the endosome due to the protonation of the DEAP. The MUC1 peptide is then processed and presented to the DCs which further triggers the activation of the CD8+ T-cells. Further analysis of the DCs and T-cells revealed that these cells showed enhanced secretion of proinflammatory cytokines like IFN-γ and TNF-α when treated with the HDEA@EVAT. With this particle, the authors were able to expedite the interplay between the DCs and the T-cells by inducing the DCs maturation by presenting the cancer-associated peptide MUC1.[130]

A new class of polymers, the modern 21st-century polymers are the PAMAM dendrimers [131] which consists of highly branched, mono-disperse man-made macromolecules with defined structures and compositions. The core of PAMAM is generally ethylenediamine while the branches are usually composed of a different number of generations of methyl acrylate and ethylenediamine. Since the structure and the composition of the PAMAMs allow efficient loading of different small molecules, there has been a lot of research done on exploiting this property. One such study was conducted using a modified PAMAM derivative dendrimer, specifically, the fourth generation-N-N-diethylaminoethyl (G4-DEEA). Wu *et al.* used the G4-DEEA and loaded it with the TLR agonist R848. The resulting formulation denoted as G4-DEEA@R848 was studied in mice 4T1 breast cancer models. The G4-DEEA@R848 particles showed the ability to polarize the TAMs to M1 macrophages in vitro, thereby displaying their functionality. In the animal models, the mice treated with the G4-DEEA@R848 showed significantly slower growth and smaller size of the tumors when compared to the controls. Further

analysis of the cells in the tumor revealed the mice group treated with G4-DEEA@R848 showed the most presence of the CD3+, and CD8+ infiltrating anti-tumor T-cells while showing the least amount of myeloid-derived suppressor cells with respect to the controls. The group treated with this formulation also showed a greater number of M1 macrophages in the tumor when compared to the control groups. Thus, the authors showed the potential of the new class of polymers to deliver immunotherapeutic drugs in a safe and non-toxic manner to treat cancer.[132]

Apart from the biomaterials that are delivered by intravenous injections, which are used to reach the cancer sites that are harder to reach otherwise, there are also other classes of biomaterials to combat cancer growth and progression. Implantable biomaterial scaffolds or hydrogels are the biomaterials that can be loaded with anticancer drugs for site-specific delivery and implanted as post-surgical treatments in cancer patients. With a similar idea, Ren *et al.* developed a degradable and implantable microporous scaffold (Dr-AIMS) that could convert the protumor TME into an anti-tumor TME. Dr-AIMS is made of two differently modified HA components. The major component or the bulk of the scaffold is made of methacrylate modified HA and the rest of the scaffold is made up of methacrylate modified oxidized HA. The ability of this soft hydrogel scaffold to degrade and release the drugs loaded in them depended on the blending ratios of the two components. The Dr-AIMS was loaded with a chemotherapeutic drug (Paclitaxel; PTX) to deplete any of the TAMs and tumor cells. Additionally, to activate the DCs and cytotoxic T-cells, R837 or imiquimod was loaded onto the scaffold. The authors also added a combination of immune checkpoint blockers in anti-CTLA-4 and anti-OX40 monoclonal antibodies (mAbs) which also helped in breaking the anergy of the T-cells. These scaffolds were then implanted in mice post removal (10% of the original tumor mass of 200 mm^3 was left behind) of the 4T1 tumors. Two weeks after the implantation of the scaffold, it was observed that there were a smaller number of TAMs and myeloid-derived suppressor cells in the drug-loaded scaffold group when compared to the untreated group. Further analysis also revealed that there were also a significantly greater number of activated DCs present in the intratumoral area in the Dr-AIMS treated mice when compared to the untreated mice. The authors here successfully demonstrated the use of hydrogel-based scaffold to deliver immunotherapeutic and chemotherapy drugs in post-surgery to prevent the recurrence of tumors.[133]

In the sections above, some of the recent advancements in the application of biomaterials for immunomodulation in anti-cancer treatments have been discussed. Most of the discussed materials are organic in nature. There are also several inorganic

materials like gold[134], iron oxide nanoparticles[135], mesoporous silica nanoparticles[136], and microneedles[137] that are being developed to deliver chemotherapy and immunotherapeutic drugs. These will not be focused on in detail as they are out of the scope of this thesis. There are also cells that are engineered to combat cancer. Chimeric antigen receptor (CAR)-T cells are cells that are engineered to express synthetic receptors that will help the T-cells to recognize and destroy cells that express a specific tumor antigen.[138] Even though there are a few limitations of using CAR T-cells for anti-cancer treatments, it has been recently shown to have successfully eliminated acute lymphoblastic leukemia in phase I clinical trials held in late 2020.[139] There are also several biomaterials that have been approved by the FDA or are undergoing approvals or clinical trials for use as anti-cancer treatments.[140,141] The number of biomaterials in the trials or waiting for approval shows the potential and the urgent need for an efficient and safe drug delivery method to treat and eliminate cancer.

2.3.3 Immunomodulation for tissue engineering and regenerative medicine

In the first part of this thesis, we have seen the role of the immune system in tissue regeneration and wound healing. We have also observed that to attain proper regeneration of tissues there has to be a fine balance that has to be reached in the way the immune system operates. If the balance is not reached the most likely scenario is the formation of scar tissue or the wound not healing due to chronic inflammation. Broadly there are many different biomaterials that have been studied to help in wound healing and tissue regeneration. There are even cell-based therapies that are being developed for the purpose of using them in regenerative medicine applications.[142] In this section, some of the current biomaterial-based and cell-based immunomodulatory methods will be discussed.

There have been many reports of using decellularized tissues as scaffolds. These decellularized matrices are considered to be key regulators for tissue regeneration.[143] In a study that Sadtler *et al.* performed, they observed that scaffolds that are derived from cardiac muscles and bone ECM components help in manipulating the immune response to a pro-regenerative response during wound healing. When they tested the efficiency of these scaffolds in a traumatic wound model in C57BL/6 mice, they observed that both the cardiac and bone ECM (C-ECM and B-ECF) attracted more myeloid cells and lymphocytes after implantation when compared to untreated controls. They also observed that in the biomaterial scaffold groups the ratio of the

CD4:CD8 cells was skewed towards the CD4+ help T-cells when compared to the untreated group. This was also correlated with the observance of the increase in the IL-4 cytokines in the injury site and a decrease in the IFN-γ cytokines. Further analysis revealed that the CD4+ helper T-cells and the IL-4 presence in these tissues derived biomaterial scaffolds group was instrumental in the complete wound healing of the injury and the animals completely regaining movements due to regenerated tissues. They successfully demonstrated the potential of tissue-derived biomaterial scaffolds in tissue regeneration.[144] It has to be remembered that one of the main disadvantages of using tissue-based decellularized scaffolds is that the immunogenicity of the scaffolds varies depending on where the scaffolds are sourced from.[145,146] To circumvent this issue, there have also been studies done on more defined and purified naturally available materials. High molecular weight HA has been used to treat failed back syndrome in rat models. The rats chosen were surgically corrected with a modified laminectomy after disc injury. When high molecular weight HA gel was applied in the epidural space post laminectomy, it was observed that there was a significant decrease in the infiltration of macrophages in the groups treated with HA gels when compared to the non-treated groups. It was also observed that there was a significantly lower amount of IL-1β and IL-6 cytokines present in the epidural space.[147] The authors speculate that the HA gel when applied can inhibit proliferative fibrosis post-laminectomy in preclinical models.

As mentioned in the sections above, creating an immunosuppressive environment in place of an inflamed environment is important for successful wound healing and tissue regeneration. To achieve this, Francesca Taraballi *et al.* exploited the properties of chondroitin sulphate (CS) to tune the immune system. Collagen scaffold (CL) was functionalized with CS to obtain a glycosaminoglycan-based functional scaffold (CSCL) that could manipulate the immune system. They tested the CSCL scaffolds in vitro by exposing them to unactivated bone marrow-derived macrophages (BMDM). It was observed there was a significant reduction in the expression of pro-inflammatory genes like TNF-α, IL-1β, IL-12β, and MMP-1 and an increase in the expression of anti-inflammatory genes like TGF-β, Arginase, MRC1, and IL-10 when compared to the CL group. To test if the scaffolds were indeed immunosuppressive, they exposed the CSCL to the BMDMs that were activated into an inflamed state by lipopolysaccharide (LPS). It was observed that there was a significant decrease in the expression of proinflammatory genes like TNF-α, IL-1β, IL-12β, and MMP-1. When these scaffolds were injected subcutaneously in rats, it was observed that the CSCL scaffolds had more cell

infiltration when compared to the CL scaffold. However, the cells that infiltrated the CSCL had lower levels of pro-inflammatory markers when compared to the CL scaffold. The authors explain that the higher infiltration of cells with low proinflammatory markers could suggest the earlier termination of inflammatory processes around the CSCL scaffold.[148]

In a similar manner, Wood *et al.* used HA-based scaffolds and added a synergistic mix of collagen-IV (Col-IV) and fibronectin (FN) to functionalize these scaffolds. The functionalization of this HA scaffold allowed them to grow astrocytes and also showed axonal outgrowth when neuronal cells were grown on them. The functionalization of these HA gels allowed the astrocytes to get activated and release immunomodulatory cytokines like IL-10 and IL-6. The release of IL-10 was significantly higher than the IL-6 in the functionalized HA gels. This increased release of an anti-inflammatory IL-10 by the astrocytes can aid to terminate the acute inflammatory activity and promote repair and regeneration and prevent cell death. The authors observed that their functionalized HA gels could help in the reduction of inflammation and promote motor functions after spinal cord injury. They theorize that the functionalized HA gels could reduce the inflammation in the astrocytes while also polarizing them towards a neuroprotective state. When the authors cultured SH-SY5Y neuronal cell lines on these scaffolds, they observed increased metabolic activity in the cells which they deduced as being the effect of increased neuronal outgrowth. They also theorized that these neuronal outgrowths could increase the therapeutic efficiency while also serving as a stimulus for the generation of relay neurons. With these observations in hand, they examined the potency of their scaffolds to promote adult axonal regrowth in an ex-vivo model of neuronal injury. Rat dorsal ganglia were isolated and used as the ex-vivo model. The studies in this model revealed results that were similar to the studies observed in vitro. There was a significant increase in the metabolic activities of the neurites and significant outgrowth was observed at much deeper locations in the functionalized HA gels when compared to the non-functionalized gels. Despite these significant results where they showed proficient neurite outgrowth and neuroprotective behaviors by the astrocytes, the authors also mention the complexity of the spinal cord in-vivo and suggest additional studies that need to be performed for their scaffold to be used as spinal cord implants.[149]

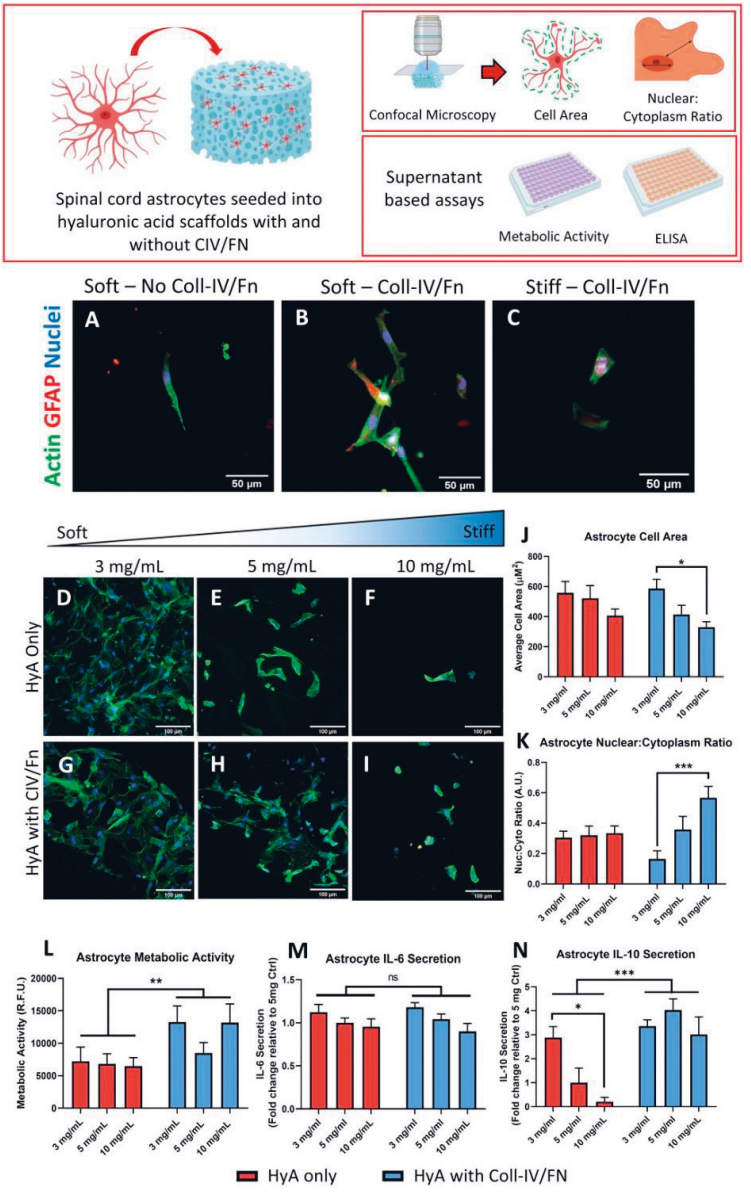

Figure 8. A–I) Soft hyaluronic acid scaffolds with collagen-IV and fibronectin mediate astrocyte polarization to a pro-regenerative phenotype. Spinal cord astrocytes cultured in scaffolds of ranging stiffness with and without Coll-IV/Fn functionalization were imaged to characterize individual cytoskeleton distribution. .J) Astrocyte cell area was the largest in soft scaffolds with Coll-IV/Fn and was significantly larger than cells grown in stiffer scaffolds. K) Nuclear: cytoplasm ratio analysis also revealed a lower reactive index for astrocytes in soft-functionalized scaffolds compared to stiffer scaffolds. L) Metabolic analysis of samples revealed a Coll-IV/Fn dependent effect supporting higher levels of astrocyte metabolic activity. M) Analysis of cytokine secretion showed no significant difference in IL-6 secretion

across scaffold groupings. N) However, significant differences in the secretion of IL-10 were observed in a Coll-IV/Fn-dependent manner. Additionally, this secretion was altered in a stiffness-dependent manner in cells cultured in scaffolds without Coll-IV/Fn. Image adapted with permission from Woods et al. 2022.[149]

Another interesting strategy that was used by Lohmann *et al.* was to absorb or attract the inflammatory chemokines and rescue the wound healing process. They designed a hydrogel that contains heparin, a GAG, that could bind to most of the chemokines, and star-shaped PEG (starPEG). The authors expected their hydrogels to work as an efficient molecular sink which would bind to all the chemokine and thereby inhibit the recruitment of more inflammatory cells and resolve the inflammation. It was also observed that the hydrogels were successful in vitro to scavenge chemokines like IL-8 and MCP-1 from conditioned medium and wound exudates of human patients. They then compared their GAG containing starPEG hydrogel with a commercially available wound healing matrix PROMOGRAN in a wound healing impaired mice model. They observed that their hydrogel was superior in terms of rescuing the wound healing when compared to PROMOGRAN in these impaired wound healing mice models. It was observed that the heparin containing starPEG hydrogels were able to sequestrate the heparin-binding chemoattractants like MCP-1 and IL-8, which caused reduced infiltration of inflammatory cells which thereby reduced the amounts of non-heparin binding chemokines like TNF-α, IL-1β. The reduction of these pro-inflammatory factors were observed to be beneficial to wound healing and was also observed to promote vascularization and re-epithelialization in the wound site, at significantly higher levels than when compared to the commercially available product.[150] The authors also mention that their successful hydrogel system can be loaded with other anti-inflammatory drugs that could aid in wound healing. These were some of the examples (out of many) in recent times where different materials were used to manipulate the immune system and promote wound healing by suppressing inflammation.

Apart from materials, there are also cells that can be transplanted and naturally be therapeutic and help in wound healing applications. The transplanted cells used for these purposes can sense and integrate different signals from the surrounding environment and can respond adequately by releasing factors to manipulate the surrounding environment. However, transplantation of cells results in poor survival of cells after transplantation. It has also been observed that only a fraction of the initial cells transplanted reach the target and reside at the target site after a period of time.[143] Biomaterials and scaffolds based on biomaterials can help in the cells reaching their potential as therapeutic agents by helping the cells survive longer and by controlling their functions. Some of the most researched cells for their potential

use in tissue engineering and regenerative medicine are the mesenchymal stem cells (MSCs). MSCs are known to release different factors that can suppress inflammation and act as pivotal components for MSC-mediated tissue repair.[151] To exploit the properties of the MSCs in the treatment of chondral effects of the knee, Akgun *et al.* grew the MSCs in a commercially available collagen membrane (Chondro-Gide; Geitschlich Biomaterials) (m-AMI) and tested it in patients with chondral defects. The authors also included a group where they used chondrocytes in the collagen membranes as the other test group (m-ACI). The authors claim that at the end of the study, the m-AMI group was found to be clinically effective in terms of significantly improving the quality of the patient's life. There were no graft failures reported in both the groups and both the group had achieved similar clinical and radiological outcomes. The authors state that considering the limitations of their study and the similar outcomes of both groups, the new m-AMI grafts could be potentially more beneficial in the long term due to the superior qualities of the MSCs.[152]

Table 1: A table showing the different scaffolds used to deliver MSCs or MSC factors in various applications. Table adapted with permission from Tsou et al. 2016.[153]

Material	Study performed
Silk	Tissue engineering with silk hydrogels
PCL	A variation of pore size modulating MSC behavior
PEG	Injectable Biodegradable hydrogel deposits for cartilage tissue engineering
HA	Functionalized hydrogel with mimetic peptide to emulate osteogenic niche
NapFF-NO	Nitric oxide releasing hydrogels to study efficacy of MSCs for myocardial infraction
Chitosan	Affinity peptide bone matrix, with chitosan hydrogel for cartilage regeneration
Agarose	Biomimetic hydrogel delivers MSC factors in spinal cord injury
PEG and Chitosan	Controlling porosity of hydrogels for tissue engineering applications
PEG	Evaluation of macroporous hydrogel for bone regeneration applications

Similarly, Corradetti *et al.* used the MSCs to test if they could treat degenerative inflammatory conditions of articular cartilage. To enhance the efficacy of the MSCs therapy, the authors encapsulated the MSCs in a chondroitin sulfate-based biomimetic scaffold (CSCL). When the immunosuppressive properties of the CSCL with MSCs was evaluated in-vitro by a lymphocyte reaction assay, it was observed that the CSCL scaffolds showed greater inhibitory effects than when the MSCs were grown in a collagen scaffold (CL). When both the scaffolds loaded with MSCs were injected subcutaneously in rats, it was observed that there was lower infiltration of immune cells in the CSCL scaffold when compared to the CL scaffold. When the differentiation of the MSCs towards chondrocytes was checked, it was observed after 21 days, that the MSCs in CSCL showed more chondrogenic differentiation in the basal and chondrogenic medium when compared to the cells in the CL scaffolds. The authors thus claim, that their strategy of using MSCs in CSCL could potentially be the solution to various problems in regenerative medicine application.[154] Similarly, HA was used by the same group to coat the plates in which they cultured murine MSCs. They observed that the HA-treated MSCs had a transient increase in the expression of CD44 and showed a two-fold increase in the migration potential when compared to cells that were not treated with HA. When these cells were injected retro-orbitally in mice with LPS-induced inflamed ear, it was found that the HA-treated MSCs showed better homing capacity when compared to the non-HA treated cells. Further analysis revealed that the accumulation of these MSCs led to the suppression of inflammation and early localization of $CD206^{+}$ /M2 macrophages. The increase in the expression of IL-10 and TGF-β in the ear further confirmed the effects of the MSCs on a molecular level. With these results, the authors have developed a method to improve the efficacy of MSCs to home into the site of inflammation and also made it an easy and ready to be used method.[155] There are many other studies that have reported the advantages of using biomaterials to deliver stem cells for regeneration purposes that have not been discussed here in detail.[156,157]

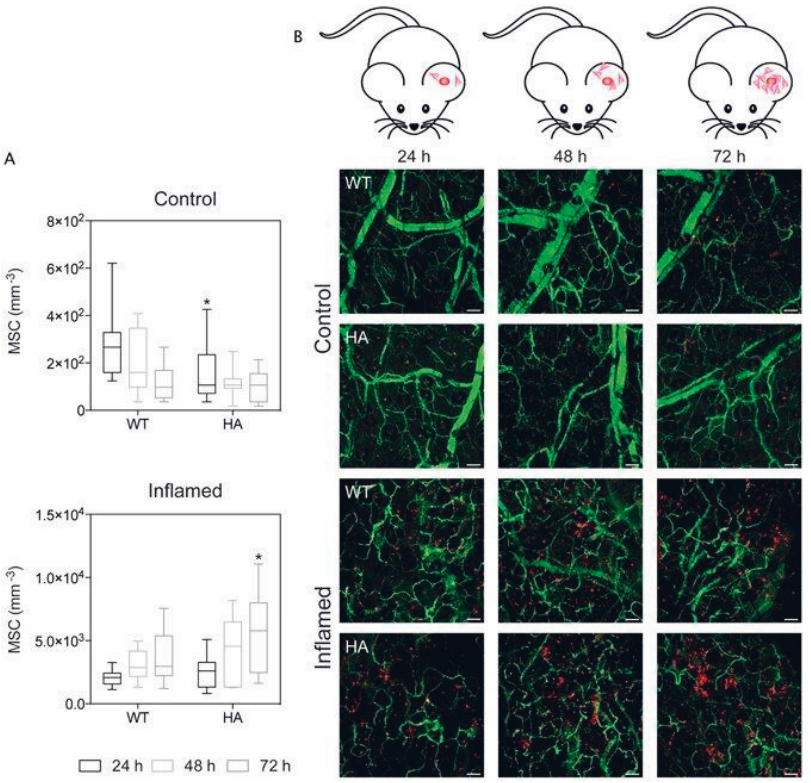

Figure 9. The in-vivo migration of the MSC was evaluated by establishing a local inflamed site in the ears. Migration of both wild type (WT) and HA-coated, towards the inflamed site, is seen in (A) representative graphs. (B) Representative microscopic staining images of the migration of MSCs. The vessels are seen in green and the MSCs in red. Image adapted with permission from Corradetti et al. 2017.[155]

For this dissertation, I have exploited the properties of biomaterials to modulate the immune system. I used HA-based nanoparticles loaded with immunosuppressive drugs and a chemotherapeutic agent to evade the systemic immune system and increase the inflammation in the tumor microenvironment. I have also used modified HA functionalized with gallic acid to develop an immunosuppressive hydrogel system that could potentially be used in wound healing applications. I have also modified MSCs with two different strategies based on biomaterials to make them more compatible and safer for transplantation.

3 AIMS OF THE STUDY

The aim of this thesis is to develop bio-engineering strategies to address the critical issues like instant blood mediated immune response and foreign body response that biomaterials and cells encounter upon implantation in-vivo.

More specifically the aim can be categorized into the following, divided into publications: -

i) Publication I- To design a biopolymer-based nanocarrier to deliver chemotherapeutic drugs while attenuating the risk of drug induced thrombosis

ii) Publications II & IV- To engineer MSCs and enhance the in-vivo survival and function while attenuating the risk of stem cell induced instant blood mediated immune response (IBMIR)

iii) Publication III- To engineer a 3D scaffold that could suppress inflammation and that could be used to deliver cells for cell-based therapies and tissue engineering applications.

4 MATERIALS AND METHODS

4.1 General Materials

For the work in **Publication I**, hyaluronic acid (HA, MW130 kDa) was purchased from LifeCore Biomedical (Chaska, USA). 1-Ethyl-3-(3-dimethylaminopropyl)-carbodiimide hydrochloride (EDC) (E7750), 1-hydroxybenzotriazole hydrate (HOBt) (54802), carbodihydrazide (CDH) (C11006) , and dexamethasone (D4902) (DEX) were purchased from Sigma-Aldrich. Doxorubicin (DOX.HCl) was purchased from Tocris Bioscience, UK. Dialysis membranes used for purification were purchased from Spectra Por-6 (MWCO 3500). All solvents were of analytical quality. The ^{1}H NMR experiments (δ scale) were carried out on JEOL ECZR 500 instruments, at a magnetic field strength of 11.7 T, operating at 500MHz. Spectra for all HA conjugates were recorded in D_2O at 293 K. All solvents used in this study were of analytical quality.

For the work in **Publication II**, the chemicals, reagents, and dry solvents for Pluronic F108 (542342) and RNA synthesis were purchased from Sigma–Aldrich (Sweden) and used without any further purification. Unmodified phosphoramidites (N6-benzoyl-rA, N2-isobutyl-rG, N4-acetyl-rC, rU and dT) and solid supports were purchased from ChemGene Corporation (USA). 1H NMR was recorded on 400 MHz instruments (Jeol JNM-ECP Series FT NMR). The chemical shifts in parts per million (δ) are reported downfield from TMS (0 ppm).

For the work in **Publication III**, heparin sulphate (H3393-500KU) was obtained from Sigma-Aldrich. Gelatin Type A was obtained from Sigma Aldrich. In **Publication IV**, HA, EDC, HOBt, CDH and the dialysis membranes were purchased from the same source as mentioned earlier. Gallic acid (3,4,5-trihydroxy benzoic acid) (G7384) was purchased from Sigma Aldrich. All spectrophotometric analysis was carried out on Shimadzu UV-3600 plus UV–VIS-NIR spectrophotometer.

4.2 Cell culture

In **Publication I**, the cell lines used were all obtained from ATCC-LGS standards. Osteosarcoma cell lines (MG63), breast adenocarcinoma (MCF7), and colorectal carcinoma (HCT116) were all obtained from ATCC-LGS standards. These cells were cultured in DMEM (Gibco, 31885023) containing 10% fetal bovine serum (FBS, 26140079) and 1% penicillin-streptomycin (Gibco, 15070063) at 37°C and 5% CO_2. Bone marrow-derived macrophages (BMDM) were isolated from C57BL/6 mice and were cultured following a standard protocol.[158] The isolated monocyte cells were differentiated into M1 phenotype were stimulated with 100 ng/mL lipopolysaccharide (LPS; Sigma Aldrich, L2630) and 20 ng/mL interferon-gamma (IFN-γ; Sigma Aldrich, I4777) for 24 hr after which they were used for experiments. For M2 macrophages, the monocytes were stimulated with 20 ng/mL TGF-β (R&D Systems), 20 ng/mL IL4 (R&D Systems) and 20 ng/mL IL10 (R&D Systems) for 24 hr after which they were used for experiments. The similar protocol was followed in **Publication III** were BMDMs were used for the experiments.

For **Publication II**, the bone marrow-derived mesenchymal stem cells (MSCs) were obtained from professor Susanna Miettinen's lab in Tampere University. The MSCs used for the **Publication III** were obtained from Professor Katerina Le Blanc's lab in Karolinska Institute, Sweden. These cells were cultured in α-MEM (Gibco) containing 10% FBS (Gibco) and 1% penicillin-streptomycin (Gibco) at 37°C and 5% CO_2. hMSCs were characterized by flow cytometry as described previously.[159,160] In **Publication II and IV**, the THP-1 (human monocytic cell line) were cultured in RPMI (Gibco, 21875034) with 10% FBS and 1% penicillin-streptomycin at 37°C and 5% CO_2. Phorbol 12-myristate 13 (PMA)(P8139) at 50 ng/mL was used to differentiate these cells into M0 phenotypic state. To differentiate these M0 cells to M1 state in **Publication II**, 500 ng/mL of LPS was used. CRL-2429 human fibroblast cells used in **Publication IV** were also cultured in DMEM (Gibco) containing 10% fetal bovine serum (FBS) and 1% penicillin-streptomycin (Gibco) at 37°C and 5% CO_2.

4.3 Synthesis of HA-DEX-DOX

The first step in the synthesis of HA-DEX-DOX was the preparation of HA-CDH. Carbodiimide coupling chemistry was used to conjugate CDH on HA to obtain hydrazide functionalized HA-CDH. Briefly, 1 mmol CDH and 1 mmol HOBt were

added to 400 mg of HA that was dissolved in 120 mL of deionized water. The pH of this reaction mixture was adjusted to 4.7 after which EDC.HCl (40 mg) was added to the mixture and stirred overnight. This mixture was then dialyzed against dilute HCl containing 100 mM NaCl followed by dialysis in HCl and then dialyzed against deionized water. Each the dialysis was done for 24 h. After dialysis, this solution was lyophilized to obtain HA-CDH. The degree of CDH modification on the HA was determined by trinitrobenzene sulfonic acid (P2297)(TNBS) assay following the previously reported protocol.[161] Following this, DEX was conjugated to the HA-CDH by hydrazone formation. Briefly, 23.5 mg of DEX was dissolved in 30 mL of dimethyl sulfoxide (DMSO)(D5879) and was added to HA-CDH that was dissolved in 50 mL of deionized water. This solution was then stirred till it dissolved after which the pH was adjusted to 4.5 by using acetic acid. After constant stirring at 50°C overnight, the mixture was then dialyzed against deionized water for 48 h. The solution after dialysis was then lyophilized to obtain HA-DEX. The DEX conjugation was quantified using UV-Vis spectroscopy, by estimating the free hydrazide moiety through TNBS assay. DOX was then loaded onto the HA-DEX. Briefly, 100 mg of HA-DEX was dissolved in 90 mL of DMSO:H_2O (2:1), and 10 mg of DOX dissolved in 10 mL of deionized water were mixed and stirred for 6 h. To this mixture, 60 mL of deionized water was added and stirred overnight. After constant stirring, the solution was dialyzed against water containing 100 mM NaCl for 72 h after which it was dialyzed again against deionized water for 24 h. This solution was then lyophilized to obtain HA-DEX-DOX. The drug loading was determined using UV-Vis measurement at 485 nm and fluorescence measurements using the FLS1000 Photoluminescence spectrometer (Edinburg Instruments).

4.4 Synthesis of Plu-SS-TF

For the preparation of Plu-SS-TF in **Publication II**, disulfide functionalized siRNA was synthesized on an automated solid-phase synthesizer using a thiol-modified solid support to the sense strand of the siRNA using the standard synthesis cycle for RNA. The strands were then deprotected and purified by polyacrylamide gel electrophoresis (PAGE). After purification, an equal amount of the strands was mixed to form a duplex. To activate the thiol group in the siRNA, 2.5 nmol (50 μL) of siRNA was mixed with dithiothreitol (Sigma Aldrich, D0632) (DTT, 50 mM, 10 μL) and water (40 μL) and incubated at 37°C for 2 h. After incubation, 3M NaCl (150 μL) was added, followed by 150 μL water. This mixture was then vortexed and

spun down. To remove the excess DTT from the mixture, 100% ethanol (1000 μL) was added, after which the mixture was vortexed and stored at -20°C for 18 h. The RNA was then centrifuged at 13,000 rpm for 20 minutes at 4°C for 10 min after which the supernatant was removed and the pellet was washed with absolute ethanol (100 μL). The centrifugation step was repeated and the pellet was directly dissolved in a disulfide-activated pluronic solution (368 μL in PBS, pH 8, 250 nmol). This mixture was then incubated overnight and at room temperature after which they were used for experiments.

For the transfection studies, cells were transfected with pyridyl disulfide Pluronic F108 conjugated TF 3 (Plu-SS-TF) siRNA with calcium chloride and RNAiMAX (Thermo Fisher Scientific, 13778150). Plu-SS-TF/Ca were prepared by adding 50 nM of Pluronic-linked TF siRNA to 25 μL of 100 mM $CaCl_2$. They were mixed by vertexing, followed by incubation at room temperature for 10 min. At the end of incubation, the Plu-SS-TF/Ca nanoparticles were added to cells in a single well of a 24-well plate. Cells were also transfected with Pluronic-linked TF siRNA by RNAiMAX (Plu-SS-TF/RNAiMAX). Unconjugated TF siRNA was transfected with both RNAiMAX (TF/RNAiMAX) and Plu-SS and calcium chloride (Plu-SS/TF/Ca) using similar amounts of siRNA and calcium chloride. RNA was then isolated and quantitative real-time polymerase chain reaction (qRT-PCR)

4.5 Coating of MSCs with heparin and gelatin

Heparin (H) 1% wt/vol was prepared by dissolving the desired amount of heparin in serum-free cell culture medium and 0.1% wt/vol gelatin type-A (G) solution were prepared separately by dissolving gelatin in the Dulbecco's phosphate-buffered saline (DPBS) (Gibco, 14190169). Approximately, 2×10^6 MSCs were resuspended in 1 mL of gelatin solution and incubated for 10 minutes under mild shaking. Cells were centrifuged at 500 g for 5 minutes and re-suspended in the heparin solution and incubated for 10 minutes under mild shaking. The two previous steps were repeated alternatively until the cells were coated with four layers of polymers. After the final coating steps, the cells were counted and cultured as per need for the experiments. As control, the same number of cells were put through similar conditions substituting the H solution with serum-free medium and G solution with PBS. A visual observation of the coating was done by transmission electron microscopy (TEM). Briefly, the H/G MSCs and MSCs without coating were cultured for 3 days after which they were fixed with 2.5% glutaraldehyde and 1%

paraformaldehyde in 0.1 M buffer. The samples were then post-fixed with 1% Osmium tetra oxide and dehydrated in ethanol. The samples were then embedded in resin (Epon) and polymerized by heating, Thereafter, ultra-thin sections were cut with an ultramicrotome and collected on grids. The samples are then contrasted with uranyl acetate and lead citrate and then air-dried. The samples are then taken for imaging in the TEM (FEI Technai G2) at 80 kV.

4.6 Preparation of HA-GA hydrogel

For the preparation of HA-GA hydrogel, GA was first functionalized with a hydrazide group. Briefly, 4 mg of GA was dissolved in 100 mL of methanol. Thereafter, 12 drops of sulfuric acid were added to the flask and the reaction mixture was refluxed overnight. Methanol was then completely removed under the reduced pressure in the rotary evaporator. The remaining product was extracted using ethyl acetate after which the organic layer was collected and dried over anhydrous sodium sulphate. After drying again in with a rotary evaporator, 60 mL of methanol and two drops of triethylamine was added to dissolve the GA methyl ester intermediate. Hydrazine monohydrate (80%, 2 mL) was then added to the reaction mixture and stirred for 48 h. The hydrazide functionalized GA was obtained as an off-white powder. The resulting product was filtered and washed 3 times in methanol and once with water. The final product was dried in vacuum and was characterized using nuclear magnetic resonance (NMR) and the chemical shifts were measured in δ (ppm) with reference to the DMSO-d6 solvent (δ = 2.50 ppm and 39.4 ppm for 1H and 13C NMR, respectively). ^{1}H (500 MHz, DMSO-d6), δ (ppm): 6.09 (s, 2H). ^{13}C NMR (126 MHz, DMSO-d6), δ (ppm): 166.3, 145.4, 136.3, 123.3 and 106.3.

The resultant product from the steps mentioned above was then utilized to prepare HA-GA-CDH. Briefly, 400 mg of HA was dissolved in 75 mL of deionized water. To this solution, 1 mmol of HOBt (153 mg) was added and 1 mmol of GA-hydrazide (184 mg in 25 mL DMSO) was added to the HA solution dropwise and stirred. The pH of this solution was then adjusted to 4.75 with the help of 1 M HCl and 1 M NaOH. After this, 0.2 mmol of EDC (39.5 mg) was added to the mixture and it was kept overnight under constant stirring. This mixture was then dialyzed against dilute HCl containing 100 mM NaCl for 48 h and then dialyzed again against deionized water for 24 h. This solution was then lyophilized to obtain HA-GA-CDH. The degree of modification was ascertained by UV-vis spectroscopy dissolving HA-GA (1 mg/mL in PBS) and measuring the absorbance at 240-340 nm.

The conjugation of CDH to HA-GA was carried out using a similar method as mentioned in section 4.3. HA-CDH was prepared and characterized in the same protocol as mention in section 4.3. HA-Aldehyde (HA-ALD) was synthesized following our already published protocol.[162]

To make the HA-GA and the HA-HA hydrogels, crosslinking between the aldehyde and the carbodihydrazide moieties of the HA derivatives were used. Both the components, HA-GA-CDH and HA-ALD were dissolved at a concentration of 16 mg/mL for all the experiments and equal volumes of these solutions were mixed together to form hydrogels. HA-CDH and HA-GA-CDH were dissolved in a 10% sucrose solution and the HA-ALD was dissolved in PBS. The materials were sterilized in UV for 20 min prior to the use in cell experiments.

4.7 Dynamic light scattering and zeta potential

In **Publication I and II**, the hydrodynamic size and the surface charges of the nanoparticles were measured by dynamic light scattering. In **publication I**, the size distribution of HA-derived nanoparticles, namely, HA-DEX and HA-DEX-DOX were performed using a laser granulometer (Zetasizer Nano ZS, Malvern, UK) using a disposable polystyrene cuvette. Briefly, the lyophilized samples were dissolved in deionized water at a 1 mg/mL concentration. The DLS measurements were performed and then subsequently the surface zeta potential was measured using disposable folded capillary DTS1070 cells.

In **publication II**, for the pluronics-derived nanoparticles (Plu-SS-TF/Ca), 100 nM equivalents of siRNA in Plu-SS-TF were added to 100mM $CaCl_2$. This was then mixed well and incubated for 10 minutes at room temperature. This mixture was then added to 700 μL of deionized water and the hydrodynamic size was measured. For the Plu-SS-TF, 100 nM of siRNA equivalents was added directly to 750 μL and the measurements were taken. The surface zeta potential was measured using disposable folded capillary DTS1070 cells.

In **publication III**, the surface zeta potentials of the cells were recorded after performing the polyelectrolyte coating steps. Briefly, a few microliters of cells were taken after each coating step and resuspended in deionized water and the surface zeta potentials were measured using the disposable folded capillary DTS1070 cells.

4.8 Measurement of rheological, degradation, and adhesive characteristics

In **Publication IV**, the HA-GA and the HA-HA hydrogels were subjected to a rheological test to assess the stiffness and deformation characteristics of the hydrogels. For this purpose, hydrogels of 250 μL volume were prepared in the form of cylinders. They were cured overnight and their rheological property was then measured using a TA instrument TRIOS Discovery HR2 rheometer. The storage and loss modulus values obtained using frequency sweep were plotted against the frequency (Hz) as this demonstrates the viscoelastic shear behavior of the material as a function of the frequency. High frequency and rapid motion were used to determine the short-term properties of the gels and the long-term properties were stimulated by the slow-motion using low frequency. This provides the time-dependent storage elastic modulus (G'), viscous loss modulus (G"), and complex viscosity (η^*). To evaluate the strain recovery, the fully recovered hydrogels were placed between 12 mm diameter stainless steel parallel plate geometry, and the G' and G" were measured by alternating low and high oscillation strain conditions at 25°C and 1 Hz oscillation frequency for 7 cycles with 60s of holding period in each step.

The swelling and the degradation properties of the HA-HA and HA-GA hydrogels were also studied in the presence of hyaluronidase, the ubiquitous enzyme responsible for HA degradation. Hyaluronidase at a concentration of 50 U/mL in PBS at pH 7.4 was used for this purpose. Three samples of each 250 μL HA-HA and HA-GA hydrogels were prepared in glass vials and were allowed to crosslink for 24 h at room temperature. After curing, the gels were weighed and submerged in PBS containing hyaluronidase. At different time points, the buffer solution was carefully removed and the weights of the gels were recorded. After each measurement, fresh buffer solution was replenished and the steps were repeated for every measurement timepoint.

The adhesive properties of HA-HA and HA-GA were measured by tack adhesion test performed using a rheometer. For this purpose, porcine muscle tissue was glued to the geometry (12 mm) to the movable top head of the rheometer and then the fully cured 250 μL HA-HA and HA-GA were placed on the bottom plate. The top plate with the porcine muscle was placed in contact with the gel with a holding period of 120 sec during which a constant force of 100 mN was applied to establish uniform contact between gels and the tissue. The top plate was then pulled apart at a constant velocity of 10 μm/sec to record the axial force (N) with respect to time. The axial

force was then plotted vs step time to observe the difference between the two hydrogels.

4.9 Hematological studies and ELISA using Chandler's loop model

In **publications I, II, and III**, the hematological studies were performed using fresh human whole blood to study the interaction between the biomaterials and the blood following Chandler's loop protocol. For this purpose, fresh human blood was drawn from healthy volunteers who had not received any medication in the last 10 days prior to donation. No anticoagulants were used in this study as it would skew the complement and coagulation cascade readouts. Loops of polyurethane tubing with 2-methacryloyloxyethyl phosphorylcholine (MPC) polymer (poly(MPC-co-n-butyl methacrylate) with a 0.3 MPC unit mole fraction were used for the whole blood experiments. Stainless steel connectors were coated with Corline heparin surface according to the manufacturer's protocol. Loops were comprised of tubing that was closed with the surface-heparinized connectors (length:30 cm, blood volume: 2.5 mL) and were loaded with the samples. The blood along with the samples were then rotated on a wheel at 50 rpm in a 37°C cabinet for 1 h. After that, the blood was collected and mixed with EDTA (Sigma Aldrich, E5134) (10 mM) and then centrifuged at 3400 rpm for 20 min at 4°C to collect the plasma. The collected plasma was then stored at -80°C before ELISA analyses as described below. The experiments were repeated three times using blood from different donors. Ethical approval was obtained from the regional ethical committee. For **Publication I**, DOX, HA-DEX, and HA-DEX-DOX (dissolved in PBS) were incubated with the blood. For **Publication II**, the untreated MSCs (1.5x 10^4 cells in each group), as well as the TF silenced MSCs (using Plu-SS-TF/Ca) were separately incubated with human whole blood. In **Publication III**, the untreated MSCs (1. 5x 10^4 cells in each group) and polyelectrolyte-coated MSCs (by layer-by-layer coating with H/G) were incubated with the human whole blood. As a negative control, the same volume of cell culture medium was used.

For the measurement of the TAT complex, complements C3a and C5b9 an ELISA analysis was performed on the blood samples after the treatment with samples. Briefly, PBS containing 1% bovine serum albumin and 0.05% Tween 20 was used as the dilution buffer. PBS containing 0.05% Tween 20 was used as the washing buffer and TMB+ substrate chromogen was used as the color substrate. Plasma levels of the TAT and complement 3a and sC5b9 were analyzed using

specific kits available from Enzyme research laboratories (South Bend, IN, USA). TAT was captured in wells coated with anti-human thrombin antibody diluted 1/20. Horseradish peroxidase (HRP)-conjugated anti-human antithrombin (AT) antibody diluted 1/20 was used for detection. Pooled human serum diluted in normal citrate-phosphate-dextrose plasma was used as a standard. C3a levels were determined and captured using mAb 4SD17.3, biotinylated polyclonal anti-C3a, and HRP-conjugated streptavidin (GE Healthcare) for detection. sC5b-9 was determined using the anti-neoC9 mAb aE11 (Diatec Monoclonal AS, Oslo, Norway) for capture, and polyclonal anti-C5 antibody (Acris, Herford, Germany) and HRP-conjugated anti-rabbit IgG (Dako) for detection. The assay was calibrated against a commercially available kit (MicroVue, Quidel Corp, Santa Clara, CA, USA).

4.10 Cell viability and toxicity studies

In **Publication I**, the cytotoxicity of DOX, HA-DEX, and HA-DEX-DOX were estimated by the MTT assay (Thermofisher, M6494). The DOX and the nanoparticles were tested on three different cell lines, namely, osteosarcoma cells (MG63), human colon cancer cells (HCT116), and human breast cancer cells (MCF7). Briefly, these cells (5000 in number) were seeded onto 96 well plates and cultured for 18-24 h. Thereafter, the cells were exposed to free DOX at concentrations of 100 nM, 500 nM, 1000 nM, 2000 nM, and 4000 nM. For the HA-DEX-DOX, concentrations equivalent to the DOX amount was used. Therefore, HA-DEX-DOX at the concentrations of 1.5 μg/mL (100 nM DOX), 7.55 μg/mL (500 nM DOX), 14.7 μg/mL (1000 nM DOX), 29.86 μg/mL (2000 nM DOX) and 61.5 μg/mL (4000 nM DOX) were incubated with the cells. In the case of HA-DEX, the concentrations of HA-DEX was chosen with reference to the amount of HA-DEX-DOX (with respect to the weight). The cells were then incubated at 37°C and 5% CO_2 for 48 h. After 48 h, MTT (5mg/mL) was added to the cells and incubated for 4 h. After 4 h, 150 μL of DMSO was added to each of the wells. The plates were shaken well and the absorbance was measured using a microplate reader. The results were expressed as percentage viability. The IC50 values for these nanoparticles were estimated by performing the logarithmic curve fitting of cell viability (%) using GraphPad Prism software against DOX equivalents. Similar protocols were also followed where free 200 nM DOX, 200 nM DEX, and a combination of both were used. The results were also expressed in percentage viability.

In **Publication II**, MSCs (5000 in number) were seeded in 96 well plates in conditions mentioned in section 4.2. The cells were then treated with Plu-SS-TF/Ca complexes or Plu-SS-TF without the calcium. The concentrations of the nanoparticles used were dependent on the siRNA concentration (50 nM). Equivalent amounts of Plu-SS were also taken from the stock of 3.2 mg/mL and added to the cells. MTT assay was then performed as mentioned above.

In **Publication III**, polyelectrolyte-coated hMSCs (H/G) and uncoated cells (C) (as control group) were seeded at 5×10^3cell/mL density in 96 well plates and were incubated at 37°C and 5% CO_2. Cellular proliferation was measured at each time point by reading the fluorescent intensity at 590 nm using a plate reader (Infinite 200 pro Tecan). For the AlamarBlue® assay, an equal amount of 10% of the volume of the medium and cells of AlamarBlue® dye (Fisher Scientific 10099022) was added to the cells after aspirating the medium and washing cells with pre-warmed DPBS for one time. The cells were incubated for 2 hours at 37℃ and 5% CO_2. Then, samples were read at 590 nm using plate reader model Infinite 200 pro Tecan.

In **Publication IV**, For the CRL2429, BMDMs were encapsulated in 200 μL hydrogels at a concentration of $2x10^6$ cells/mL in a 48-well plate. The cells were cultured in the conditioned media as mentioned in section 4.2 for their respective time periods. The LIVE/DEAD staining was performed using the Viability/Cytotoxicity kit (Thermofisher, L3224) and a fluorescence microscope (Nikon TS2). The assay was carried out by aspirating the medium from the cells and then washing the hydrogels with PBS. After washing, 300 μL of live/dead staining solution containing 2 μM Calcein Am and 1 μM Ethidium homodimer in 1X PBS was added to the cells and incubated for 1.5 h at 37°C. Post incubation the hydrogels were washed and visualized under the microscope. For the CyQuant assay, the gels were frozen at the respective time points along with the cells at -80°C, and the DNA amount was determined by the use of the CyQuant Cell proliferation assay following the manufacturer's protocol.

4.11 Nuclear localization of HA-DEX-DOX

To visualize the nuclear localization of the HA-DEX-DOX in publication I, HCT116 and MCF7 cells were used. In short, 7000 cells were seeded in 96-well plate and cultured in conditions mentioned in section 4.2. After 24 h, the cell culture medium was replaced with medium containing HA-DEX-DOX with the loaded DOX concentration being 1 μM and the cells were incubated for 4 h. The medium

was then removed and the cells were washed 3x in PBS after which they were fixed with 4% paraformaldehyde (Sigma Aldrich, 100496) for ten minutes. The nuclei were stained using DAPI (Sigma Aldrich, D9542) and the cell were analyzed by fluorescence microscopy (Nikon Eclipse TS2).

4.12 Immunomodulation studies using BMDMs and THP-1

In **Publication I, and IV**, BMDMs were isolated and cultured as mentioned in section 4.2. In **Publication I**, briefly, TGF-β, IL4, and IL10 activated M2-like-BMDMs (50,000 in number) were plated in 24 well plates and incubated overnight. After incubation, the cells were treated with 200 nM DOX or DOX equivalent in HA-DEX-DOX for 48 h. The equivalent weight ratio of HA and HA-DEX as control groups were adopted for comparison. RNA was extracted using Qiagen RNeasy Mini Kit and cDNA was synthesized following the iScript cDNA synthesis kit (Bio-Rad). iQ SYBR green supermix was used to prepare samples for the PCR, which was then performed on the CFX96 instrument. The expression levels of genes (TNFα, IL1β, iNOS, and IL6) were analyzed with and without exposure to the nanoparticles. Hypoxanthine guanine phosphoribosyl transferase (HPRT) was used as housekeeping gene for internal normalization. In **Publication IV**, BMDMs were cultured without activation in the HA-HA and the HA-GA hydrogels at a concentration of $2x10^6$ cells/mL and incubated for two weeks. After incubation, the gene expression analysis of the different pro-inflammatory and anti-inflammatory genes were performed as mentioned earlier by extraction of RNA followed by qRT-PCR. The qRT-PCR data were normalized and calculated using the ΔΔCT method.

In **Publication II**, **III**, **and IV**, THP-1 cells were cultured as mentioned in section 4.2. Briefly, THP-1 cells were differentiated with 50 ng/mL phorbol myristic acid (PMA; Sigma) for 24 h at 37°C and 5% CO_2. The cells were then treated with 500 ng/mL lipopolysaccharide for 24 h at 37°C and 5% CO_2 to make them M1 macrophage-like. In **Publication II and III**, the cells were then detached using 2mM EDTA (Sigma) and plated in 24-well plates (60,000 cells in number). In **publication II**, these cells were incubated with a conditioned medium from the MSCs that were treated with and without Plu-SS-TF/Ca. The THP-1 cells were incubated in the conditioned medium for a period of 3 days after which the RNA was extracted and the expression level of pro-inflammatory genes was analyzed through qRT-PCR. Briefly, RNA was extracted using RNeasy Plus Mini kit from Qiagen. The cDNA was prepared using Maxima First Strand cDNA kit according

to manufacturer's protocol (Thermo Fisher Scientific, Vantaa, Finland) and qRT-PCR was performed with cDNA and TaqMan® Fast Advanced Master Mix (2X) (Applied Biosystems). Reference gene, β-actin (ACTB) (Taqman primers, Thermo Fisher, Finland) were selected as a control for normalization of real-time PCR data. The amplification was carried out using the Bio-Rad CFX1000 (Bio-Rad) using a 40-cycle program. The CFX manager software automatically calculates the raw Ct (cycle threshold) values. Data from samples with a Ct value equal to or below 33 were further analyzed. Samples were normalized relative to endogenous control and differences in cycle number thresholds were calculated using the comparative quantitation $2-\Delta\Delta CT$ method (also called the $\Delta\Delta CT$ method), which is commonly used for analyzing siRNA induced gene knockdown efficiency. In **Publication III**, the conditioned medium from the coated MSCs and uncoated MSCs were exposed to the M1 polarized THP-1 cells. The cells were incubated in these conditions for a period of 3 days after which this medium was collected and analyzed my multiplex bead-based assay as mentioned below. In **publication IV**, $4x10^6$ THP-1 cells were encapsulated in 200 μL HA-HA and HA-GA hydrogels. These cells were cultured in the hydrogels for a period of 10 days, after which RNA was extracted using the RNeasy Mini kit from Qiagen. cDNA was then prepared using the cDNA First-strand synthesis kit from Thermofisher. The qPCR reactions were prepared and the gene expression analysis was performed as mentioned earlier.

4.13 Differentiation studies with MSCs

The differentiation studies with the MSCs were performed with commercially available kits from Gibco. For the osteogenic differentiation, the StemPro Osteogenic differentiation kit (Thermofisher, A1007201) was used and for the adipogenic differentiation (Thermofisher, A1007001), the StemPro Adipogenic differentiation kit was used. Briefly, the cells were cultured in these media for a period of 14 days after which they were taken for differentiation analysis. For the osteogenic differentiation, calcium deposits formed were stained using 2% alizarin red solution after the cells were fixed with 4% paraformaldehyde and washed with PBS. The cells were then visualized using microscopy. Adipogenic differentiation was observed by staining the fixed cells with 300 nM of Nile red solution in **Publication II**, whereas Oil red O staining was performed in **publication III**. In both conditions, the cells were then visualized through microscopy. To further confirm the differentiation, qRT-PCR analysis was done on the cells. Osteogenic

genes like ALPL, DLX5, and BGLAP were analyzed and adipogenic markers like PPARG and LPL were analyzed by qRT-PCR.

4.14 Multiplex bead-based assay

Protein level analyses were done with the detection of cytokines from the medium. In **Publications III and IV**, bead-based cytokine detection immunoassay from LEGENDplex (BioLegend, NordicBiosite, 740509) were used to identify the secreted cytokines following in-vitro cell culture. The cell culture supernatants were collected at the respective timepoints and stored at -80°C before use. The mouse macrophage/microglia cytokine panel was used in **publication IV** and the human macrophage/microglia cytokine panel was used in **publication III**. The assays were performed following the manufacturer's protocol. The analysis was done using the LEGENDplex data analysis software (BioLegend) and the cytokines were quantified by comparing samples to a set of standards.

4.15 Implantation of HA-HA and HA-GA hydrogels in C57BL/6 mice

In **publication IV**, the HA-HA and the HA-GA hydrogels were injected subcutaneously in 8-9 weeks old C57BL/6 female mice. 200 µL of HA-HA and HA-GA hydrogels were injected into each side of the lower back area in the same mice. The gels were then collected 5 days post-injection and the cells were infiltrating the gels were harvested by digesting the gels in 500 µL PBS containing 0.4 mg/mL hyaluronidase (Sigma) and trypsin (1 g/mL; Gibco) for 50 min at 37°C. The cell suspension was then filtered using a strainer and was then centrifuged at 350g for 5 min at 4°C. The cocktail of anti-body solutions contained D45-PeCy7 1:100, CD11b-PercpCy5.5 1:100, CD36-Pe 1:100, CD86-APC 1:100, MHCII-A700 1:100, CD40-FITC 1:100, live dead marker – Near-infrared 1:500). The pellet was then resuspended in a cocktail of antibody solution for 30 min at 4°C. After a wash with PBS, the cells were centrifuged and pelleted, and transferred to FACS tubes. The cells were then analyzed using BD LSR Fortessa. Flowjo V 10.8.0 was used to analyze the data. Ethical permission was obtained from the regional ethical committee.

5 RESULTS AND DISCUSSION

5.1 Engineering biomaterials and cells that can evade the systemic immune system

The importance of evading the systemic immune system by the biomaterials has already been mentioned. We have also seen that there are several biomaterials that can cause adverse immune reactions which eventually lead to the failure of the implants and devices. In this thesis, I have developed a nanoparticle system that suppressed systemic inflammation mediated by the drug molecule while targeting the CD44 receptors overexpressed on cancer cells and delivering a chemotherapeutic drug. I also devised two different strategies for MSCs to evade the systemic immune system. Lastly, I have developed an immunosuppressive hydrogel that has partially exhibited its potential to evade the systemic immune response.

In **Publication I,** an HA-based immunomodulatory nanoparticle was developed through a supramolecular self-assembly approach as an anti-cancer therapy. During chemotherapy, there is a high risk of the chemotherapeutic drug activating the platelets. These activated platelets amplify the pro-inflammatory response and can secrete over 300 different proteins and small molecules like cytokines, chemokines, growth factors, and coagulation factors that can trigger blood-mediated inflammatory responses and induce hypersensitivity reactions in several patients.[163] The chemotherapeutic drugs are also known to damage the lymphohematopoietic cells that can result in leukocytopenia and thrombocytopenia. To combat this, the chemotherapeutic patients are often infused with platelets from healthy donors and factors like granulocyte stimulating factor to aid in the recovery of these cells. These methods are expensive with a low success rate. It has been known that for patients undergoing chemotherapy, immunosuppressive drugs like dexamethasone (DEX), prednisone or prednisolone have been given as co-medications to suppress the side effects caused by the chemotherapy drugs like doxorubicin (DOX).[164] Drugs like DEX have been known to possess immunosuppressive properties and can help in alleviating side effects like nausea, and weight loss that the chemotherapy patients experience. We designed a nanoparticle with HA due to its relative non-toxic and non-sensitizing characteristics and that there are already many commercially HA

based products available in the market.[165] This HA-based nanoparticle (HA-DEX-DOX) was designed to deliver the immunosuppressive drug dexamethasone (DEX) along with the chemotherapeutic drug doxorubicin (DOX) to the tumor site using the targeting ability of HA.

To design the HA-DEX-DOX, HA was first functionalized with carbohydrazide (CDH) to make HA-CDH following our previously reported protocol.[166] The percentage of CDH functionalization on the HA was quantified by TNBS assay, which was estimated to be ~12% with respect to the disaccharide repeat units. The hydrazide functionalization was exploited to graft DEX to form a pH-responsive drug delivery system that disassembles in the endosomal compartment after cellular uptake. The amount of DEX conjugated to HA that forms HA-DEX micelles was estimated to be ~5.2% with respect to the disaccharide repeats units. The percentage modification of DEX in HA-DEX was quantified by estimating the number of free hydrazide units after the conjugation of DEX to HA-CDH. As mentioned earlier, we expected the conjugation of DEX to promote the supramolecular self-assembly of these polymers in water, resulting in the formation of nanomicelles. The hydrodynamic size of the HA-DEX nanoparticle was analyzed by dynamic light scattering and was observed to be 511± 47 nm (Z-average). (Figure 10) When the chemotherapeutic drug DOX was loaded onto the HA-DEX, a ~50% reduction in the hydrodynamic size (252± 20 nm) of the particle (HA-DEX-DOX) was observed. This reduction in the size of HA-DEX-DOX after the loading of DOX could be due to the hydrophobic interactions between the DEX and the hydrophobic segments of DOX. The amount of DOX loaded onto the HA-DEX-DOX was estimated by UV-vis spectroscopy and was found to be around 4.6% by weight. The encapsulation of DOX was further confirmed by observing the characteristic absorbance of DOX at 485 nm and fluorescence at 580 nm. The drug release kinetics for the release of DOX from the HA-DEX-DOX was also performed using stimulated body fluids (SBF) at pH 7.4. A slow and sustained release of DOX from HA-DEX-DOX (only 10.6% of the 4.6% by weight that was loaded) was observed after 96 hr with near zero-order kinetics as compared to free DOX.

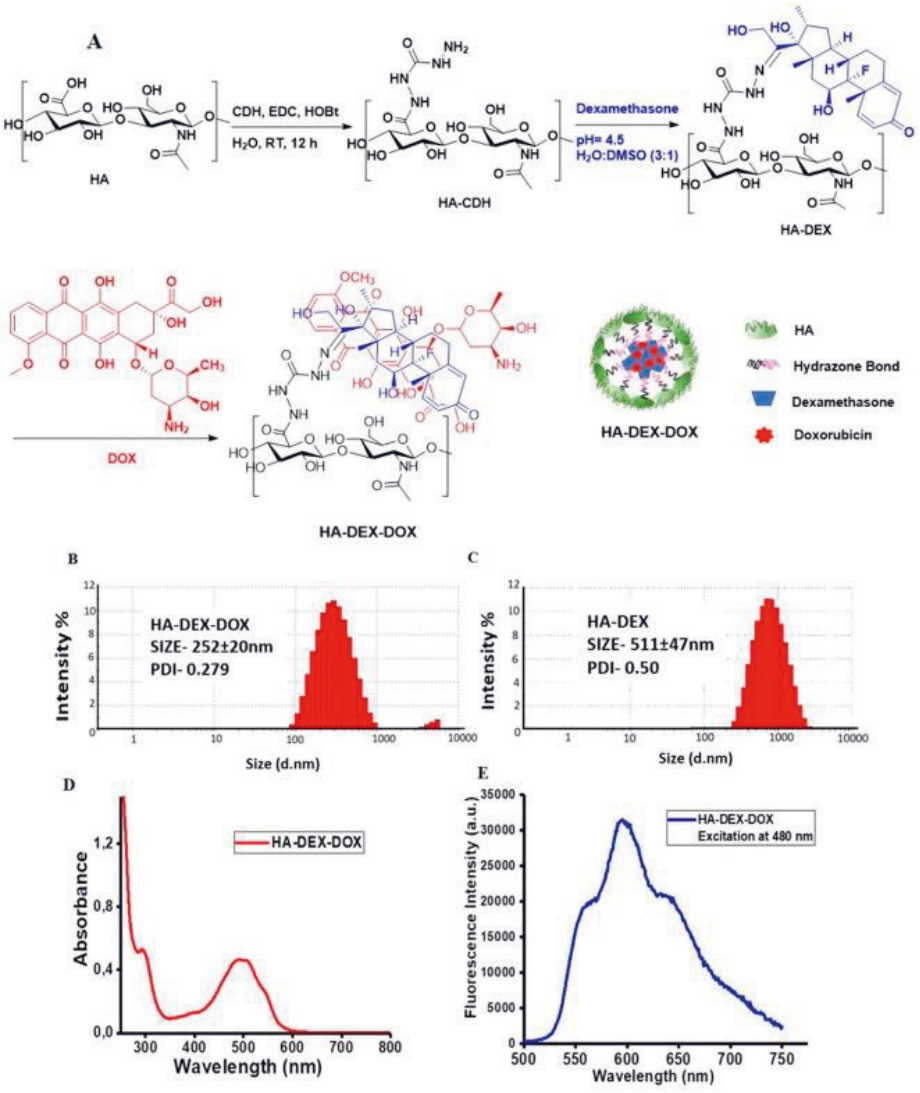

Figure 10. : (A) Schematic representation of the strategy to synthesize HA-DEX-DOX as described in the materials and methods section. Hydrodynamic size (Z-average) of (B) HA-DEX-DOX and (C) HA-DEX obtained by dynamic light scattering. (D) UV-vis spectrum of HA-DEX-DOX and (E) Fluorescence spectra of HA-DEX-DOX showing the characteristic peaks in water.

In **Publication II**, a nanoparticle was developed that could efficiently silence the F3 gene that encodes tissue factor (TF) or CD142 or factor III, that was reported to be a key driving factor causing the procoagulant activities of MSCs.[167] Even though the MSCs are believed to be immunoprevileged, there are several recent reports suggesting that MSCs can be prone to immune rejection by activating the

complement pathways with markers like CD46, CD55 and CD59 expressed on their surface. [168,169] Infusion of MSCs in patients has also been known to cause thromboembolism mediated by the activation of the coagulation cascade and has also led to fatalities in some cases.[170,171] Silencing TF has been reported to improve the hemocompatibility of the MSCs and reduce the implications of blood-mediated inflammatory reaction (IBMIR).[172] In **publication II**, to make the MSCs more hemocompatible and safe for transplantation, we developed a nanoparticle system that safely delivers a siRNA targeting TF to MSCs.

Considering the success of the nucleic acid-based mRNA vaccines, we made use of RNAi or RNA interference, a well-known Nobel prize winning nucleic acid-based mechanism. In the last decade, RNAi has been one of the most promising and rapidly advancing areas in biology. Due to the siRNAs ability to target many mRNAs, RNAi has been proposed as a therapy in various diseases like cardiac diseases, neurodegenerative diseases, and a wide range of cancers.[173] One of the major issues with RNAi has been the delivery of the siRNAs. The naked delivery of siRNA has been known to be problematic due to the siRNAs being vulnerable to rapid hydrolytic cleavage and degradation.[174] Even though there have been attempts to make siRNAs resistant to degradation through GalNac modifications[175] there seems to be a need for the rapid development of carrier molecules. Lipofectamine a commercially available carrier agents for siRNA has been successful in in-vitro conditions but has had limited clinical utility due to its cytotoxicity and limited capacity of efficiently deliver siRNA in-vivo.[174]

To address the above-mentioned issues and to develop a carrier molecule for siRNA, we made use of pluronic F108, a block copolymer possessing a poly(ethylene glycol)-block or PEG as a hydrophilic arm, and poly(propylene glycol) forming the hydrophobic core that self-assembles to form nanoparticles. Pluronic F108 also known as Poloxamer 338 has already been declared to be safe to be used in cosmetic ingredients and also has been proposed to be used as an anti-fouling agent in the management of catheter associated urinary tract infections.[176,177]

Considering the ease with which the pluronics form micelles and its considerably non-toxic safety profile, pluronic-based nanoparticles complexed with calcium phosphate are known to deliver siRNA to mammalian cells.[178] Such nanocomplexes are not known to be very efficient as the physical association does not provide good control over siRNA loading efficiency, resulting in inhomogeneous particle distribution. The release of the cargo molecules could also be affected by the temperature (as Pluronic is a thermoresponsive polymer) as well as by the presence of different biomolecules in the milieu. We, therefore, adopted a covalent grafting

strategy where siRNA was covalently conjugated on the hydrophilic arm of the block polymer that facilitated efficient micelle formation, and promoted intracellular transport of the cargo molecule. We achieved this by incorporating redox-responsive disulfide groups that provide the dual advantage of fast delivery to the cytosol and glutathione-mediated selective dissociation inside the cells. To manufacture these nanocarriers, we first conjugated disulfide pyridyl groups to the terminal hydroxyls present on PEG units by activating the hydroxyls with 4-nitrophenyl chloroformate, followed by a nucleophilic displacement reaction with 2-(pyridin-2-yldisulfaneyl)ethan-1-amine, also termed as the amino disulfide pyridyl molecule. We succeeded in obtaining an unprecedented degree of PEG functionalization of over 95% with respect to the available hydroxyls, as verified by UV–vis measurements. Next, the disulfide pyridyl-functionalized Pluronic F108 was conjugated with thiol-modified siRNA targeting the TF gene where the thiol groups were incorporated at the 3' end of the sense strand (Figure 11). We succeeded in obtaining good conjugation of the siRNA to the nanocarrier, as evidenced by gel electrophoresis (20% PAGE). The covalent conjugation resulted in retardation of mobility, indicating higher-molecular-weight species in lane 2 and lane 3, which represents the Pluronic F108-siRNA conjugate (Plu-SS-TF) and the Pluronic F108-siRNA conjugate complexed with 5 mmol Ca2+ (Plu-SS-TF/Ca). The siRNA conjugated polymer self-assembled to form micelles that showed a hydrodynamic size of ∼274 nm with unimodal distribution (Figure 12A), which upon complexation with Ca2+ displayed a hydrodynamic size of ∼370 nm (Figure 12B), as determined by the DLS experiment. We also confirmed the presence of elemental carbon, phosphate, and calcium in the particles by EDS analysis (Figure 12E). The zeta potential of Plu-SS-TF was estimated to be −12.1 mV, which changed to −0.515 mV upon complexation with Ca2+ (Plu-SS-TF/Ca). This indicates that the addition of Ca2+ ions neutralized the net negative charge of phosphates, maintaining an overall near-neutral charge. Interestingly, Plu-SS-TF/Ca also displayed thermoresponsive properties as the hydrodynamic size of the micelles reduced from 370 to 254 nm when the DLS experiment was performed at 37 °C instead of 25 °C.

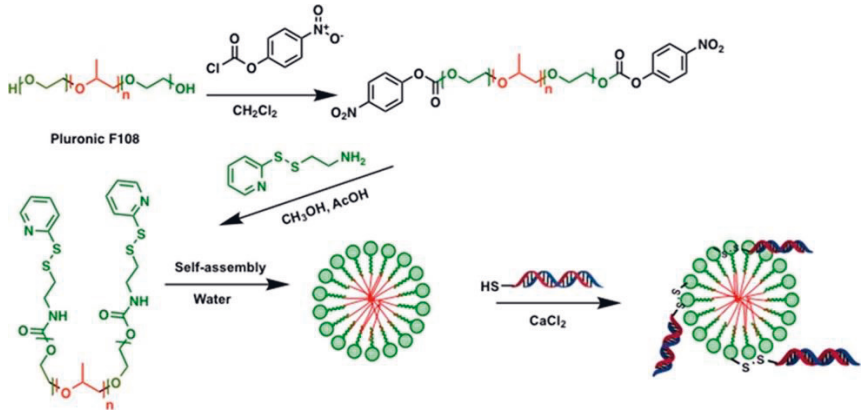

Figure 11. Schematic representation of the steps involved in the synthesis of Plu-SS-TF/Ca. Pluronic F108 is reacted with para-nitrochlroformate to get an intermediate product, which is then reacted with amino S-S pyridyl to give pluronic S-S pyridyl which can self-assemble in water.

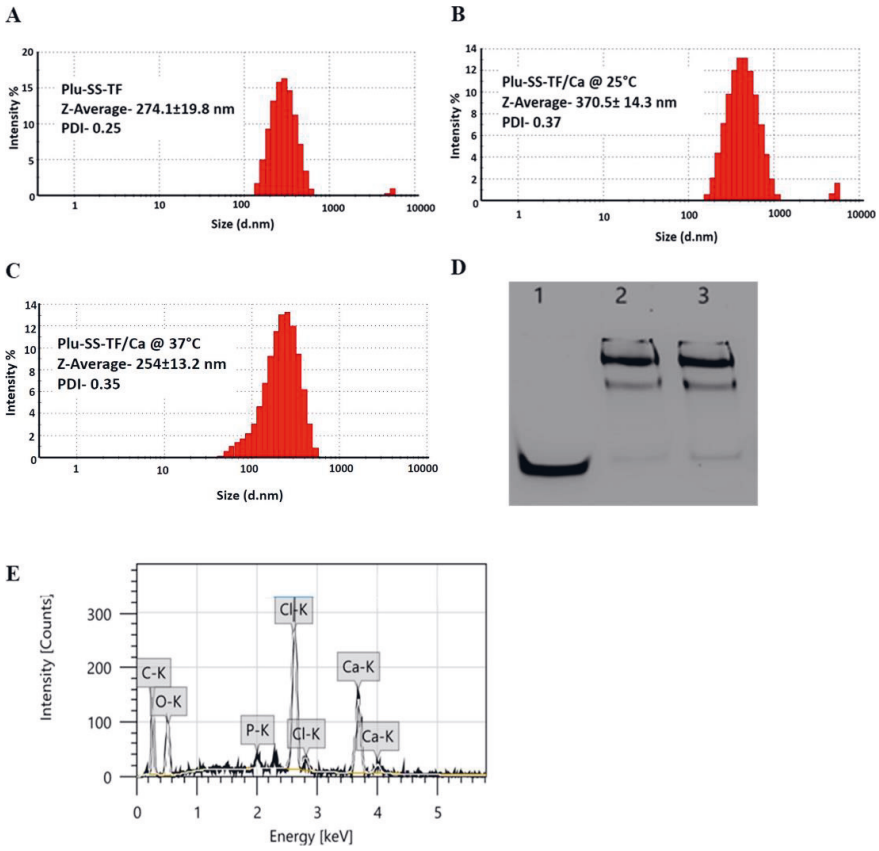

Figure 12. (A) Hydrodynamic size of Plu-SS-TF without calcium complexation and (B, C) with calcium complexation at 25 and 37 °C, respectively. (D) Gel electrophoresis indicates nanoparticle formation. Lane 1 = free siRNA; lane 2 = Plu-SS-TF with calcium complexation; lane 3 = Plu-SS-TF without calcium complexation. (E) EDS elemental mapping indicating the presence of carbon, phosphate, and calcium in Plu-SS-TF/Ca.

After the successful preparation and characterization of the Plu-SS-TF nanoparticles, the ability of these nanoparticles to silence TF in the MSCs were tested in vitro. When the Plu-SS-TF were used on MSCs of higher passages (4-6) we observed that the Plu-SS-TF/Ca formulation showed a 72% knockdown of the TF with 50 nM of siRNA. (Figure 13A) As controls, Plu-SS-TF was also transfected using commercially available lipofectamine RNAiMAX (Plu-SS-TF/RNAiMAX) that resulted in 84% knockdown of TF on the MSCs. To prove that the physical conjugation of the TF siRNA is required for the efficient knockdown of the gene in the cells, we coated the siRNA/Ca+2 complexes with pluronic functionalized with disulfide groups (Plu-SS/TF/Ca). The Plu-SS/TF/Ca showed a modest silencing effect of the TF, silencing around 20% of the gene in the MSCs. MSCs in general are known to be hard to transfect cells[179] and we believe the enhanced transfection efficiency of the Plu-SS-TF/Ca is due to the dithiol groups which are reported to improve the rapid internalization of the conjugates.[180] It has also been reported that the higher transfection efficiency has always come at the cost of higher toxicity due to the cationic nature of most of the transfecting agents. The Plu-SS-TF/Ca with a net neutral charge was observed to show minimal toxicity when cell viability studies were performed. The Plu-SS-TF/Ca showed ~90% cell viability when treated on MSCs and the individual components of the nanoparticle Plu-SS and Plu-SS-TF did not show any significant toxicity. (Figure 13B)

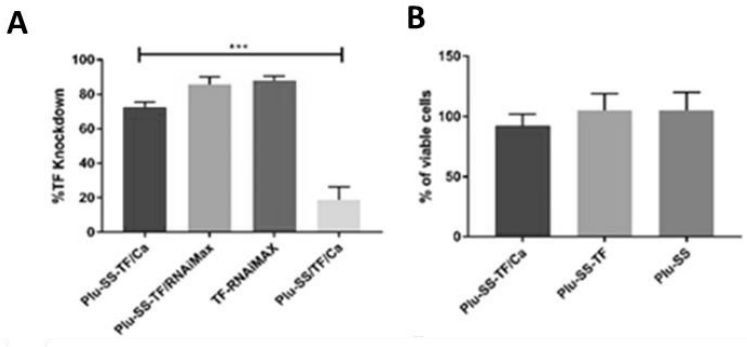

Figure 13. (A) In vitro KD efficiency of different formulations of the nanoparticles with calcium complexation and RNAiMAX. Statistics were done by ANOVA on GraphPad Prism (***P < 0.001). (B) Cell viability percentages were obtained for the nanoparticles and their components through the MTT assay.

In **Publication III**, we have used a different strategy to make the MSCs compatible for transplantation. In **Publication II**, we used a nanoparticle to knockdown TF to make the MSCs evade the systemic immune system. Here in **Publication III**, we coated the MSCs with polyelectrolyte layers to protect the MSCs from activating the systemic immune system. Creating a polymeric thin film on the cells has shown promising effects on cell survival and functionality.[181,182] Single-cell encapsulations are a promising technique which have shown beneficial outcomes in both adherent and non-adherent cells.[183,184] These techniques are mainly used to increase cell survival and functionality after in-vivo transplantation. Although very promising, several limitations exist as the polymers used for cell encapsulation often cause undesired complications. Gelatin and alginate are currently the most used substances used in coating of stem cells. One of the major issues of these types of coatings are the procoagulant nature of the alginate in the coating that could induce thrombosis.[185] In section 2.1, we have seen that dextran sulfate can be used to reduce the risk of thrombotic complications when islet cell are transplanted into the body. However, dextran sulfate is used to make mouse models of inflammatory bowel syndrome as they induce inflammation of the colon after oral administration and mimic Crohn's disease in humans.[186] Moreover, it is also used as a potent adjuvant for vaccines.[187] Thus we anticipated heparin being a natural ECM polymer with a known degradation profile and pharmacokinetics, heparin would be ideal for stem cell coating applications. To address this challenge, we developed a strategy where MSCs from bone marrow are coated with a gelatin-heparin layer, which are natural polymers with opposite charges. The opposite charge of the polyelectrolyte facilitates the coating of cells in a layer-by-layer fashion. As the cell surface are inherently anionic due to sialic acid and glycosaminoglycans expressed on the cell surface, the first layer that complex with the anionic cell surface is gelatin, which is followed by the heparin layer. This coating of gelatin and heparin was again repeated to achieve two layers each of gelatin (G) and heparin (H). To observe if our coating (H/G) was successful and stable under culture conditions, we performed a transmission electron microscopy (TEM) analysis on the cells, three days after coating. As a control, we used cells that were not coated. The TEM analysis showed a clear coating around the cells even after three days in culture, which were not observed in the control cells. To further confirm the cellular coating, we estimated the charge on the cell surface by zeta potential measurement of the cells. As anticipated, we observed charge neutralization as evidenced by an increase in the zeta potential from ~-27.2 mV (native cell surface) to ~-5.17 mV after the first layer of gelatin coating. Subsequent coating with heparin layer resulted in a drop-in zeta potential to ~-31.72

mV. The addition of the second layer of gelatin and heparin resulted in a similar change in surface charge as evidenced by the change in zeta potential from ~-31.72 mV to ~-6.08 mV and ~-29.1 respectively, after the second cycle of polyelectrolyte treatment. These alternations between the charges after each cycle of polyelectrolyte treatment clearly demonstrate the successful coating of the MSCs (c-MSCs) (Figure 14). Next, we investigated if polyelectrolyte coating influences cell proliferation by performing Alamar blue. We found that both the c-MSCs and control MSCs showed proliferation with time, however, unlike c-MSCs, the control MSCs displayed lower proliferation after 5 days in culture. This clearly shows the H/G coating enhances the metabolic activity of cells which could be due to the presence of gelatin and heparin which are known to enhance the proliferation of these cells.[188,189]

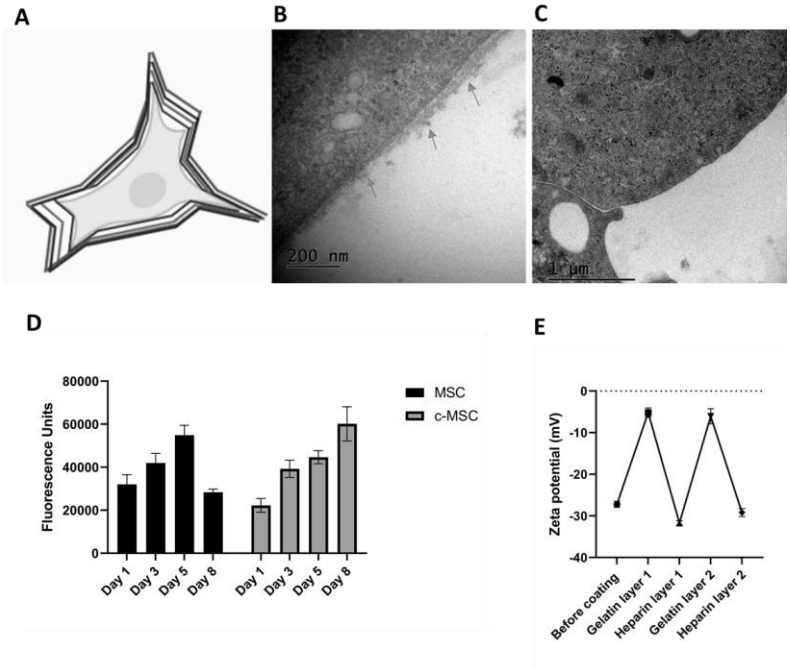

Figure 14. (A) Schematic representation of the c-MSCs with the layers of heparin and gelatin. Transmission electron microscopy images of (B) c-MSCs and (C) MSCs after 3 days in culture. The red arrows depict the presence of coating in c-MSCs. (D) Alamar blue proliferation assay performed on the MSCs and c-MSCs in different timepoints depicting the proliferation rates. (E) Zeta potential reading was observed after each layer of coating of the cells with H/G coating.

In **Publication IV**, a glycosaminoglycan-based hydrogel scaffold with immunosuppressive properties were developed. Innovative scaffold designs that modulate inflammation through favorable macrophage polarization and by reducing oxidative stress are the most sought-after for the successful clinical translation of regenerative therapies. Subsequently, we designed a hydrazone crosslinked gallol functionalized HA-based hydrogel (HA-GA). The HA was functionalized with gallic acid (GA) so as to exploit the immunosuppressive and antioxidant properties of the gallic acid.[190,191] To design this HA-based hydrogel scaffold, we first synthesized hydrazide functionalized GA by two-step method, namely, synthesizing methyl ester derivative of GA followed by nucleophilic displacement with aqueous hydrazine (80% solution) to get GA-hydrazide in quantitative yields. The HA was functionalized with this GA-hydrazide through EDC coupling. This GA functionalized HA was then grafted with carbodihydrazide (CDH) groups as a biorthogonal moiety that facilitates covalent crosslinking reaction with an aldehyde functionalized HA derivative (HA-ALD). The CDH modified HA-GA would then form hydrogels with the HA-ALD through the CDH derived hydrazone bonds that are known to exhibit exceptional stability under physiological conditions.[192] The degree of GA functionalization on the HA was 6% with respect to the disaccharide repeat units as determined by UV spectrometry. The degree of hydrazone crosslinking on the hydrogels was fixed at ~10%. As controls, we used HA gels without GA by using the same hydrazone chemistry with a similar degree of cross-linking density using 10% modified HA-ALD. To check if the addition of the GA in the GA functionalized HA gels (HA-GA) changed the anti-oxidant properties when compared to the hydrogels without GA functionalization (HA-HA), a DPPH radical scavenging assay was performed. The DPPH reagent underwent a visual change in color from deep purple to deep orange in the HA-GA, indicating the antioxidant property imparted by the HA-GA.

The viscoelastic properties of the HA gels (HA-HA) and HA gels with 6% GA (HA-GA gels) were evaluated by rheological studies by amplitude and frequency sweeps. The rheological analyses revealed that both HA-HA and HA-GA gels remained stable during the rheological testing and consistently yielded higher storage modulus (G') values as compared to loss modulus (G") indicating the viscoelastic nature of the matrix (Figure 16A). For HA-HA gels, a storage modulus, G', of 995 ± 4 Pa and a loss modulus G" of 7 ± 3 Pa was observed, while for HA-GA gels the G' and G" values were 747 ± 57 and 4 ± 1 Pa, respectively. We then observed the changes in the stiffness of both the hydrogels in phosphate buffer saline (PBS) at pH 7.4. It was observed matrix stiffening in HA-GA hydrogels on day 2 compared

to day 0 when immersed in PBS at pH 7.4 (Figure 16B). Thereafter, the HA-GA gels exhibited exceptional stability in storage modulus, when compared to HA-HA hydrogels until day 21 (Figure 16B). This suggests that the grafting of GA in HA gels promotes the formation of a secondary network that stabilizes the gel and prevents excessive swelling. We believe this is attributed to the unique capability of the gallol moiety to undergo oxidation (leading to the generation of radicals) and undergo intermolecular dimerization.[190]

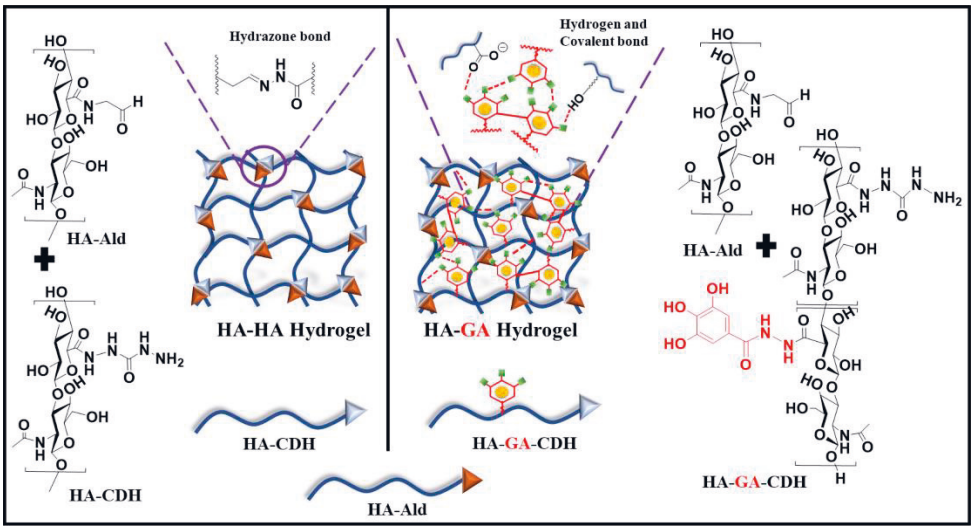

Figure 15. Schematic representation of the formation of the HA-HA and the HA-GA hydrogels.

We next evaluated the tissue adhesive property of the two gels by performing tissue adhesion tack tests using porcine muscle tissue as a model. The tack test revealed that HA-GA gels had significantly greater adhesion to the wet muscle tissue, as a greater negative force was required to induce cohesive failure between the top plate and the gel. To further prove the gallol-mediated secondary network formation in the HA-GA hydrogels we performed an enzymatic degradation study in the presence of hyaluronidase in PBS at pH 7.4. Enzymatically, the HA-GA gels illustrated slower degradation in the presence of hyaluronidase than did the HA-HA gels, especially after day 2 (Figure 16F). We believe that the additional GA-mediated secondary crosslinking network along with the primary hydrazone network in the HA-GA hydrogel restricts the hydrogel swelling and thus prevents enzymatic degradation.

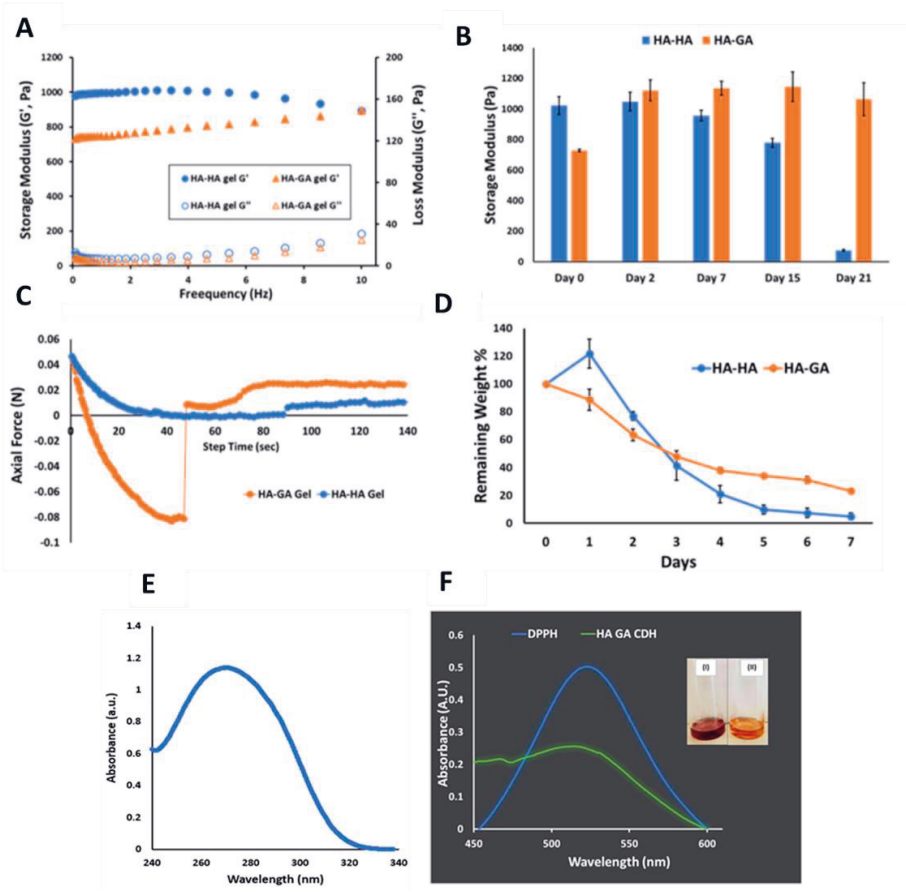

Figure 16. (A) Rheological measurements were obtained from frequency sweep for 250 µL HA-HA and HA-GA hydrogels (*n* = 3). (B) Rheological measurements of HA-HA and HA-GA hydrogels (*n* = 3) immersed in PBS buffer (pH 7.40). Dynamic strain recovery of a (C) Measurement of tissue adhesion force of the two hydrogels by rheological tack adhesion test (250 µL gels). (D) Degradation profiles of HA-HA and HA-GA hydrogels (250 µL, *n* = 3) in neutral PBS (pH 7.4) buffer containing 50 U/mL hyaluronidase. (E) UV-Vis spectra of conjugated gallic modified hyaluronic acid (HA-GA) (F) DPPH radical scavenging assay were carried out to assess the antioxidant property of HA-GA-CDH (green) with the 6 mol% GA. The picture (in the inset) depicts qualitatively the reagent underwent a color change (I) deep purple (DPPH) to (II) deep orange (DPPH + HA-GA hydrogel), which is due to the higher antioxidant property imparted by gallic acid.

5.2 Biopolymer-based nanocarriers that modulate immune response towards anti-cancer immunity

One of the aims of this thesis was to modulate the immune system with the help of biomaterials and increase the local inflammation. In diseases like cancer, the TME is highly immunosuppressive in nature due to the role of TAMs that are the most abundant cells in the TME.[193] Targeting the TME and modulating the TME to anti-tumor phenotype have been studied as cancer treatment options.[194,195] In Paper I, we designed a nanoparticle HA-DEX-DOX that could effectively co-deliver the chemotherapeutic agent (DOX) and an anti-inflammatory drug (DEX). The co-delivery of these two therapeutic modalities would synergistically facilitate DOX-mediated apoptosis, suppress side effects, and inflammation, and promote HA-mediated targeted delivery.

As mentioned earlier, a major risk of chemotherapy is thromboembolism which causes hypersensitivity reactions in cancer patients. The chemotherapeutic drugs are known to activate the platelets and trigger procoagulant activity that leads to thrombus formations.[196] It is now established that the platelets are the key initiators of inflammation and also assist in the activation of other immune cells like the neutrophils, macrophages and also activate the complement pathways.[197] Therefore, evaluating the activation of platelets and complement-coagulation cascade is of paramount importance. To study the thrombotic activity of HA-DEX-DOX and DOX, we performed an ex vivo experiment using Chandler's loop model with fresh human whole blood (non- coagulated blood without the addition of anticoagulants) from six healthy donors. (Figure 17) These experiments revealed that when 60 μM DOX was incubated with fresh blood, about 50% of the donors aggressively reacted to DOX where severe platelet aggregation was observed (3 donors from Group 1). The other 3 healthy donors (Group 2) were not responsive to DOX and no platelet aggregation was detected. When HA-DEX-DOX was incubated in the blood, suppression of the DOX-induced platelet aggregation was observed in Group 1. In group 2, the HA-DEX-DOX similar to the free DOX did not trigger any platelet aggregation. The reason and the mechanism for this discrepancy of DOX reacting to blood need to be further researched.

When the thrombin-antithrombin (TAT) complex were measured in the blood samples by ELISA after incubation with HA-DEX-DOX and DOX, it was observed that similar to the platelet aggregation there was no reaction from the donors in group 2. However, in group 1, DOX showed significant activation of the TAT corresponding to the platelet aggregation. HA-DEX-DOX, on the other hand,

showed significantly lower activation of the TAT when compared to the DOX. Surprisingly in group 1, when HA-DEX was incubated with blood we observed a significant elevation of TAT. We believe that this elevation of TAT in the HA-DEX groups could be due to the large hydrodynamic size of the HA-DEX when compared to HA-DEX-DOX. It has been previously reported that nanoparticles with lower curvatures (larger size) denatured the factor XII more when compared with nanoparticles having higher curvatures (lower size) triggering the activation of TAT.[198] It has also been reported that TAT activation is influenced by the amphiphilic surfaces[199] and we believe the larger size of the HA-DEX exposes more hydrophobic surfaces resulting in higher plasma protein adsorption resulting in higher TAT activation when compared to HA-DEX-DOX. When the levels of anaphylatoxin C3a was measured, to our surprise it was observed that there were no significant differences between DOX, HA-DEX, and HA-DEX-DOX which were all similar to the control PBS group in both the groups 1 and 2. All these observations taken together suggest that the encapsulation of DOX in HA-DEX-DOX nanoparticles prevents platelet aggregation and thrombo-inflammation in human whole blood. The discrepancy in how DOX reacts with blood also suggests that a personalized approach is required in patients before standard chemotherapeutics are administered as some patients might be more sensitive to the treatments.[200] These observations also suggest that the HA-DEX-DOX nanoparticle is capable of evading the systemic immune system.

In section 5.1, we have already discussed the design and the rationale behind the design of HA-DEX-DOX. The ability of HA-DEX-DOX to evade the systemic immune system by not triggering the platelets and the coagulation cascade has also been discussed. After witnessing these observations, we analyzed the ability of the HA-DEX-DOX to target the tumor cells. We believe that HA being the major component in HA-DEX-DOX, the nanoparticle would be able to target the HA-specific CD44 receptor that is known to be overexpressed in cancer cells and is also a known cancer stem cell marker.[201] For this purpose, we used three different human cancer cell lines with different levels of CD44 receptor expression. MG63 osteosarcoma cell lines and HCT116 human colon carcinoma cell lines are known to have high expression of the CD44 receptors, whereas the third cell line MCF7 is reported to have very low levels of CD44 expression. When HA-DEX-DOX was used on these cells, the uptake of the HA-DEX-DOX was analyzed by flow cytometry, exploiting the inherent fluorescent property of DOX. These experiments revealed that the MG63 and the HCT116 cells demonstrated 83% and 87% nanoparticle uptake while only 60% nanoparticle uptake was observed in the MCF7

cell lines. The lower uptake in the MCF7 cell line could be explained due to the lower levels of the CD44 receptors. To further confirm if HA-DEX-DOX is taken up by these cells through the CD44 receptor-mediated uptake, we observed the uptake of the HA-DEX-DOX in these cells after blocking the CD44 receptors with 5kDa HA. Blocking the CD44 resulted in ~1.5 folds and ~1.7 folds reduction in the uptake in the MG63 and HCT116 cells, while MCF7 cells displayed ~1.3 folds reduction in uptake of HA-DEX-DOX. These observations suggest that the cell surface HA receptors are involved in the uptake of the particles. We also performed fluorescence microscopy to ascertain the intracellular localization of DOX and DOX in HA-DEX-DOX. Interestingly, DOX in HA-DEX-DOX displayed nuclear localization similar to free DOX, validating the uptake and intracellular bio distribution of nanoparticles.

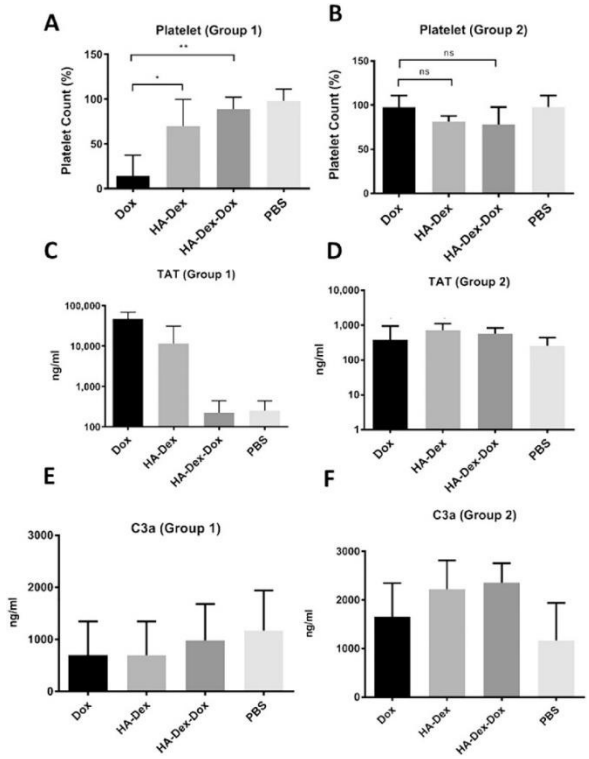

Figure 17. The left panel represents Group 1 donors and the right panel represents Group 2 donors. (A, B) Normalized Platelet aggregation. (C, D) ELISA of Thrombin-antithrombin complex, a marker for coagulation using EDTA plasma (N = 3 donors); (E, F) ELISA of C3a, a marker for complement activation using EDTA plasma (N = 3 donors). Statistical analysis was done by one-way ANOVA *P < 0.05, **P < 0.01.

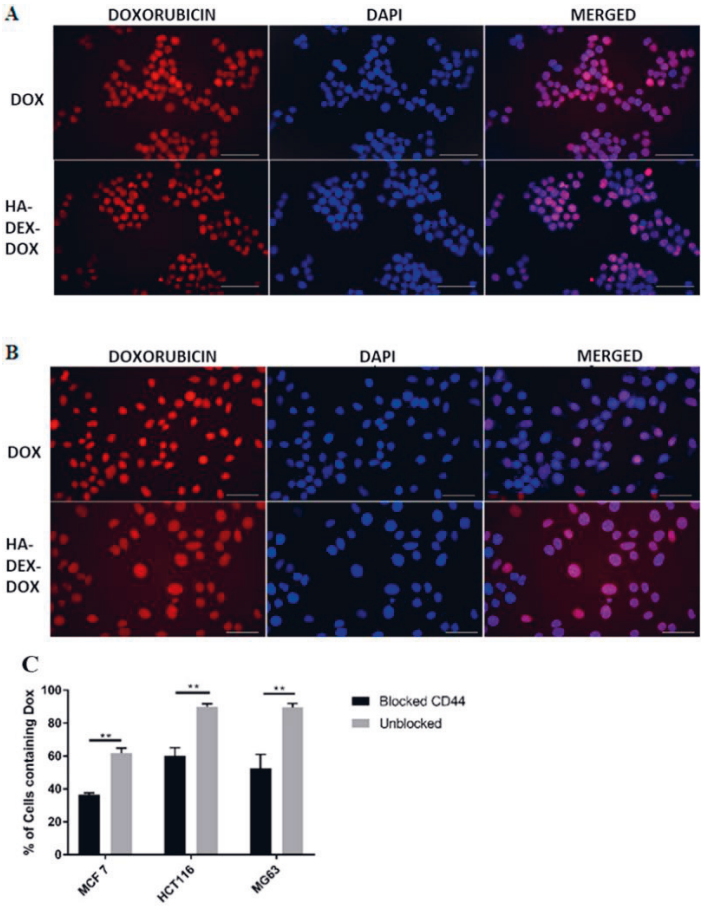

Figure 18. Nuclear localization of the free DOX and HA-DEX-DOX along with nuclear staining (DAPI) in (A) HCT116 colon carcinoma cell line and (B) MCF7 breast cancer cell line after 4 hr incubation. Scale bar 50 μm (C) Competitive CD44 blocking assay. The dependence of the nanoparticle uptake on the HA-specific cell surface receptor CD44 when the CD44 receptor was blocked and unblocked as estimated by flow cytometry analysis. Statistics were done for individual groups by Mann-Whitney U-test in GraphPad Prism. (**P<0.01).

We then investigated the in vitro toxicity of the combination therapy. A dose-dependent MTT assay of DOX, HA-DEX, and HA-DEX-DOX was performed on the three cell lines. (Figure 19 A-D & Table 2) As expected, we observed toxicity in a dose-dependent manner in DOX and HA-DEX-DOX, while the HA-DEX did not show any significant toxicity. When we calculated the IC50 values, we surprisingly found that the toxicity of the HA-DEX-DOX was ~3 folds lower that the DOX in all the cell lines irrespective of the CD44 expression. To understand this

paradoxical effect, we examined the cytotoxic effect of free DOX, free DEX, and the mixture of DEX and DOX (combination effect) on these cell lines. Surprisingly we found that free DEX (200 nM) displayed significant toxicity to the MCF7 and MG63 cell lines. Specifically, it was observed that only 56% and 59.17% of the cells were viable in the MCF and MG63 cells respectively after 48 h as determined by the MTT assay. The HCT116 cells, however, did not display any signs of toxicity with cell viability being around 93% after 48 h. Interestingly, when the HCT116 cells were treated with 200 nM DEX and 200 nM DOX, it was observed that the DEX had suppressed the effect of DOX on the HCT116 cells (56.75% in DOX compared to 76.9% in DEX-DOX). On the contrary, DEX increased the cytotoxic effects of DOX from 41.38% to 30.3% when in combination. In the MG63 cells, even though the DEX was shown to have toxicity (59.17% cell viability), a combination of DEX+DOX did not show any significant effect when compared to DOX alone (38.6% cell viability with DEX+DOX and 38.91% with DOX alone). This clearly suggests that nanoparticles combining DEX and DOX form a powerful synergistic system for breast cancer, while contrary to the reported literature,[202] DEX plays an inhibitory role in HCT116 colon cancer cells (Figure 19A). Such effects were negligible in MG63 osteosarcoma cells.

Since the TAMs are one of the most abundantly found cells in the TME, we wanted to see if the HA-DEX-DOX could manipulate the TAMs into producing anti-tumor factors. For this purpose, we evaluated the immunomodulatory properties of DOX and HA-DEX-DOX on mouse bone marrow-derived macrophages (BMDMs) that were differentiated to mimic the TAMs. To ascertain the immunomodulatory effects of the HA-DEX-DOX, we treated the TAMs like cells with 200 nM of HA-DEX-DOX and measured the expression of proinflammatory markers like TNF-α, IL1β, iNOS, and IL6, which are known to be hallmarks of proinflammatory M1 macrophages.[203] We observed that all these proinflammatory markers were elevated when these cells were treated with HA-DEX-DOX when compared to untreated controls. (Figure 22 A-D) The elevated levels of these markers indicate the modulation of macrophage activation state from the M2 (TAMs) like state towards the M1 like state that favors anti-cancer immunity. All these results taken together show that we have developed a nanoparticle HA-DEX-DOX that could evade the systemic immune system and target the tumor to deliver a chemotherapeutic drug while also modulating the TME to an anti-tumor environment.

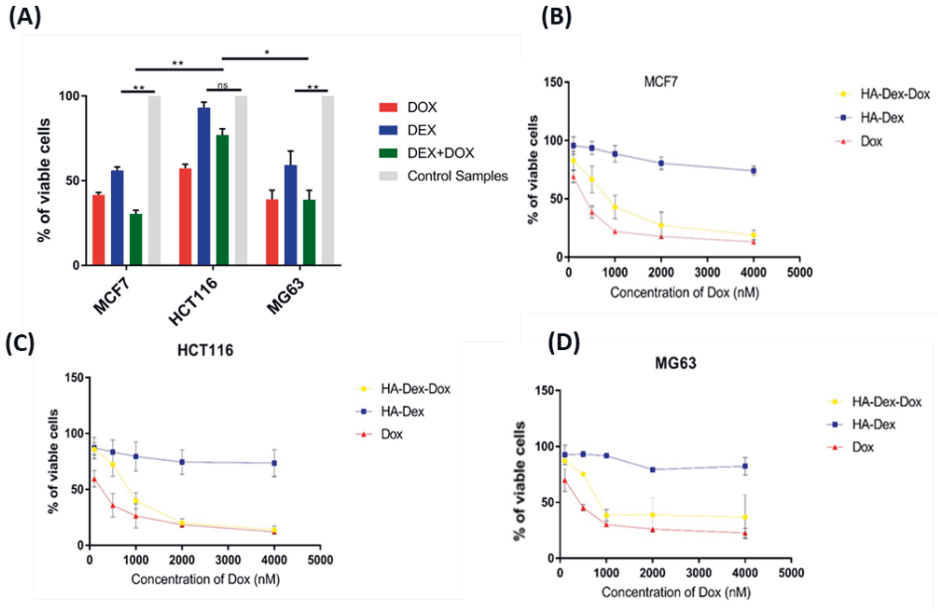

Figure 19. (A) Cell viability percentages after treating with either 200 nM free DOX, 200 nM DEX, or a combination of 200 nM DOX and 200 nM DEX. The experiments were performed on MCF7, HCT116, and MG63 cell lines. Statistical analysis was done by Kruskal-Wallis test (**p < 0.01 *p < 0.05). Cell viability percentages after the introduction of HA-DEX-DOX, DOX and HA-DEX at concentrations of 100nM, 500nM, 1000nM, 2000nM and 4000nM. The concentration HA-DEX chosen was equivalent to HA-DEX-DOX. The cytotoxicity studies were performed on different cell lines (B) MCF7, (C) HCT116, and (D) MG63.

Table 2: Cytotoxicity of DOX and HA-DEX-DOX on the different cell lines. IC50 values were estimated by the logarithmic curve fitting of the cell viability percentage using GraphPad Prism software.

Cell lines	DOX IC50 (nM)	HA-DEX-DOX IC50 (nM)
MCF-7	226.03 ± 42.2	702.03 ± 76.3 (3.1 fold)
HCT-116	192.6 ± 59.9	585.7 ± 40 (3.04 fold)
MG-63	195.4 ± 26.4	576.4 ± 65.2 (2.95 fold)

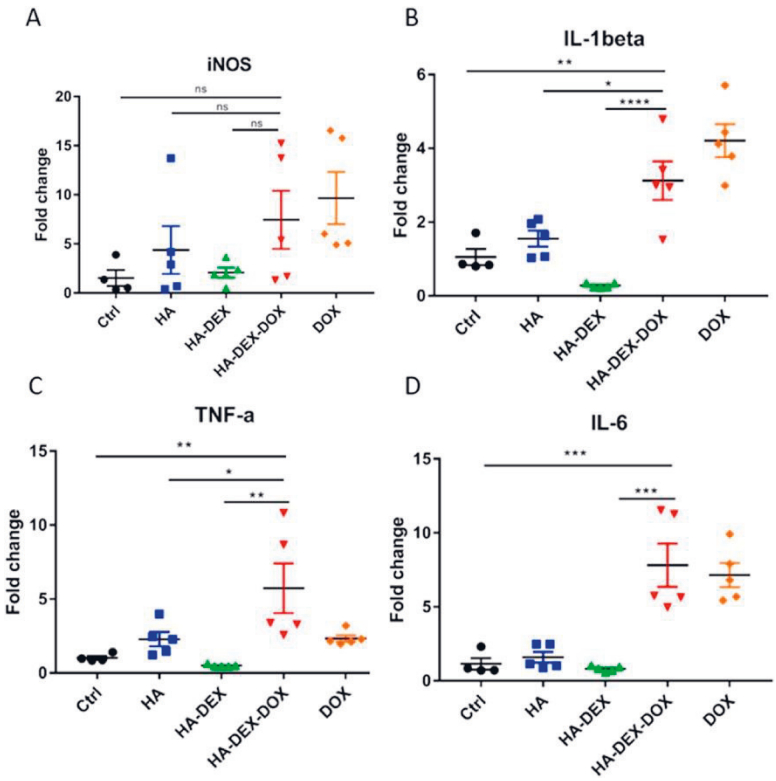

Figure 20. mRNA expression of pro-inflammatory genes by TAMs as estimated by qRT-PCR and normalized by HPRT gene expression. A) iNOS B) IL-1β C) TNF-α and D) IL-6. Statistical analysis done by one-way Anova *P < 0.05, **P < 0.01, ***P < 0.001.

5.3 Designing covert MSCs with enhanced hemocompatibility and functions

Along with increasing the local inflammation with the help of biomaterials, another aim of this thesis is to suppress the local inflammation. Suppressing local inflammation can be useful in cases where wound healing and tissue repairs are necessary. Here in this dissertation, I have exploited the MSCs to impart immunosuppressive properties while enhancing the safety and functions of these cells. In the section below the results of the **Publication II, III** where multipotent MSCs have been studied have been discussed.

In **Publication II**, we used the Plu-SS-TF/Ca nanoparticle to silence the TF or CD142 gene on the MSCs. Therefore, we evaluated the functional activity of TF knockdown (TF-KD) MSCs as we anticipated that TF knockdown would suppress the activation of the coagulation cascade and complement system. Using a modified chandler's loop, we incubated the MSCs and TF-KD MSCs (for 1 h) in non-anticoagulated blood and estimated platelet activation. (Figure 21A) Interestingly, the TF silencing attenuated the platelet aggregation as we observed ~93% free platelets in the TF-KD MSCs group when compared to the normal MSCs which had only ~22% free platelets. These results were further corroborated with the TAT complex activation where the TF-KD MSCs showed significantly lower TAT formation when compared to the normal MSCs. (Figure 21B) Interestingly, when the early and late complement activation markers were measured, we did not see any significant difference between the normal untreated MSCs and the TF-KD MSCs. These results unequivocally show that TF silencing using Plu-SS-TF/Ca alleviate platelet activation and systemic inflammation which will significantly enhance stem cell survival after transplantation as the MSCs will evade the systemic immune system.

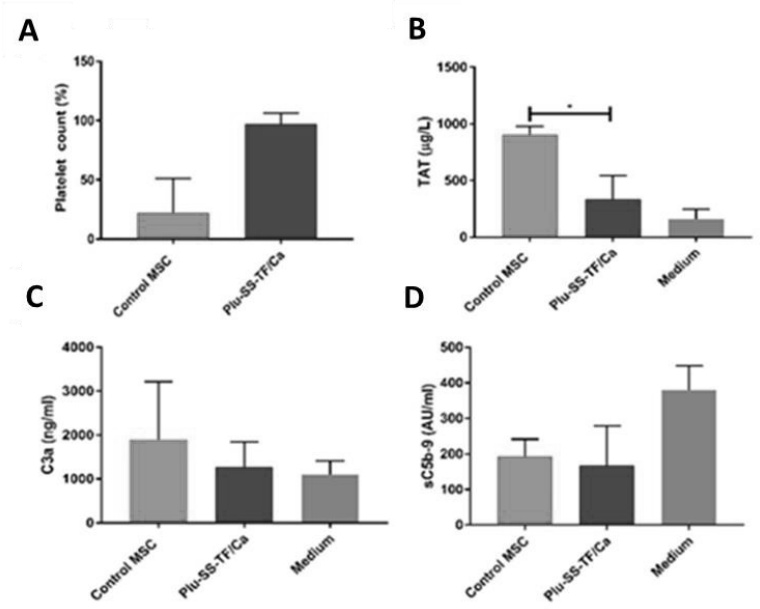

Figure 21. (A) Platelet counts normalized against the growth medium. (B) TAT complex, a marker for coagulation in whole blood (N = 3). (C, D) C3a and sC5b-9, markers for complement activation in whole blood (N = 3). Statistical analysis was done by the Kruskal–Wallis T-test, *P < 0.05.

The results obtained earlier depict that the TF-KD MSCs could evade the systemic immune system by suppressing platelet aggregation and mitigating activation of the coagulation cascade (TAT complex). As knockdown of genes in MSCs could potentially cause unprecedented responses leading to altered phenotype and cellular function. To ascertain that TF silencing does not affect cellular phenotype, we first estimated the expression of key MSC markers like CD105, CD73, and CD90 in the TF-KD MSCs through staining and flow cytometry. MSCs are also classified by the absence of certain markers and for this reason, we also test the expression of CD34 in the TF-KD MSCs. We found that a similar percentage of cells in the control MSC and the TF-KD groups expressing the MSCs markers CD73 (92.1± 1.62% in MSCs to 89.2± 2.2% in TF-KD MSCs), and CD105 (91.4±1.8% in MSCs to 90.8± 1.6% in TF-KD MSCs). The negative MSC marker CD34 was found to be lacking in the majority of the cells in both the MSCs and TF-KD MSCs(0.4± 0.2% in MSCs to 1.2± 0.6% in TF-KD MSCs). Interestingly, the number of cells expressing the CD90 marker was found to be lower in the TF-KD MSCs (74.1± 1.9%) when compared to the control MSCs (82.5± 2.2%). The CD90 in the MSCs signifies the undifferentiated state of the MSCs and it is also known to control the differentiation of the MSCs by acting as an impediment towards the pathway of differentiation commitment. Lower expression of CD90 is correlated with temporal lineage commitment in vitro.[204] Thus, we believe the lower amount of CD90 expressing cells in the TF-KD MSCs group could signify the increase in the differentiation ability of these cells. In order to validate the effect of TF-KD on stemness, we measured the expression of OCT4 and the NANOG gene by qRT-PCR as they are the key transcription factors that are crucial for maintaining multipotency and the self-renewal state.[205] Interestingly, the qRT-PCR study revealed higher expression of the NANOG gene as a result of TF-KD (though non-significant); however, no significant differences were observed in the OCT4 expression. (Figure 22A)

The differentiation potential of the MSCs and the TF-KD MSCs was then evaluated by culturing these cells in osteogenic conditions and adipogenic conditions. (Figure 22 B-E) Interestingly, when the TF-KD MSCs were cultured under osteogenic conditions, increase mineralization was observed when compared to the control MSCs, as evidenced by higher calcium deposits observed by alizarin red staining. This observation was further confirmed by qRT-PCR which also revealed the increased expression of osteogenic markers ALP, BGLAP, and DLX5 in the TF-KD MSCs when compared to the control MSCs grown in osteogenic

conditions. Interestingly, the TF-KD MSCs also exhibited an increase in the expression of adipogenic markers (LPL and PPARG) compared to control MSCs in adipogenic conditions, albeit not as significant as under the osteogenic conditions.

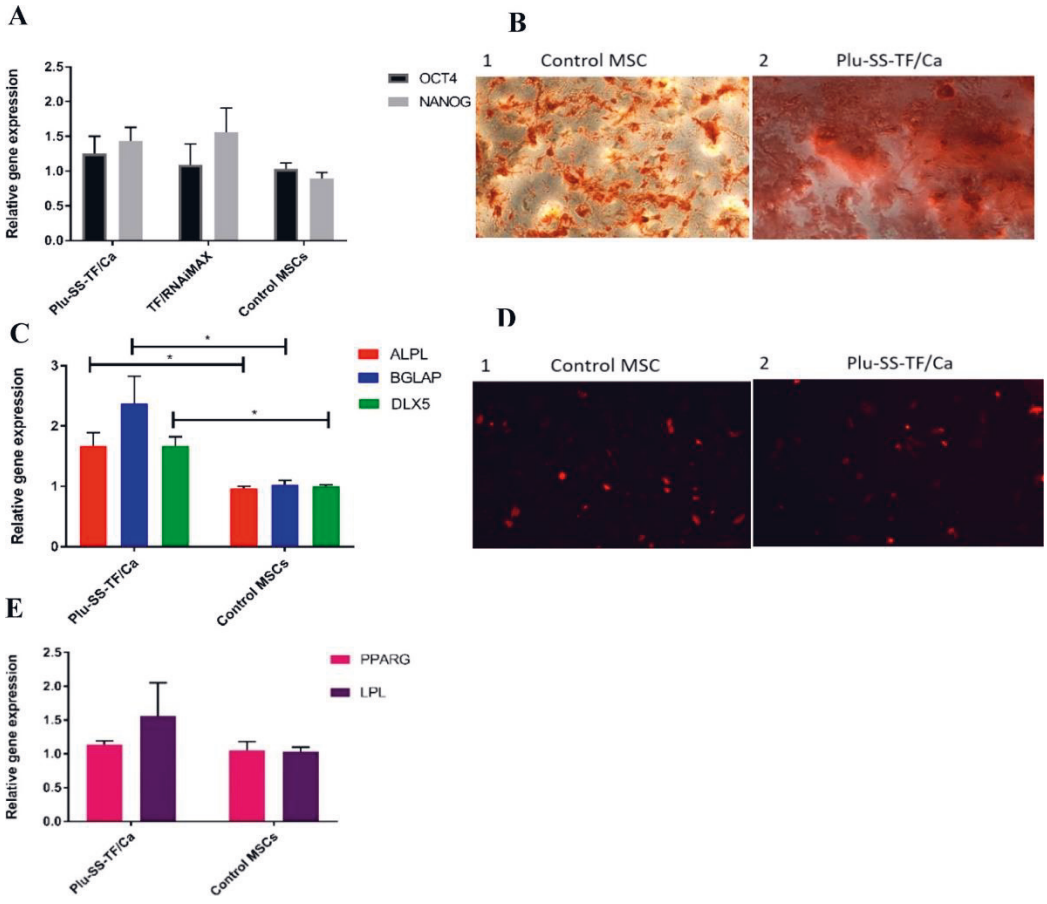

Figure 22. : A) qRT-PCR analysis was done to determine the level of OCT4 and NANOG to analyze the stemness of the TF-KD cells and untreated MSCs. (B) qRT-PCR analysis of osteogenic markers. Statistics were done by the Mann–Whitney test on GraphPad Prism (*P < 0.05). (C, D) Differentiation studies of TF-KD MSCs and MSCs after 16 days of culture. (C) Alizarin red staining to detect the presence of calcium deposits of MSCs cultured under osteogenic conditions. (C1) Control MSCs and (C2) MSCs after treatment with Plu-SS-TF/Ca. (D) Nile red staining of MSCs to detect the presence of lipid vacuoles cultured under adipogenic conditions. (D1) Control MSCs and (D2) MSCs after treatment with Plu-SS-TF/Ca. (E) qRT-PCR analysis of adipogenic markers.

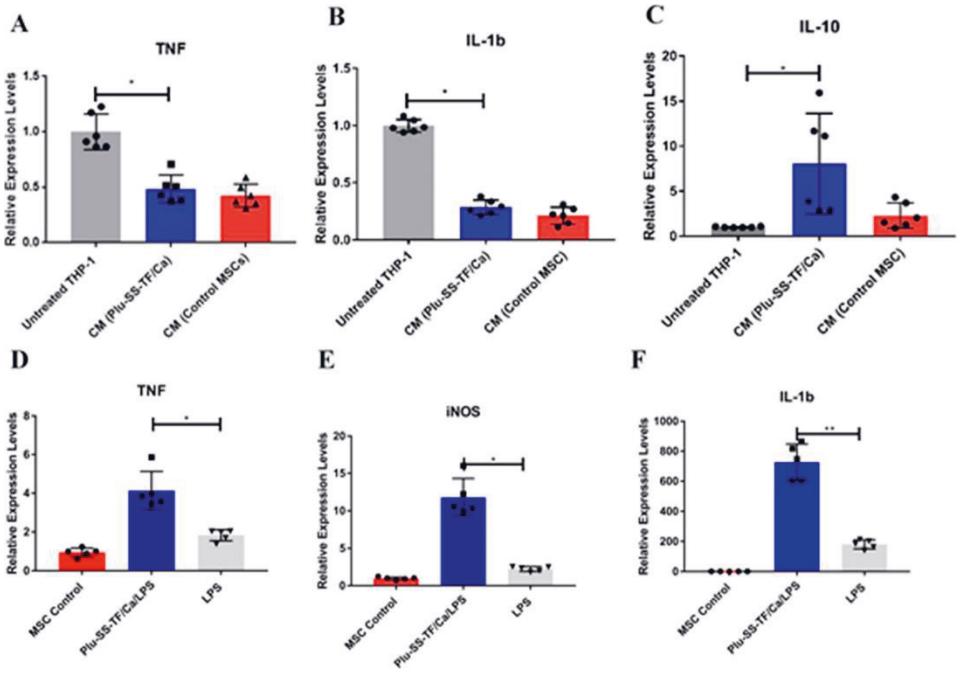

Figure 23. (A–C) Effect of the MSC secretome (CM) on proinflammatory M1 macrophages derived from THP-1 cells. qRT-PCR analysis quantifying the cytokine mRNA levels of (A) TNF, (B) IL-1β, and (C) IL-10. (D–F) Paracrine signaling of MSCs and TF-KD MSCs by direct stimulation with endotoxin LPS (2 μg/mL) relative to the untreated MSC control. qRT-PCR analysis quantifying the cytokine mRNA levels of (D) TNF, (E) iNOS, and (F) IL-1β. Gene expression is relative to β-actin. Statistics were done by the Kruskal–Wallis method (*P ≤ 0.05, **P ≤ 0.01).

We then investigated if the immunomodulatory properties of TF-KD MSCs are different from the control MSCs. (Figure 23 A-C) It has been reported that MSCs impart their functional benefits by secreting soluble factors and by paracrine signaling.[206] For this purpose, we studied the effect of the MSC and TF-KD MSC secretome on THP-1 human monocyte cell lines that were differentiated to the proinflammatory M1 phenotype. When the conditioned medium (CM) from the MSCs and TF-KD MSCs were exposed to the M1 macrophages, we observed a significant decrease in the expression of proinflammatory markers TNF-α and IL1β when compared to the M1 macrophages that were not exposed to the CM. We also analyzed the levels of IL10, an anti-inflammatory marker. It was observed that when the M1 macrophages were exposed to the CM from the TF-KD MSCs they showed a significant increase in the production of IL10. The CM from the control MSCs also increases the IL10 production but is not as significant as the TF-KD group. These results suggest that the TF-KD MSCs retained their immunosuppressive

properties similar to the control MSCs. The increase in the IL10 expression in the M1 macrophages after the exposure of CM of TF-KD MSCs, when compared to the CM from control MSCs, shows that the TF-KD MSCs might be partially superior that the control MSCs in the resolution of inflammation. We believe this because IL10, being a master anti-inflammatory response regulator, can suppress the activity of other proinflammatory immune cells and subsequently regulate the T-helper cell responses.[207] We then examined if TF-KD MSCs respond differently to stimulants when compared to control MSCs. It has been reported that MSCs can exhibit a proinflammatory phenotype when stimulated with external agents.[208] For this purpose, we stimulated the MSCs with endotoxin LPS (lipopolysaccharides) and surprisingly observed that the TF-KD MSCs displayed significantly higher expression of proinflammatory cytokines TNF-α, IL1β, and iNOS when compared to the stimulated MSCs and unstimulated MSCs. This clearly suggests that the TF-KD MSCs were more sensitive to stimulation. Thus, TF silencing of MSCs by Plu-SS-TF/Ca as reported in **Publication II**, clearly demonstrate that TF-KD MSCs possess enhanced hemocompatibility, differentiation potential, and paracrine functionalities, which would enhance the stem cell survival and function after transplantation.

In **Publication III**, we used heparin and gelatin to coat the MSCs. This H/G coating on the MSCs made them more proliferative in-vitro. We then analyzed if this coating could help these cells evade immune surveillance after infusion in blood. Similar to the hematological experiments in **Publication II**, the MSCs and c-MSCs were incubated with non-anticoagulated human whole blood in a modified chandlers' loop for one hour. These experiments revealed that the c-MSCs attenuated the platelet aggregation when compared to the MSCs, as demonstrated by ~94% free platelets in the c-MSCs group when compared to the control MSCs (~2% free platelets). (Figure 24) These observations were further corroborated with the TAT activation, which were significantly lower in the c-MSCs when compared to the control MSC group. The lower TAT activation by the c-MSCs group could be attributed to the outer heparin coating. Heparin is a known anti-coagulant which is known to reduce thrombin generation in a dose-dependent manner.[209] When the early and late markers for complement activation were measured, we observed the c-MSCs to have lower levels of both the C3a and the C5b-9 markers. The C3a levels in the c-MSCs were significantly lower (~600 ng/mL) when compared to the MSCs (~1300 ng/mL). The C5b-9 marker levels were lower in the c-MSCs (~30 IU/mL) when compared to the control MSCs (~81 IU/mL), however, they were not significant. Thus, heparin coating significantly improves the hematological response

as confirmed by lower platelet aggregation and lower expression of complement markers. The unfractionated heparin, the glycosaminoglycan used in this study for coating cells, is known to sequester complement proteins and thus neutralize the activation of the complement cascade.[210,211] These results, taken together suggest that the c-MSCs could successfully evade the systemic immune system when compared to the control MSCs.

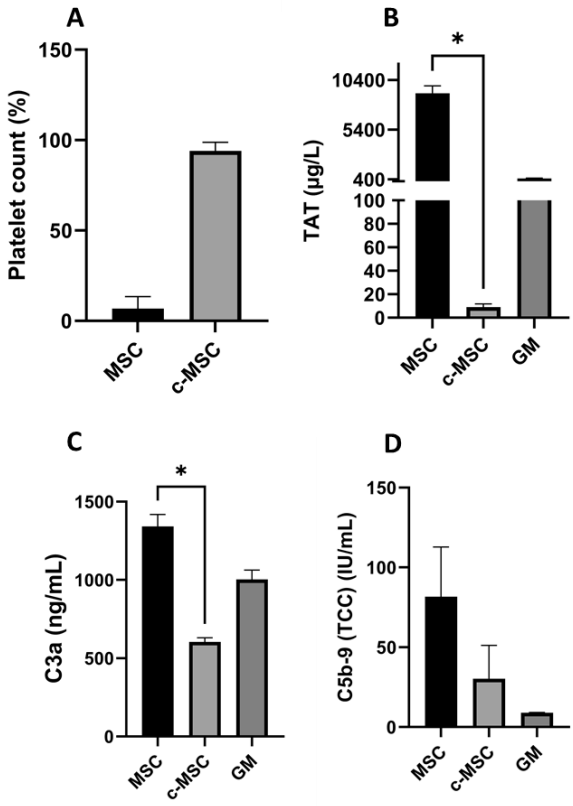

Figure 24. (A) Platelet counts observed after incubation of c-MSCs and MSCs in non-anticoagulated blood, normalized against the growth medium (GM). (B) TAT complex, a marker for coagulation in whole blood (N = 3). (C, D) C3a and sC5b-9, markers for complement activation in whole blood (N = 3).

After establishing that the c-MSCs did not trigger the coagulation cascade, we investigated the cytokines released by the MSCs. (Figure 25) Since it has already been established that the MSCs could be used as cell therapy to treat cartilage lesions and osteoarthritis,[212] we looked for the release of IL8 and IL6 which are known to be

involved in the repair of these conditions.[213] For this purpose, we analyzed the secretome of the c-MSCs and the uncoated MSCs after three days by ELISA. Interestingly, we observed that the levels of IL6 and IL8 secreted by the c-MSCs were much lower than the uncoated MSCs. Further analysis revealed that even after stimulation of the MSCs and c-MSCs with IFNγ and TNFα, the c-MSCs secretome contained a much lower amount of IL6 and IL8 after three days. We speculated that the factors released by the c-MSCs could adhere to the heparin in the H/G coating as heparin is known to bind to a lot of biological molecules.[214] To further confirm if the c-MSCs indeed produce a lower amount of IL6 and IL8, we analyzed the mRNA levels of these cytokines in the c-MSCs and MSCs. Interestingly, we observed that on day 3, the c-MSCs had significantly more mRNA levels of IL6 and IL8 when compared to the uncoated MSCs. The c-MSCs showed higher levels of IL6 and IL8 even when analyzed 7 days after culturing, though this increase was non-significant. We also looked for markers like VEGF, HIF1, and TGFβ that are important markers for immunomodulation, tissue repair, and regeneration. When the mRNA levels of the markers we analyzed on day 3, we found that there were no significant differences in the mRNA levels of these markers. Intriguingly, we observed a non-significant increase of the VEGF, HIF1, and TGFβ mRNA levels on day 7 when compared to the uncoated MSCs. The increased levels of HIF1 could help in the survival, proliferation, and differentiation.[215] HIF1 is also known to influence the production of VEGF,[216] which is known to be a potent angiogenic factor.[217] The increase in TGFβ could suggest that the c-MSCs could be more efficient than the uncoated MSCs in inducing the production of regulatory T-cells that are known to partake in tissue repair and regeneration.[218] These observations suggest that the H/G coating does not significantly reduce or inhibit the mRNA expression of these important markers that are involved in immunomodulation and tissue repair.

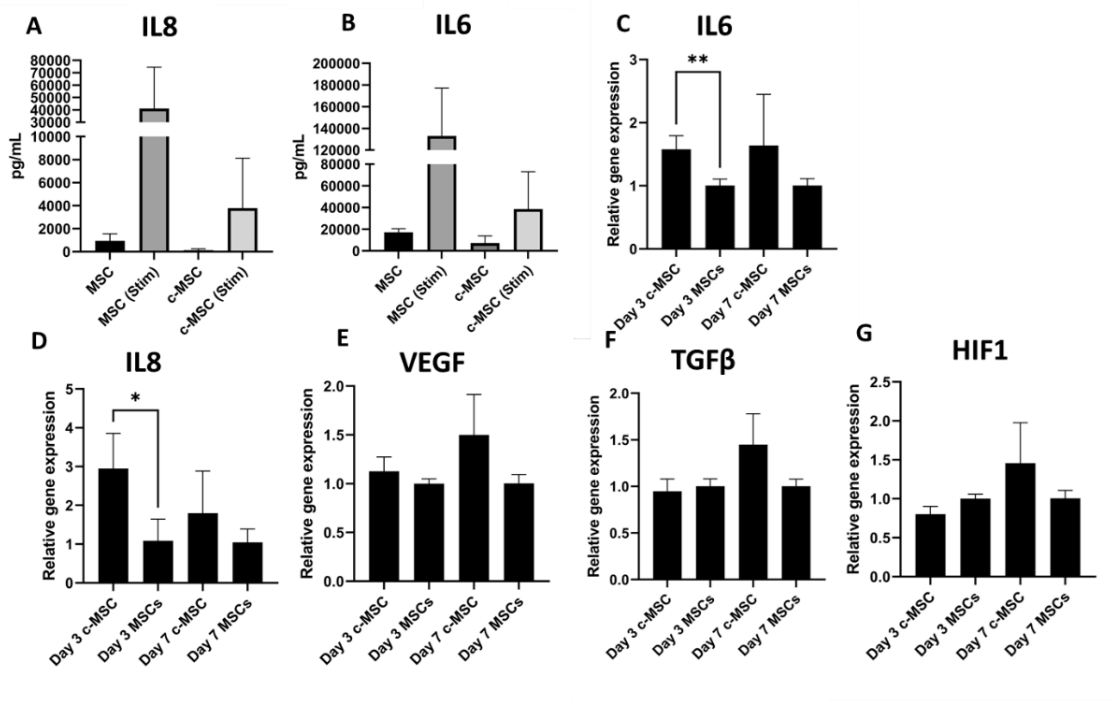

Figure 25. A&B) Levels of the IL8 and IL6 cytokines (in pg/mL) as analyzed through ELISA of the c-MSCs, uncoated MSCs, and c-MSCs, and uncoated MSCs stimulated by IFNγ and TNFα. (C – G) mRNA expression levels of the IL6, IL8, VEGF, TGFβ, and HIF1 in uncoated and c-MSCs.

The discrepancy in the level of cytokines secreted by the c-MSCs in ELISA and the mRNA levels of the cytokines prompted us to investigate the paracrine signaling abilities of the c-MSCs. For this purpose, we stimulated the C28/i2 chondrocytes to a pro-inflammatory phenotype by treating them with lipopolysaccharides (LPS, 1 μg/mL) for 24 h. (Figure 26) The conditioned medium from c-MSCs and uncoated MSCs were collected after 3 days in culture and exposed to the stimulated chondrocytes. We analyzed the levels of the major pro-inflammatory genes IL1β and TNFα. As expected, when the conditioned medium from the uncoated MSCs was exposed to the stimulated chondrocytes, there was a decrease in the levels of IL1β and TNFα. Similarly, a significant decrease in the mRNA levels of the IL1β and TNFα was observed when the conditioned medium of the c-MSCs was exposed to the stimulated chondrocytes. We also measured the levels of the anti-inflammatory marker TGFβ and observed that in there was a moderate increase in both the c-MSCs and the uncoated MSCs. These results suggest that the c-MSCs are as effective

as the uncoated MSCs and that the H/G coating does not interfere in the paracrine signaling of the MSCs.

To further confirm that the immunomodulatory properties of the MSCs are retained after the H/G coating, we exposed the conditioned medium of the c-MSCs and uncoated MSCs to THP1 cells differentiated into M1-like macrophages. (Figure 26) The medium was then collected and the cytokines were analyzed through a multiplex bead-based assay. We specifically analyzed the proinflammatory cytokines TNFα and IL1β which are the hallmarks of pro-inflammatory macrophages. Expectedly, we saw a decrease in the production of TNFα and IL1β when the conditioned medium of c-MSCs and MSCs were exposed to the M1 polarized THP1 cells. We also observed the cytokine levels of IP10 (CXCL10), a proinflammatory cytokine that is known to be produced by IFNγ or LPS stimulated cells.[219] We observed a drastic decrease in the production of IP10 when the conditioned medium of c-MSCs and the MSCs were exposed to the proinflammatory THP1 cells. The decrease in the levels of pro-inflammatory markers released by the M1 polarized could be due to the predominantly immunosuppressive nature of the MSCs.[220] We also analyzed the levels of IL6, a pleiotropic cytokine that is known to be involved in both pro-inflammatory as well as anti-inflammatory roles.[221] Interestingly, we observed a drastic increase in the production of IL6, when the conditioned medium of the c-MSCs was exposed to the M1-like THP1 cells. The conditioned medium from the uncoated MSCs had similar levels of IL6 secretion when compared to the control THP1 cells. The increase in the IL6 secretion with the conditioned medium of the c-MSCs could be explained due to the fact that c-MSCs showed an increased expression of IL6. The reduction of the proinflammatory TNFα, as well as the IL1β, seen in the THP1 cells also strengthens our belief that this IL6 expression could be a direct effect of the increased amount of IL6 present in the conditioned media of the c-MSCs. We also hypothesize that this IL6 release could be of the anti-inflammatory type as there have been reports where the IL6 is involved in the regulation of macrophages and has been known to increase CD206 expression (a major anti-inflammatory marker) in macrophages.[222] Taking all the results together, it can clearly be inferred that the H/G coating of the MSCs does not hinder the paracrine signaling capabilities and immunomodulatory functions of the MSCs.

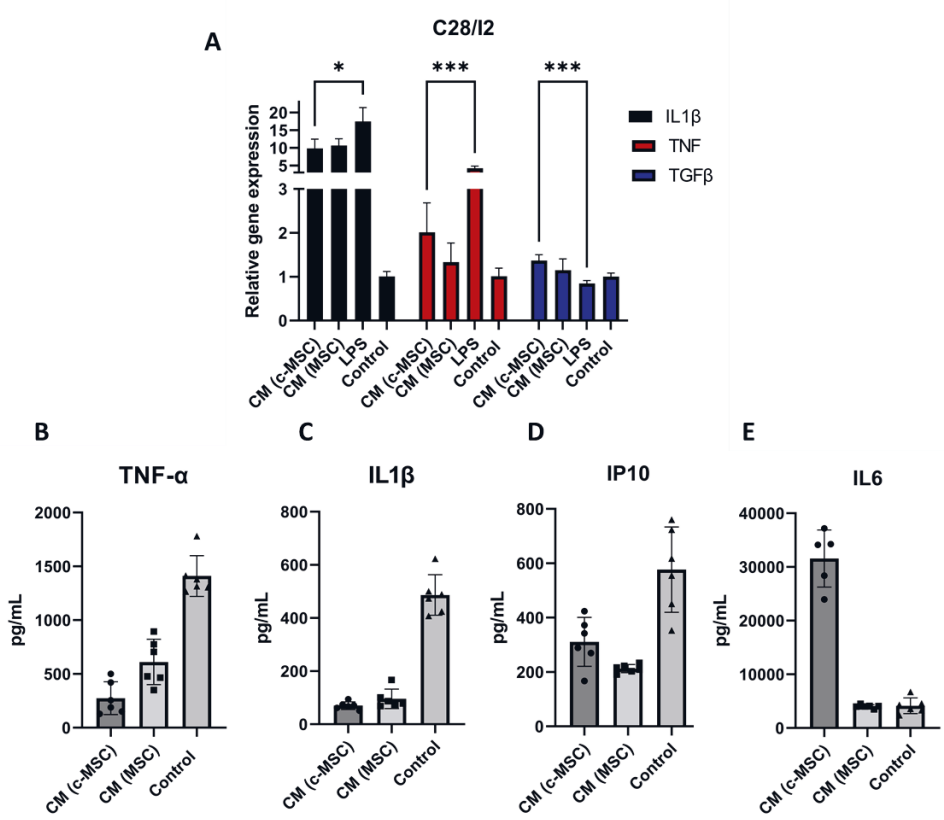

Figure 26. Immunomodulatory properties of the c-MSCs. (A) The effect of the conditioned media (CM) from c-MSCs and MSCs on the LPS stimulated C28/I2 chondrocytes. The effect of the CM of c-MSCs and MSCs on the M1 polarized THP1 cells was measured by analyzing the levels of (B) TNFα (C) IL1β (D) IP10 and (E) IL6.

Finally, after analyzing the paracrine signaling abilities of the c-MSCs, we investigated if the H/G coating had an effect on the differentiation abilities of the MSCs. Most of the cell therapies where the MSCs have exploited their immunomodulatory properties rather than their differentiation potential.[223] However, there have been reports that when the MSCs have differentiated into cardiomyocytes when they were used in mice myocardial infraction models.[224] Therefore, to evaluate the differentiation potentials of the c-MSCs, we cultured the H/G in osteogenic and adipogenic conditions for a period of two weeks. As controls, uncoated MSCs were also cultured under osteogenic and adipogenic conditions for a period of two weeks. We also included a group where the c-MSCs and uncoated MSCs were cultured in basal medium for two weeks. To analyze the

osteogenic differentiation potential, the cells were stained with alizarin red stain. We observed that there were similar amounts of calcium deposits in the c-MSCs and uncoated MSCs in osteogenic conditions as seen in figure 27 B&C. The c-MSCs and uncoated MSCs in basal medium did not show any significant calcium deposits as seen in Figure 27 A&D. To further confirm that the c-MSCs did not lose their differentiation ability, we examined the mRNA levels of the two osteogenic markers, ALPL and BGLAP. We observed similar increase in the BGLAP and ALPL in the c-MSCs and uncoated MSCs in osteogenic conditions when compared to the c-MSCs and uncoated MSCs in basal medium (BM). To analyze the adipogenic differentiation, the cells were stained with oil red S stain which would stain the lipid present in the cells. These experiments did not reveal any significant differences in the adipogenic differentiation between the c-MSCs and uncoated MSCs, as seen in Figure 27 F&G. The c-MSCs and uncoated MSCs did not show any adipogenic differentiation in the basal medium conditions. (Figure 27 E&H) To confirm this, we analyzed the mRNA levels of the adipogenic markers (PPARG, LPL) in the c-MSCs and uncoated MSCs. The mRNA levels correlated with the oil red stain S results and elevated levels of PPARG and LPL were observed in the c-MSCs and uncoated MSCs in adipogenic conditions when compared to the cells grown in basal medium conditions. These results taken together show that the H/G coating of the MSCs does not hinder the differentiation potential of the MSCs.

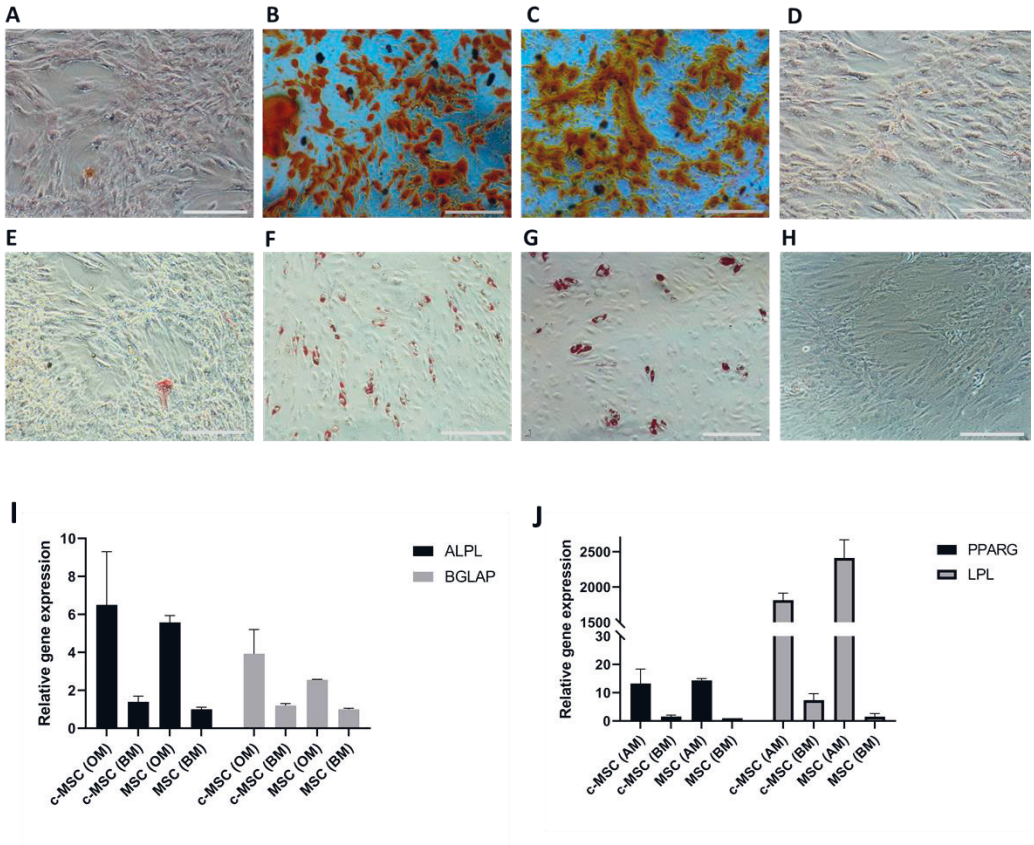

Figure 27. Differentiation potential of the c-MSCs and uncoated MSCs. Alizarin red staining was used to stain the calcium deposits formed in (A) c-MSCs in basal medium, (B) c-MSCs in osteogenic medium, (C) Uncoated MSCs in osteogenic medium, and (D) uncoated MSCs in basal medium. Oil red S stain was used to stain the lipids present in (E) c-MSCs in basal medium, (F) c-MSCs in adipogenic medium, (G) Uncoated MSCs in adipogenic medium, and (H) uncoated MSCs in basal medium. Scale bar- 500 µm. mRNA levels of (I) osteogenic markers and (J) adipogenic markers. AM= adipogenic medium OM= osteogenic medium BM= basal medium

5.4 Designing ECM mimetic hydrogel scaffold with immunosuppressive characteristics

In **Publication IV**, we made a hyaluronic acid-based extracellular matrix mimetic injectable scaffold that is grafted with immunomodulatory gallol moiety.

First, we evaluated the biocompatibility of these hydrogels by encapsulating CRL2429 fibroblast cells in both HA-HA and HA-GA hydrogels. The

biocompatibility assays were performed by Live/dead staining and we observed that both the HA-GA and HA-HA gels were highly compatible for these cells for up to two weeks when encapsulated. (Figure 28A) We then encapsulated the primary mouse BMDM in these hydrogels and observed no significant toxicity at the respective time points. Further, we also encapsulated MSCs in these hydrogels and measured the DNA content of these cells using CyQuant cell proliferation assays. These experiments revealed that the MSCs were viable and proliferating from day 1 to day 21 in HA-HA gels. However, in the HA-GA gels, the MSCs showed slower proliferation between days 1 and 14 compared to the HA-HA gels and subsequently showed an increase in the proliferation up to day 21. This reduction in the proliferation ability of MSCs in the HA-GA gels could be attributed to the inhibitory effect of gallol on MSC proliferation.[225] We then evaluated the antioxidant effects of the HA-GA on CRL2429 cells. (Figure 28B,C) For this purpose, we incubated the components of the hydrogels (HA-CDH and HA-GA-CDH) with these cells in the presence or absence of 200 μM hydrogen peroxide (H_2O_2). We observed a reduction in the cell viability (~50% reduction) when the cells were exposed to the H_2O_2 without the hydrogel components. We observed a similar reduction (~55%) in the cell viability when the cells were treated with HA-CDH (1 mg/mL) and then exposed to H_2O_2. Interestingly, when the cells were treated with HA-GA (1 mg/mL) and then exposed to the H_2O_2, we observed that there was only ~36% reduction in cell viability when compared to ~50-55% in the non-treated controls and the HA-CDH group. This clearly suggests that the GA moiety in the HA-GA polymer contributed to the radical scavenging property when exposed to H_2O_2.

To further validate the antioxidant property in the hydrogels, we performed 3D cellular oxidative stress measurement experiments. The CRL2429 cells were encapsulated in the HA-GA and HA-HA hydrogels and then exposed to 250 μM H_2O_2. In the HA-HA gels, the CRL2429 cells showed the effects of oxidative stress and the cell viability was observed to be around 50% when compared to the no H_2O_2 treated HA-HA gel. As expected, in the HA-GA hydrogels there was higher cell viability when treated with H_2O_2 when compared to the HA-GA gels that were not treated with H_2O_2. These experiments clearly suggest that the GA moiety in the hydrogel network shielded the encapsulated cells from oxidative stress by scavenging free radicals induced by the addition of H_2O_2.

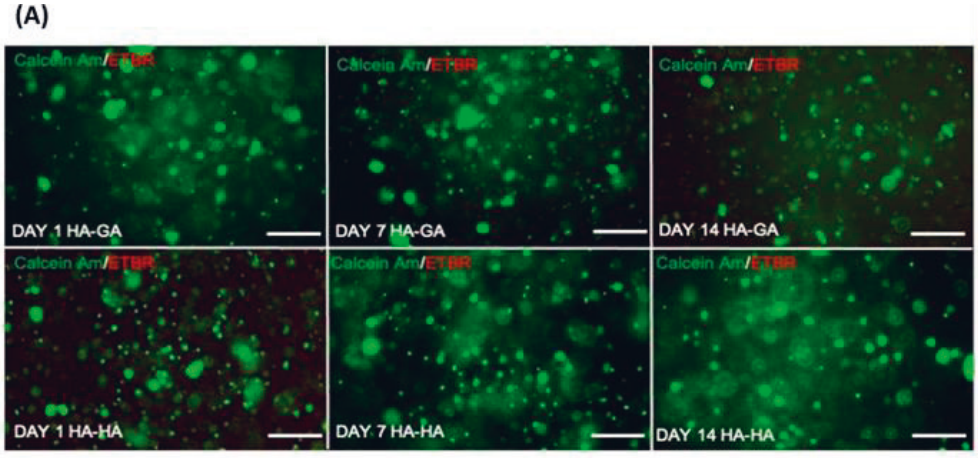
(A)
Calcein Am/ETBR
DAY 1 HA-GA
DAY 7 HA-GA
DAY 14 HA-GA
DAY 1 HA-HA
DAY 7 HA-HA
DAY 14 HA-HA

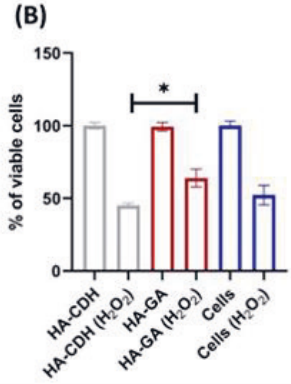
(B)
% of viable cells
150
100
50
0
*
HA-CDH
HA-CDH (H2O2)
HA-GA
HA-GA (H2O2)
Cells
Cells (H2O2)

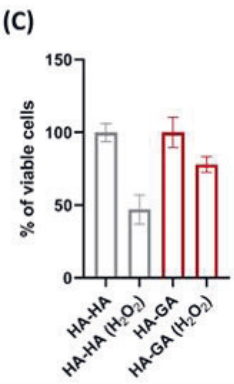
(C)
% of viable cells
150
100
50
0
HA-HA
HA-HA (H2O2)
HA-GA
HA-GA (H2O2)

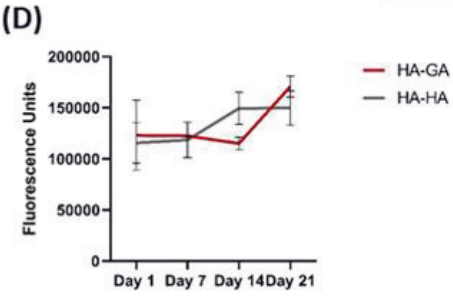
(D)
Fluorescence Units
200000
150000
100000
50000
0
Day 1
Day 7
Day 14
Day 21
HA-GA
HA-HA

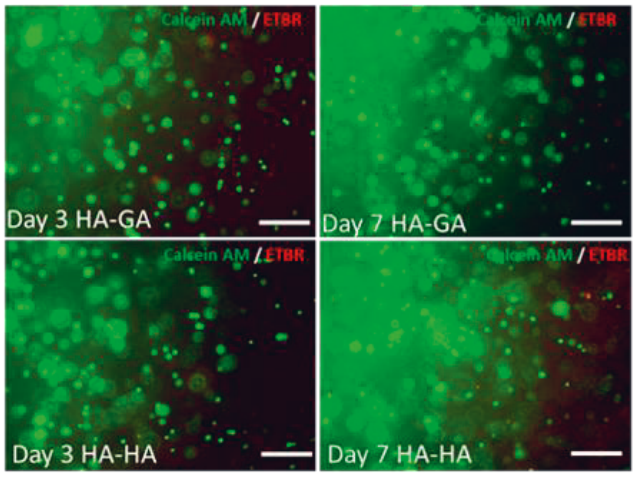
(E)
Calcein AM / ETBR
Day 3 HA-GA
Day 7 HA-GA
Day 3 HA-HA
Day 7 HA-HA

Figure 28. (A) LIVE/DEAD staining of CRL2429 fibroblasts encapsulated inside hydrogels on 1, 7, and 14 days of culture. Cells stained in green (Calcein AM) represent live cells while cells stained in red (EtBr) represent dead cells. (Scale bar = 500 μm, Cell density = 2×10^6/mL). (B) 2D monolayer and (C) 3D encapsulated cells Presto Blue viability assays showing the antioxidant effect of GA moieties on CRL2429 cells during induced oxidative stress. HA-GA improves cell viability during oxidative stress in (B) monolayer and (C) 3D cultures. (Cell density = 5×10^4 cells/well for 2D (n = 6) and 2×10^6/mL for 3D cultures, (n = 3)). Statistical analysis used the Mann-Whitney Test *P<0.05. (D) CyQuant Cell proliferation assay of MSCs encapsulated in HA-HA and HA-GA gels over a time period. (E) Live dead assay of murine bone marrow-derived macrophages in HA-HA and HA-GA hydrogels at Day 3 and Day 7. (Scale bar = 500 μm, Cell density = 2×10^6/mL)

To assess the immunomodulatory property of the HA-GA hydrogel, we encapsulated human monocyte cell line THP-1 in the gels. The THP-1 cells were encapsulated in the HA-GA and HA-HA hydrogels without the addition of any differentiation factors or immunomodulatory agents. After 8 days in culture, we analyzed the expression of selected pro-inflammatory and anti-inflammatory genes. In the HA-GA gels, we observed a 125-fold increase in the IL10 and a 2.5-fold increase in the IL1ra when compared to the cells in HA-HA gels. (Figure 29) The increase in the IL10 and IL1ra suggests that the macrophages had polarized towards an immunosuppressive M2 phenotype. Interestingly, we observed a 20-fold increase in the proinflammatory IL1β in the HA-GA gels when compared to the HA-HA gels. It is important to consider that it is the net sum of inflammatory genes that determine the final macrophage activation phenotype, so the co-expression of both pro-inflammatory and immunosuppressive markers is expected. We believe that the substantial amount of IL10 produced by these cells in the HA-GA gels would inhibit the differentiation of the neighboring cells into pro-inflammatory by the suppression of proinflammatory genes through the IL10/STAT3 pathway [226] and thereby allowing the macrophage population to be self-regulating.[227] This property of the macrophages could be useful in reducing inflammation and could facilitate wound healing and tissue regeneration. The immunosuppressive macrophages are reported to mitigate tissue damage and promote recovery from conditions like spinal cord injury and myocardial ischemia.[228,229]

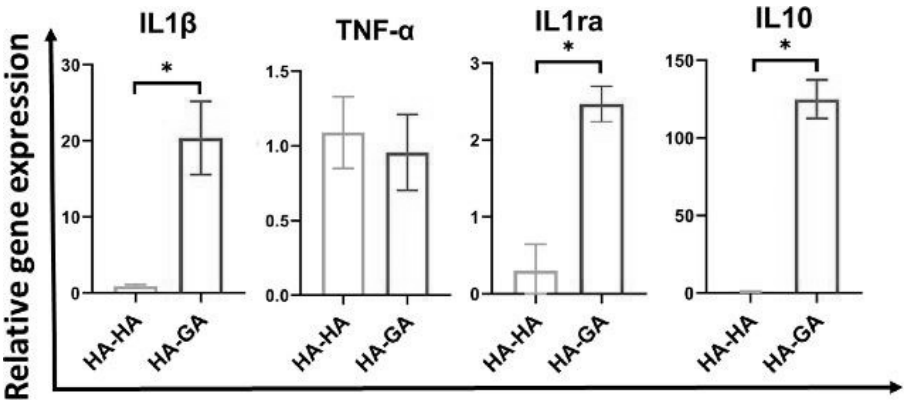

Figure 29. Gene expression analysis of pro-inflammatory markers TNF-α and IL-1β and anti-inflammatory markers IL-10 and IL-1ra in THP-1 cells encapsulated in HA-GA hydrogels for 8 days in basal medium, as compared to HA-HA gels. Expression of anti-inflammatory markers was increased in HA-GA gels as compared to HA-HA gels, suggesting increased immunosuppressive polarization (200 µL gels. THP-1 density = 4×10^6/mL, $n = 6$). Statistics used Mann-Whitney Test *P<0.05

To further confirm that the HA-GA hydrogels polarize macrophages towards the immunosuppressive phenotype, we encapsulated murine bone marrow-derived primary macrophages (BMDM) in their resting state (M0 macrophage) in the HA-GA and HA-HA gels for 10 days. The medium in which these cells were cultured was collected on day 1 and day 10 and analyzed using a multiplex bead-based assay for the cytokines released by the cells. (Figure 30 A&B) We observed that the cells in the HA-GA gels produced lower levels of pro-inflammatory cytokines like IL6 1.6 ± 0.5 ng/mL in HA-GA vs 2.5 ± 0.5 ng/mL in HA-HA), IL-12p40 (0.6 ± 0.4 ng/mL in HA-GA vs 3 ± 1 ng/mL in HA-HA) and MDC (1 ± 0.3 ng/mL in HA-GA vs 3 ± 1 ng/mL in HA-HA) when compared to the HA-HA gels. Interestingly, in the same samples, there was no significant difference in the levels of the anti-inflammatory genes TGF-β in both the HA-HA and HA-GA gels. When the day 10 mediums were analyzed, a similar trend was observed whereby the HA-GA gels had released significantly lower amounts of pro-inflammatory cytokines when compared to HA-HA gels. Specifically, IL-6 (187 ± 28 ng/mL in HA-HA vs 104 ± 5 ng/mL in HA-GA), IL-12p40 (174 ± 78 ng/mL in HA-HA vs 5 ± 2 ng/mL in HA-GA), MDC (284 ± 140 ng/mL in HA-HA vs 7 ± 3 ng/mL in HA-GA) and TNF-α (1086 ± 257 ng/mL in HA-HA vs 695 ± 45 ng/mL in HA-GA) expression were significantly lower in the HA-GA gels, while IL-18 released by both the gels was at similar levels. Unexpectedly, TGF-β was less abundant in the HA-GA gels (6 ± 2 ng/mL) compared to the HA-HA gels (36 ± 22 ng/mL). These

results indicate that HA-GA gels have the potential to drive BMDM towards a less inflammatory phenotype than do the HA-HA gels. We also did an mRNA level analysis of the genes by doing a qRT-PCR of the cells from the HA-HA and HA-GA gels. (Figure 30C) First, we observed that these cells matured into macrophages from their resting M0 phenotype in both the HA-GA and the HA-HA gels as evidenced by the equally present F4/80 murine macrophage marker. Interestingly, we observed an increase in the expression levels of anti-inflammatory genes; il10 (~2-fold), tgfb-1 (~3-fold), il4 (~1.5-fold), il4ra (~3-fold), and tgfb-r1 (~2.5-fold) in the HA-GA gels when compared to the cells in the HA-HA gels. As observed in the study with the THP-1 cells, we observed an increase in the expression levels of pro-inflammatory markers such as socs3 (~2-fold), il6 (~1.5-fold), and tnfa (~2.5-fold) in the HA-GA gels when compared to the cells in the HA-HA gels. The results obtained in the multiplex bead assay and the qRT-PCR concord with our hypothesis that the GA functionalization of HA could act as a cue to polarize the macrophages towards an immunosuppressive phenotype. The increase in the expression of proinflammatory markers could be attributed to the flexible phenotypic paradigms of the macrophages.[230] There have also been reports suggesting that the temporality and responsiveness of macrophage functions necessitate this flexibility, with M2-activated macrophages being able to display M1-like features or to repolarize completely.[231]

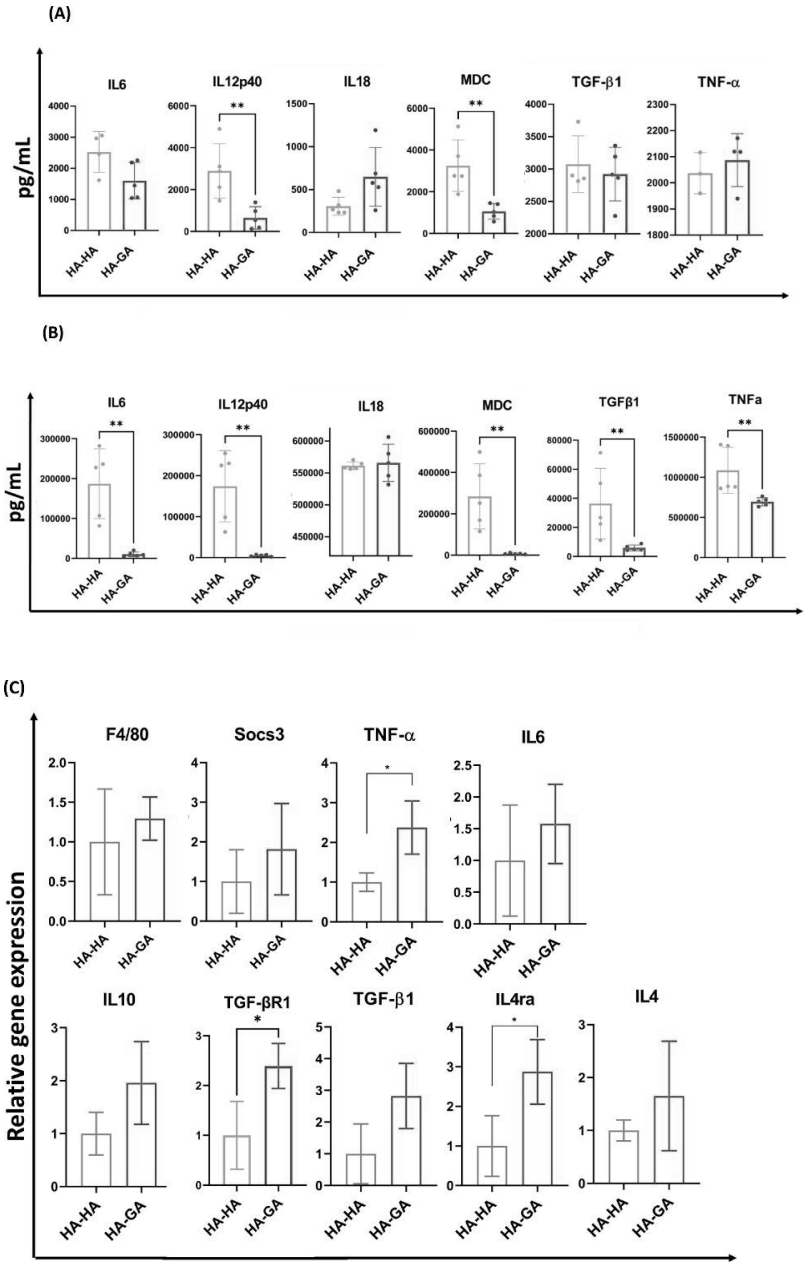

Figure 30. Cytokine release in the medium by the primary murine BMDM cells was analyzed by capture bead assay on (A) day 1 and (B) day 10. Statistical analysis was done by Mann-Whitney Test using GraphPad Prism. ***P*<0.01 (C) Cytokine mRNA levels produced by the BMDM cells as determined by qRT-PCR when encapsulated within HA-HA and HA-GA gels (*n* = 5) for 14 days. Statistical analysis using student T-test **P*<0.05.

Although the results with the M0 macrophages showed promising signs of the cells polarizing towards the immunosuppressive phenotype, the extent of the polarization was not very clear. For this purpose, we tested the immunosuppressive property of the gels by encapsulating BMDM that were differentiated towards a pro-inflammatory M1 phenotype. (Figure 31) As expected, we did observe a significant decrease in the pro-inflammatory genes like socs3, iNOS, and il6 and a non-significant decrease in tnfa and il1β in the HA-GA when compared to the HA-HA gels. Unexpectedly, we observed a decrease in the expression of il4 in the HA-GA gels when compared to the HA-HA gels. A significant decrease in the expression of chemokine-derived cx3cr1 was also observed. There have been studies that state the lower expression of cx3cr1 in the macrophages allows these cells to express both pro-inflammatory and anti-inflammatory markers.[232] These kinds of cells could be vital in the early and late stages of wound healing and repair in spinal cord injuries.[233] To further confirm these observations, we analyzed the medium in which these cells were cultured. The mediums were analyzed for different pro-inflammatory and anti-inflammatory cytokines using the multiplex bead-based assay. The observations from these experiments corroborated with the qRT-PCR results where we observed a significant decrease in the levels of the pro-inflammatory cytokines. Specifically, we observed a reduction in the levels of IL-23 (10 ± 3 ng/mL in HA-HA vs 4.5 ± 2 ng/mL in HA-GA), IL-6 (3.6 ± 1 ng/mL in HA-HA vs 1.7 ± 1 ng/mL in HA-GA), macrophage-derived chemokine (MDC; 39 ± 12 ng/mL in HA-HA vs 20 ± 8 ng/mL in HA-GA) and IL-12p40 (30 ± 4 ng/mL in HA-HA vs 15 ± 4 ng/mL in HA-GA) in the HA-GA gels when compared to the HA-HA gels. Unexpectedly, we observed an increase in the some of the pro-inflammatory markers such as TNF-α (16 ± 0.3 ng/mL in HA-HA vs 16 ± 0.4 ng/mL in HA-GA) and IL-18 (19 ± 7 ng/mL in HA-HA vs 42 ± 7 ng/mL in HA-GA) in the HA-GA gels when compared to the HA-HA gels. Interestingly, we also observed the there was an increase in the production of anti-inflammatory cytokines from the cells in the HA-GA gels when compared to the HA-HA gels. The levels of granulocyte colony stimulating factors (20 ± 7 ng/mL in HA-HA vs 40 ± 11 ng/mL in HA-GA), IL-10 (9 ± 4 ng/mL in HA-HA vs 14 ± 9 ng/mL in HA-GA) and TGF-β (5 ± 2 ng/mL in HA-HA vs 16 ± 7 ng/mL in HA-GA) were found to be higher in the HA-GA gels. The qRT-PCR results together with the multiplex bead-based assay results clearly suggest that the HA-GA gels predominantly possess an immunosuppressive characteristic compared to the HA-HA gels.

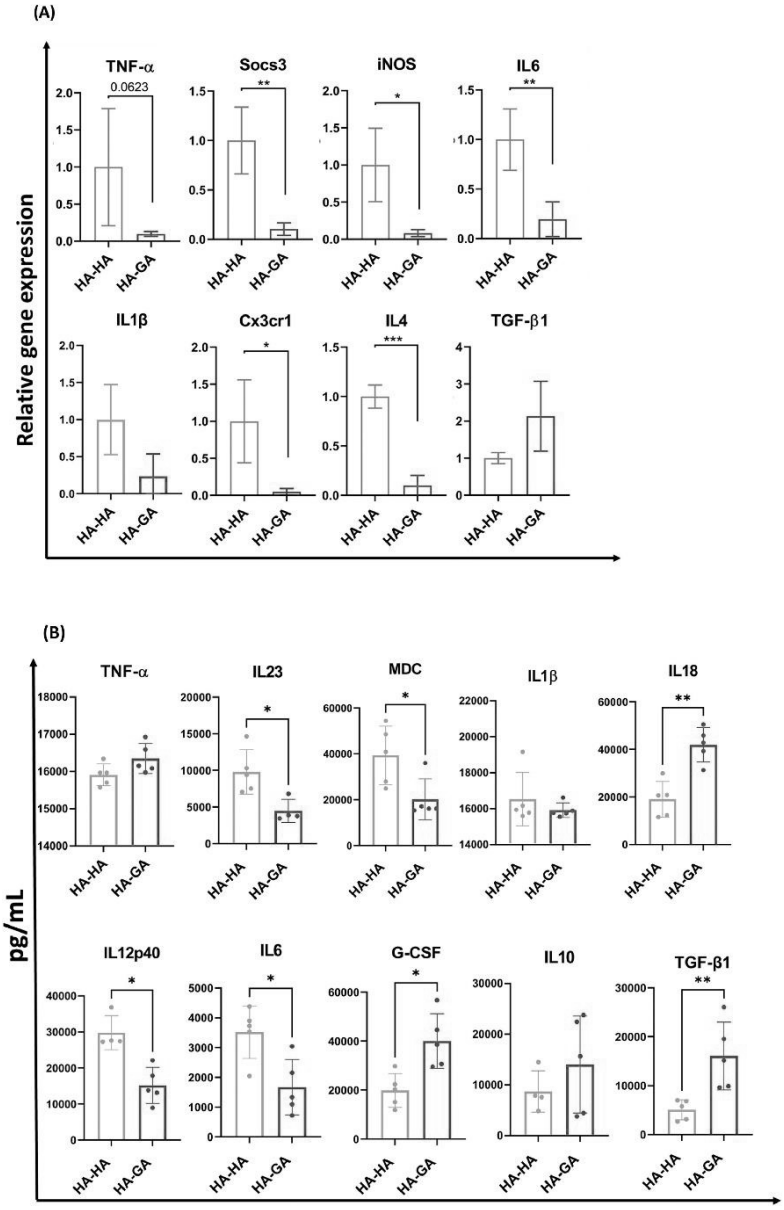

Figure 31. (A) Primary murine BMDM cells were stimulated with LPS/IFNγ for 16 h and then encapsulated in HA-HA and HA-GA gels (n = 4) for 3 days. The expression of different inflammatory markers was determined by qRT-PCR. Statistics were done by T-test using GraphPad Prism. *P<0.05, **P<0.005, ***P<0.001 (B) Cytokine present in the medium detected by multiplex bead-based assay after 3 days. Statistical analysis used Mann-Whitney Test. *P<0.05, **P<0.01.

Unlike **Publications I, II, and III**, in **Publication IV**, the HA-GA hydrogel was not designed to evade the systemic immune. These hydrogel scaffolds were designed to modulate the immune system. As seen in the literature review section, any biomaterial when implanted into the body triggers the innate immune system and activates the pro-inflammatory immune cells that accumulate at the site of the implantation ultimately leading to the failure of the biomaterial. In our case, we injected the HA-HA and HA-GA gels into two different subcutaneous pockets in healthy C57BL/6 mice and analyzed the immune cells recruited by these gels. Five days after implantation when these gels were recovered and the cells that infiltrated the gels were harvested, stained, and analyzed by flow cytometry, we were surprised to find that the HA-GA gels had attracted more myeloid cells ($CD45^+CD11^+$) cells relative to the HA-HA gels. When these cells were analyzed further for the proinflammatory markers CD86 and MHCII (major histocompatibility factor), it was observed that the HA-GA gels had lower amounts of cells expressing $CD86^+MHCII^+$ when compared to the HA-HA gels. A similar trend was observed when analyzed for $CD86^+MHCII^+CD40^+$ expressing cells, where HA-GA gels has a significantly lower number of cells expressing when compared to the HA-HA gels. (Figure 32) It is our belief that the intrinsic property of the HA-GA gel to stimulate the immune cells to produce IL-10 could be responsible for the lower amount of $CD86^+MHCII^+$ cells.[234] Interestingly, when we left the hydrogels for a longer period of 10 days in the subcutaneous pockets of the mice, we found that the HA-GA gels were completely resorbed and the HA-HA gels were intact. We speculate that this unique degradation could be attributed to the higher number of M2-like macrophages in the cells recruited by the HA-GA gels. It has also been reported that such fast degradations have been observed in collagen-containing scaffolds in mice which was attributed to the M2-like macrophages that are known to dramatically enhance the turnover of extracellular matrix through intracellular pathways.[235] Thus these, results show that we have designed a hydrogel scaffold that could modulate the systemic immune system reaction and succeed in bringing an immunosuppressive environment in its surroundings.

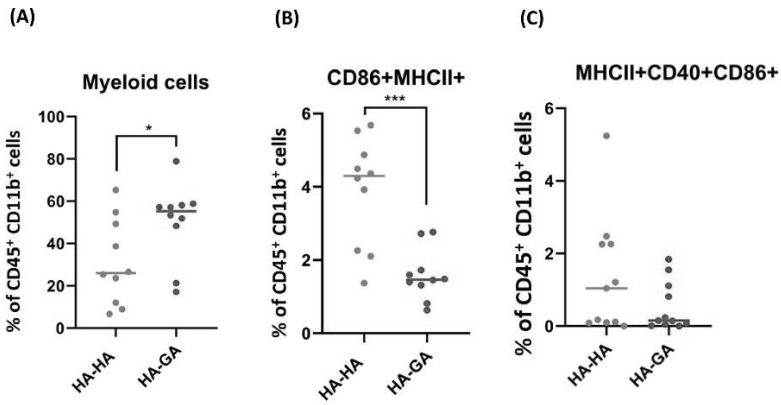

Figure 32. Flow cytometric analysis of the cells recruited into the HA-HA and the HA-GA hydrogels when implanted subcutaneously in C57L/B6 mice. The hydrogels were excised and the cells recovered after the dissolution of the hydrogels using hyaluronidase enzyme. The cells were then stained with CD86, MHCII, CD40, and CD45 antibodies and analyzed using flow cytometry. Statistics used student T-test. **P*<0.05, ***P*<0.005, ****P*<0.0005.

Furthermore, as seen above the HA-GA recruited a lower number of pro-inflammatory macrophages compared to HA-HA gels when implanted in subcutaneous pockets in mice. These results clearly suggest that GA functionalized gels display radical scavenging activity and promote polarization of macrophages into an immunosuppressive phenotype have great potential to be used as scaffolds for regenerative therapies. The ability of the HA-GA gels to suppress the major pro-inflammatory genes and an increase in the TGF-β and IL-10 suggests that these hydrogels may be a valuable tool for tissue engineering applications, especially for wound healing during which suppression of inflammation is crucial.

6 CONCLUSIONS

In conclusion, the findings from the study presented in this thesis prove that glycosaminoglycan derived polymers such as hyaluronic acid and heparin are a valuable building block with diverse bioactivity and cellular function for engineering different materials. We have successfully exploited these polymers for engineering nanocarriers, bulk hydrogels and used them to encapsulate stem cells and have shown that they can modulate the immune system. Specifically, the findings from the four studies in this dissertation show that

1) nanocarriers designed using HA can be successfully used to provide stealth properties that evade the systemic immune system, that allow controlled drug release and modulate immune response. For example, the study in **Publication I** can be used in cancer treatment. The combined delivery of an immunosuppressive drug and chemotherapeutic drug using a tumor targeting nanoparticle could help in mitigating the side effects of chemotherapy. Moreover, apart from inducing DOX mediated cytotoxicity, our nanoparticle was also shown to manipulate the TAMs to release pro-inflammatory cytokines which could lead to the faster elimination of the tumor.

2) synthetic block polymers such as pluronic F108 can also be used to design nanocarriers for siRNA delivery that successfully silenced tissue factor gene that enhancing the safety and function of these therapeutic cells. For example, in **Publication II**, the silencing of TF lead to the MSCs being more hemocompatible and to our surprise it enhanced the functions and the differentiation potential of the MSCs.

3) in **Publication III**, we show that biopolymers such as gelatin and heparin can be exploited to engineer stem cells that overcome thrombotic risk associated with stem cell transplantation thus making them more compatible for clinical applications.

4) the biomaterials can be used to create an immunosuppressive environment suitable for wound healing and tissue regeneration. For example, **Publication IV**, show that GA functionalized hydrogel display antioxidant properties and immunosuppressive properties by polarizing macrophages to an immunosuppressive phenotype, thus has great potential for regenerative medicine and for designing living scaffold with stem cells. The GA functionalized hydrogels

suppressed major pro-inflammatory genes in the endotoxin stimulated macrophages. They also showed increase in anti-inflammatory gene expression in the endotoxin stimulated macrophages, suggesting that these hydrogels could be a valuable tool for wound healing and other tissue engineering applications.

The findings of this thesis also show that the manipulation of the immune system has a huge potential for treating various diseases. The manipulation of the immune system however needs spatiotemporal control of the immune activity, which is currently difficult to provide in the traditional treatment methods. The ability of the biomaterial scaffolds to provide spatiotemporal control of immune activity makes them perfectly suited for these applications. For example, in the case of cancer immunotherapy, the immunotherapeutic agents react differently in patients with cancer.[236] The ability of biomaterials to be flexible and tailored in different ways, could help in increasing the efficacy of these immunotherapeutic agents. To make these biomaterial-based immunotherapies successful in the transition to the clinic, the biomaterials require new design approaches so they could be fabricated for each patient group or even individual patients. In the case of tissue regeneration or wound healing, a balance between the pro-inflammatory activities and anti-inflammatory activities. The design of the biomaterials in these cases also would depend on the severity and complexity of the wound. With the evolution of 3D printing and synthetic biology, these could be integrated into the design of future biomaterials in tissue engineering and wound healing. The lessons learned from designing biomaterials for cancer immunotherapy and tissue engineering could be translated to other complex diseases like autoimmune and neurodegenerative diseases. Thus, the future of medicine could be heavily reliant on the development and the advancement of biomaterials.

REFERENCES

1. Dhandayuthapani, B., Yoshida, Y., Maekawa, T. & Kumar, D. S. Polymeric scaffolds in tissue engineering application: A review. *International Journal of Polymer Science* vol. 2011 (2011).
2. Wiles, K., Fishman, J. M., De Coppi, P. & Birchall, M. A. The host immune response to tissue-engineered organs: Current problems and future directions. *Tissue Engineering - Part B: Reviews* vol. 22 208–219 (2016).
3. Roseti, L. *et al.* Scaffolds for Bone Tissue Engineering: State of the art and new perspectives. *Materials Science and Engineering C* vol. 78 1246–1262 (2017).
4. Keselowsky, B. G., Collard, D. M. & García, A. J. Surface chemistry modulates focal adhesion composition and signaling through changes in integrin binding. *Biomaterials* **25**, 5947–5954 (2004).
5. Gasperini, L., Mano, J. F. & Reis, R. L. Natural polymers for the microencapsulation of cells. *Journal of the Royal Society Interface* vol. 11 (2014).
6. Matlaga, B. F., Yasenchak, L. P. & Salthouse, T. N. Tissue response to implanted polymers: The significance of sample shape. *J. Biomed. Mater. Res.* **10**, 391–397 (1976).
7. Yuan, Y., Lin, D., Chen, F. & Liu, C. Clinical translation of biomedical materials and the key factors towards product registration. *J. Orthop. Transl.* **2**, 49–55 (2014).
8. Mariani, E., Lisignoli, G., Borzì, R. M. & Pulsatelli, L. Biomaterials: Foreign bodies or tuners for the immune response? *International Journal of Molecular Sciences* vol. 20 (2019).
9. Italiani, P. & Boraschi, D. New Insights Into Tissue Macrophages: From Their Origin to the Development of Memory. *Immune Netw.* **15**, 167 (2015).
10. Wynn, T. A. & Vannella, K. M. Macrophages in Tissue Repair, Regeneration, and Fibrosis. *Immunity* **44**, 450–462 (2016).
11. Stabler, C. L., Li, Y., Stewart, J. M. & Keselowsky, B. G. Engineering immunomodulatory biomaterials for type 1 diabetes. *Nat. Rev. Mater. 2019 46* **4**, 429–450 (2019).
12. Bloise, N. *et al.* Engineering Immunomodulatory Biomaterials for Regenerating the Infarcted Myocardium. *Front. Bioeng. Biotechnol.* **8**, 292 (2020).
13. Vishwakarma, A. *et al.* Engineering Immunomodulatory Biomaterials To Tune the Inflammatory Response. *Trends in Biotechnology* vol. 34 470–482 (2016).
14. Whitaker, R., Hernaez-Estrada, B., Hernandez, R. M., Santos-Vizcaino, E. & Spiller, K. L. Immunomodulatory Biomaterials for Tissue Repair. *Chem. Rev.* **121**, 11305–11335 (2021).
15. Roitt, I., Delves, P., Martin, S. & Burton, D. Roitt's Essential Immmonology. (2016).
16. Vanguri, V. K. The Adaptive Immune System. in *Pathobiology of Human Disease: A Dynamic Encyclopedia of Disease Mechanisms* 1–4 (Garland Science, 2014). doi:10.1016/B978-0-12-386456-7.01101-1.
17. Anderson, J. M., Rodriguez, A. & Chang, D. T. Foreign body reaction to biomaterials. *Seminars in Immunology* vol. 20 86–100 (2008).
18. Boccafoschi, F., Mosca, C. & Cannas, M. Cardiovascular biomaterials: When the inflammatory response helps to efficiently restore tissue functionality? *Journal of Tissue Engineering and Regenerative Medicine* vol. 8 253–267 (2014).
19. Wilson, C. J., Clegg, R. E., Leavesley, D. I. & Pearcy, M. J. Mediation of biomaterial-cell interactions by adsorbed proteins: A review. *Tissue Engineering* vol. 11 1–18 (2005).
20. Milleret, V. *et al.* Protein adsorption steers blood contact activation on engineered cobalt chromium alloy oxide layers. *Acta Biomater.* **24**, 343–351 (2015).
21. Vitte, J., Benoliel, A. M., Pierres, A., Bongrand, P. & Curtis, A. S. G. Is there a predictable relationship between surface physical-chemical properties and cell behaviour at the interface? *Eur. Cells Mater.* **7**, 52–63 (2004).
22. Anderson, J. M., Rodriguez, A. & Chang, D. T. Foreign body reaction to biomaterials. *Semin.*

Immunol. **20**, 86–100 (2008).
23. Nilsson, B., Ekdahl, K. N., Mollnes, T. E. & Lambris, J. D. The role of complement in biomaterial-induced inflammation. *Mol. Immunol.* **44**, 82–94 (2007).
24. Ekdahl, K. N. *et al.* Innate immunity activation on biomaterial surfaces: a mechanistic model and coping strategies. *Adv. Drug Deliv. Rev.* **63**, 1042–1050 (2011).
25. Leonard, E. F. & Vroman, L. Is the Vroman effect of importance in the interaction of blood with artificial materials? *J. Biomater. Sci. Polym. Ed.* **3**, 95–107 (1992).
26. Chen, X., Chen, J. & Huang, N. The structure, formation, and effect of plasma protein layer on the blood contact materials: A review. *Biosurface and Biotribology* **8**, 1–14 (2022).
27. Zhang, L. *et al.* Zwitterionic hydrogels implanted in mice resist the foreign-body reaction. *Nat. Biotechnol. 2013 316* **31**, 553–556 (2013).
28. Liu, Q. *et al.* Developing mechanically robust, triazole-zwitterionic hydrogels to mitigate foreign body response (FBR) for islet encapsulation. *Biomaterials* **230**, 119640 (2020).
29. Keselowsky, B. G. *et al.* Role of plasma fibronectin in the foreign body response to biomaterials. *Biomaterials* **28**, 3626–3631 (2007).
30. Swartzlander, M. D. *et al.* Linking the foreign body response and protein adsorption to PEG-based hydrogels using proteomics. *Biomaterials* **41**, 26–36 (2015).
31. Herant, M., Heinrich, V. & Dembo, M. Mechanics of neurophil phagocytosis: Experiments and quantitative models. *J. Cell Sci.* **119**, 1903–1913 (2006).
32. Jhunjhunwala, S. *et al.* Neutrophil responses to sterile implant materials. *PLoS One* **10**, e0137550 (2015).
33. Labow, R. S., Meek, E. & Santerre, J. P. Neutrophil-mediated biodegradation of medical implant materials. *J. Cell. Physiol.* **186**, 95–103 (2001).
34. Brinkmann, V. *et al.* Neutrophil Extracellular Traps Kill Bacteria. *Science (80-.).* **303**, 1532–1535 (2004).
35. Kolaczkowska, E. & Kubes, P. Neutrophil recruitment and function in health and inflammation. *Nat. Rev. Immunol.* **13**, 159–175 (2013).
36. Selders, G. S., Fetz, A. E., Radic, M. Z. & Bowlin, G. L. An overview of the role of neutrophils in innate immunity, inflammation and host-biomaterial integration. *Regen. Biomater.* **4**, 55–68 (2017).
37. Fetz, A. E., Neeli, I., Rodriguez, I. A., Radic, M. Z. & Bowlin, G. L. Electrospun Template Architecture and Composition Regulate Neutrophil NETosis in Vitro and in Vivo. *Tissue Eng. - Part A* **23**, 1054–1063 (2017).
38. Doloff, J. C. *et al.* Colony stimulating factor-1 receptor is a central component of the foreign body response to biomaterial implants in rodents and non-human primates. *Nat. Mater. 2017 166* **16**, 671–680 (2017).
39. Veiseh, O. *et al.* Size- and shape-dependent foreign body immune response to materials implanted in rodents and non-human primates. *Nat. Mater. 2014 146* **14**, 643–651 (2015).
40. Yamashiro, S. *et al.* Phenotypic and functional change of cytokine-activated neutrophils: inflammatory neutrophils are heterogeneous and enhance adaptive immune responses. *J. Leukoc. Biol.* **69**, 698–704 (2001).
41. Witherel, C. E., Abebayehu, D., Barker, T. H. & Spiller, K. L. Macrophage and Fibroblast Interactions in Biomaterial-Mediated Fibrosis. *Adv. Healthc. Mater.* **8**, (2019).
42. Jones, J. A. *et al.* Proteomic analysis and quantification of cytokines and chemokines from biomaterial surface-adherent macrophages and foreign body giant cells. *J. Biomed. Mater. Res. A* **83**, 585–596 (2007).
43. Broughton, G., Janis, J. E. & Attinger, C. E. The basic science of wound healing. *Plast. Reconstr. Surg.* **117**, (2006).
44. Zhao, Q. *et al.* Foreign-body giant cells and polyurethane biostability: in vivo correlation of cell adhesion and surface cracking. *J. Biomed. Mater. Res.* **25**, 177–183 (1991).
45. Mooney, J. E. *et al.* Cellular Plasticity of Inflammatory Myeloid Cells in the Peritoneal Foreign Body Response. *Am. J. Pathol.* **176**, 369–380 (2010).
46. Dondossola, E. *et al.* Examination of the foreign body response to biomaterials by nonlinear intravital microscopy. *Nat. Biomed. Eng. 2016 11* **1**, 1–10 (2016).
47. Amer, L. D. *et al.* Inflammation via myeloid differentiation primary response gene 88 signaling mediates the fibrotic response to implantable synthetic poly(ethylene glycol) hydrogels. *Acta Biomater.* **100**, 105–117 (2019).

48. Malik, A. F. *et al.* Inflammasome components Asc and caspase-1 mediate biomaterial-induced inflammation and foreign body response. *Proc. Natl. Acad. Sci. U. S. A.* **108**, 20095–20100 (2011).
49. Kyriakides, T. R. *et al.* The CC Chemokine Ligand, CCL2/MCP1, Participates in Macrophage Fusion and Foreign Body Giant Cell Formation. *Am. J. Pathol.* **165**, 2157–2166 (2004).
50. Johansson, H. ACTA UNIVERSITATIS UPSALIENSIS UPPSALA 2007. in.
51. Kourtzelis, I., Magnusson, P. U., Kotlabova, K., Lambris, J. D. & Chavakis, T. Regulation of Instant Blood Mediated Inflammatory Reaction (IBMIR) in pancreatic islet xeno-transplantation: Points for therapeutic interventions. *Adv. Exp. Med. Biol.* **865**, 171–188 (2015).
52. Ilinskaya, A. N. & Dobrovolskaia, M. A. Nanoparticles and the blood coagulation system. Part II: safety concerns. *Nanomedicine (Lond).* **8**, 969 (2013).
53. Amara, U. *et al.* Molecular Intercommunication between the Complement and Coagulation Systems. *J. Immunol.* **185**, 5628 (2010).
54. Hayama, M. *et al.* Nanoscopic behavior of polyvinylpyrrolidone particles on polysulfone/polyvinylpyrrolidone film. *Biomaterials* **25**, 1019–1028 (2004).
55. Jin, Z., Feng, W., Zhu, S., Sheardown, H. & Brash, J. L. Protein-resistant polyurethane by sequential grafting of poly(2-hydroxyethyl methacrylate) and poly(oligo(ethylene glycol) methacrylate) via surface-initiated ATRP. *J. Biomed. Mater. Res. A* **95**, 1223–1232 (2010).
56. Futamura, K., Matsuno, R., Konno, T., Takai, M. & Ishihara, K. Rapid development of hydrophilicity and protein adsorption resistance by polymer surfaces bearing phosphorylcholine and naphthalene groups. *Langmuir* **24**, 10340–10344 (2008).
57. Liu, X. *et al.* Blood compatible materials: state of the art. *J. Mater. Chem. B* **2**, 5718–5738 (2014).
58. Johansson, H. *et al.* Low molecular weight dextran sulfate: A strong candidate drug to block IBMIR in clinical islet transplantation. *Am. J. Transplant.* **6**, 305–312 (2006).
59. Goto, M. *et al.* Low molecular weight dextran sulfate prevents the instant blood-mediated inflammatory reaction induced by adult porcine islets. *Transplantation* **77**, 741–747 (2004).
60. Study to Evaluate Safety and Efficacy of IBsolvMIR in Islet Transplantation. *Case Med. Res.* (2019) doi:10.31525/ct1-nct03867851.
61. Cabric, S. *et al.* A New Method for Incorporating Functional Heparin onto the Surface of Islets of Langerhans. *Tissue Eng. Part C. Methods* **14**, 141 (2008).
62. Cabric, S. *et al.* Islet Surface Heparinization Prevents the Instant Blood-Mediated Inflammatory Reaction in Islet Transplantation. *Diabetes* **56**, 2008–2015 (2007).
63. Teramura, Y. & Iwata, H. Surface modification of islets with PEG-lipid for improvement of graft survival in intraportal transplantation. *Transplantation* **88**, 624–630 (2009).
64. Mellman, I., Coukos, G. & Dranoff, G. Cancer immunotherapy comes of age. *Nat. 2011 4807378* **480**, 480–489 (2011).
65. Chen, D. S. & Mellman, I. Oncology meets immunology: the cancer-immunity cycle. *Immunity* **39**, 1–10 (2013).
66. Hinshaw, D. C. & Shevde, L. A. The tumor microenvironment innately modulates cancer progression. *Cancer Res.* **79**, 4557–4567 (2019).
67. Kim, J. & Bae, J. S. Tumor-associated macrophages and neutrophils in tumor microenvironment. *Mediators of Inflammation* vol. 2016 (2016).
68. Zeng, X. Y. *et al.* M2-like tumor-associated macrophages-secreted EGF promotes epithelial ovarian cancer metastasis via activating EGFR-ERK signaling and suppressing lncRNA LIMT expression. *Cancer Biol. Ther.* **20**, 956 (2019).
69. Goswami, S. *et al.* Macrophages promote the invasion of breast carcinoma cells via a colony-stimulating factor-1/epidermal growth factor paracrine loop. *Cancer Res.* **65**, 5278–5283 (2005).
70. Wyckoff, J. *et al.* A paracrine loop between tumor cells and macrophages is required for tumor cell migration in mammary tumors. *Cancer Res.* **64**, 7022–7029 (2004).
71. Zheng, X. *et al.* Redirecting tumor-associated macrophages to become tumoricidal effectors as a novel strategy for cancer therapy. *Oncotarget* **8**, 48436–48452 (2017).
72. Petrova, V., Annicchiarico-Petruzzelli, M., Melino, G. & Amelio, I. The hypoxic tumour microenvironment. *Oncog. 2018 71* **7**, 1–13 (2018).
73. Hanna, A. *et al.* Inhibition of Hedgehog signaling reprograms the dysfunctional immune microenvironment in breast cancer. *Oncoimmunology* **8**, (2018).
74. Collin, M. & Bigley, V. Human dendritic cell subsets: an update. *Immunology* **154**, 3–20 (2018).
75. Gandhi Huang, C. R. *et al.* Induction of IDO Dendritic Cells via STAT3-Dependent

Allostimulatory Function of Liver Myeloid Hepatic Stellate Cells Undermine the. *J Immunol* **189**, 3848–3858 (2012).
76. Motta, J. M. & Rumjanek, V. M. Sensitivity of dendritic cells to microenvironment signals. *Journal of Immunology Research* vol. 2016 (2016).
77. Aspord, C. *et al.* Breast cancer instructs dendritic cells to prime interleukin 13-secreting CD4+ T cells that facilitate tumor development. *J. Exp. Med.* **204**, 1037–1047 (2007).
78. Chaput, N., Conforti, R., Viaud, S., Spatz, A. & Zitvogel, L. The Janus face of dendritic cells in cancer. *Oncogene 2008 2745* **27**, 5920–5931 (2008).
79. Fridlender, Z. G. & Albelda, S. M. Tumor-associated neutrophils: friend or foe? *Carcinogenesis* **33**, 949–955 (2012).
80. He, M. *et al.* Peritumoral stromal neutrophils are essential for c-Met-elicited metastasis in human hepatocellular carcinoma. *Oncoimmunology* **5**, (2016).
81. Demers, M. *et al.* Priming of neutrophils toward NETosis promotes tumor growth. *Oncoimmunology* **5**, (2016).
82. Flügge, U. I., Westhoff, P. & Leister, D. Recent advances in understanding photosynthesis. *F1000Research* vol. 5 (2016).
83. Stabile, H., Fionda, C., Gismondi, A. & Santoni, A. Role of distinct natural killer cell subsets in anticancer response. *Frontiers in Immunology* vol. 8 (2017).
84. Imai, K., Matsuyama, S., Miyake, S., Suga, K. & Nakachi, K. Natural cytotoxic activity of peripheral-blood lymphocytes and cancer incidence: an 11-year follow-up study of a general population. *Lancet (London, England)* **356**, 1795–1799 (2000).
85. Jacobs, N., Langers, Renoux, Thiry & Delvenne. Natural killer cells: role in local tumor growth and metastasis. *Biol. Targets Ther.* **6**, 73 (2012).
86. Pickup, M. W., Mouw, J. K. & Weaver, V. M. The extracellular matrix modulates the hallmarks of cancer. *EMBO Rep.* **15**, 1243–1253 (2014).
87. Lakins, M. A., Ghorani, E., Munir, H., Martins, C. P. & Shields, J. D. Cancer-associated fibroblasts induce antigen-specific deletion of CD8 + T Cells to protect tumour cells. *Nat. Commun.* **9**, 1–9 (2018).
88. Institute, N. C. Immune System Modulators for Cancer Therapy. https://www.cancer.gov/about-cancer/treatment/types/immunotherapy/immune-system-modulators.
89. Lu, W. *et al.* Reprogramming immunosuppressive myeloid cells facilitates immunotherapy for colorectal cancer. *EMBO Mol. Med.* **13**, e12798 (2021).
90. Zheng, Y. *et al.* Reprogramming Tumor-Associated Macrophages via ROS-Mediated Novel Mechanism of Ultra-Small Cu2−xSe Nanoparticles to Enhance Anti-Tumor Immunity. *Adv. Funct. Mater.* **32**, 2108971 (2022).
91. McKinlay, C. J. *et al.* Charge-altering releasable transporters (CARTs) for the delivery and release of mRNA in living animals. *Proc. Natl. Acad. Sci. U. S. A.* **114**, E448–E456 (2017).
92. Cai, X. *et al.* Re-polarization of tumor-associated macrophages to pro-inflammatory M1 macrophages by microRNA-155. *J. Mol. Cell Biol.* **4**, 341–343 (2012).
93. Kamerkar, S. *et al.* Exosome-mediated genetic reprogramming of tumor-associated macrophages by exoASO-STAT6 leads to potent monotherapy antitumor activity. *Sci. Adv.* **8**, 7002 (2022).
94. Forbes, S. J. & Rosenthal, N. Preparing the ground for tissue regeneration: from mechanism to therapy. *Nat. Med. 2014 208* **20**, 857–869 (2014).
95. Kono, H., Onda, A. & Yanagida, T. Molecular determinants of sterile inflammation. *Curr. Opin. Immunol.* **26**, 147–156 (2014).
96. Julier, Z., Park, A. J., Briquez, P. S. & Martino, M. M. Promoting tissue regeneration by modulating the immune system. *Acta Biomaterialia* vol. 53 13–28 (2017).
97. Hirsiger, S., Simmen, H. P., Werner, C. M. L., Wanner, G. A. & Rittirsch, D. Danger signals activating the immune response after trauma. *Mediators of Inflammation* vol. 2012 (2012).
98. Adair-Kirk, T. L. & Senior, R. M. Fragments of extracellular matrix as mediators of inflammation. *International Journal of Biochemistry and Cell Biology* vol. 40 1101–1110 (2008).
99. Takeuchi, O. & Akira, S. Pattern Recognition Receptors and Inflammation. *Cell* **140**, 805–820 (2010).
100. Tang, S. C. *et al.* Pivotal role for neuronal Toll-like receptors in ischemic brain injury and functional deficits. *Proc. Natl. Acad. Sci.* **104**, 13798–13803 (2007).
101. Oyama, J. I. *et al.* Reduced Myocardial Ischemia-Reperfusion Injury in Toll-Like Receptor 4-

Deficient Mice. *Circulation* **109**, 784–789 (2004).
102. Dasu, M. R. & Rivkah Isseroff, R. Toll-like receptors in wound healing: Location, accessibility, and timing. *J. Invest. Dermatol.* **132**, 1955–1958 (2012).
103. Zemans, R. L. *et al.* Neutrophil transmigration triggers repair of the lung epithelium via β-catenin signaling. *Proc. Natl. Acad. Sci. U. S. A.* **108**, 15990–15995 (2011).
104. Kolaczkowska, E. & Kubes, P. Neutrophil recruitment and function in health and inflammation. *Nature Reviews Immunology* vol. 13 159–175 (2013).
105. Horckmans, M. *et al.* Neutrophils orchestrate post-myocardial infarction healing by polarizing macrophages towards a reparative phenotype. *Eur. Heart J.* **38**, 187–197 (2017).
106. Novak, M. L., Weinheimer-Haus, E. M. & Koh, T. J. Macrophage activation and skeletal muscle healing following traumatic injury. *J. Pathol.* **232**, 344–355 (2014).
107. Wynn, T. A. & Vannella, K. M. Macrophages in Tissue Repair, Regeneration, and Fibrosis. *Immunity* vol. 44 450–462 (2016).
108. Essandoh, K., Li, Y., Huo, J. & Fan, G. C. MiRNA-mediated macrophage polarization and its potential role in the regulation of inflammatory response. *Shock* vol. 46 122–131 (2016).
109. Vinish, M. *et al.* Dendritic cells modulate burn wound healing by enhancing early proliferation. *Wound Repair Regen.* **24**, 6–13 (2016).
110. Gregorio, J. *et al.* Plasmacytoid dendritic cells sense skin injury and promote wound healing through type i interferons. *J. Exp. Med.* **207**, 2921–2930 (2010).
111. Trujillo, G., Hartigan, A. J. & Hogaboam, C. M. T regulatory cells and attenuated bleomycin-induced fibrosis in lungs of CCR7-/- mice. *Fibrogenes. Tissue Repair 2010 31* **3**, 1–9 (2010).
112. Lei, H., Schmidt-Bleek, K., Dienelt, A., Reinke, P. & Volk, H. D. Regulatory T cell-mediated anti-inflammatory effects promote successful tissue repair in both indirect and direct manners. *Front. Pharmacol.* **6**, 184 (2015).
113. Nosbaum, A. *et al.* Cutting Edge: Regulatory T Cells Facilitate Cutaneous Wound Healing. *J. Immunol.* **196**, 2010–2014 (2016).
114. Lai, L. W., Yong, K. C. & Lien, Y. H. H. Pharmacologic recruitment of regulatory T cells as a therapy for ischemic acute kidney injury. *Kidney Int.* **81**, 983–992 (2012).
115. Moghimi, S. M. *et al.* Complement activation cascade triggered by PEG–PL engineered nanomedicines and carbon nanotubes: The challenges ahead. *J. Control. Release* **146**, 175–181 (2010).
116. Moein Moghimi, S. *et al.* Methylation of the phosphate oxygen moiety of phospholipid-methoxy(polyethylene glycol) conjugate prevents PEGylated liposome-mediated complement activation and anaphylatoxin production. *FASEB J.* **20**, 2591–2593 (2006).
117. Adler, A. *et al.* Effect of liposome surface modification with water-soluble phospholipid polymer chain-conjugated lipids on interaction with human plasma proteins. *J. Mater. Chem. B* **10**, 2512–2522 (2022).
118. Gurav, D. *et al.* Chondroitin sulfate coated gold nanoparticles: a new strategy to resolve multidrug resistance and thromboinflammation. *Chem. Commun.* **52**, 966–969 (2016).
119. Teramura, Y., Ekdahl, K. N., Fromell, K., Nilsson, B. & Ishihara, K. Potential of Cell Surface Engineering with Biocompatible Polymers for Biomedical Applications. *Langmuir* **36**, 12088–12106 (2020).
120. Asawa, K. *et al.* Cell Surface Functionalization with Heparin-Conjugated Lipid to Suppress Blood Activation. *Adv. Funct. Mater.* **31**, 2008167 (2021).
121. Nilsson, P. H. *et al.* Autoregulation of thromboinflammation on biomaterial surfaces by a multicomponent therapeutic coating. *Biomaterials* **34**, 985–994 (2013).
122. Yang, F. *et al.* Advanced biomaterials for cancer immunotherapy. *Acta Pharmacologica Sinica* vol. 41 911–927 (2020).
123. Stephan, S. B. *et al.* Biopolymer implants enhance the efficacy of adoptive T-cell therapy. *Nat. Biotechnol.* **33**, 97–101 (2015).
124. Fontana, F., Liu, D., Hirvonen, J. & Santos, H. A. Delivery of therapeutics with nanoparticles: what's new in cancer immunotherapy? *Wiley Interdisciplinary Reviews: Nanomedicine and Nanobiotechnology* vol. 9 (2017).
125. National Institutes of Health (NIH). Experimental mRNA HIV vaccine safe, shows promise in animals. *Press Release* https://www.nih.gov/news-events/news-releases/experimental-mrna-hiv-vaccine-safe-shows-promise-animals (2021).
126. Lai, C. *et al.* The enhanced antitumor-specific immune response with mannose- and CpG-ODN-

coated liposomes delivering TRP2 peptide. *Theranostics* **8**, 1723–1739 (2018).
127. Zhang, Y., Li, N., Suh, H. & Irvine, D. J. Nanoparticle anchoring targets immune agonists to tumors enabling anti-cancer immunity without systemic toxicity. *Nat. Commun.* **9**, 1–15 (2018).
128. Liu, L. *et al.* ROS-Inducing Micelles Sensitize Tumor-Associated Macrophages to TLR3 Stimulation for Potent Immunotherapy. *Biomacromolecules* **19**, 2146–2155 (2018).
129. Liu, Y. *et al.* Dual pH-responsive multifunctional nanoparticles for targeted treatment of breast cancer by combining immunotherapy and chemotherapy. *Acta Biomater.* **66**, 310–324 (2018).
130. Lee, H. *et al.* Dendritic cell-targeted ph-responsive extracellular vesicles for anticancer vaccination. *Pharmaceutics* **11**, 54 (2019).
131. Sohail, I. *et al.* Polyamidoamine (PAMAM) dendrimers synthesis, characterization and adsorptive removal of nickel ions from aqueous solution. *J. Mater. Res. Technol.* **9**, 498–506 (2020).
132. Wu, J. S. *et al.* A polyamidoamine (PAMAM) derivative dendrimer with high loading capacity of TLR7/8 agonist for improved cancer immunotherapy. *Nano Res.* **15**, 510–518 (2022).
133. Ren, L. & Lim, Y. T. Degradation-Regulatable Architectured Implantable Macroporous Scaffold for the Spatiotemporal Modulation of Immunosuppressive Microenvironment and Enhanced Combination Cancer Immunotherapy. *Adv. Funct. Mater.* **28**, 1804490 (2018).
134. Li, X. *et al.* Doxorubicin-loaded dextran-modified GoldMag nanoparticles for targeting hepatocellular carcinoma. *J. Biomed. Nanotechnol.* **14**, 1135–1146 (2018).
135. Hauksdóttir, H. L. & Webster, T. J. Selenium and Iron Oxide Nanocomposites for Magnetically-Targeted Anti-Cancer Applications. *J. Biomed. Nanotechnol.* **14**, 510–525 (2018).
136. Kempe, K. *et al.* Engineered Hydrogen-Bonded Glycopolymer Capsules and Their Interactions with Antigen Presenting Cells. *ACS Appl. Mater. Interfaces* **9**, 6444–6452 (2017).
137. Wang, C., Ye, Y., Hochu, G. M., Sadeghifar, H. & Gu, Z. Enhanced Cancer Immunotherapy by Microneedle Patch-Assisted Delivery of Anti-PD1 Antibody. *Nano Lett.* **16**, 2334–2340 (2016).
138. Sterner, R. C. & Sterner, R. M. CAR-T cell therapy: current limitations and potential strategies. *Blood Cancer J. 2021 114* **11**, 1–11 (2021).
139. Roddie, C. *et al.* Durable responses and low toxicity after fast off-rate cd19 chimeric antigen receptor-t therapy in adults with relapsed or refractory b-cell acute lymphoblastic leukemia. *J. Clin. Oncol.* **39**, 3352–3364 (2021).
140. Li, J. *et al.* Implantable and Injectable Biomaterial Scaffolds for Cancer Immunotherapy. *Frontiers in Bioengineering and Biotechnology* vol. 8 1363 (2020).
141. Kim, E.-M. & Jeong, H.-J. Liposomes: Biomedical Applications. *Chonnam Med. J.* **57**, 27 (2021).
142. Fischbach, M. A., Bluestone, J. A. & Lim, W. A. Cell-based therapeutics: The next pillar of medicine. *Science Translational Medicine* vol. 5 (2013).
143. Dellacherie, M. O., Seo, B. R. & Mooney, D. J. Macroscale biomaterials strategies for local immunomodulation. *Nat. Rev. Mater. 2019 46* **4**, 379–397 (2019).
144. Sadtler, K. *et al.* Developing a pro-regenerative biomaterial scaffold microenvironment requires T helper 2 cells. *Science (80-.).* **352**, 366–370 (2016).
145. Wang, Y. *et al.* Genipin crosslinking reduced the immunogenicity of xenogeneic decellularized porcine whole-liver matrices through regulation of immune cell proliferation and polarization. *Sci. Reports 2016 61* **6**, 1–16 (2016).
146. Wong, M. L. & Griffiths, L. G. Immunogenicity in xenogeneic scaffold generation: antigen removal vs. decellularization. *Acta Biomater.* **10**, 1806–1816 (2014).
147. Schimizzi, A. L. *et al.* High-molecular-weight hyaluronan inhibits macrophage proliferation and cytokine release in the early wound of a preclinical postlaminectomy rat model. *Spine J.* **6**, 550–556 (2006).
148. Taraballi, F. *et al.* Biomimetic collagenous scaffold to tune inflammation by targeting macrophages. *J. Tissue Eng.* **7**, 2041731415624667 (2016).
149. Woods, I. *et al.* Biomimetic Scaffolds for Spinal Cord Applications Exhibit Stiffness-Dependent Immunomodulatory and Neurotrophic Characteristics. *Adv. Healthc. Mater.* **11**, 2101663 (2022).
150. Lohmann, N. *et al.* Glycosaminoglycan-based hydrogels capture inflammatory chemokines and rescue defective wound healing in mice. *Sci. Transl. Med.* **9**, (2017).
151. Vasandan, A. B. *et al.* Human Mesenchymal stem cells program macrophage plasticity by altering their metabolic status via a PGE2-dependent mechanism. *Sci. Reports 2016 61* **6**, 1–17 (2016).
152. Akgun, I. *et al.* Matrix-induced autologous mesenchymal stem cell implantation versus matrix-induced autologous chondrocyte implantation in the treatment of chondral defects of the knee: a

2-year randomized study. *Arch. Orthop. Trauma Surg.* **135**, 251–263 (2015).
153. Tsou, Y. H., Khoneisser, J., Huang, P. C. & Xu, X. Hydrogel as a bioactive material to regulate stem cell fate. *Bioactive Materials* vol. 1 39–55 (2016).
154. Corradetti, B. *et al.* Chondroitin Sulfate Immobilized on a Biomimetic Scaffold Modulates Inflammation While Driving Chondrogenesis. *Stem Cells Transl. Med.* **5**, 670–682 (2016).
155. Corradetti, B. *et al.* Hyaluronic acid coatings as a simple and efficient approach to improve MSC homing toward the site of inflammation. *Sci. Reports 2017 71* **7**, 1–12 (2017).
156. Peng, H. *et al.* Polymer Cell Surface Coating Enhances Mesenchymal Stem Cell Retention and Cardiac Protection. *ACS Appl. Bio Mater.* **4**, 1655–1667 (2021).
157. Liu, G. *et al.* A VEGF delivery system targeting MI improves angiogenesis and cardiac function based on the tropism of MSCs and layer-by-layer self-assembly. *Biomaterials* **127**, 117–131 (2017).
158. Weischenfeldt, J. & Porse, B. Bone Marrow-Derived Macrophages (BMM): Isolation and Applications. *Cold Spring Harb. Protoc.* **2008**, pdb.prot5080 (2008).
159. Lindroos, B. *et al.* Serum-free, xeno-free culture media maintain the proliferation rate and multipotentiality of adipose stem cells in vitro. *Cytotherapy* **11**, 958–972 (2009).
160. Dominici, M. *et al.* Minimal criteria for defining multipotent mesenchymal stromal cells. The International Society for Cellular Therapy position statement. *Cytotherapy* **8**, 315–317 (2006).
161. Varghese, O. P., Kisiel, M., Martinez-Sanz, E., Ossipov, D. A. & Hilborn, J. Synthesis of Guanidinium-Modified Hyaluronic Acid Hydrogel. *Macromol. Rapid Commun.* **31**, 1175–1180 (2010).
162. Varghese, O. P., Wang, S., Oommen, O. P. & Yan, H. Mild and efficient strategy for site-selective aldehyde modification of glycosaminoglycans: Tailoring hydrogels with tunable release of growth factor. *Biomacromolecules* **14**, 2427–2432 (2013).
163. Stokes, K. Y. & Granger, D. N. Platelets: a critical link between inflammation and microvascular dysfunction. *J. Physiol.* **590**, 1023–1034 (2012).
164. Lin, K. T. & Wang, L. H. New dimension of glucocorticoids in cancer treatment. *Steroids* vol. 111 84–88 (2016).
165. Becker, L. C. *et al.* Final report of the safety assessment of hyaluronic acid, potassium hyaluronate, and sodium hyaluronate. *Int. J. Toxicol.* **28**, 5–67 (2009).
166. Kisiel, M. *et al.* Critical assessment of rhBMP-2 mediated bone induction: An in vitro and in vivo evaluation. *J. Control. Release* **162**, 646–653 (2012).
167. Moll, G. *et al.* Intravascular Mesenchymal Stromal/Stem Cell Therapy Product Diversification: Time for New Clinical Guidelines. *Trends Mol. Med.* **25**, 149–163 (2019).
168. Li, Y. & Lin, F. Mesenchymal stem cells are injured by complement after their contact with serum. *Blood* **120**, 3436–3443 (2012).
169. Berglund, A. K., Fortier, L. A., Antczak, D. F. & Schnabel, L. V. Immunoprivileged no more: measuring the immunogenicity of allogeneic adult mesenchymal stem cells. *Stem Cell Res. Ther.* **8**, (2017).
170. Özdemir, E. & Kansu, E. Deep vein thrombosis following non-myeloablative allogeneic stem cell transplantation: Presentation of three cases and literature review. *Turkish Journal of Hematology* vol. 30 188–190 (2013).
171. Cyranoski, D. Korean deaths spark inquiry. *Nature* vol. 468 485 (2010).
172. Oeller, M. *et al.* Selection of Tissue Factor-Deficient Cell Transplants as a Novel Strategy for Improving Hemocompatibility of Human Bone Marrow Stromal Cells. *Theranostics* **8**, 1421–1434 (2018).
173. Tian, Z. *et al.* Insight Into the Prospects for RNAi Therapy of Cancer. *Frontiers in Pharmacology* vol. 12 308 (2021).
174. Kraja, I. *et al.* Preliminary study of a novel transfection modality for in vivo siRNA delivery to vocal fold fibroblasts. *Laryngoscope* **127**, E231 (2017).
175. Springer, A. D. & Dowdy, S. F. GalNAc-siRNA Conjugates: Leading the Way for Delivery of RNAi Therapeutics. *Nucleic Acid Ther.* **28**, 109 (2018).
176. McLain, V. C. Safety assessment of poloxamers 101, 105, 108, 122, 123, 124, 181, 182, 183, 184, 185, 188, 212, 215, 217, 231, 234, 235, 237, 238, 282, 284, 288, 331, 333, 334, 335, 338, 401, 402, 403, and 407, poloxamer 105 benzoate, and poloxamer 182 dibenzoate as use. *Int. J. Toxicol.* **27**, 93–128 (2008).
177. Stirpe, M., Brugnoli, B., Donelli, G., Francolini, I. & Vuotto, C. Poloxamer 338 affects cell adhesion and biofilm formation in escherichia coli: Potential applications in the management of catheter-

associated urinary tract infections. *Pathogens* **9**, 1–16 (2020).
178. Qin, L. *et al.* F127/Calcium phosphate hybrid nanoparticles: a promising vector for improving siRNA delivery and gene silencing. *J. Biomater. Sci. Polym. Ed.* **24**, 1757–1766 (2013).
179. Hamann, A., Nguyen, A. & Pannier, A. K. Nucleic acid delivery to mesenchymal stem cells: A review of nonviral methods and applications. *Journal of Biological Engineering* vol. 13 (2019).
180. Shu, Z. *et al.* Disulfide-Unit Conjugation Enables Ultrafast Cytosolic Internalization of Antisense DNA and siRNA. *Angew. Chemie* **131**, 6683–6687 (2019).
181. Teramura, Y., Kaneda, Y. & Iwata, H. Islet-encapsulation in ultra-thin layer-by-layer membranes of poly(vinyl alcohol) anchored to poly(ethylene glycol)-lipids in the cell membrane. *Biomaterials* **28**, 4818–4825 (2007).
182. Li, W. *et al.* The effect of layer-by-layer assembly coating on the proliferation and differentiation of neural stem cells. *ACS Appl. Mater. Interfaces* **7**, 3018–3029 (2015).
183. Teramura, Y., Oommen, O. P., Olerud, J., Hilborn, J. & Nilsson, B. Microencapsulation of cells, including islets, within stable ultra-thin membranes of maleimide-conjugated PEG-lipid with multifunctional crosslinkers. *Biomaterials* **34**, 2683–2693 (2013).
184. Komeri, R., Thankam, F. G. & Muthu, J. Influence of matrix and bulk behaviour of an injectable hydrogel on the survival of encapsulated cardiac cells. *RSC Adv.* **5**, 31439–31449 (2015).
185. Gravastrand, C. *et al.* Alginate microbeads are coagulation compatible, while alginate microcapsules activate coagulation secondary to complement or directly through FXII. *Acta Biomater.* **58**, 158–167 (2017).
186. Dieleman, L. A. *et al.* Chronic experimental colitis induced by dextran sulphate sodium (DSS) is characterized by Th1 and Th2 cytokines. *Clin. Exp. Immunol.* **114**, 385–391 (2001).
187. Mccarthy, R. E., Arnold, L. W., Babcock, G. F. & Present, *. Dextran sulphate: an adjuvant for cell-mediated immune responses. *Immunology* **32**, 963 (1977).
188. Susanto, A., Putera, B. W., Wijaya, A. & Muhtadi, A. Effect of heparin on proliferation mesencymal stem cell. *Cytotherapy* **21**, S87–S88 (2019).
189. Lee, H. *et al.* Gelatin Directly Enhances Neurogenic Differentiation Potential in Bone Marrow-Derived Mesenchymal Stem Cells Without Stimulation of Neural Progenitor Cell Proliferation. *DNA Cell Biol.* **35**, 530–536 (2016).
190. Samanta, S. *et al.* An unexpected role of an extra phenolic hydroxyl on the chemical reactivity and bioactivity of catechol or gallol modified hyaluronic acid hydrogels. *Polym. Chem.* **12**, 2987–2991 (2021).
191. Prathiba, S., Ponnulakshmi, R., Jayaraman, S., P, M. K. & Kasturi, R. A Review on Therapeutic Perspectives of Anticancer Properties of Chebulagic Acid. *Nat. Volatiles Essent. Oils* **8**, 7598–7612 (2021).
192. Oommen, O. P. *et al.* Smart Design of Stable Extracellular Matrix Mimetic Hydrogel: Synthesis, Characterization, and In Vitro and In Vivo Evaluation for Tissue Engineering. *Adv. Funct. Mater.* **23**, 1273–1280 (2013).
193. Wang, J., Li, D., Cang, H. & Guo, B. Crosstalk between cancer and immune cells: Role of tumor-associated macrophages in the tumor microenvironment. *Cancer Medicine* vol. 8 4709–4721 (2019).
194. Binnemars-Postma, K., Bansal, R., Storm, G. & Prakash, J. Targeting the Stat6 pathway in tumor-associated macrophages reduces tumor growth and metastatic niche formation in breast cancer. *FASEB J.* **32**, 969–978 (2018).
195. Liguori, M. *et al.* Functional TRAIL receptors in monocytes and tumor-associated macrophages: A possible targeting pathway in the tumor microenvironment. *Oncotarget* **7**, 41662 (2016).
196. Kim, S. H. *et al.* Doxorubicin-induced platelet procoagulant activities: An important clue for chemotherapy-associated thrombosis. *Toxicol. Sci.* **124**, 215–224 (2011).
197. Garraud, O. & Cognasse, F. Are platelets cells? And if yes, are they immune cells? *Frontiers in Immunology* vol. 6 (2015).
198. Sanfins, E., Augustsson, C., Dahlbäck, B., Linse, S. & Cedervall, T. Size-dependent effects of nanoparticles on enzymes in the blood coagulation cascade. *Nano Lett.* **14**, 4736–4744 (2014).
199. Zhao, J., Yang, D. & Zheng, D. Coagulation is more affected by quick than slow bleeding in patients with massive blood loss. *Blood Coagul. Fibrinolysis* **28**, 121–125 (2017).
200. Kim, S. H. *et al.* Doxorubicin-Induced Platelet Procoagulant Activities: An Important Clue for Chemotherapy-Associated Thrombosis. *Toxicol. Sci.* **124**, 215–224 (2011).

201. De Beca, F. F. *et al.* Cancer stem cells markers CD44, CD24 and ALDH1 in breast cancer special histological types. *J. Clin. Pathol.* **66**, 187–191 (2013).
202. He, J. *et al.* Dexamethasone affects cell growth/apoptosis/chemosensitivity of colon cancer via glucocorticoid receptor α/NF-κB. *Oncotarget* **8**, 67670–67683 (2017).
203. Martinez, F. O. & Gordon, S. The M1 and M2 paradigm of macrophage activation: Time for reassessment. *F1000Prime Rep.* **6**, (2014).
204. Moraes, D. A. *et al.* A reduction in CD90 (THY-1) expression results in increased differentiation of mesenchymal stromal cells. *Stem Cell Res. Ther.* **7**, (2016).
205. Tsai, C. C., Su, P. F., Huang, Y. F., Yew, T. L. & Hung, S. C. Oct4 and Nanog Directly Regulate Dnmt1 to Maintain Self-Renewal and Undifferentiated State in Mesenchymal Stem Cells. *Mol. Cell* **47**, 169–182 (2012).
206. Baraniak, P. R. & McDevitt, T. C. Stem cell paracrine actions and tissue regeneration. *Regen. Med.* **5**, 121–143 (2010).
207. O'Garra, A., Barrat, F. J., Castro, A. G., Vicari, A. & Hawrylowicz, C. Strategies for use of IL-10 or its antagonists in human disease. *Immunol. Rev.* **223**, 114–131 (2008).
208. Kurte, M. *et al.* Time-dependent LPS exposure commands MSC immunoplasticity through TLR4 activation leading to opposite therapeutic outcome in EAE. *Stem Cell Res. Ther.* **11**, 1–14 (2020).
209. Welsby, I. J. *et al.* Effect of Combined Anticoagulation Using Heparin and Bivalirudin on the Hemostatic and Inflammatory Responses to Cardiopulmonary Bypass in the Rat. *Anesthesiology* **106**, 295–301 (2007).
210. Yu, H., Muñoz, E. M., Edens, R. E. & Linhardt, R. J. Kinetic studies on the interactions of heparin and complement proteins using surface plasmon resonance. *Biochim. Biophys. Acta - Gen. Subj.* **1726**, 168–176 (2005).
211. Zaferani, A. *et al.* Heparin/heparan sulphate interactions with complement—a possible target for reduction of renal function loss? *Nephrol. Dial. Transplant.* **29**, 515–522 (2014).
212. Zhang, R., Ma, J., Han, J., Zhang, W. & Ma, J. Mesenchymal stem cell related therapies for cartilage lesions and osteoarthritis. *Am. J. Transl. Res.* **11**, 6275 (2019).
213. ng Li, Y. I., ang, B. W. & Li, G. SendOrders for Reprintsto reprints@benthamscience.net The Roles of Mesenchymal Stem Cells in Tissue Repair and Disease Modification. *Curr. Stem Cell Res. Ther.* **9**, 424–431 (2014).
214. Page, C. Heparin and Related Drugs: Beyond Anticoagulant Activity. *ISRN Pharmacol.* **2013**, 1–13 (2013).
215. Stubbs, S. L. *et al.* Hypoxic preconditioning enhances survival of human adipose-derived stem cells and conditions endothelial cells in vitro. *Stem Cells Dev.* **21**, 1887–1896 (2012).
216. Samal, J. R. K., Rangasami, V. K., Samanta, S., Varghese, O. P. & Oommen, O. P. Discrepancies on the Role of Oxygen Gradient and Culture Condition on Mesenchymal Stem Cell Fate. *Advanced Healthcare Materials* vol. 10 2002058 (2021).
217. Ge, Q. *et al.* VEGF secreted by mesenchymal stem cells mediates the differentiation of endothelial progenitor cells into endothelial cells via paracrine mechanisms. *Mol. Med. Rep.* **17**, 1667 (2018).
218. English, K. *et al.* Cell contact, prostaglandin E2 and transforming growth factor beta 1 play non-redundant roles in human mesenchymal stem cell induction of CD4+CD25Highforkhead box P3+ regulatory T cells. *Clin. Exp. Immunol.* **156**, 149–160 (2009).
219. Dufour, J. H. *et al.* IFN-γ-Inducible Protein 10 (IP-10; CXCL10)-Deficient Mice Reveal a Role for IP-10 in Effector T Cell Generation and Trafficking. *J. Immunol.* **168**, 3195–3204 (2002).
220. Liu, S. *et al.* Immunosuppressive Property of MSCs Mediated by Cell Surface Receptors. *Frontiers in Immunology* vol. 11 1076 (2020).
221. Casella, G. *et al.* IL4 induces IL6-producing M2 macrophages associated to inhibition of neuroinflammation in vitro and in vivo. *J. Neuroinflammation* **13**, 1–10 (2016).
222. Luckett-Chastain, L., Calhoun, K., Schartz, T. & Gallucci, R. M. IL-6 influences the balance between M1 and M2 macrophages in a mouse model of irritant contact dermatitis. *J. Immunol.* **196**, 196.17 LP-196.17 (2016).
223. Wu, T., Liu, Y., Wang, B. & Li, G. The Roles of Mesenchymal Stem Cells in Tissue Repair and Disease Modification. *Curr. Stem Cell Res. Ther.* **9**, 424–431 (2014).
224. Orlic, D. *et al.* Bone marrow stem cells regenerate infarcted myocardium. *Pediatr. Transplant.* **7 Suppl 3**, 86–88 (2003).
225. Abnosi, M. H. & Yari, S. The toxic effect of gallic acid on biochemical factors, viability and

proliferation of rat bone marrow mesenchymal stem cells was compensated by boric acid. *J. Trace Elem. Med. Biol.* **48**, 246–253 (2018).
226. Hutchins, A. P., Diez, D. & Miranda-Saavedra, D. The IL-10/STAT3-mediated anti-inflammatory response: recent developments and future challenges. *Brief. Funct. Genomics* **12**, 489–498 (2013).
227. Couper, K. N., Blount, D. G. & Riley, E. M. IL-10: The Master Regulator of Immunity to Infection. *J. Immunol.* **180**, 5771–5777 (2008).
228. Gensel, J. C. & Zhang, B. Macrophage activation and its role in repair and pathology after spinal cord injury. *Brain Res.* **1619**, 1–11 (2015).
229. Yue, Y. *et al.* M2b macrophages reduce early reperfusion injury after myocardial ischemia in mice: A predominant role of inhibiting apoptosis via A20. *Int. J. Cardiol.* **245**, 228–235 (2017).
230. Mosser, D. M. & Edwards, J. P. Exploring the full spectrum of macrophage activation. *Nat. Rev. Immunol. 2008 812* **8**, 958–969 (2008).
231. Atri, C., Guerfali, F. Z. & Laouini, D. Role of Human Macrophage Polarization in Inflammation during Infectious Diseases. *Int. J. Mol. Sci. 2018, Vol. 19, Page 1801* **19**, 1801 (2018).
232. Burgess, M., Wicks, K., Gardasevic, M. & Mace, K. A. Cx3CR1 Expression Identifies Distinct Macrophage Populations That Contribute Differentially to Inflammation and Repair. *ImmunoHorizons* **3**, 262–273 (2019).
233. Freria, C. M. *et al.* Deletion of the Fractalkine Receptor, CX3CR1, Improves Endogenous Repair, Axon Sprouting, and Synaptogenesis after Spinal Cord Injury in Mice. *J. Neurosci.* **37**, 3568–3587 (2017).
234. Nova-Lamperti, E. *et al.* IL-10-produced by human transitional B-cells down-regulates CD86 expression on B-cells leading to inhibition of CD4+T-cell responses. *Sci. Reports 2016 61* **6**, 1–8 (2016).
235. Madsen, D. H. *et al.* M2-like macrophages are responsible for collagen degradation through a mannose receptor-mediated pathway. *J. Cell Biol.* **202**, 951–966 (2013).
236. Jiang, P. *et al.* Signatures of T cell dysfunction and exclusion predict cancer immunotherapy response. *Nat. Med.* **24**, 1550–1558 (2018).

PUBLICATION 1

Harnessing hyaluronic acid-based nanoparticles for combination therapy: A novel approach for suppressing systemic inflammation and to promote antitumor macrophage polarization

V.K. Rangasami, S. Samanta, V.S. Parihar, K. Asawa, K. Zhu, O.P. Varghese, Y. Teramura, B. Nilsson, J. Hilborn, R.A. Harris, O.P. Oommen

Carbohydrate Polymers, Volume 254, 2021, 117291
https://doi.org/10.1016/j.carbpol.2020.117291

Carbohydrate Polymers 254 (2021) 117291

Contents lists available at ScienceDirect

Carbohydrate Polymers

journal homepage: www.elsevier.com/locate/carbpol

Harnessing hyaluronic acid-based nanoparticles for combination therapy: A novel approach for suppressing systemic inflammation and to promote antitumor macrophage polarization

Vignesh K. Rangasami [a], Sumanta Samanta [a], Vijay Singh Parihar [a], Kenta Asawa [b], Keying Zhu [c], Oommen P. Varghese [a], Yuji Teramura [b,e], Bo Nilsson [e], Jöns Hilborn [d], Robert A. Harris [c], Oommen P. Oommen [a,*]

[a] Bioengineering and Nanomedicine Lab, Faculty of Medicine and Health Technologies, Tampere University and BioMediTech Institute, 33720, Tampere, Finland
[b] Department of Bioengineering, The University of Tokyo, 7-3-1 Hongo, Bunkyo-ku, Tokyo, 113-8656, Japan
[c] Applied Immunology and Immunotherapy, Department of Clinical Neuroscience, Karolinska Institutet, Centre for Molecular Medicine, Karolinska University Hospital, 171 76, Solna, Stockholm, Sweden
[d] Translational Chemical Biology Laboratory, Department of Chemistry, Ångström Laboratory, Uppsala University, 751 21, Uppsala, Sweden
[e] Department of Immunology, Genetics and Pathology, Rudbeck Laboratory, Uppsala University, SE-75105, Sweden

ARTICLE INFO

Keywords:
Hyaluronic-acid
Nanoparticles
Immune system
Macrophages
Doxorubicin
Dexamethasone

ABSTRACT

Anti-inflammatory drugs such as dexamethasone (DEX) are commonly administered to cancer patients along with anticancer drugs, however, the effect of DEX on human cancers is poorly understood. In this article, we have tailored self-assembled nanoparticles derived from hyaluronic acid (HA) wherein, anti-inflammatory DEX was used as a hydrophobic moiety for inducing amphiphilicity. The HA-DEX micelles were subsequently loaded with chemotherapeutic agent, doxorubicin (DOX) (HA-DEX-DOX) and was utilized to deliver drug cargo to human cancer cells expressing different levels of CD44 receptors. We found that DEX suppressed the cytotoxicity of DOX in HCT116, while it synergistically enhanced cytotoxicity in MCF-7 cells. When we tested DOX and HA-DEX-DOX in an ex-vivo human whole blood, we found activation of complement and the coagulation cascade in one group of donors. Encapsulation of DOX within the nanoparticle core eliminated such deleterious side-effects. The HA-DEX-DOX also polarized bone-marrow-derived anti-inflammatory M2 macrophages, to pro-inflammatory M1 phenotype with the upregulation of the cytokines TNF-α, iNOS and IL-1β.

1. Introduction

Most of the current clinically used chemotherapeutic agents are DNA intercalating molecules targeting rapidly dividing cells. These drugs invariably damage the DNA of the lymphohematopoietic precursor cells, resulting in leukocytopenia and thrombocytopenia. Platelets are natural effector cells that amplify the inflammatory response (von Hundelshausen & Weber, 2007). Upon activation by chemotherapeutic agents platelets secrete over 300 proteins and small molecules including cytokines, chemokines, growth factors and coagulation factors that trigger blood-mediated inflammatory responses that in turn induce hypersensitivity reactions in several patients (Stokes & Granger, 2012). The depletion of the effector cells from the circulation following chemotherapy poses an additional risk of infection. Patients are therefore often infused with platelets from healthy donors after each chemotherapy cycle or are treated with hematopoietic growth factors such as granulocyte colony stimulating factor (G-CSF) and granulocyte macrophage colony stimulating factor (GM-CSF) as these are both known to accelerate the proliferation and promote the recovery of hematopoietic cells (Bennett, Djulbegovic, Norris, & Armitage, 2013). Unfortunately, these methods are expensive and fail to mitigate the damage to the hematopoietic progenitor cells. The supportive co-medication of corticosteroids such as dexamethasone (DEX), prednisone or prednisolone is also used to alleviate the inevitable side-effects in cancer patients undergoing

* Corresponding author.
E-mail addresses: vignesh.rangasami@tuni.fi (V.K. Rangasami), sumanta.samanta@tuni.fi (S. Samanta), vijay.parihar@tuni.fi (V.S. Parihar), asawa@celly.t.u-tokyo.ac.jp (K. Asawa), keying.zhu@ki.se (K. Zhu), oommen.varghese@kemi.uu.se (O.P. Varghese), teramura@bioeng.t.u-tokyo.ac.jp (Y. Teramura), bo.nilsson@igp.uu.se (B. Nilsson), jons.hilborn@kemi.uu.se (J. Hilborn), Robert.harris@ki.se (R.A. Harris), oommen.oommen@tuni.fi (O.P. Oommen).

https://doi.org/10.1016/j.carbpol.2020.117291
Received 17 June 2020; Received in revised form 15 October 2020; Accepted 19 October 2020
Available online 27 October 2020

chemotherapy (Lin & Wang, 2016). These drugs possess anti-inflammatory and immunosuppressive properties and are used as an antiemetic or adjuvant as they help in reducing weight loss, overcoming nausea, and help in alleviating pain and improving appetite (Grunberg, 2007). However, several studies demonstrate the deleterious effect of DEX on anticancer effect of chemotherapeutic agents by various mechanism. The pretreatment of DEX suppressed the uptake of chemotherapeutic agents in tumor (Wang, Li, Rinehart, & Zhang, 2004). Other studies reported that DEX promoted cell proliferation and inhibited apoptosis by activating glucocorticoid receptors in bladder cancer (Zheng, Izumi, Li, Ishiguro, & Miyamoto, 2012) or by activating Stat5/Bcl-xL pathway in C6 glioma models (Qian, Xiao, Chen, & Xu, 2009). The glucocorticoid also depletes the key effector immune cells such as T and B lymphocytes and NK cells resulting in suppression of the efficacy of immunochemotherapy treatment (Aston et al., 2019). On the contrary, DEX display anticancer and anti-estrogenic activity in human non-small cell lung cancer (NSCLC) (Wang et al., 2016). These conflicting studies motivated us to analysis the effect of DEX when co-delivered with a chemotherapeutic agent using a biomimetic delivery system that provide stealth properties and specifically targets the tumor specific cell surface receptor.

Nanomedicine provides the ideal opportunities to design combination therapies (Aminu, Chan, Yam, & Toh, 2019), as nanoparticles could be grafted with ligands that target cell-surface receptors overexpressed in cancer cells and tailored to deliver multiple drug payloads with controlled drug release profile. One such ligand is hyaluronic acid (HA) which targets CD44 receptors that are known to be overexpressed 6–7 fold in solid tumors (Plattt & Szoka, 2008). Recent efforts to develop nanomedicine for immuno-oncology aim to boost our immune system to recognize the malignant cells. Nanoparticles can be armed with targeting ligands, antigens or adjuvants to promote prophylactic therapeutics triggering immunotherapy. However, a key challenge in nanoparticle-mediated immuno-oncology is the immunosuppressive nature of the tumor microenvironment that neutralizes the infiltration and antitumoral activity of effector immune cells. The tumor microenvironment is immunosuppressive due to the presence of anti-inflammatory tumor-associated macrophages (TAMs) and regulatory lymphocytes. Strategies that can deliver drug payload to the target site and activate immune effector cells, disrupting this immunosuppressive activity, would therefore offer multimodal and enhanced efficiency of antitumor therapies.

In this study we aimed to design an immunomodulatory nanoparticle derived from hyaluronic acid (HA), a natural extracellular matrix-based biopolymer, using a supramolecular self-assembly approach. HA is a non-sulfated glycosaminoglycan composed of disaccharides repeat units, D-glucuronic acid and N-acetyl-D-glucosamine which are linked through alternating β-(1→4) and β-(1→3) glycosidic bonds. HA is an attractive choice for engineering such nanoparticles as it plays multiple roles in immunomodulation, cell proliferation, cell signaling, and differentiation (Plattt & Szoka, 2008). In addition to its capability to target CD44 receptors overexpressed on several solid tumors, it can effectively target macrophages, a key regulator of inflammation as macrophages express several HA-specific receptors such as CD44, ICAM-1, RHAMM, and LYVE-1 (Foley et al., 2012). HA could provide stealth properties by shielding encapsulated cytotoxic drugs from interacting with blood components, thereby preventing hypersensitivity reactions in patients. We hypothesized that nanoparticles derived from low molecular weight HA can target and polarize TAMs, thereby assisting in anti-tumor immunity as HA display molecular weight-dependent macrophage polarization (Rayahin, Buhrman, Zhang, Koh, & Gemeinhart, 2015). We have previously reported that HA nanoparticles can be used for delivering cytotoxic drugs (Oommen, Garousi, Sloff, & Varghese, 2014) and short interfering RNA or siRNA (Paidikondala et al., 2019). The most common strategy to tailor HA derived nanoparticles involves conjugating small hydrophobic molecules such as cholesterol (Nakai et al., 2012), fatty acids (Cho et al., 2012), fluorescein (Oommen, Duehrkop, Nilsson, Hilborn, & Varghese, 2016) etc. that impart sufficient amphiphilicity promoting self-assembly, however these hydrophobic molecules do not impart any functional bioactivity. In this study, we aimed to tailor HA-derived nanocarriers by conjugating DEX by pH responsive hydrazone linkages. To the best of our knowledge, the HA-DEX micelles developed in this study is the first example of a bioactive nanocarrier design that does not use any inert excipients and could be effectively used to co-deliver the chemotherapeutic agent (Doxorubicin or DOX) and an anti-inflammatory drug (DEX). The co-delivery of two therapeutic modalities would synergistically facilitate DOX-mediated apoptosis, suppress inflammation and promote HA-mediated targeted delivery.

2. Experimental section

2.1. Synthesis of HA-CDH conjugate

The conjugation of carbodihydrazide (CDH) on hyaluronic acid (HA) was carried out by carbodiimide coupling chemistry, as previously optimized by our group (Oommen et al., 2013). Briefly, 1 mmol of HA (400 mg, 1 equivalent) was dissolved in 120 mL of deionized water. Thereafter, 1 mmol CDH (90 mg, 1 equivalent) and 1 mmol HOBt (153 mg, 1 equivalent) was added to the aqueous HA solution. The pH of the reaction mixture was adjusted to 4.7. Finally, 0.2 mmol EDC·HCl (40 mg, 0.2 equivalent) was added and allowed to stir overnight. The solution was loaded into dialysis bag (Spectra Por-3, MWCO 3500) and dialyzed against dilute HCl (pH = 3.5) containing 100 mM NaCl (2 × 2 L, 24 h) followed by dialysis in dilute HCl (pH 3.5) (2 × 2 L, 24 h) and then dialyzed against deionized water (2 × 2 L, 24 h). The solution was lyophilized to obtain HA-CDH. The degree of hydrazide modifications was determined by trinitrobenzene sulfonic acid (TNBS) assay, following reported procedure (Varghese, Kisiel, Martinez-Sanz, Ossipov, & Hilborn, 2010).

2.2. Synthesis of HA-DEX-DOX conjugate

The conjugation of DEX on HA-CDH was achieved by hydrazone formation. Briefly, HA-CDH (200 mg; 0.5 mmol of disaccharide repeating units) was dissolved in 50 mL of deionized water. DEX (23.5 mg, 0.06 mmol) was dissolved in 30 mL of dimethyl sulfoxide was added to above solution and stirred until it was completely dissolved. Thereafter, the pH of the resultant solution was adjusted to 4.5 by using acetic acid and kept overnight at 50 °C with constant stirring. The reaction mixture was then dialyzed against deionized water (2 × 2 L, 48 h). The solution was lyophilized to obtain HA-DEX. The conjugation efficiency of DEX was determined using UV–vis spectroscopy, by estimating the free hydrazide moiety through TNBS assay, after DEX conjugation. Additionally, the DEX conjugation was also confirmed by performing ^{1}H NMR spectroscopy further described in supporting information.

100 mg of HA-DEX was then dissolved in 90 mL of DMSO:H_2O (2:1) and DOX (10 mg) pre-dissolved in 10 mL of deionized water was added and stirred for 6 h ; then 60 mL of deionized water was added and stirred overnight. The solution was loaded into a dialysis bag (Spectra Por-3, MWCO 3500) and dialyzed against deionized water containing 100 mM NaCl (3 × 2 L, 72 h) and then dialyzed against deionized water (2 × 2 L, 24 h). The solution was lyophilized to obtain HA-DEX-DOX.

2.3. Cytotoxicity studies

Both HA-DEX and HA-DEX-DOX were assessed for their cytotoxic properties by MTT (3-(4, 5-dimethylthiazol-2-yl)-2, 5-diphenyltetrazolium bromide) assay. Three different human cell lines, MG63 (osteosarcoma), HCT116 (colorectal carcinoma) and MCF7 (breast adenocarcinoma) were used. Briefly, 5000 cells were seeded in 96-well plates with 100 μL DMEM (Gibco) containing 10 % fetal bovine serum (Gibco, South American) and 1% penicillin-streptomycin (Gibco). After

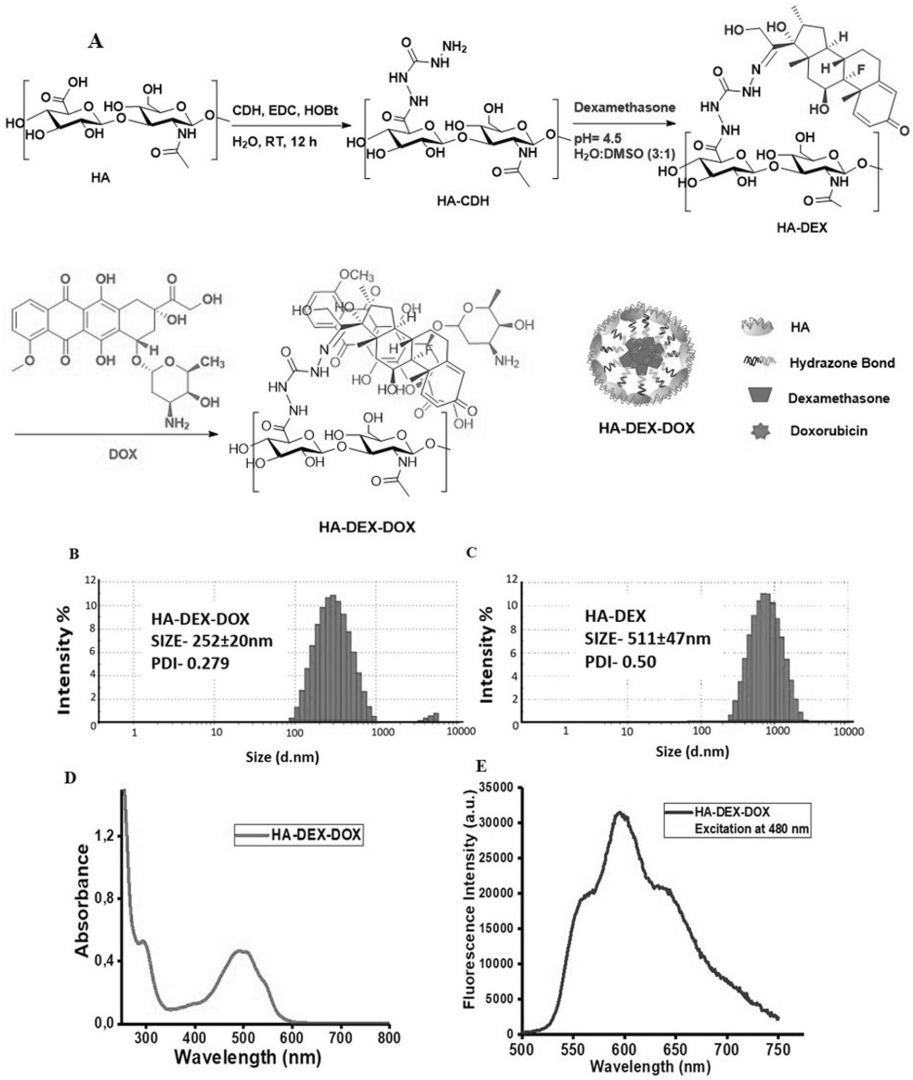

Fig. 1. (A) Schematic representation of the synthetic strategy for designing self-assembled HA-DEX-DOX nanoparticles. Representation of particle size distribution (B) HA-DEX-DOX (C) HA-DEX defined by dynamic light scattering (D) UV–vis spectrum of HA-DEX-DOX and (E) Fluorescence spectra of HA-DEX-DOX in water showing the characteristic peaks of DOX.

18−24 h the cells were exposed to free DOX at concentrations of 100 nM, 500 nM, 1000 nM, 2000 nM and 4000 nM, respectively. The amount of the HA-DEX-DOX was based on the amount of DOX loaded. HA-DEX-DOX at the concentrations of 1.5 μg/mL (100 nM DOX), 7.55 μg/mL (500 nM DOX), 14.7 μg/mL (1000 nM DOX), 29.86 μg/mL (2000 nM Dox) and 61.5 μg/mL (4000 nM DOX) were exposed to the cells. The amount of HA-DEX was made similar to that of HA-DEX-DOX. The cells were then incubated for 48 h at 37 °C and 5% CO_2, after which MTT (5 mg/mL) was added to the cells. After 4 h of incubation 150 μl of DMSO was added to each of the wells and the plates were shaken well. The absorbance was measured using a microplate reader. Results were expressed as percent viability $= \left\{ \frac{A_{540(treated\ cells)} - Background}{A_{540(untreated\ cells)} - Background} \right\} \times 100$.

The IC50 estimation (50 % inhibitory concentration) for HA-DEX-DOX NPs and free DOX was performed by logarithmic curve fitting of cell viability (%) using Graphpad Prism software against DOX equivalents. We also did the cytotoxicity studies where the viability of the cells was tested with free DOX and free DEX and a combination of both. Briefly, 200 nM of DOX and 200 nM of DEX and a mixture of 200 nM DOX and 200 nM DEX were exposed to HCT116, MCF7 and MG63 cell lines for 48 h. The percentage viability was obtained following the protocol mentioned above.

2.4. Fluorescence microscopy

Two different human cell lines, HCT116 (colorectal carcinoma) and

MCF7 (breast adenocarcinoma) were used. Briefly, 7000 cells were seeded in 96-well plates with 100 μL DMEM (Gibco) containing 10 % fetal bovine serum (Gibco, South American) and 1% penicillin-streptomycin (Gibco) and incubated overnight at 37 °C, 5% CO_2. After 24 h the cell culture medium was replaced with fresh medium containing HA-DEX-DOX and DOX. The amount of HA-DEX-DOX applied contained 1 μM of the loaded DOX. Four hours after incubation the medium was removed, and the cells were washed thrice with PBS. Thereafter, the cells were fixed with 4% paraformaldehyde (Sigma-Aldrich) for ten minutes and permeabilized using 0.1 % Triton X-100 (Sigma-Aldrich) for 5 min. The nuclei were stained with DAPI (Sigma) and the cells were analyzed by fluorescence microscopy (Nikon Eclipse Ts2).

2.5. Hematological studies/ ex vivo chandler loop studies

Fresh human whole blood was obtained from healthy volunteers who had not received any medication for at least 10 days prior to donation, and no heparin was added into the blood. Loops of polyurethane tubing (inner diameter of 6.3 mm) with 2-methacryloyloxyethyl phosphorylcholine (MPC) polymer (poly(MPC-co-*n*-butyl methacrylate) with a 0.30 MPC unit mole fraction were used for the whole blood experiments (Asif et al., 2019). Stainless-steel connectors were coated with Corline heparin surface (Corline Systems AB, Uppsala, Sweden) according to the manufacturer's protocol. Loops were comprised of tubing that was closed with surface-heparinized connectors (length: 30 cm, blood volume: 2.5 mL) were loaded with samples (DOX, HA-DEX, and HA-DEX-DOX in PBS). They were then rotated on a wheel at 50 rpm in a 37 °C cabinet for 1 h. As a negative control the same volume of PBS was used. 60 μM the amount of DOX taken and the concentration of DOX, HA-DEX and HA-DEX-DOX was according in the whole blood. The blood was collected and mixed with EDTA (10 mM), and then centrifuged (3400 rpm, 20 min, 4 °C) to collect plasma. The collected plasma was stored at −80 °C before ELISA analyses which are described further in the supporting information. These experiments were repeated three times using blood from different donors for each group. Ethical approval was obtained from the regional ethics committee.

2.6. Evaluation of the particles on bone marrow derived macrophages

Bone marrow-derived macrophages from mice (C57BL/6) were isolated and cultured using a standard protocol (Weischenfeldt & Porse, 2008). The isolated monocyte cells were differentiated to an immunosuppressive phenotype through stimulation with 20 ng/mL TGF-β (R&D Systems), 20 ng/mL IL-4 (R&D Systems) and 20 ng/mL IL-10 (R&D Systems) for 24 h. For the M1 phenotype the cells were stimulated with 100 ng/mL lipopolysaccharide (LPS) and 20 ng/mL interferon gamma (IFN-γ). The activated cells were then plated (50,000 in number) in 24-well plates overnight and subsequently treated with 200 nM DOX or DOX equivalent in HA-DEX-DOX for 48 h. The equivalent weight ratio of native HA and HA-DEX was used for comparison. RNA was then extracted using a commercially available kit (RNeasy Mini kit, Qiagen). cDNA first strand was synthesized following the protocol from iScript cDNA synthesis kit (BioRad). iQ SYBR Green Supermix was used to prepare the samples for qPCR on a CFX96 instrument from BioRad. The proinflammatory genes (TNF-α, IL-1β, iNOS, IL-6) were selected and their expression levels analyzed with and without exposure to the HA-DEX and HA-DEX-DOX particles. Hypoxanthine guanine phosphoribosyltransferase (HPRT) was used as housekeeping gene for normalization. The primers for the qPCR were obtained from Sigma Aldrich, Sweden.

3. Results and discussions

3.1. Synthesis and characterization of HA-DEX-DOX

To design the HA nanoparticle we first synthesized carbodihydrazide (CDH)-functionalized HA in accordance with our reported protocol (Kisiel et al., 2012), followed by conjugation of DEX with a hydrazone linkage (Fig. 1A). We have previously shown that CDH assists in the formation of hydrazone bonds that are stable under physiological conditions due to an urea-type linkage (Oommen et al., 2013). The percentage of CDH functionalization on the HA backbone was determined to be 12 % (with respect to the disaccharide repeat units) as estimated by the TNBS assay. The amount of DEX loaded in HA-DEX was quantified as 5.2 % (with respect to the disaccharide repeat units) by estimating the free hydrazide moiety after DEX conjugation. Additionally, we confirmed the conjugation of DEX by ^{1}H NMR spectroscopy (Figure S1 in SI). The DEX conjugation of HA (HA-DEX) promotes supramolecular self-assembly of the amphiphilic polymers in water, resulting in the forming of nanoparticles with hydrodynamic size 511 ± 47 nm (Z-average) as estimated by dynamic light scattering (DLS) analysis. Consistent with the literature, the ^{1}H NMR spectrograph of HA-DEX underestimate the amount of DEX due to the core-shell structure as a result of self-assembly in D_2O (Bütün et al., 2001). Subsequent loading of DOX into these particles led to a reduction in size to 252 ± 20 nm (Z-average)with a zeta potential of -26.1 ± 5.4 mV (Fig. 1B,C and S2 in SI). This reduction in size is due to strong hydrophobic interactions between DEX and hydrophobic segments of DOX. Further, the size of the DOX loaded nanoparticles (HA-DEX-DOX) were analyzed using AFM surface topology assessment, which confirms that HA-DEX-DOX nanoparticles were spherical in nature, and 250−350 nm in size. (Figure S2 in SI). These particles displayed long shelf-life when stored as a lyophilized powder at −20 °C, as the size remained stable upon dispersion even after 1 year of storage (Figure S2D & S2E in SI). The amount of DOX loading was ascertained by UV–vis spectroscopy to be 4.6 % by weight. The encapsulation of DOX in HA-DEX-DOX was also confirmed by observing the characteristic absorbance of DOX at 485 nm, and fluorescence emission at 580 nm (Fig. 1D, E). We further performed drug release experiments using the dialysis method to assess the relative drug release kinetic from HA-DEX-DOX using simulated body fluids (SBF) at pH 7.4, mimicking physiological conditions. These experiments indicated a slow and sustained release of DOX in HA-DEX-DOX nanoparticles with only 10.6 % of DOX released (of the 4.6 % by weight) after 96 h with near zero-order kinetics as compared to free DOX (Figure S3 in SI).

3.2. Cellular Uptake and cytotoxic effects of HA-DEX-DOX in cancer cell lines

Because HA is known to target the CD44 receptor, a known cancer stem cell marker (Beça et al., 2013), we also evaluated the receptor targeting capability of HA-DEX-DOX nanoparticles. In this study we used three different human cancer cell lines with different levels of CD44 receptors. We quantified the relative CD44 expression in osteosarcoma cells (MG63), human colon carcinoma cells (HCT116) and human breast cancer cells (MCF-7) by flow cytometry (Figure S4 in SI) following a previously reported protocol (Oommen, Duehrkop, Nilsson, Hilborn, & Varghese, 2016). We found that MCF-7 expressed lowest levels of CD44 receptors while MG-63 expressed highest levels with a relative CD44 expression of 1:6.4:11.25 for MCF-7, HCT116 and MG-63 respectively. In order to evaluate the role of CD44-receptors we performed a competitive assay using low molecular weight HA (5 kDa) to block the CD44 receptors and determined the intracellular uptake of HA-DEX-DOX NPs following our reported protocol (Oommen et al., 2016b). The cellular uptake was quantified by fluorescence-activated cell sorting (FACS) analysis (described in detail in Supporting Information) and fluorescence microscopy, exploiting the inherent fluorescent property of DOX. This analysis revealed that after 4 h of incubation with

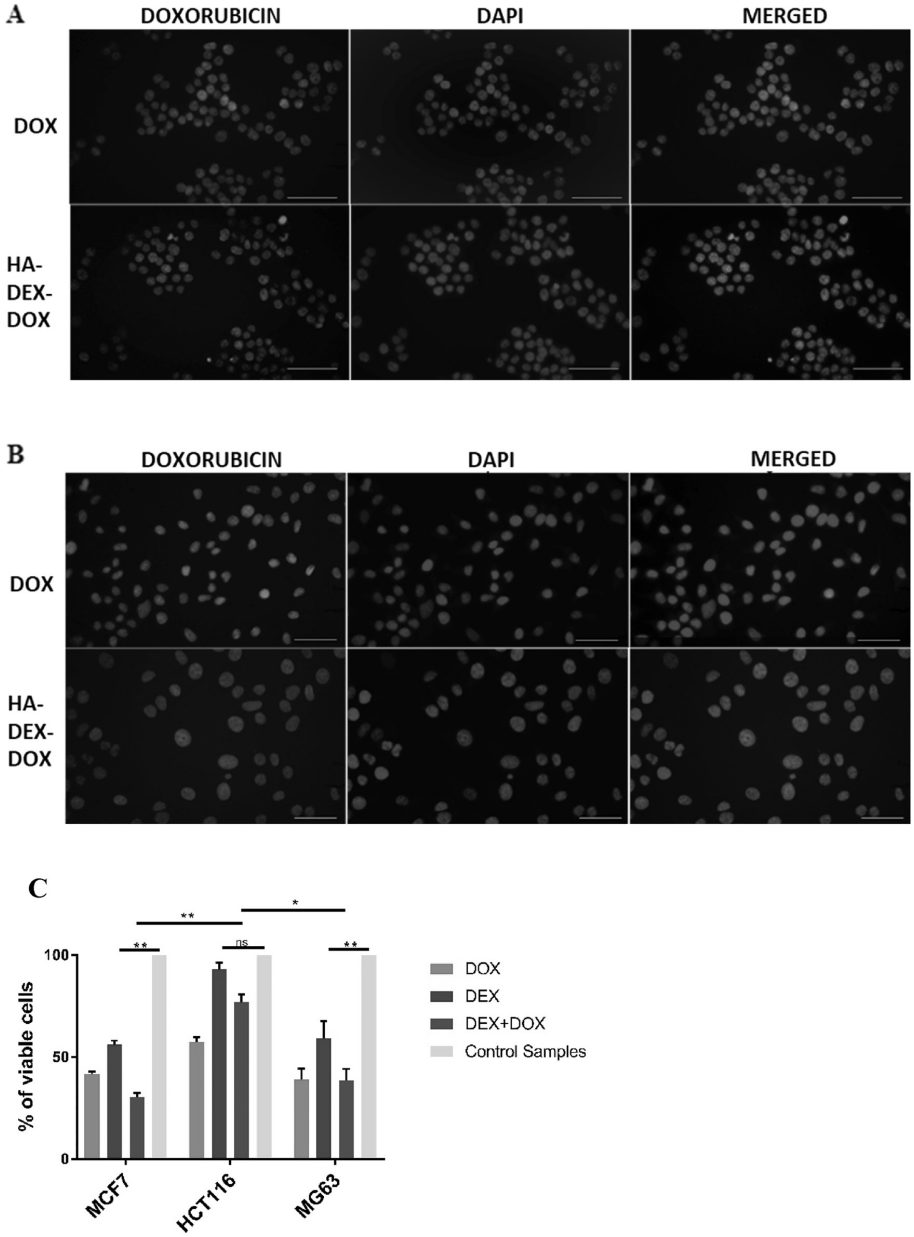

Fig. 2. Nuclear localization of the free DOX and HA-DEX-DOX along with nuclear staining (DAPI) in (A) HCT116 colon carcinoma cell line and (B) MCF7 breast cancer cell line. Scale bar 50 μm (C) Cell viability percentages after treating with either 200 nM free DOX, 200 nM DEX or a combination of 200 nM DOX and 200 nM DEX. The experiments were performed on MCF7, HCT116 and MG63 cell lines. Statistical analysis was done by Kruskal-Wallis test (**$p < 0.01$ *$p < 0.05$).

HA-DEX-DOX the HCT116 and MG63 cells demonstrated 87 % and 83 % nanoparticle uptake respectively while only 60 % uptake was observed in MCF-7 cells that express lower levels of CD44 receptors (Figure S5 in SI). Interestingly, when we blocked the cell surface CD44 receptors using 5 kDa HA, we observed ~1.7 folds and ~1.5 folds reduction in uptake in HCT116 and MG63 cells, while MCF-7 cells displayed ~1.3-folds decrease in uptake. This suggests that cell surface HA receptors are involved in the uptake of these particles. Finally, we performed fluorescence microscopy to ascertain the intracellular localization of DOX and DOX in HA-DEX-DOX (Fig. 2A, B). Interestingly, DOX in HA-DEX-DOX displayed nuclear localization similar to free DOX, validating the uptake and intracellular bio distribution of nanoparticles.

Table 1
Cytotoxicity of DOX and HA-DEX-DOX on the different cell lines. IC50 values were estimated by the logarithmic curve fitting of the cell viability percentage using GraphPad Prism software.

Cell lines	DOX IC50 (nM)	HA-DEX-DOX IC50 (nM)
MCF-7	226.03 ± 42.2	702.03 ± 76.3 (3.1 fold)
HCT-116	192.6 ± 59.9	585.7 ± 40 (3.04 fold)
MG-63	195.4 ± 26.4	576.4 ± 65.2 (2.95 fold)

In order to investigate the *in vitro* toxicity of combination therapy, we next performed a dose-dependent MTT assay of DOX, HA-DEX, and HA-DEX-DOX, respectively, in HCT-116, MCF-7 and a human osteosarcoma cell line (MG-63) that possess varying levels of CD44 receptors. The amount of HA-DEX used was equivalent to the weight of HA-DEX-DOX. As anticipated, we observed a dose-dependent cytotoxicity of DOX and HA-DEX-DOX, while HA-DEX did not exhibit any toxicity (Figure S8 in SI). Surprisingly, the cytotoxicity of HA-DEX-DOX was ~3-fold lower than free DOX (presumably due to differences in uptake mechanisms) in all three cell lines irrespective of their CD44 expression levels (Table 1). In order to understand this paradox, we examined the cytotoxic effects of free DEX, free DOX and the combination effect (i.e., mixture of DEX and DOX) in these cell lines (Fig. 2C). Surprisingly, we found that free DEX (200 nM) displayed significant toxicity to MCF-7 and MG63 cells while it showed no toxicity to HCT116 cells. Specifically, we observed a cell viability of 56 % and 59.17 % in MCF-7 and MG63 cells respectively after 48 h as determined by MTT assay. On the other hand, 200 nM DEX did not show any significant cytotoxicity to HCT116 cells (93 % viable cells after 48 h). Intriguingly, DEX suppressed the cytotoxicity of DOX in HCT116 cells as the cell viability of HCT116 cells increased from 56.75 % to 76.9 % when the cells were incubated with a mixture of 200 nM DEX and 200 nM DOX relative to when treated with 200 nM DOX alone. On the contrary, incubation of MCF-7 cells with the mixture of 200 nM DEX and 200 nM DOX increased the cytotoxic effects of DOX, as seen by the reduction of cell viability from 41.38 % to 30.3 %. Although, incubation of 200 nM DEX to MG63 cells also showed some toxicity (as cell viability reduced to 59.17 % in 48 h), this effect was not prominent in the combination treatment (viability of MG63 was 38.91 % and 38.6 % when treated with free DOX and DEX + DOX combination respectively). This clearly suggest that nanoparticles combining DEX and DOX forms a powerful synergistic system for breast cancer, while contrary to the reported literature (He et al., 2017), DEX plays an inhibitory role in HCT116 colon cancer cells (Fig. 2C). Such effects were negligible in MG63 osteosarcoma cells.

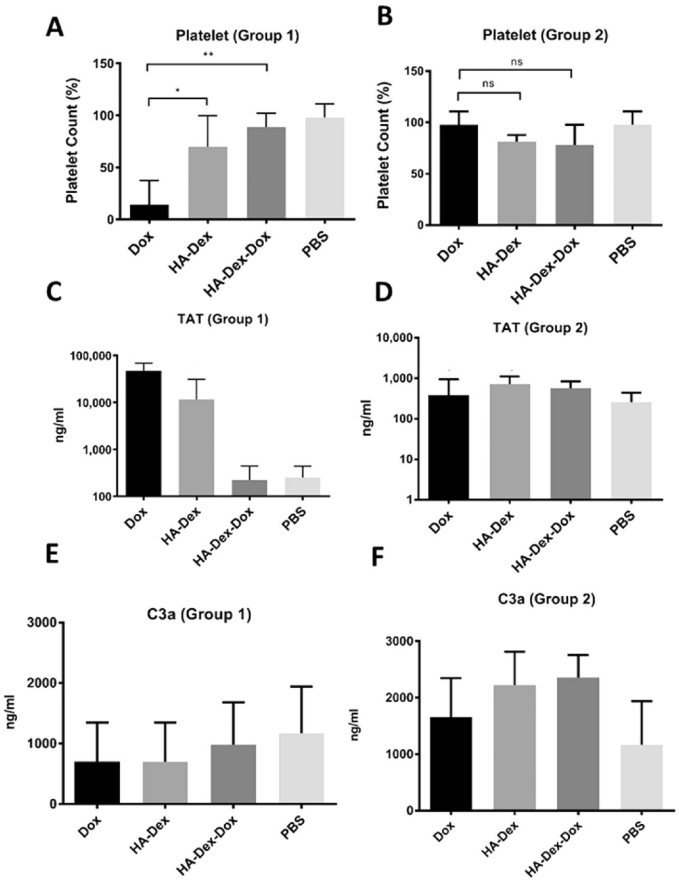

Fig. 3. Left panel represents Group 1 donors and right panel represents Group 2 donors. (A, B) Normalized Platelet aggregation. (C, D) ELISA of Thrombin-antithrombin complex, a marker for coagulation using EDTA plasma (N = 3 donors); (E, F) ELISA of C3a, a marker for complement activation using EDTA plasma (N = 3 donors). Statistical analysis was done by one-way Anova *P < 0.05, **P < 0.01.

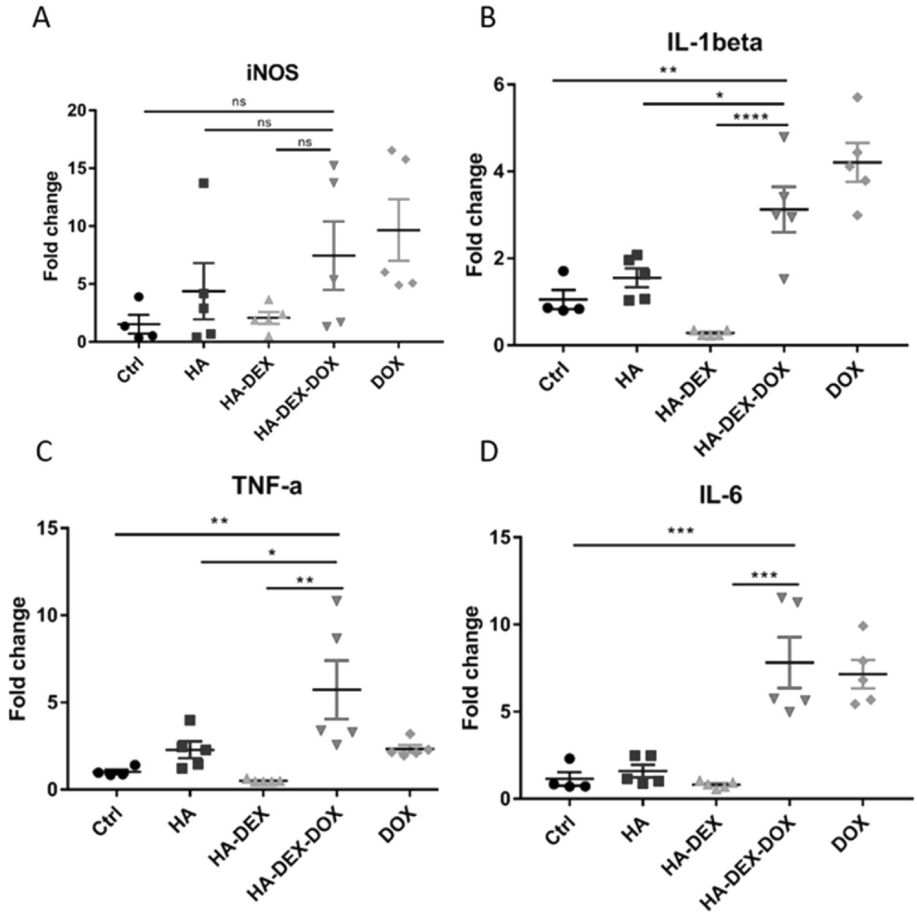

Fig. 4. mRNA expression of pro-inflammatory genes by TAMs as estimated by qRT-PCR and normalized by HPRT gene expression. A) iNOS B) IL-1β C) TNF-α and D) IL-6. Statistical analysis done by one-way Anova *P < 0.05, **P < 0.01, ***P < 0.001.

3.3. Hematological studies and the effect of HA-DEX-DOX on complement system

One of the major drawbacks of chemotherapy is thromboembolism, which causes hypersensitivity reactions in cancer patients (Chanan--Khan et al., 2003; Lyman, Eckert, Wang, Wang, & Cohen, 2013), and is suggested to be the second major cause of cancer-associated deaths among these patients (Caine, Stonelake, Lip, & Kehoe, 2002). In order to evaluate the impact of DOX on platelet aggregation and activation of the complement and coagulation cascades, we performed an *ex vivo* experiment using fresh non-anticoagulated human whole blood (i.e., non-coagulated blood without using any anticoagulants) from six healthy donors. We utilized the modified Chandler loop model to ascertain the hematological responses of free DOX and HA-DEX-DOX nanoparticles (Gurav et al., 2016). Surprisingly, when DOX (60 μM) was incubated with fresh blood from healthy volunteers, blood from 50 % of the healthy donors (i.e. 3 donors; Group 1) aggressively reacted to DOX, triggering aggregation of blood platelets, while the blood from other three donors (Group 2 donors) was non-responsive. The combined data of all the donors are provided in the supporting information (Figure S6 in SI). The reason or the mechanism of activation platelets by DOX in three healthy donors is not clearly understood and warrants further investigation. Conversely, encapsulation of DOX in the HA-DEX-DOX nanoparticles suppressed the DOX induced platelet aggregation (Fig. 3).

We next estimated the activation of coagulation and complement cascade reactions induced by DOX, HA-DEX and HA-DEX-DOX in human whole blood by measuring thrombin-antithrombin (TAT) and anaphylatoxin C3a, respectively, by ELISA. We observed significantly higher TAT generation by DOX in Group 1 donors and this was suppressed when DOX was encapsulated in HA-DEX-DOX. Surprisingly, Group-2 donors did not evoke any TAT activation by DOX or HA-DEX-DOX. However, we were intrigued to find elevated levels of TAT by HA-DEX in both the donor groups. Several factors contribute to the contact activation of coagulation cascade such as the nanoscale curvature (or size of the nanoparticles), the exposed amphiphilic surfaces, the cationic nature of DOX and the chemical composition of the nanoparticles. However, as we do not observe any burst release of ionically bound DOX from the nanoparticle, the TAT activation by DOX in HA-DEX-DOX is improbable. The nanoparticles with higher curvature (smaller size) did not denature Factor XII to the extent as the nanoparticles with lower curvature (larger size) (Sanfins, Augustsson, Dahlbäck, Linse, &

Cedervall, 2014). In addition, the contact activation of coagulation is also influenced by the amphiphilic surfaces (Hunt, Parratt, Cable, Finch, & Yacoub, 1997). We believe the higher TAT activation is attributed to the higher hydrodynamic size (~511 nm) of HA-DEX as compared to the HA-DEX-DOX (~252 nm). The larger HA-DEX particles, will presumably expose higher hydrophobic surfaces, resulting in higher plasma protein adsorption which further activate the coagulation system more than the compact HA-DEX-DOX particle, even though they have identical zeta potential (-23 to −26 mV) and identical chemistry (Kushida, Saha, Subramani, Nandwana, & Rotello, 2014).

Interestingly, when we assessed complement marker (C3a) we did not observe significant differences between DOX, HA-DEX or HA-DEX-DOX, which was comparable with the PBS control. Taken together our data suggests that the encapsulation of DOX in HA-DEX-DOX nanoparticles prevents platelet aggregations and thrombo-inflammation in human whole blood (Fig. 3). This suggests the need for a personalized approach before treating patients with standard chemotherapeutics as DOX in known to trigger blood-mediated thromboinflammation in some patients (Kim et al., 2011).

3.4. Effect of HA-DEX-DOX on bone marrow derived macrophages

Next, we evaluated the immunomodulatory properties of DOX and HA-DEX-DOX nanoparticles on mouse bone-marrow derived macrophages that were pre-activated into an immunosuppressive M2 phenotype following our previously optimized protocol (Parsa et al., 2016). The M2 macrophages mimic the tumor-associated macrophages (TAMs) that comprise nearly 50 % of the tumor bulk (Kim & Bae, 2016). TAMs, enable the tumor to resist immunogenic attacks (Murdoch, Giannoudis, & Lewis, 2004). and diminish the cytotoxic effect of chemotherapeutic drugs (Larionova et al., 2019). To ascertain the immunomodulatory effects of NPs we measured the expression of pro-inflammatory cytokines by immunosuppressive M2 macrophages. When treated with 200 nM DOX or DOX equivalent in HA-DEX-DOX particles for 48 h, we observed elevated levels of iNOS (not statistically significant) (Xue, Yan, Zhang, & Xiong, 2018), IL-1β, TNF-α and IL-6 which are hallmarks of proinflammatory M1 macrophages (Martinez & Gordon, 2014) (Fig. 4). This indicates modulation of macrophage activation state from the M2-like state towards the M1-like state that favors anti-cancer immunity (Jiang et al., 2017). HA-DEX-DOX on the other hand did not show significant effect on pro-inflammatory M1 like macrophages (Figure S7 in SI). Interestingly, encapsulation of DOX in HA-DEX-DOX suppressed the pro-inflammatory response of DOX on the pro-inflammatory M1 like macrophages.

4. Conclusions

In conclusion, we developed a novel HA-derived nanoparticle having an anti-inflammatory drug and loaded with a chemotherapeutic agent (HA-DEX-DOX) designed for combination therapy. Immunological evaluation of the drug-loaded nanoparticles in human whole blood indicated that free DOX induces platelet aggregation in some individuals (but not in others) and that this effect was mitigated upon nano formulation. Our study suggests the need for *ex vivo* immunogenicity models for screening thrombogenic activation induced by chemotherapeutic drugs as a personalized approach in treating patients. The HA-DEX-DOX was effective in inducing modulation of the immunosuppressive M2 macrophages towards the pro-inflammatory M1 phenotype. The therapeutic validation of the two drugs suggested that DEX augmented the toxic effect to DOX in breast cancer and osteosarcoma cell lines while it suppressed the cytotoxicity in colon cancer cells. This implies the need for a careful evaluation of the combination therapy while treating patients. Our approach to develop HA-DEX-DOX nanoparticles has an advantage that it could be stored as a lyophilized powder facilitating long shelf-life and stability allowing easy handling and administration and would be an ideal platform for developing effective anticancer therapeutics.

CRediT authorship contribution statement

Vignesh K. Rangasami: Data curation, Methodology, Writing - review & editing, Formal analysis. **Sumanta Samanta:** Data curation, Methodology, Writing - review & editing. **Vijay Singh Parihar:** Data curation, Methodology. **Kenta Asawa:** Data curation, Methodology. **Keying Zhu:** Data curation, Methodology. **Oommen P. Varghese:** Writing - review & editing. **Yuji Teramura:** Supervision. **Bo Nilsson:** Writing - review & editing. **Jöns Hilborn:** Writing - review & editing. **Robert A. Harris:** Writing - review & editing. **Oommen P. Oommen:** Conceptualization, Methodology, Writing - review & editing, Supervision.

Acknowledgements

We would like to thank Prof. Kristina N Ekdahl from Uppsala University for assisting in the hematological experiments. We would also like to thank Maiju Juusela from Faculty of Medicine and health technologies, Tampere University for assisting in processing the AFM images. SS acknowledge the financial support received from the European Union's Horizon 2020 Marie Sklodowska-Curie grant program(agreement No 713645).

Appendix A. Supplementary data

Supplementary material related to this article can be found, in the online version, at doi:https://doi.org/10.1016/j.carbpol.2020.117291.

References

Aminu, N., Chan, S. Y., Yam, M. F., & Toh, S. M. (2019). A dual-action chitosan-based nanogel system of triclosan and flurbiprofen for localised treatment of periodontitis. *International Journal of Pharmaceutics, 570*. https://doi.org/10.1016/j.ijpharm.2019.118659

Asif, S., Asawa, K., Inoue, Y., Ishihara, K., Lindell, B., Holmgren, R., … Ekdahl, K. N. (2019). Validation of an MPC polymer coating to attenuate surface-induced crosstalk between the complement and coagulation systems in whole blood in in vitro and in vivo models. *Macromolecular Bioscience, 19*(5), Article 1800485. https://doi.org/10.1002/mabi.201800485

Aston, W. J., Hope, D. E., Cook, A. M., Boon, L., Dick, I., Nowak, A. K., … Lesterhuis, W. J. (2019). Dexamethasone differentially depletes tumour and peripheral blood lymphocytes and can impact the efficacy of chemotherapy/checkpoint blockade combination treatment. *OncoImmunology, 8*(11), Article e1641390. https://doi.org/10.1080/2162402X.2019.1641390

Beça, F. F., Caetano, P., Gerhard, R., Alvarenga, C. A., Gomes, M., Paredes, J., & Schmitt, F. (2013). Cancer stem cells markers CD44, CD24 and ALDH1 in breast cancer special histological types. *Journal of Clinical Pathology, 66*(3), 187–191. https://doi.org/10.1136/jclinpath-2012-201169

Bennett, C. L., Djulbegovic, B., Norris, L. B., & Armitage, J. O. (2013). Colony-stimulating factors for febrile neutropenia during Cancer therapy. *The New England Journal of Medicine, 368*(12), 1131–1139. https://doi.org/10.1056/NEJMct1210890

Bütün, V., Armes, S. P., Billingham, N. C., Tuzar, Z., Rankin, A., Eastoe, J., & Heenan, R. K. (2001). The remarkable "Flip−Flop" self-assembly of a diblock copolymer in aqueous solution. *Macromolecules, 34*(5), 1503–1511. https://doi.org/10.1021/ma0018392

Caine, G. J., Stonelake, P. S., Lip, G. Y. H., & Kehoe, S. T. (2002). The hypercoagulable state of malignancy: Pathogenesis and current debate. *Neoplasia, 4*(6), 465–473. https://doi.org/10.1038/sj.neo.7900263

Chanan-Khan, A., Szebeni, J., Savay, S., Liebes, L., Rafique, N. M., Alving, C. R., & Muggia, F. M. (2003). Complement activation following first exposure to pegylated liposomal doxorubicin (Doxil??): Possible role in hypersensitivity reactions. *Annals of Oncology, 14*(9), 1430–1437. https://doi.org/10.1093/annonc/mdg374

Cho, H. J., Yoon, I. S., Yoon, H. Y., Koo, H., Jin, Y. J., Ko, S. H., … Kim, D. D. (2012). Polyethylene glycol-conjugated hyaluronic acid-ceramide self-assembled nanoparticles for targeted delivery of doxorubicin. *Biomaterials, 33*(4), 1190–1200. https://doi.org/10.1016/j.biomaterials.2011.10.064

Foley, J. P., Lam, D., Jiang, H., Liao, J., Cheong, N., McDevitt, T. M., … Savani, R. C. (2012). Toll-like receptor 2 (TLR2), transforming growth factor-β, hyaluronan (HA), and receptor for HA-mediated motility (RHAMM) are required for surfactant protein A-stimulated macrophage chemotaxis. *The Journal of Biological Chemistry, 287*(44), 37406–37419. https://doi.org/10.1074/jbc.M112.360982

Grunberg, S. M. (2007). Antiemetic activity of corticosteroids in patients receiving cancer chemotherapy: Dosing, efficacy, and tolerability analysis. *Annals of Oncology*. https://doi.org/10.1093/annonc/mdl347

Gurav, D., Varghese, O. P., Hamad, O. A., Nilsson, B., Hilborn, J., & Oommen, O. P. (2016). Chondroitin sulfate coated gold nanoparticles: A new strategy to resolve multidrug resistance and thromboinflammation. *Chemical Communications, 52*(5), 966–969. https://doi.org/10.1039/C5CC09215A

He, J., Zhou, J., Yang, W., Zhou, Q., Liang, X., Pang, X., … Liang, H. (2017). Dexamethasone affects cell growth/apoptosis/chemosensitivity of colon cancer via glucocorticoid receptor α/NF-κB. *Oncotarget, 8*(40), 67670–67683. https://doi.org/10.18632/oncotarget.18802

Hunt, B. J., Parratt, R., Cable, M., Finch, D., & Yacoub, M. (1997). Activation of coagulation and platelets is affected by the hydrophobicity of artificial surfaces. *Blood Coagulation & Fibrinolysis, 8*(4), 223–231. https://doi.org/10.1097/00001721-199706000-00003

Jiang, W., Von Roemeling, C. A., Chen, Y., Qie, Y., Liu, X., Chen, J., & Kim, B. Y. S. (2017). Designing nanomedicine for immuno-oncology. *Nature Biomedical Engineering, 1*(2), 0029. https://doi.org/10.1038/s41551-017-0029

Kim, J., & Bae, J.-S. (2016). Tumor-associated macrophages and neutrophils in tumor microenvironment. *Mediators of Inflammation, 2016*, Article 6058147. https://doi.org/10.1155/2016/6058147

Kim, S.-H., Lim, K.-M., Noh, J.-Y., Kim, K., Kang, S., Chang, Y. K., … Chung, J.-H. (2011). Doxorubicin-induced platelet procoagulant activities: An important clue for chemotherapy-associated thrombosis. *Toxicological Sciences, 124*(1), 215–224. https://doi.org/10.1093/toxsci/kfr222

Kisiel, M., Ventura, M., Oommen, O. P., George, A., Walboomers, X. F., Hilborn, J., & Varghese, O. P. (2012). Critical assessment of rhBMP-2 mediated bone induction: An in vitro and in vivo evaluation. *Journal of Controlled Release : Official Journal of the Controlled Release Society, 162*(3), 646–653. https://doi.org/10.1016/j.jconrel.2012.08.004

Kushida, T., Saha, K., Subramani, C., Nandwana, V., & Rotello, V. M. (2014). Effect of nano-scale curvature on the intrinsic blood coagulation system. *Nanoscale, 6*(23), 14484–14487. https://doi.org/10.1039/c4nr04128c

Larionova, I., Cherdyntseva, N., Liu, T., Patysheva, M., Rakina, M., & Kzhyshkowska, J. (2019). Interaction of tumor-associated macrophages and cancer chemotherapy. *OncoImmunology*. https://doi.org/10.1080/2162402X.2019.1596004

Lin, K. T., & Wang, L. H. (2016). New dimension of glucocorticoids in cancer treatment. *Steroids*. https://doi.org/10.1016/j.steroids.2016.02.019

Lyman, G. H., Eckert, L., Wang, Y., Wang, H., & Cohen, A. (2013). Venous thromboembolism risk in patients with Cancer Receiving chemotherapy: A real-world analysis. *The Oncologist, 18*(12), 1321–1329. https://doi.org/10.1634/theoncologist.2013-0226

Martinez, F. O., & Gordon, S. (2014). The M1 and M2 paradigm of macrophage activation: Time for reassessment. *F1000prime Reports, 6*, 13. https://doi.org/10.12703/P6-13

Murdoch, C., Giannoudis, A., & Lewis, C. E. (2004). Mechanisms regulating the recruitment of macrophages into hypoxic areas of tumors and other ischemic tissues. *Blood*. https://doi.org/10.1182/blood-2004-03-1109

Nakai, T., Hirakura, T., Sakurai, Y., Shimoboji, T., Ishigai, M., & Akiyoshi, K. (2012). Injectable hydrogel for sustained protein release by salt-induced association of hyaluronic acid nanogel. *Macromolecular Bioscience, 12*(4), 475–483. https://doi.org/10.1002/mabi.201100352

Oommen, O. P., Garousi, J., Sloff, M., & Varghese, O. P. (2014). Tailored doxorubicin-hyaluronan conjugate as a potent anticancer glyco-drug: An alternative to prodrug approach. *Macromolecular Bioscience, 14*(3), 327–333. https://doi.org/10.1002/mabi.201300383

Oommen, O. P., Wang, S., Kisiel, M., Sloff, M., Hilborn, J., & Varghese, O. P. (2013). Smart design of stable extracellular matrix mimetic hydrogel: Synthesis, characterization, and in vitro and in vivo evaluation for tissue engineering. *Advanced Functional Materials, 23*(10), 1273–1280. https://doi.org/10.1002/adfm.201201698

Oommen, O. P., Duehrkop, C., Nilsson, B., Hilborn, J., & Varghese, O. P. (2016a). Multifunctional hyaluronic acid and chondroitin sulfate nanoparticles: Impact of glycosaminoglycan presentation on receptor mediated cellular uptake and immune activation. *ACS Applied Materials & Interfaces, 8*(32), 20614–20622. https://doi.org/10.1021/acsami.6b06823

Oommen, O. P., Duehrkop, C., Nilsson, B., Hilborn, J., & Varghese, O. P. (2016b). Multifunctional hyaluronic acid and chondroitin sulfate nanoparticles: Impact of glycosaminoglycan presentation on receptor mediated cellular uptake and immune activation. *ACS Applied Materials & Interfaces, 8*(32), 20614–20622. https://doi.org/10.1021/acsami.6b06823

Paidikondala, M., Rangasami, V. K., Nawale, G. N., Casalini, T., Perale, G., Kadekar, S., … Varghese, O. P. (2019). An unexpected role of hyaluronic acid in trafficking siRNA across the cellular barrier: The first biomimetic, anionic, non-viral transfection method. *Angewandte Chemie - International Edition, 58*(9), 2815–2819. https://doi.org/10.1002/anie.201900099

Parsa, R., Lund, H., Tosevski, I., Zhang, X.-M., Malipiero, U., Beckervordersandforth, J., … Harris, R. A. (2016). TGFβ regulates persistent neuroinflammation by controlling Th1 polarization and ROS production via monocyte-derived dendritic cells. *Glia, 64*(11), 1925–1937. https://doi.org/10.1002/glia.23033

Plattt, V. M., & Szoka, F. C. (2008). Anticancer therapeutics: Targeting macromolecules and nanocarriers to hyaluronan or CD44, a hyaluronan receptor. In *Molecular pharmaceutics* (Vol. 5, pp. 474–486). American Chemical Society. https://doi.org/10.1021/mp800024g

Qian, Y.-H., Xiao, Q., Chen, H., & Xu, J. (2009). Dexamethasone inhibits camptothecin-induced apoptosis in C6-glioma via activation of Stat5/Bcl-xL pathway. *Biochimica et Biophysica Acta, 1793*(5), 764–771. https://doi.org/10.1016/j.bbamcr.2009.01.017

Rayahin, J. E., Buhrman, J. S., Zhang, Y., Koh, T. J., & Gemeinhart, R. A. (2015). High and low molecular weight hyaluronic acid differentially influence macrophage activation. *ACS Biomaterials Science & Engineering, 1*(7), 481–493. https://doi.org/10.1021/acsbiomaterials.5b00181

Sanfins, E., Augustsson, C., Dahlbäck, B., Linse, S., & Cedervall, T. (2014). Size-dependent effects of nanoparticles on enzymes in the blood coagulation cascade. *Nano Letters, 14*(8), 4736–4744. https://doi.org/10.1021/nl501863u

Stokes, K. Y., & Granger, D. N. (2012). Platelets: A critical link between inflammation and microvascular dysfunction. *The Journal of Physiology*. https://doi.org/10.1113/jphysiol.2011.225417

Varghese, O. P., Kisiel, M., Martinez-Sanz, E., Ossipov, D. A., & Hilborn, J. (2010). Synthesis of guanidinium-modified hyaluronic acid hydrogel. *Macromolecular Rapid Communications, 31*(13), 1175–1180. https://doi.org/10.1002/marc.200900906

von Hundelshausen, P., & Weber, C. (2007). Platelets as immune cells. *Circulation Research, 100*(1), 27–40. https://doi.org/10.1161/01.res.0000252802.25497.b7

Wang, H., Li, M., Rinehart, J. J., & Zhang, R. (2004). Dexamethasone as a chemoprotectant in cancer chemotherapy: Hematoprotective effects and altered pharmacokinetics and tissue distribution of carboplatin and gemcitabine. *Cancer Chemotherapy and Pharmacology, 53*(6), 459–467. https://doi.org/10.1007/s00280-003-0759-9

Wang, L. J., Li, J., Hao, F. R., Yuan, Y., Li, J. Y., Lu, W., & Zhou, T. Y. (2016). Dexamethasone suppresses the growth of human non-small cell lung cancer via inducing estrogen sulfotransferase and inactivating estrogen. *Acta Pharmacologica Sinica, 37*(6), 845–856. https://doi.org/10.1038/aps.2016.39

Weischenfeldt, J., & Porse, B. (2008). Bone marrow-derived macrophages (BMM): Isolation and applications. *Cold Spring Harbor Protocols, 2008*(12). https://doi.org/10.1101/pdb.prot5080. pdb.prot5080-pdb.prot5080.

Xue, Q., Yan, Y., Zhang, R., & Xiong, H. (2018). Regulation of iNOS on immune cells and its role in diseases. *International Journal of Molecular Sciences, 19*(12), 3805. https://doi.org/10.3390/ijms19123805

Zheng, Y., Izumi, K., Li, Y., Ishiguro, H., & Miyamoto, H. (2012). Contrary regulation of bladder cancer cell proliferation and invasion by dexamethasone-mediated glucocorticoid receptor signals. *Molecular Cancer Therapeutics, 11*(12), 2621–2632. https://doi.org/10.1158/1535-7163.MCT-12-0621

PUBLICATION 2

Pluronic micelle-mediated tissue factor silencing enhances hemocompatibility, stemness, differentiation potential, and paracrine signaling of mesenchymal stem cells

V.K. Rangasami, G. Nawale, K. Asawa, S. Kadekar, S. Samanta, B. Nilsson, K.N. Ekdahl, S. Miettinen, J. Hilborn, Y. Teramura, O.P. Varghese, O.P. Oommen

Biomacromolecules, Volume 22, 5, 2021, 1980-1989
https://doi.org/10.1021/acs.biomac.1c00070

BioMACROMOLECULES

pubs.acs.org/Biomac

Article

Pluronic Micelle-Mediated Tissue Factor Silencing Enhances Hemocompatibility, Stemness, Differentiation Potential, and Paracrine Signaling of Mesenchymal Stem Cells

Vignesh K. Rangasami, Ganesh Nawale, Kenta Asawa, Sandeep Kadekar, Sumanta Samanta, Bo Nilsson, Kristina N. Ekdahl, Susanna Miettinen, Jöns Hilborn, Yuji Teramura, Oommen P. Varghese, and Oommen P. Oommen*

Cite This: *Biomacromolecules* 2021, 22, 1980–1989

Read Online

ACCESS | Metrics & More | Article Recommendations | Supporting Information

ABSTRACT: Mesenchymal stem/stromal cells (MSCs) evoke great excitement for treating different human diseases due to their ability to home inflamed tissues, suppress inflammation, and promote tissue regeneration. Despite great promises, clinical trial results are disappointing as allotransplantation of MSCs trigger thrombotic activity and are damaged by the complement system, compromising their survival and function. To overcome this, a new strategy is presented by the silencing of tissue factor (TF), a transmembrane protein that mediates procoagulant activity. Novel Pluronic-based micelles are designed with the pendant pyridyl disulfide group, which are used to conjugate TF-targeting siRNA by the thiol-exchange reaction. This nanocarrier design effectively delivered the payload to MSCs resulting in ∼72% TF knockdown (KD) without significant cytotoxicity. Hematological evaluation of MSCs and TF-KD MSCs in an ex vivo human whole blood model revealed a significant reduction in an instant-blood-mediated-inflammatory reaction as evidenced by reduced platelet aggregation (93% of free platelets in the TF-KD group, compared to 22% in untreated bone marrow-derived MSCs) and thrombin−antithrombin complex formation. Effective TF silencing induced higher MSC differentiation in osteogenic and adipogenic media and showed stronger paracrine suppression of proinflammatory cytokines in macrophages and higher stimulation in the presence of endotoxins. Thus, TF silencing can produce functional cells with higher fidelity, efficacy, and functions.

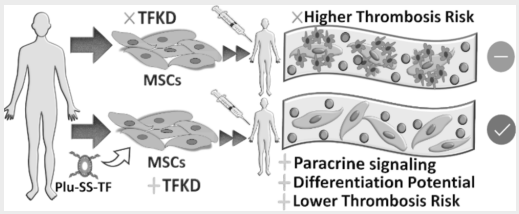

■ INTRODUCTION

Mesenchymal stem/stromal cells (MSCs) are adult stem cells that orchestrate immunoregulatory functions and have been extensively evaluated in clinical trials for treating various diseases such as graft-versus-host disease, liver cirrhosis, Crohn disease, stroke, myocardial infarction, allograft rejection, and multiple sclerosis.[1] MSCs are believed to be immunoprivileged and are transplanted to patients across the major histocompatibility complex barriers. However, recent studies suggest that upon transplantation, patients generate antibodies against these cells, leading to immune rejection.[2,3] MSCs express C3a and C5a receptors that help in the recruitment of these cells to the injury site.[4] MSCs also express key regulators such as CD46, CD55, and CD59 that provide defense against the autologous complement.[5] However, despite these factors, stem cells receive limited protection from complement-mediated cell lysis. Several studies reveal that infusion of MSCs in patients leads to pulmonary thromboembolism mediated by activation of the coagulation cascade[6−8] with some patients suffering fatal consequences.[9] Among different factors that drive thrombotic response, the tissue factor (TF, also called CD142 or factor III) encoded by the *F3* gene and expressed on the MSC surface is believed to be the most dominating factor and a key determinant of hemocompatibility.[10] TF expression activates coagulation and leads to elevated levels of the thrombin−antithrombin (TAT) complex.[7,11]

Careful selection of bone marrow-derived MSCs (BMSCs) that are deficient in TF is therefore proposed as a novel strategy to improve the hemocompatibility of the transplanted cells.[12] MSCs derived from the adipose tissue (ASCs) express higher TF and show elevated procoagulant activity as compared to the BMSCs.[13] Therefore, systemic administration of ASCs results in a lower in vivo survival rate than BMSCs.[14] Hence, there is a pressing need to develop new tools to engineer MSCs that could suppress the instant blood-mediated

Received: January 20, 2021
Revised: March 25, 2021
Published: April 5, 2021

inflammatory reaction (IBMIR), which significantly suppress the efficacy of MSCs after in vivo infusion. There is also a need to enhance the stemness and differentiation potential of MSCs for safer and effective translation of cell-based products. One of the promising strategies to engineer stem cells with enhanced in vivo survival and paracrine functions is by ex vivo manipulation of these cells. Engineered cell-based therapies have gained prominence over the past decade and even gained approval from the Center for Biologics Evaluation and Research in the United States[15] and the European Medicines Agency in Europe.[16,17] There have already been studies using engineered stem cells to treat pancreatic cancer using MSCs armed with the TRAIL gene[18] to deliver growth factors in an ALS model[19] and CRISPR edited stem cells to produce erythroid protein to treat disorders that require protein replacement therapy.[20] As TF expressed on the stem cell surface is one of the key drivers of the coagulation cascade, we hypothesized that effective silencing of procoagulative pathways in MSCs before infusion would potentially suppress the damage caused by IBMIR. Such engineered cells could not only increase cell survival but also display higher fidelity, efficacy, and functions upon transplantation.

We have recently reported the first anionic transfection method to deliver siRNA molecules to MSCs using hyaluronic acid-coated nanoparticles, which could efficiently transfect cells under standard culture conditions[21] as well as under suspension conditions.[22] However, such strategies require a significantly higher concentration of RNA for effective knockdown (KD) as complexation with two anionic polymers is not very efficient and the use of excess biopolymer also blocks the nanoparticle uptake. We, therefore, envisioned developing a charge-neutral nanoparticle system where siRNA is covalently conjugated to the nanocarrier. To engineer such a system that safely delivers TF-targeting siRNA to MSCs, we utilized Pluronic F108, a block copolymer possessing a poly(ethylene glycol)-*block* or PEG as a hydrophilic arm and poly(propylene glycol) forming the hydrophobic core that self-assembles to form nanoparticles (NPs).

■ EXPERIMENTAL SECTION

Synthesis of Pluronic-siRNA Conjugates with Disulfide Linkage. Disulfide functional siRNA was synthesized on an automated solid-phase synthesizer using a thiol-modified solid support to the sense strand of siRNA employing the standard synthesis cycle for RNA. Further, both the strands were deprotected and purified by polyacrylamide gel electrophoresis (PAGE), and the equimolar amount was mixed to form a duplex. To the solution of duplex RNA (50 μL, 2.5 nmol, 25 μM), dithiothreitol (DTT, 10 μL, 50 mM) and H_2O (40 μL) were added. The reaction mixture was incubated at 37 °C for 2 h. Thereafter, 3 M NaCl (150 μL) was added, followed by H_2O (150 μL), and the mixture was vortexed and centrifuged down. Then, ethanol (100%, 1000 μL) was added, vortexed, and stored at −20 °C for 18 h. The RNA was micro-centrifuged at 13,000 rpm for 20 min at 4 °C. The supernatant was removed. The pellet was washed with absolute ethanol (100 μL) and micro-centrifuged at 13,000 rpm at 4 °C for 10 min, and the supernatant was removed. The pellet was directly dissolved in disulfide-activated Pluronic solution [368 μL, phosphate-buffered saline (PBS), pH 8, 250 nmol] (detailed description in the Supporting Information). The reaction mixture was incubated at room temperature overnight. Then, the reaction mixture was directly used for conjugation analysis and gene KD experiments.

Particle Size Distribution by Dynamic Light Scattering. The particle size distribution of the nanoparticles was carried out using a laser granulometer (Zetasizer Nano ZS, Malvern, UK) using a disposable polystyrene cuvette. For the Plu-SS-TF/Ca particles, 100 nM equivalents of siRNA in Plu-SS-TF were added to 50 μL of 100 mM $CaCl_2$. This mixture was then vortexed and incubated at room temperature for 10 min. An aliquot of 700 μL of deionized water was added to the solution, and the dynamic light scattering (DLS) experiments were performed. The experiments at 25 °C were performed immediately, whereas the solution was incubated at 37 °C for 30 min before the recordings were done at 37 °C. For the Plu-SS-TF particles without the calcium complexation, 100 nM of siRNA equivalent in Plu-SS-TF was added directly to 750 μL of deionized water, and the DLS measurement was recorded. The surface zeta potential for both the formulations was subsequently measured using a Zetasizer Nano ZS at 25 °C using disposable folded capillary DTS1070 cells.

Cell Culture. The BMSCs were isolated from a bone marrow aspirate sample obtained from a surgical procedure at the Department of Orthopedics and Traumatology, Tampere University Hospital, with the patient's consent. The study was conducted in accordance with the Ethics Committee of the Pirkanmaa Hospital District, Tampere (R15174). These BMSCs cells were cultured in α-MEM high glucose (Thermo Fisher Scientific, Vantaa, Finland) with 10% fetal bovine serum (FBS) and 1% penicillin−streptomycin (Penstrep). The cells used in this study were between passages 4 and 6. StemPro osteogenesis and adipogenesis differentiation kits from Gibco were used in the differentiation experiments. THP-1 cells were cultured in RPMI with 10% FBS and 1% Penstrep. Phorbol 12-myristate 13-acetate (PMA) (50 ng/mL) was used to differentiate the THP-1 cells to the M0 state. 500 ng/mL lipopolysaccharide (LPS) was used to activate the M0 cells into the M1 phase.

Transfection of Cells. Cells were transfected with pyridyl disulfide Pluronic F108 conjugated TF 3 (Plu-SS-TF) siRNA with calcium chloride and RNAiMAX (Thermo Fisher Scientific, Vantaa, Finland). Nanoparticles of Pluronic-linked siRNA and calcium chloride (Plu-SS-TF/Ca) were prepared by adding 50 nM of Pluronic-linked TF siRNA to 25 μL of 100 mM $CaCl_2$. They were mixed by vortexing, followed by incubation at room temperature for 10 min. At the end of incubation, the Plu-SS-TF/Ca nanoparticles were added to cells in a single well of a 24-well plate. Cells were also transfected with Pluronic-linked TF siRNA by RNAiMAX (Plu-SS-TF/RNAiMAX). Unconjugated TF siRNA was transfected with both RNAiMAX (TF/RNAiMAX) and Plu-SS and calcium chloride (Plu-SS/TF/Ca) using similar amounts of siRNA and calcium chloride. The cells were incubated for 24 h after transfection at 37 °C and 5% CO_2. RNA was then isolated and quantitative real-time polymerase chain reaction (qRT-PCR) was performed, as described in the Supporting Information.

Hematological Studies. Fresh human whole blood was obtained from three healthy volunteers who had not received any medication for at least 10 days before donation, and no heparin was added into the blood. Loops of the polyurethane tubing (an inner diameter of 6.3 mm) with the 2-methacryloyloxyethyl phosphorylcholine (MPC) polymer [poly(MPC-*co*-*n*-butyl methacrylate)] with a 0.30 MPC unit mole fraction were used for the whole blood experiments.[23] Stainless-steel connectors were coated with the Corline heparin surface (Corline Systems AB, Uppsala, Sweden) according to the manufacturer's protocol. Loops were composed of the tubing that was closed with surface-heparinized connectors (length: 30 cm, blood volume: 2.5 mL) and were loaded with samples. There were two groups of 1.5×10^4 cells each, the cells after the KD of TF (Plu-SS-TF/Ca) and cells without TF-KD (control MSCs). They were then rotated on a wheel at 50 rpm in a 37 °C cabinet for 1 h. As a negative control, the same volume of the cell culture medium was used. The blood was collected and mixed with ethylenediaminetetraacetic acid (EDTA) (10 mM) and then centrifuged (3400 rpm, 20 min, 4 °C) to collect plasma. The collected plasma was stored at −80 °C before enzyme-linked immunosorbent assay (ELISA) analysis (described in detail in the Supporting Information). These experiments were repeated three times using blood from different donors for each group. Ethical approval was obtained from the regional ethics committee in Uppsala (#2008-264).

https://doi.org/10.1021/acs.biomac.1c00070
Biomacromolecules 2021, 22, 1980−1989

Scheme 1. Schematic Description of the Steps Involved in the Synthesis of Plu-SS-TF/Ca

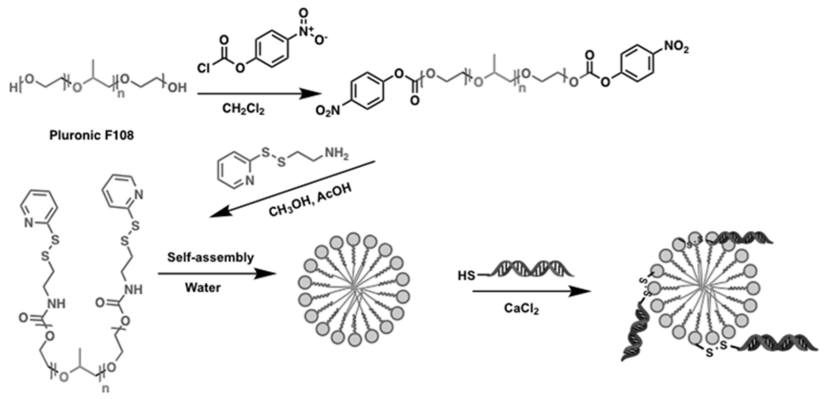

Differentiation Experiments. The cells were transfected with Plu-SS-TF and incubated for 24 h under normal culture conditions. The mediums were then replaced with the osteogenic medium (StemPro Osteogenesis Differentiation Kit from Gibco) and adipogenic mediums separately for 16 days. Osteogenic differentiation of cells was analyzed by alizarin red (Sigma-Aldrich) staining.[24] Briefly, the cells were fixed with 4% paraformaldehyde for 15 min. They were washed with PBS twice and stained with 2% alizarin red solution for 5 min. The samples were then washed twice with water and observed under a microscope. The adipogenic differentiation of the cells was observed by staining the cells with Nile red (Sigma-Aldrich).[25] Briefly, the cells were fixed with 4% paraformaldehyde for 15 min. They were washed with PBS twice and stained with 300 nM of Nile red solution. The samples were incubated with the dye for 30 min, after which they were washed with PBS and observed under a fluorescence microscope (Nikon Eclipse Ti2). The expression levels of the osteogenic markers alkaline phosphatase (ALP), osteocalcin (BGLAP), and distal-less homeobox 5 (DLX5) and the adipogenic markers lipoprotein lipase (LPL) and peroxisome proliferator activated receptor gamma (PPARG) were analyzed by qRT-PCR. The expression levels of these Plu-SS-TF/Ca-treated MSCs were compared with untreated controls.

Condition Medium on THP-1 Cells. The THP-1 cells were first differentiated with 50 ng/mL of PMA (Sigma-Aldrich) for 24 h at 37 °C and 5% CO_2. The cells were then differentiated 500 ng/mL LPS (Sigma-Aldrich) for 24 h at 37 °C and 5% CO_2. These cells were then detached with 2 mM EDTA (Sigma-Aldrich) and plated in 24-well plates (60,000 cells/well). These macrophage were incubated with a conditioned medium (CM) collected from the MSCs that were either treated with Plu-SS-TF/Ca or untreated control (CM collected after 2 days). The cells were then incubated for 3 days, after which RNA was extracted, and the expression levels of proinflammatory genes were analyzed by qRT-PCR. The TaqMan primers for IL-1β, TNF, and IL-10 were obtained from Thermo Fisher Scientific, Finland.

BMSC Stimulation with LPS. Briefly, 50,000 cells were seeded in 24-well plates with 500 μL of α-MEM (Gibco) containing 10% FBS (Gibco, South America) and 1% Penstrep (Gibco) and incubated overnight at 37 °C and 5% CO_2. The cells were then exposed to 50 nM of the Plu-SS-TF/Ca complex. The cells were then incubated for 48 h at 37 °C and 5% CO_2, after which LPS (2 μg/mL) was added to the cells. For the purpose of control, one group of cells not treated with Plu-SS-TF/Ca and treated with 2 μg/mL LPS and one group of untreated cells were used. After 24 h of incubation, RNA was extracted, and the expression levels of proinflammatory genes were analyzed by qRT-PCR as mentioned above. The TaqMan primers for IL-1β, TNF, and iNOS were obtained from Thermo Fisher Scientific, Finland.

RESULTS AND DISCUSSION

Pluronic-based nanocarriers are effectively used for delivering chemotherapeutic drugs, plasmid DNA, and siRNA molecules as they can coat amphiphilic molecules by hydrophobic interactions.[26−28] Pluronic F127-coated siRNA/calcium phosphate nanocomplexes are also developed for siRNA delivery to mammalian cells.[29] Such nanocomplexes are not very efficient as a physical association does not provide good control over siRNA loading efficiency, resulting in inhomogeneous particle distribution. The release of the cargo molecules could also be affected by the temperature (as Pluronic is a thermoresponsive polymer) as well as by the presence of different biomolecules in the milieu. We, therefore, envisaged adopting a covalent grafting strategy where siRNA is covalently conjugated on the hydrophilic arm of the block polymer that would facilitate efficient micelle formation and promote intracellular transport of the cargo molecule. To achieve this aim, we incorporated redox-responsive disulfide groups that provide the dual advantage of fast delivery to the cytosol and glutathione-mediated selective dissociation inside the cells. The excess disulfide groups present on the particle surface after siRNA conjugation can also be exploited for conjugating targeting peptides. To engineer redox-responsive nanocarriers, we first conjugated disulfide pyridyl groups to the terminal hydroxyls present on PEG units by activating the hydroxyls with 4-nitrophenyl chloroformate, followed by nucleophilic displacement reaction with 2-(pyridin-2-yldisulfaneyl)ethan-1-amine, also termed as the amino disulfide pyridyl molecule. We succeeded in obtaining an unprecedented degree of PEG functionalization of over 95% with respect to the available hydroxyls, as verified by UV−vis measurements. In the next step, the disulfide pyridyl-functionalized Pluronic F108 was conjugated with thiol-modified siRNA targeting the TF gene where the thiol groups were incorporated at the 3′ end of the sense strand (Scheme 1). The ratio of siRNA thiol groups and disulfide pyridyl groups was fixed at 10 mol % to achieve quantitative coupling. Indeed, we succeeded in obtaining over 95% conjugation, as evidenced by gel electrophoresis (20% PAGE; Figure 1D). The covalent conjugation resulted in retardation of mobility, indicating higher-molecular-weight species in lane 2 and lane 3, which represents the Pluronic F108-siRNA conjugate (Plu-SS-TF) and the Pluronic F108-siRNA conjugate complexed with 5 mmol Ca^{2+} (Plu-SS-TF/

https://doi.org/10.1021/acs.biomac.1c00070
Biomacromolecules 2021, 22, 1980−1989

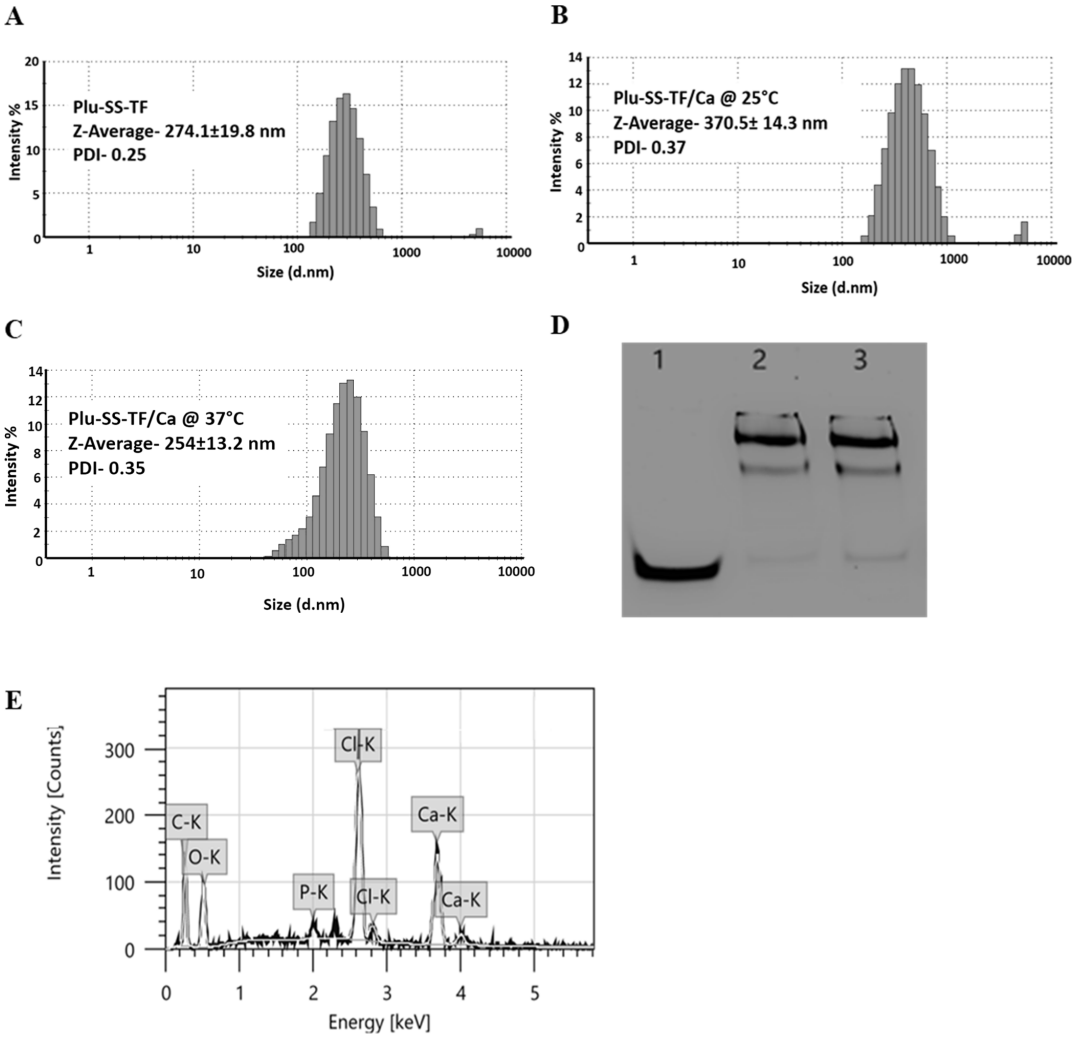

Figure 1. (A) Hydrodynamic size of Plu-SS-TF without calcium complexation and (B, C) with calcium complexation at 25 and 37 °C, respectively. (D) Gel electrophoresis indicating nanoparticle formation. Lane 1 = free siRNA; lane 2 = Plu-SS-TF with calcium complexation; lane 3 = Plu-SS-TF without calcium complexation. (E) EDS elemental mapping indicating the presence of carbon, phosphate, and calcium in Plu-SS-TF/Ca.

Ca). The native siRNA is presented in lane 1. The siRNA conjugated polymer self-assembled to form micelles that showed a hydrodynamic size of ∼274 nm with unimodal distribution (Figure 1A), which upon complexation with Ca^{2+} displayed a hydrodynamic size of ∼370 nm (Figure 1B), as determined by the DLS experiment. We also confirmed the presence of elemental carbon, phosphate, and calcium in the particles by EDS analysis (Figure 1E). The zeta potential of Plu-SS-TF was estimated to be −12.1 mV, which changed to −0.515 mV upon complexation with Ca^{2+} (Plu-SS-TF/Ca) (Figure S2 in the Supporting Information). This indicates that the addition of Ca^{2+} ions neutralized the net negative charge of phosphates, maintaining an overall near neutral charge. Interestingly, Plu-SS-TF/Ca also displayed thermoresponsive properties as the hydrodynamic size of the micelles reduced from 370 to 254 nm when the DLS experiment was performed at 37 °C instead of 25 °C (Figure 1C). This was also confirmed by scanning electron microscopy (SEM) analysis, which confirmed spherical nanoparticle formation with a ∼200 nm in size (Figure S3 in the Supporting Information).

After successful conjugation of TF siRNA with a releasable disulfide linker to Pluronic micelles (Plu-SS-TF), we performed transfection studies of BMSCs. Since clinical studies with MSCs limit the cell expansion to a maximum of four passages to retain the differentiation potential,[30] we decided to use BMSCs of higher passages (passages 4−6) in our study. Higher passages are expected to increase the expression of TF,[8] and we believe that efficient KD of TF in

https://doi.org/10.1021/acs.biomac.1c00070
Biomacromolecules 2021, 22, 1980−1989

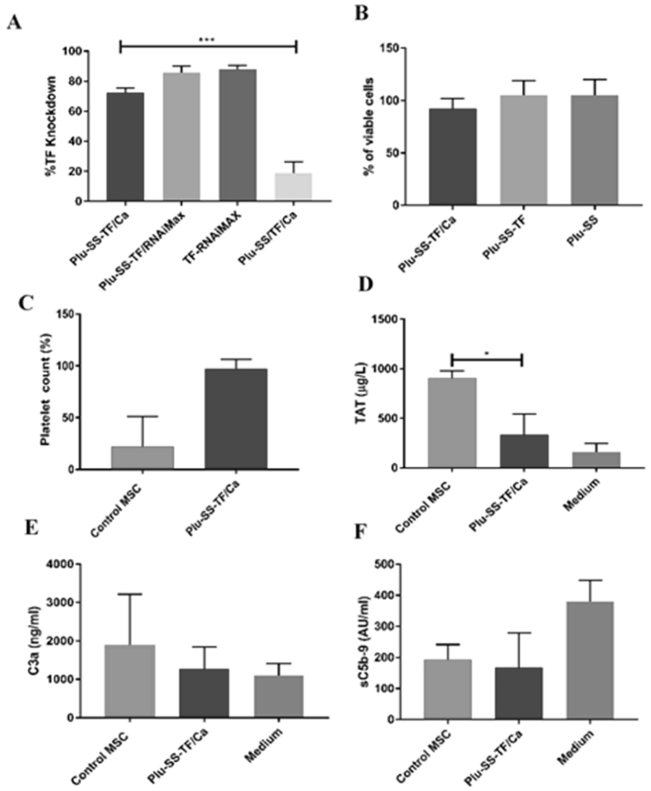

Figure 2. (A) In vitro KD efficiency of different formulations of the nanoparticles with calcium complexation and RNAiMAX. Statistics was done by ANOVA on GraphPad Prism (***$P < 0.001$). (B) Cell viability percentages obtained for the nanoparticles and their components through the MTT assay. (C) Platelet counts normalized against the growth medium. (D) TAT complex, a marker for coagulation in whole blood ($N = 3$). (E, F) C3a and sC5b-9, markers for complement activation in whole blood ($N = 3$). Statistical analysis was done by the Kruskal–Wallis T-test, *$P < 0.05$.

these cells could overcome the deleterious performance of such MSCs, improving its in vivo survival and function. To test the gene silencing efficiency, we first tested the physical coating of the siRNA/Ca^{2+} nanocomplex with the Pluronics F108 polymer functionalized with disulfide pyridyl groups (Plu-SS/TF/Ca) as Pluronics coating of the complex is reported to enhance siRNA delivery.[29] However, we observed a modest 20% gene silencing with a 50 nM concentration using this system. On the contrary, the positive control experiment with RNAiMAX (TF-RNAiMAX) gave an 86% mRNA silencing efficiency, indicating that the siRNA sequence is effective in silencing the TF gene. Interestingly, the covalently conjugated Plu-SS-TF complexed with Ca^{2+} (Plu-SS-TF/Ca) showed a TF-KD efficiency of 72% when the same concentration of siRNA (50 nM) was used. MSCs are known to be hard-to-transfect cells,[31] and we believe that the enhanced transfection efficiency of our nanocarrier is due to dithiol groups which are reported to improve the rapid internalization of molecular conjugates.[32] Earlier reports of high transfection efficiency in MSCs have always come at the cost of poor viability due to the toxicity of the nanocarrier.[31] This is mainly attributed to the cationic charges on the surface of the particles.[33] We have previously reported that coating of cationic nanoparticles with anionic polymers not only mitigates cellular toxicity but also assists in the endosomal release of the cargo molecules.[34] Since the Plu-SS-TF/Ca nanoparticle has a net neutral charge, we anticipated such particles to have minimal toxicity. To evaluate the cytotoxicity of our nanocarrier system, we measured the cellular metabolic activity using the MTT assay, which is an indicator of cell viability, proliferation, and cytotoxicity, and compared it with commercially available RNAiMAX. Interestingly, neither the Pluronic-based micelles (Plu-SS and Plu-SS-TF) nor RNAiMAX showed any toxicity (~100% cell viability); however, upon complexation with Ca^{2+} (Plu-SS-TF/Ca), the micelles showed ~90% cell viability (Figure 2B).

Next, we evaluated the effect of TF-KD of BMSCs on the activation of the coagulation cascade using an ex vivo chandler loop model.[35] We incubated the 1×10^4 BMSCs for 1 h in non-anti-coagulated human whole blood. As anticipated, the TF-KD BMSCs displayed enhanced stability and attenuated platelet aggregation in blood, as evidenced by the availability of ~93% free platelets (normalized against the growth medium) when compared with untreated BMSCs (22% free platelets) (Figure 2C). This is further corroborated with the TAT complex determination where the TF-KD BMSCs showed significantly lower TAT complex formation when compared to

https://doi.org/10.1021/acs.biomac.1c00070
Biomacromolecules 2021, 22, 1980−1989

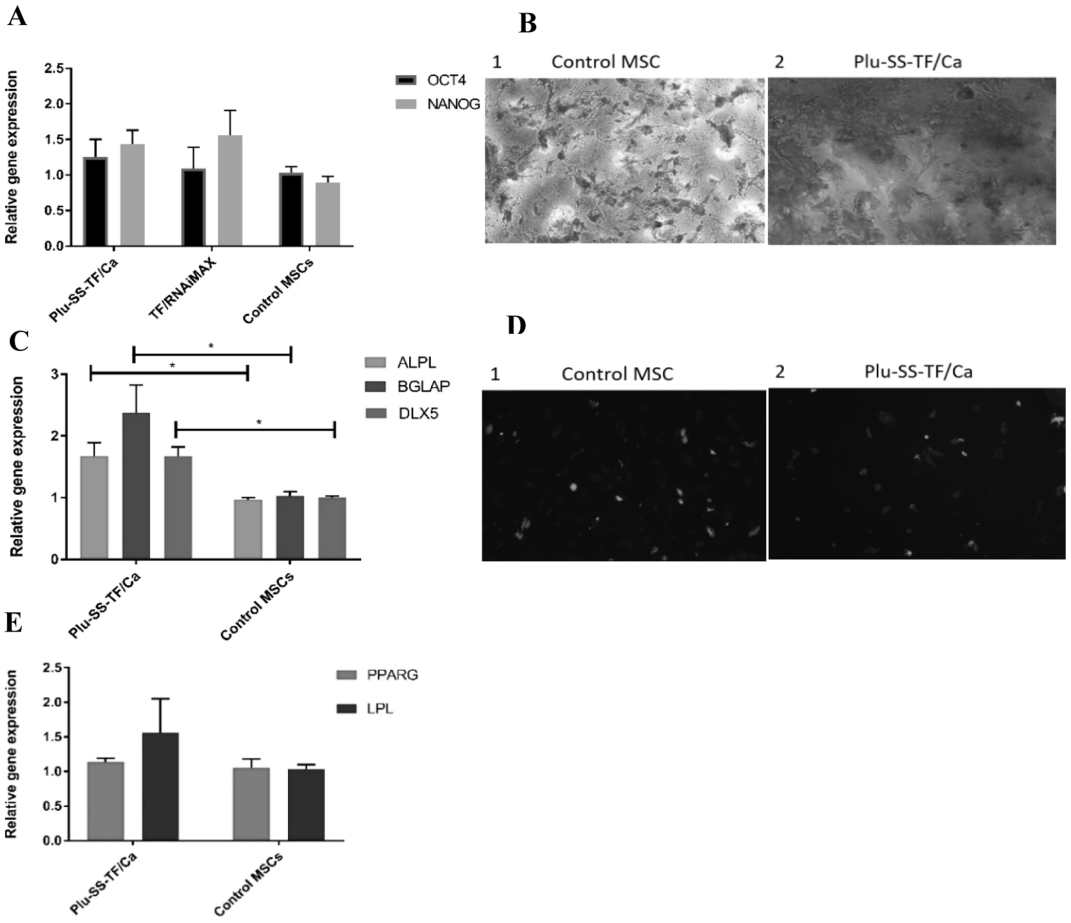

Figure 3. (A) qRT-PCR analysis done to determine the level of OCT4 and NANOG to analyze the stemness of the TF-KD cells and untreated MSCs. (B) qRT-PCR analysis of osteogenic markers. Statistics was done by the Mann−Whitney test on GraphPad Prism (*P < 0.05). (C, D) Differentiation studies of TF-KD MSCs and MSCs after 16 days of culture. (C) Alizarin red staining to detect the presence of calcium deposits of MSCs cultured under osteogenic conditions. (C1) Control MSCs and (C2) MSCs after treatment with Plu-SS-TF/Ca. (D) Nile red staining of MSCs to detect the presence of lipid vacuoles cultured under adipogenic conditions. (D1) Control MSCs and (D2) MSCs after treatment with Plu-SS-TF/Ca. (E) qRT-PCR analysis of adipogenic markers.

the untreated cells (Figure 2D). Interestingly, we did not see any significant difference in the early and late complement activation markers, namely, C3a and sC5b-9 between the two groups (Figure 2E,F).

As KD of genes in BMSCs could potentially evoke unprecedented responses by altering the paracrine function or by reducing the multipotency of the cells, we investigated the BMSC function by different biochemical methods. We first tested the expression of key cell surface markers that characterize the stem cell physiognomies. It is universally accepted that cells that exhibit positive co-expression of CD105, CD73, and CD90 and are negative for CD45, CD34, and CD14 are characterized as MSCs.[36] We performed flow cytometry studies to ascertain the impact of TF-KD on the expression of these key cell surface markers. We found that the control BMSCs displayed good population of cells that exhibited high expressions of CD73 (92.1 ± 1.62%), CD105 (91.4 ± 1.8%), and CD90 (82.5 ± 3.2%) and lacked the expression of CD34 (0.4 ± 0.2%) (Figure S4 in the Supporting Information). Gratifyingly, the expression of these markers on the TF-KD BMSC population did not show significant changes. We found that CD73 (89.2 ± 2.2%), CD105 (90.8 ± 1.6%), and CD34 (1.2 ± 0.6%) remained similar, whereas we observed an 8% loss of cells that expressed CD90 (74.1 ± 1.9%) molecules (Figure S3 in the Supporting Information). CD90 is a glycoprotein expressed on the cell surface and is a stem cell marker that signifies the undifferentiated status of MSCs. CD90 (THY-1) controls the differentiation of MSCs as it acts as an impediment toward the pathway of differentiation commitment, and lower expression of CD90 correlates with temporal lineage commitment in vitro.[37] Thus, lower expression of CD90 as a result of TF-KD could help to increase the differentiation capability of MSCs.[37] In order to validate the effect of TF-KD on stemness, we measured the

https://doi.org/10.1021/acs.biomac.1c00070
Biomacromolecules 2021, 22, 1980−1989

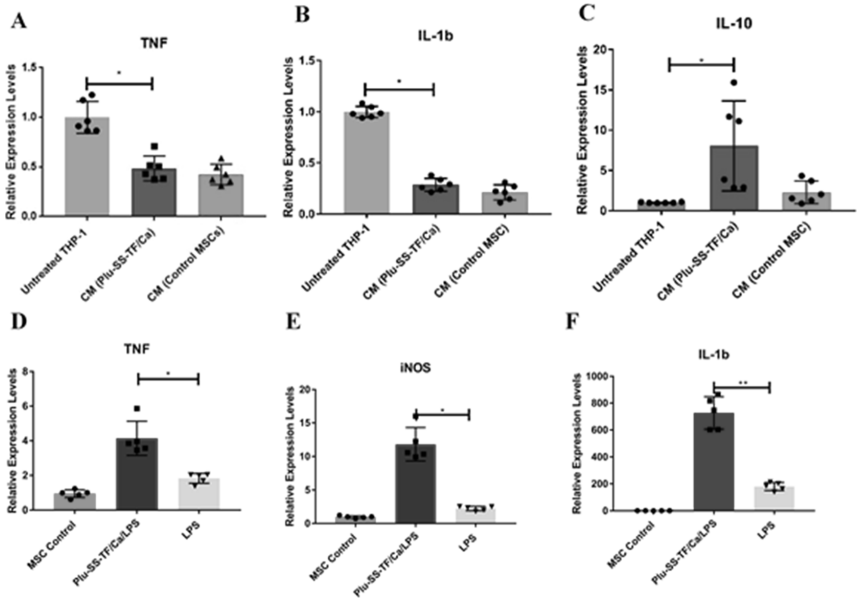

Figure 4. (A–C) Effect of the MSC secretome (CM) on proinflammatory M1 macrophages derived from THP-1 cells. qRT-PCR analysis quantifying the cytokine mRNA levels of (A) TNF, (B) IL-1β, and (C) IL-10. (D–F) Paracrine signaling of MSCs and TF-KD MSCs by direct stimulation with endotoxin LPS (2 μg/mL) relative to the untreated MSC control. qRT-PCR analysis quantifying the cytokine mRNA levels of (D) TNF, (E) iNOS, and (F) IL-1β. Gene expression is relative to β-actin. Statistics was done by the Kruskal–Wallis method ($^*P \leq 0.05$, $^{**}P \leq 0.01$).

expression of OCT4 and the NANOG gene by qRT-PCR as they are the key transcription factors that are crucial for maintaining pluripotency and the self-renewal state.[38] Interestingly, the qRT-PCR study revealed higher expression of the NANOG gene as a result of TF-KD; however, no significant differences were observed in the OCT4 expression (Figure 3A).

We further validated the impact of TF-KD on the differentiation potential of BMSCs by culturing these cells under osteogenic and adipogenic differentiation conditions. Interestingly, under osteogenic conditions, we observed increased mineralization, as evidenced by higher calcium deposits observed by Alizarin red staining in the TF-KD cells when compared to the control MSCs (Figure 3B). This observation was further validated by qPCR analysis of osteogenic markers under these conditions. We found that the expression of osteogenic markers, namely, ALP, osteocalcein (BGLAP), and DLX5, was on an average 2-fold higher than that in control MSCs under osteogenic conditions (Figure 3C). Interestingly, the TF-KD cells when cultured under adipogenic conditions also showed an increase in the expression of adipogenic markers (LPL and PPARG), albeit not as significantly as under the osteogenic conditions (Figure 3D,E).

We then investigated the immunomodulatory properties of the MSCs by studying the effect of the MSC secretome on proinflammatory M1 macrophages. It is believed that MSCs impart functional benefits in tissue repair and mitigate inflammation by secreting soluble factors by paracrine signaling.[39,40] In order to assess the immunosuppressive nature of the TF-KD MSCs, we exposed the CM of TF-KD MSCs and control MSCs to the THP-1 human monocyte cell line that was differentiated to the proinflammatory M1 phenotype. We subsequently analyzed the expression of proinflammatory cytokines, namely, TNF and IL-1β as well as the IL-10 cytokine, a master regulator of anti-inflammatory response. As anticipated, incubation of M1 macrophages with the secretome in condition media from TF-KD MSCs and control MSCs suppressed the production of the proinflammatory cytokines TNF and IL-1β, relative to M1 macrophages that were not exposed to the condition media (control) (Figure 4A–C). This suggests that the TF-KD MSCs retained the immunosuppressive ability similar to untreated MSCs. Surprisingly, we observed an increase in the production of the anti-inflammatory IL-10 cytokine when the M1 macrophages were treated with conditioned media from the TF-KD cells. IL-10 is a broad anti-inflammatory cytokine that suppresses the activity of other proinflammatory immune cells and subsequently regulates T-helper cell (Th1 and Th2) responses[41] and plays an important role in tissue regeneration,[42] mitigation of liver injury,[43] and alleviation of fibrosis.[44] This suggests that the TF-KD MSCs were partially superior to control MSCs in the resolution of inflammation.

Finally, we examined the paracrine capability of BMSCs by directly stimulating the cells with endotoxin LPS (Figure 4D–F). We first silenced TF using Plu-SS-TF/Ca, and after 48 h, we treated the cells with LPS. Surprisingly, TF-KD MSCs displayed significantly higher expression of proinflammatory cytokine TNF, IL-1β, and iNOS than the untreated BMSCs control. This clearly suggests that the TF-KD MSCs were more sensitive to stimulation.

https://doi.org/10.1021/acs.biomac.1c00070
Biomacromolecules 2021, 22, 1980–1989

CONCLUSIONS

In conclusion, we have engineered a novel Pluronic-based nanocarrier for the efficient delivery of siRNA to stem cells. We exploited this system to deliver siRNA that targets TF or CD142 in BMSCs and evaluated the procoagulative activities in human whole blood as well as its differentiation and paracrine function. The Pluronic nanoparticle-mediated siRNA delivery displayed over 70% TF silencing without eliciting any significant cytotoxicity. Hematological evaluation of BMSCs and TF-KD MSCs in an ex vivo human whole blood model revealed a significant reduction in IBMIR, as evidenced by reduced platelet aggregation (93% of the free platelets in the TF-KD group as compared to only 22% in untreated BMSCs) and TAT complex formation. Effective silencing of TF enhanced the differentiation of BMSCs in osteogenic and adipogenic media, as evidenced by increased mineralization as well as higher expression of ALP, BGLAP, and DLX5 genes relative to untreated BMSCs. The TF-KD BMSCs displayed higher paracrine signaling as they exhibited enhanced stimulation upon exposure to endotoxin. This is evident from higher expression of TNF, iNOS, and IL-1β. Furthermore, the soluble factors produced by TF-KD BMSCs and untreated BMSCs competently suppressed the proinflammatory cytokines such as TNF and IL-1β and increased the production of the anti-inflammatory IL-10 cytokine when supplemented to proinflammatory M1 macrophages. Collectively, this work provides compelling evidence that efficient silencing of TF in BMSCs by Plu-SS-TF micelles provides a novel strategy to minimize the risk associated with thrombotic complications. Surprisingly, the engineered cells also exhibit enhanced immunosuppressive properties and superior paracrine functions and differentiation potential, which may increase the patient safety and benefits in existing BMSC-based therapies.

ASSOCIATED CONTENT

Supporting Information

The Supporting Information is available free of charge at https://pubs.acs.org/doi/10.1021/acs.biomac.1c00070.

Synthesis protocol for synthesizing Pluronic derivatives; siRNA sequence; zeta potential data; PAGE assay; SEM protocol and data; qRT-PCR; cytotoxicity study; ELISAs for coagulation and complement activation markers; and flow cytometry study for stem cell marker assessment (PDF)

AUTHOR INFORMATION

Corresponding Author

Oommen P. Oommen − *Bioengineering and Nanomedicine Group, Faculty of Medicine and Health Technologies, Tampere University, Tampere 33720, Finland;* orcid.org/0000-0003-2768-0133; Email: oommen.oommen@tuni.fi

Authors

Vignesh K. Rangasami − *Bioengineering and Nanomedicine Group, Faculty of Medicine and Health Technologies, Tampere University, Tampere 33720, Finland*

Ganesh Nawale − *Translational Chemical Biology Laboratory, Department of Chemistry, Ångström Laboratory, Uppsala University, Uppsala 751 21, Sweden;* orcid.org/0000-0002-7256-0758

Kenta Asawa − *Department of Bioengineering, The University of Tokyo, Bunkyo-ku, Tokyo 113-8656, Japan*

Sandeep Kadekar − *Translational Chemical Biology Laboratory, Department of Chemistry, Ångström Laboratory, Uppsala University, Uppsala 751 21, Sweden*

Sumanta Samanta − *Bioengineering and Nanomedicine Group, Faculty of Medicine and Health Technologies, Tampere University, Tampere 33720, Finland*

Bo Nilsson − *Department of Immunology, Genetics, and Pathology, Rudbeck Laboratory, Uppsala University, Uppsala SE-75105, Sweden*

Kristina N. Ekdahl − *Department of Immunology, Genetics, and Pathology, Rudbeck Laboratory, Uppsala University, Uppsala SE-75105, Sweden; Department of Chemistry and Biomedical Sciences, Faculty of Health and Life Sciences, Linnaeus University, Kalmar SE-391 82, Sweden*

Susanna Miettinen − *Adult Stem Cells Group, Faculty of Medicine and Health Technologies, Tampere University, Tampere 33014, Finland; Research, Development and Innovation Center, Tampere University Hospital, Tampere 33520, Finland*

Jöns Hilborn − *Polymer Chemistry, Department of Chemistry—Ångström Laboratory, Uppsala University, Uppsala 751 21, Sweden*

Yuji Teramura − *Department of Bioengineering, The University of Tokyo, Bunkyo-ku, Tokyo 113-8656, Japan; Department of Immunology, Genetics, and Pathology, Rudbeck Laboratory, Uppsala University, Uppsala SE-75105, Sweden;* orcid.org/0000-0002-0709-1000

Oommen P. Varghese − *Department of Bioengineering, The University of Tokyo, Bunkyo-ku, Tokyo 113-8656, Japan;* orcid.org/0000-0001-8872-9928

Complete contact information is available at: https://pubs.acs.org/10.1021/acs.biomac.1c00070

Notes

The authors declare no competing financial interest.

ACKNOWLEDGMENTS

This project was supported by the Swedish Foundation for Strategic Research; project SBE13-0028 "Strategies for stem cell survival". K.N.E. also thanks the support from the Swedish Research Council 2018-04199, 2016-2075-5.1, and 2016-04519 and Eurostar RELIEF 2020-00438, faculty grants from the Linnaeus University. The authors thank Dr. Vipul Sharma, Tampere University, for assisting in SEM analysis. S.S. acknowledges the financial support received from the European Union's Horizon 2020 Marie Sklodowska-Curie BioMEP program (agreement no. 713645). The authors acknowledge the Tampere facility of Flow Cytometry for their service.

REFERENCES

(1) Pittenger, M. F.; Discher, D. E.; Péault, B. M.; Phinney, D. G.; Hare, J. M.; Caplan, A. I. Mesenchymal Stem Cell Perspective: Cell Biology to Clinical Progress. *npj Regener. Med.* **2019**, *4*, 1−15.

(2) Berglund, A. K.; Fortier, L. A.; Antczak, D. F.; Schnabel, L. V. Immunoprivileged No More: Measuring the Immunogenicity of Allogeneic Adult Mesenchymal Stem Cells. *Stem Cell Res. Ther.* **2017**, *8*, 288.

(3) Ankrum, J. A.; Ong, J. F.; Karp, J. M. Mesenchymal Stem Cells: Immune Evasive, Not Immune Privileged. *Nat. Biotechnol.* **2014**, *32*, 252−260.

(4) Schraufstatter, I. U.; DiScipio, R. G.; Zhao, M.; Khaldoyanidi, S. K. C3a and C5a Are Chemotactic Factors for Human Mesenchymal Stem Cells, Which Cause Prolonged ERK1/2 Phosphorylation. *J. Immunol.* **2009**, *182*, 3827−3836.
(5) Li, Y.; Lin, F. Mesenchymal Stem Cells Are Injured by Complement after Their Contact with Serum. *Blood* **2012**, *120*, 3436−3443.
(6) Özdemir, E.; Kansu, E. Deep Vein Thrombosis Following Non-Myeloablative Allogeneic Stem Cell Transplantation: Presentation of Three Cases and Literature Review. *Turk. J. Hematol.* **2013**, *30*, 188−190.
(7) Tatsumi, K.; Ohashi, K.; Matsubara, Y.; Kohori, A.; Ohno, T.; Kakidachi, H.; Horii, A.; Kanegae, K.; Utoh, R.; Iwata, T.; Okano, T. Tissue Factor Triggers Procoagulation in Transplanted Mesenchymal Stem Cells Leading to Thromboembolism. *Biochem. Biophys. Res. Commun.* **2013**, *431*, 203−209.
(8) Moll, G.; Rasmusson-Duprez, I.; Von Bahr, L.; Connolly-Andersen, A.-M.; Elgue, G.; Funke, L.; Hamad, O. A.; Lönnies, H.; Magnusson, P. U.; Sanchez, J.; Teramura, Y.; Nilsson-Ekdahl, K.; Ringdén, O.; Korsgren, O.; Nilsson, B.; Le Blanc, K. Are Therapeutic Human Mesenchymal Stromal Cells Compatible with Human Blood? *Stem Cells* **2012**, *30*, 1565−1574.
(9) Cyranoski, D. Korean Deaths Spark Inquiry. *Nature* **2010**, *468*, 485.
(10) Moll, G.; Ankrum, J. A.; Kamhieh-Milz, J.; Bieback, K.; Ringdén, O.; Volk, H.-D.; Geissler, S.; Reinke, P. Intravascular Mesenchymal Stromal/Stem Cell Therapy Product Diversification: Time for New Clinical Guidelines. *Trends Mol. Med.* **2019**, *25*, 149−163.
(11) Perlee, D.; De Vos, A. F.; Scicluna, B. P.; Maag, A.; Mancheño, P.; De La Rosa, O.; Dalemans, W.; Florquin, S.; van't Veer, C.; Lombardo, E.; Van Der Poll, T. Role of Tissue Factor in the Procoagulant and Antibacterial Effects of Human Adipose-Derived Mesenchymal Stem Cells during Pneumosepsis in Mice. *Stem Cell Res. Ther.* **2019**, *10*, 286.
(12) Oeller, M.; Laner-Plamberger, S.; Hochmann, S.; Ketterl, N.; Feichtner, M.; Brachtl, G.; Hochreiter, A.; Scharler, C.; Bieler, L.; Romanelli, P.; Couillard-Despres, S.; Russe, E.; Schallmoser, K.; Strunk, D. Selection of Tissue Factor-Deficient Cell Transplants as a Novel Strategy for Improving Hemocompatibility of Human Bone Marrow Stromal Cells. *Theranostics* **2018**, *8*, 1421−1434.
(13) Christy, B. A.; Herzig, M. C.; Montgomery, R. K.; Delavan, C.; Bynum, J. A.; Reddoch, K. M.; Cap, A. P. Procoagulant activity of human mesenchymal stem cells. *J. Trauma Acute Care Surg.* **2017**, *83*, S164−S169.
(14) Shiratsuki, S.; Terai, S.; Murata, Y.; Takami, T.; Yamamoto, N.; Fujisawa, K.; Burganova, G.; Quintanilha, L. F.; Sakaida, I. Enhanced Survival of Mice Infused with Bone Marrow-Derived as Compared with Adipose-Derived Mesenchymal Stem Cells. *Hepatol. Res.* **2015**, *45*, 1353−1359.
(15) FDA (Food and Drug Administration). *Regulatory Considerations for Human Cells, Tissues, and Cellular and Tissue-Based Products: Minimal Manipulation and Homologous Use*; Guidance for Industry and Food and Drug Administration Staff, 2017.
(16) The European Parliament and The Council of the European Union. Regulation (EC) No 1394/2007 of the European Parliament and of the Council of 13 November 2007 on Advanced Therapy Medicinal Products and Amending Directive 2001/83/EC and Regulation (EC) No 726/2004. *Off. J. Eur. Union* **2007**, *L324*, 121−137.
(17) EMA. Advanced Therapy Medicinal Products: Overview| European Medicines Agency. https://www.ema.europa.eu/en/human-regulatory/overview/advanced-therapy-medicinal-products-overview#stem-cells-section (accessed Jan 16, 2021).
(18) Spano, C.; Grisendi, G.; Golinelli, G.; Rossignoli, F.; Prapa, M.; Bestagno, M.; Candini, O.; Petrachi, T.; Recchia, A.; Miselli, F.; Rovesti, G.; Orsi, G.; Maiorana, A.; Manni, P.; Veronesi, E.; Piccinno, M. S.; Murgia, A.; Pinelli, M.; Horwitz, E. M.; Cascinu, S.; Conte, P.; Dominici, M. Soluble TRAIL Armed Human MSC As Gene Therapy For Pancreatic Cancer. *Sci. Rep.* **2019**, *9*, 1−14.
(19) Suzuki, M.; Svendsen, C. N. Ex Vivo Gene Therapy Using Human Mesenchymal Stem Cells to Deliver Growth Factors in the Skeletal Muscle of a Familial ALS Rat Model. *Gene Therapy for Neurological Disorders*; Methods in Molecular Biology; Humana Press Inc., 2016; Vol. *1382*, pp 325−336.
(20) Pavani, G.; Laurent, M.; Fabiano, A.; Cantelli, E.; Sakkal, A.; Corre, G.; Lenting, P. J.; Concordet, J.-P.; Toueille, M.; Miccio, A.; Amendola, M. Ex Vivo Editing of Human Hematopoietic Stem Cells for Erythroid Expression of Therapeutic Proteins. *Nat. Commun.* **2020**, *11*, 3778.
(21) Paidikondala, M.; Rangasami, V. K.; Nawale, G. N.; Casalini, T.; Perale, G.; Kadekar, S.; Mohanty, G.; Salminen, T.; Oommen, O. P.; Varghese, O. P. An Unexpected Role of Hyaluronic Acid in Trafficking siRNA Across the Cellular Barrier: The First Biomimetic, Anionic, Non-Viral Transfection Method. *Angew. Chem., Int. Ed.* **2019**, *58*, 2815−2819.
(22) Paidikondala, M.; Nawale, G. N.; Varghese, O. P. Insights into SiRNA Transfection in Suspension: Efficient Gene Silencing in Human Mesenchymal Stem Cells Encapsulated in Hyaluronic Acid Hydrogel. *Biomacromolecules* **2019**, *20*, 1317−1324.
(23) Asif, S.; Asawa, K.; Inoue, Y.; Ishihara, K.; Lindell, B.; Holmgren, R.; Nilsson, B.; Rydén, A.; Jensen-Waern, M.; Teramura, Y.; Ekdahl, K. N. Validation of an MPC Polymer Coating to Attenuate Surface-Induced Crosstalk between the Complement and Coagulation Systems in Whole Blood in In Vitro and In Vivo Models. *Macromol. Biosci.* **2019**, *19*, 1800485.
(24) Yin, X.-x.; Chen, Z.-q.; Liu, Z.-j.; Ma, Q.-j.; Dang, G.-t. Icariine Stimulates Proliferation and Differentiation of Human Osteoblasts by Increasing Production of Bone Morphogenetic Protein 2. *Chin. Med. J.* **2007**, *120*, 204−210.
(25) Rumin, J.; Bonnefond, H.; Saint-Jean, B.; Rouxel, C.; Sciandra, A.; Bernard, O.; Cadoret, J.-P.; Bougaran, G. The Use of Fluorescent Nile Red and BODIPY for Lipid Measurement in Microalgae. *Biotechnol. Biofuels* **2015**, *8*, 42.
(26) Wang, H.; Li, Y.; Zhang, M.; Wu, D.; Shen, Y.; Tang, G.; Ping, Y. Redox-Activatable ATP-Depleting Micelles with Dual Modulation Characteristics for Multidrug-Resistant Cancer Therapy. *Adv. Healthcare Mater.* **2017**, *6*, 1601293.
(27) Lee, S. H.; Choi, S. H.; Kim, S. H.; Park, T. G. Thermally Sensitive Cationic Polymer Nanocapsules for Specific Cytosolic Delivery and Efficient Gene Silencing of SiRNA: Swelling Induced Physical Disruption of Endosome by Cold Shock. *J. Controlled Release* **2008**, *125*, 25−32.
(28) Lee, E.; Oh, C.; Kim, I.-S.; Kwon, I. C.; Kim, S. Co-Delivery of Chemosensitizing SiRNA and an Anticancer Agent via Multiple Monocomplexation-Induced Hydrophobic Association. *J. Controlled Release* **2015**, *210*, 105−114.
(29) Qin, L.; Sun, Y.; Liu, P.; Wang, Q.; Han, B.; Duan, Y. F127/Calcium Phosphate Hybrid Nanoparticles: A Promising Vector for Improving SiRNA Delivery and Gene Silencing. *J. Biomater. Sci., Polym. Ed.* **2013**, *24*, 1757−1766.
(30) Hanley, P. J.; Mei, Z.; Da Graca Cabreira-Hansen, M.; Klis, M.; Li, W.; Zhao, Y.; Durett, A. G.; Zheng, X.; Wang, Y.; Gee, A. P.; Horwitz, E. M. Manufacturing Mesenchymal Stromal Cells for Phase i Clinical Trials. *Cytotherapy* **2013**, *15*, 416−422.
(31) Hamann, A.; Nguyen, A.; Pannier, A. K. Nucleic Acid Delivery to Mesenchymal Stem Cells: A Review of Nonviral Methods and Applications. *J. Biol. Eng.* **2019**, *13*, 7.
(32) Shu, Z.; Tanaka, I.; Ota, A.; Fushihara, D.; Abe, N.; Kawaguchi, S.; Nakamoto, K.; Tomoike, F.; Tada, S.; Ito, Y.; Kimura, Y.; Abe, H. Disulfide-Unit Conjugation Enables Ultrafast Cytosolic Internalization of Antisense DNA and siRNA. *Angew. Chem., Int. Ed.* **2019**, *58*, 6611−6615.
(33) Lv, H.; Zhang, S.; Wang, B.; Cui, S.; Yan, J. Toxicity of Cationic Lipids and Cationic Polymers in Gene Delivery. *J. Controlled Release* **2006**, *114*, 100−109.

https://doi.org/10.1021/acs.biomac.1c00070
Biomacromolecules 2021, 22, 1980−1989

(34) Yan, H.; Oommen, O. P.; Yu, D.; Hilborn, J.; Qian, H.; Varghese, O. P. Chondroitin Sulfate-Coated DNA-Nanoplexes Enhance Transfection Efficiency by Controlling Plasmid Release from Endosomes: A New Insight into Modulating Nonviral Gene Transfection. *Adv. Funct. Mater.* **2015**, *25*, 3907−3915.
(35) Gurav, D.; Varghese, O. P.; Hamad, O. A.; Nilsson, B.; Hilborn, J.; Oommen, O. P. Chondroitin Sulfate Coated Gold Nanoparticles: A New Strategy to Resolve Multidrug Resistance and Thromboinflammation. *Chem. Commun.* **2016**, *52*, 966−969.
(36) Dominici, M.; Le Blanc, K.; Mueller, I.; Slaper-Cortenbach, I.; Marini, F. C.; Krause, D. S.; Deans, R. J.; Keating, A.; Prockop, D. J.; Horwitz, E. M. Minimal Criteria for Defining Multipotent Mesenchymal Stromal Cells. The International Society for Cellular Therapy Position Statement. *Cytotherapy* **2006**, *8*, 315−317.
(37) Moraes, D. A.; Sibov, T. T.; Pavon, L. F.; Alvim, P. Q.; Bonadio, R. S.; Da Silva, J. R.; Pic-Taylor, A.; Toledo, O. A.; Marti, L. C.; Azevedo, R. B.; Oliveira, D. M. A Reduction in CD90 (THY-1) Expression Results in Increased Differentiation of Mesenchymal Stromal Cells. *Stem Cell Res. Ther.* **2016**, *7*, 97.
(38) Tsai, C.-C.; Su, P.-F.; Huang, Y.-F.; Yew, T.-L.; Hung, S.-C. Oct4 and Nanog Directly Regulate Dnmt1 to Maintain Self-Renewal and Undifferentiated State in Mesenchymal Stem Cells. *Mol. Cell* **2012**, *47*, 169−182.
(39) Baraniak, P. R.; McDevitt, T. C. Stem Cell Paracrine Actions and Tissue Regeneration. *Regener. Med.* **2010**, *5*, 121−143.
(40) Ranganath, S. H.; Levy, O.; Inamdar, M. S.; Karp, J. M. Harnessing the Mesenchymal Stem Cell Secretome for the Treatment of Cardiovascular Disease. *Cell Stem Cell* **2012**, *10*, 244−258.
(41) O'Garra, A.; Barrat, F. J.; Castro, A. G.; Vicari, A.; Hawrylowicz, C. Strategies for Use of IL-10 or Its Antagonists in Human Disease. *Immunol. Rev.* **2008**, *223*, 114−131.
(42) Peranteau, W. H.; Zhang, L.; Muvarak, N.; Badillo, A. T.; Radu, A.; Zoltick, P. W.; Liechty, K. W. IL-10 Overexpression Decreases Inflammatory Mediators and Promotes Regenerative Healing in an Adult Model of Scar Formation. *J. Invest. Dermatol.* **2008**, *128*, 1852−1860.
(43) Louis, H.; Le Moine, O.; Goldman, M.; Devière, J. Modulation of Liver Injury by Interleukin-10. *Acta Gastro-Enterol. Belg.* **2003**, *66*, 7−14.
(44) Garantziotis, S.; Brass, D. M.; Savov, J.; Hollingsworth, J. W.; McElvania-TeKippe, E.; Berman, K.; Walker, J. K. L.; Schwartz, D. A. Leukocyte-Derived IL-10 Reduces Subepithelial Fibrosis Associated with Chronically Inhaled Endotoxin. *Am. J. Respir. Cell Mol. Biol.* **2006**, *35*, 662−667.

https://doi.org/10.1021/acs.biomac.1c00070
Biomacromolecules 2021, 22, 1980−1989

PUBLICATION 3

Immuno-isolation of mesenchymal stem cells via layer by layer polyelectrolyte coating enhances its survival in human blood and retains its immunomodulatory properties

V.K. Rangasami, K. Asawa, L. Davies, J. Hilborn, K. LeBlanc, Y. Teramura, B. Nilsson, O.P. Varghese, O.P. Oommen

Unpublished

PUBLICATION 4

Interpenetrating gallol functionalized tissue adhesive hyaluronic acid hydrogel polarizes macrophages to an immunosuppressive phenotype

S. Samanta ±, V.K. Rangasami ±, H. Sarlus, J.R.K. Samal, A.D. Evans, V.S. Parihar, O.P. Varghese, R.A. Harris, O.P. Oommen

± Equal contribution

Acta Biomaterialia, Volume 142, 2022, 36-48
https://doi.org/10.1016/j.actbio.2022.01.048

Acta Biomaterialia 142 (2022) 36–48

Contents lists available at ScienceDirect

Acta Biomaterialia

journal homepage: www.elsevier.com/locate/actbio

Full length article

Interpenetrating gallol functionalized tissue adhesive hyaluronic acid hydrogel polarizes macrophages to an immunosuppressive phenotype

Sumanta Samanta[a,1], Vignesh K. Rangasami[a,b,1], Heela Sarlus[c], Jay R.K. Samal[a,d], Austin D. Evans[a], Vijay S. Parihar[a], Oommen P. Varghese[b], Robert A. Harris[c], Oommen P. Oommen[a,*]

[a] *Bioengineering and Nanomedicine Group, Faculty of Medicine and Health Technologies, Tampere University and BioMediTech Institute, 33720, Tampere, Finland*

[b] *Translational Chemical Biology Laboratory, Department of Chemistry, Ångström Laboratory, Uppsala University, 751 21, Uppsala, Sweden*

[c] *Applied Immunology and Immunotherapy, Department of Clinical Neuroscience, Karolinska Institutet, Stockholm, Centre for Molecular Medicine, Karolinska University Hospital, 171 76, Solna, Stockholm, Sweden*

[d] *Department of Instructive Biomaterial Engineering, MERLN Institute for Technology-Inspired Regenerative Medicine, Maastricht University, Maastricht, 6229 ER, Netherlands*

ARTICLE INFO

Article history:
Received 11 November 2021
Revised 19 January 2022
Accepted 20 January 2022
Available online 24 January 2022

Keywords:
Hyaluronic acid
Gallic acid
Tissue-adhesive hydrogel
Interpenetrating network
Macrophage polarization

ABSTRACT

Innovative scaffold designs that modulate the local inflammatory microenvironment through favorable macrophage polarization and suppressing oxidative stress are needed for successful clinical translation of regenerative cell therapies and graft integration. We herein report derivation of a hydrazone-crosslinked gallol functionalized hyaluronic acid (HA-GA)-based hydrogel that displayed outstanding viscoelastic properties and immunomodulatory characteristics. Grafting of 6% gallol (GA) to a HA-backbone formed an interpenetrative network by promoting an additional crosslink between the gallol groups in addition to hydrazone crosslinking. This significantly enhanced the mechanical stability and displayed shear-thinning/self-healing characteristics, facilitated tissue adhesive properties to porcine tissue and also displayed radical scavenging properties, protecting encapsulated fibroblasts from peroxide challenge. The THP-1 human macrophage cell line or primary bone-marrow-derived murine macrophages cultured within HA-GA gels displayed selective polarization to a predominantly anti-inflammatory phenotype by upregulating IL4ra, IL-10, TGF-β, and TGF-βR1 expression when compared with HA-HA gels. Conversely, culturing of pro-inflammatory activated primary murine macrophages in HA-GA gels resulted in a significant reduction of pro-inflammatory TNF-α, IL-1β, SOCS3 and IL-6 marker expression, and upregulated expression of anti-inflammatory cytokines including TGF-β. Finally, when the gels were implanted subcutaneously into healthy mice, we observed infiltration of pro-inflammatory myeloid cells in HA-HA gels, while immunosuppressive phenotypes were observed within the HA-GA gels. Taken together these data suggest that HA-GA gels are an ideal injectable scaffold for viable immunotherapeutic interventions.

Statement of significance

Host immune response against the implanted scaffolds that are designed to deliver stem cells or therapeutic proteins in vivo significantly limits the functional outcome. For this reason, we have designed immunomodulatory injectable scaffolds that can favorably polarize the recruited macrophages and impart antioxidant properties to suppress oxidative stress. Specifically, we have tailored a hyaluronic acid-based extracellular matrix mimetic injectable scaffold that is grafted with immunomodulatory gallol moiety. Gallol functionalization of hydrogel not only enhanced the mechanical properties of the scaffold by form-

* Corresponding author.
E-mail addresses: oommen.oommen@tuni.fi (O.P. Varghese), oommen.oommen@tuni.fi (O.P. Oommen).
[1] Authors contributed equally.

https://doi.org/10.1016/j.actbio.2022.01.048

ing an interpenetrating network but also induced antioxidant properties, tissue adhesive properties, and polarized primary murine macrophages to immunosuppressive phenotype. We believe such immunoresponsive implants will pave the way for developing the next-generation of biomaterials for regenerative medicine applications.

1. Introduction

During recent years there has been an exponential increase in the biomaterial research field of developing extracellular matrix-derived biopolymers for engineering bioactive scaffolds [1,2], nanocarriers [3] and other biomedical implants [4]. Several biomaterials trigger a cascade of cellular events that are initiated post-implantation by fibrinogen deposition, followed by neutrophil infiltration and monocyte recruitment that differentiate into macrophages in the tissue and cause inflammation and scar tissue formation [5]. The inflammation caused by these cellular and molecular events at the implant site is identified as a key bottleneck for using biomaterials for tissue engineering or as medical implants [6]. Excessive inflammation triggered by the host immune system can cause tissue destruction or poor implant integration, leading to failure or rejection. Similarly, the survival of encapsulated cells in these biomaterials poses a great challenge as the encapsulated cells undergo oxidative stress during inflammatory reactions, leading to poor cell survival and function [7,8]. There is thus a pressing need to engineer scaffolds with inherent antioxidant properties that will not only suppress oxidative stress but also suppress senescence and improve self-renewal [8].

Cells of the innate immune system such as macrophages are believed to be early responders in an immune response that dictates the success of implant integration [9]. Macrophages exist as specialized guardians in our tissues (tissue-resident cells) or are differentiated from circulating blood monocytes following immune activati [10]. They act as phagocytes as well as antigen-presenting cells, activating the adaptive immune system. Macrophages have been traditionally considered to be polarized into differential functional states that either broadly lead to tissue damage (pro-inflammatory or M1 macrophages) or immune suppression and tissue-healing macrophages (immunosuppressive or M2 macrophages) [11], although these properties are disease context-specific and the modern view reflects a spectrum of activation states.

Controlling or regulating the immune response by tuning macrophage activation at the implant site is one of the key challenges in biomaterials research [12]. Macrophages have enormous plasticity and their activation states can be modulated in response to the biophysical and biochemical cues encompassed in the injured or inflamed tissue [13,14]. The most common strategy to control this activation is by encapsulating specific signaling molecules or stimulants that dictate the phenotype of infiltrating monocytes following implantation [12]. For example, a pro-inflammatory macrophage activation state can be induced by IFN-γ, TNF-α, or endotoxin lipopolysaccharide (LPS), while an immunosuppressive macrophage activation state can be induced by IL-4, IL-10, IL-13 or by using a cocktail of cytokines such as M-CSF, IL-4, IL-10, and TGF-β [15,16].

Although these immunoregulatory strategies could be very useful for regulating the fate of the infiltrating cells, the cytokines used for developing the immune responsive scaffolds have limited half-life and are also expensive. Most of the 3D scaffolds derived from biopolymers such as chitosan [17] or alginate [18] themselves induce pro-inflammatory activation of macrophages. Conversely, scaffolds that selectively increase the population of immunosuppressive macrophages significantly improve the compatibility of the material for in vivo applications [19]. However, there is currently a paucity of scaffolds with the latter function.

In this report we address this challenge by engineering tissue instructive scaffolds utilizing extracellular matrix (ECM) polymers possessing appropriate physicochemical properties that modulate the host inflammatory response and ameliorate adverse immune reactions [20]. Hyaluronic acid (HA) is one such biopolymer and an important component of the ECM that is known to possess immune-responsive properties and could be used to fabricate bioactive nanomaterials and hydrogels.

From an engineering perspective, HA offers great advantages as it possesses several reactive functional groups that allow the conjugation of biorthogonal moieties and bioactive molecules. HA of different molecular weights have been reported to differentially activate macrophages [21] and HA-derived nanoparticles loaded with doxorubicin have been designed to regulate macrophage polarization [22]. HA-based nanoparticles have also been developed to target pro-inflammatory macrophages by targeting CD44 receptors [23] and are proposed for atherosclerosis treatment [24].

We have previously designed several drug delivery systems [25,26] and hydrogels [27,28] using HA as the base material. We have recently demonstrated that HA could effectively complex with nucleic acids through hydrophobic interactions [29], and that scaffolds tailored using HA possess growth factor-sequestering properties [30]. These scaffolds inherently do not change the immune-activating behavior of the materials and therefore have their limitations.

Herein, we aimed to overcome this problem by designing an HA-based scaffold with optimal biochemical cues that could differentiate infiltrating monocytes into immunosuppressive macrophages, achieved without the necessity of loading any immunoregulatory molecules. We believe such immunosuppressive scaffolds will be better tolerated for tissue regeneration applications.

2. Materials and methods

Hyaluronic acid (MW 130 kDa) was purchased from LifeCore Biomedical (Chaska, USA). Gallic acid (3,4,5-trihydroxy benzoic acid), 1-ethyl-3-(3-dimethyl aminopropyl)-carbodiimide hydrochloride (EDC), 1–hydroxy benzotriazole hydrate (HOBt), carbohydrazide (CDH), 3- amino 1,2- propanediol, and sodium periodate were purchased from Sigma-Aldrich. Dialysis membranes used for purification were purchased from Spectra Por-6 (MWCO 3500). All solvents were of analytical quality. All spectrophotometric analysis was carried out on Shimadzu UV-3600 plus UV–VIS-NIR spectrophotometer.

2.1. Hydrogel preparation

HA-HA and HA-GA hydrogels were prepared using hydrazone crosslinking between aldehyde and carbodihydrazide moieties of the hyaluronic acid derivative. The details of the synthesis and characterizations of the hyaluronic acid components, HA-CDH, HA-Ald, and HA-GA-CDH are described in the supporting information.

The components were dissolved at a concentration of 16 mg/mL for all experiments, and equal volumes of aldehyde and carbodihydrazide derivatives were used to form the hydrogels. HA-CDH and HA-GA-CDH were dissolved in 10% sucrose solution, while HA-Ald was dissolved in phosphate-buffered saline (1x PBS). Prior to experiments involving cell encapsulation, the materials were UV sterilized for 20 min and subsequently dissolved in sterile solutions.

2.2 Rheological properties

Hydrogels of 250 µL volume were prepared in the form of cylinders with 12 mm diameter, cured overnight and their rheological property was measured using a TA instruments' TRIOS Discovery HR 2 rheometer. The values for storage and loss modulus were obtained using the frequency sweep and were plotted against the frequency (Hz). This demonstrates the viscoelastic shear behavior of materials as a function of frequency, which is the inverse value of time. Short-term properties stimulated at rapid motion using high frequency and long-term properties stimulated at slow motion using low frequency provides time-dependent storage elastic-modulus (G'), viscous loss-modulus (G") and complex viscosity (η^*) to name a few under controlled testing conditions. The hydrogels were cured for 24 h prior to the measurements. To evaluate strain recovery of the fully crosslinked hydrogels, G' and G" was measured under alternating low (1%) and high oscillation strain (100%) conditions at 25 °C and 1 Hz oscillation frequency for seven cycles with 60 s of holding period in each step using 12 mm diameter stainless steel parallel plate geometry.

2.3. Swelling and degradation study

To study the degradation and swelling characteristics of the material, three parallel samples of hydrogels were subjected to acidic, basic, and neutral pH conditions. Briefly, 250 µL gels were prepared in glass vials and the initial weight of the hydrogels was recorded. The gels were then submerged in 1 mL acetate buffer with pH 5, 1 mL 1x PBS with pH 7.4, and 1 mL bicarbonate buffer with pH adjusted to 9.0 using 1 M NaOH, for the acidic, neutral, and basic pH conditions respectively. To observe the swelling and subsequent degradation characteristics of the gels, the gels were weighed, and the buffer was replaced daily for the first four days and subsequently every alternate day until the sample degraded or for a total of 30 days. The remaining weight percentage was calculated by using the formula:

$$\text{Remaining weight}\,\% = \frac{\text{Measured weight}}{\text{Initial Weight}} \times 100$$

Further enzymatic degradation and swelling study of the material was conducted using hyaluronidase at a concentration of 50 U/mL in PBS at pH 7.4. Three parallel samples of 250 µL HA-HA and HA-GA gels were prepared in glass vials of known recorded blank weight, allowed to crosslink for 24 h, weighed with the formed gels, and subsequently submerged in 1 mL hyaluronidase PBS solution. In a similar fashion to the aforementioned swelling and degradation experiment, the hyaluronidase buffer solution was carefully removed prior to measurement every 24 h, the gels were weighed and the enzyme buffer was replaced after each measurement. The degradation weight percentage was calculated using the formula:

$$\text{Remaining weight}\,\% = \frac{\text{Measured weight}}{\text{Initial Weight}} \times 100$$

2.4. Tissue-adhesive tack test

To observe any difference in the adhesive properties of the two hydrogels (HA-HA and HA-GA), a tack adhesion test was performed using a rheometer. We first glued the porcine muscle having the same diameter to that of the geometry (12 mm) to the movable top head of the rheometer and then placed the fully cured 250 µL of HA-HA and HA-GA gels of 2 mm thickness on the bottom plate. Subsequently, the top plate attached with the muscle tissue was placed in contact with the gel with a holding period of 120 s (residence time) during which a constant compressive force of 100 mN was applied to establish a uniform molecular contact between the tissue and the gels. Thereafter, the top plate was pulled up at a constant velocity of 10 µm/*sec* to record the change in axial force (N) with respect to time. The experiments were performed in triplicate at 25 °C. A graph of axial force (N) vs step time was plotted to observe differences between the two hydrogels.

2.5. Anti-oxidant property

To evaluate the free radical scavenging activity of the HA-GA, the DPPH (2,2,1-diphenyl-1-picrylhydrazyl) method was used [31]. Aqueous HA-GA-CDH solution was obtained by dissolution of 1 mg of polymers in 1 mL of deionized water, followed by the addition of an equal volume of a methanol stock solution containing 1 mg of DPPH radical in 12.5 mL methanol. After incubation at 25 °C for 30 min, the absorbance of the resulting solution was measured at 517 nm using a UV−Vis spectrophotometer.

$$\text{The DPPH scavenging activity}(\%) = [(A_0 - A_1)/A_0] \times 100$$

Where, A_0 is the absorbance of blank DPPH solution that was used under the same reaction conditions in the absence of synthesized polymers, and A_1 is the absorbance of DPPH solution in the presence of polymer samples.

2.6. Cell culture

CRL-2429 cells are human fibroblast cells obtained from skin tissue. These cells were cultured in T-75 cell culture flasks in Dulbecco's Modified Eagle Medium (DMEM, Gibco) with 10% fetal bovine serum (Gibco) and 1% Penicillin-Streptomycin as an antibiotic (DMEM complete medium) in a cell culture incubator at 37 °C and 5% CO_2. The medium was changed every alternate day. TrypLE Select (Gibco) was used to detach the cells from the flasks during passaging. Cells were passaged upon reaching around 80% confluency. Cells from passage 18–20 were used for experiments.

THP-1 cells (human monocytic cell line) were cultured in suspension culture in T-25 cell culture flasks in Roswell Park Memorial Institute (RPMI) 1640 medium (Gibco) with 10% fetal bovine serum (FBS) and 1% Penicillin-Streptomycin as an antibiotic (RPMI complete medium) in a cell culture incubator at 37 °C and 5% CO_2. Cells from passage 14–15 were used for experiments.

For isolating murine bone marrow-derived macrophages (BMDM) femurs were collected from mice. After aspirating the cells from the bone marrow, they were cultured in the flasks for two weeks in MEM high glucose medium (Gibco) supplemented with 10% FBS and 10 ng/mL of mCSF. The medium was replenished every 3 days. For the experiments with unactivated phenotypes, these cells were detached using trypsin/EDTA (Gibco) and counted and resuspended in the hydrogels at a concentration of 2×10^6 cells/mL. To induce a proinflammatory activation state, BMDM was treated with 20 ng/mL lipopolysaccharide (LPS) (Invitrogen) and 10 ng/mL INF-γ (R&D systems) for 16 hrs.

Prior to encapsulation, cells were detached from the flasks, centrifuged, and resuspended in complete medium, counted, and the required number of cells was further centrifuged, and the pellets resuspended in HA-GA-CDH or HA-CDH, respectively. Hydrogels were formed by mixing HA-GA-CDH or HA-CDH cell suspension with HA-Ald in equal volumes in cell culture plates. The hydrogels were incubated for 20 min at room temperature to ensure gelation and then 500 µL complete medium was added to each well. The medium was changed every alternate day or as otherwise indicated.

2.7. Live/Dead staining

For live/dead staining, CRL2429 fibroblasts were encapsulated in 200 µL hydrogels at a concentration of 2×10^6 cells/mL in a 48-well plate. The encapsulated cells were cultured for 14 days, with a medium change every alternate day, and cell viability, as well as changes in morphology of the cells, was visualized by LIVE/DEAD staining (Viability/Cytotoxicity Kit for mammalian cells, Molecular Probes, USA) using a fluorescence microscope. To carry out the Live/Dead staining, the medium was aspirated from the wells and the gels were washed with 1x PBS twice. 300 µL Live/Dead staining solution containing 2 µM Calcein AM and 1 µM Ethidium homodimer in 1X PBS was added to the wells and the plates were incubated at 37 °C for 1.5 h. Post-incubation the hydrogels were washed with 1x PBS once and imaged using a 10x objective and a Nikon Eclipse Ts 2 fluorescence microscope. Live/Dead staining was performed on days 1,7 and 14 after the hydrogel formation. Images obtained from the microscope were post-processed using Nikon NIS Viewer and ImageJ software.

2.8. Cell viability under oxidative stress

To observe the effect of the antioxidant property on cellular behavior, CRL-2429 human fibroblast cells were exposed to hydrogen peroxide (H_2O_2) to stimulate free radical formation, along with exposure to the hydrogel material, and subsequently cell viability was quantified using PrestoBlue (Thermofisher) cell viability assays.

For monolayer cultures, cells were plated in 24-well plates at a density of 50,000 cells/well and incubated for 24 h. Post-incubation, 1 mg/mL of HA-CDH and HA-GA-CDH were exposed to the cells. Oxidative stress was induced by adding 200 µM of H_2O_2 along with the materials. The plates were further incubated for 2 days and cell viability was quantified using PrestoBlue cell viability assay.

For 3D cultures, 2×10^6 cells/mL were encapsulated in 200 µL of HA-HA or HA-GA gels in 24 well plates and incubated for 2 days. Post-incubation, 250 µM H_2O_2 was added to the wells to induce oxidative stress. The gels were incubated for 2 days and the medium was replaced. After 2 days, the PrestoBlue cell viability assay was carried out.

2.9. Immunomodulatory property

To observe the immunomodulatory effects of the gels, 4×10^6 THP-1 cells/mL were encapsulated in 200 µL HA-HA or HA-GA gels. The medium was changed every 2 days to account for medium loss due to swelling of gels. Gene expression analysis was performed by RNA extraction, followed by cDNA synthesis from the extracted RNA. The synthesized cDNA was then subjected to a quantitative polymerase chain reaction (qPCR) to quantify the fold change in gene expression levels. RNeasy Plus Mini Kit (Qiagen) was used for RNA extraction. Briefly, the gels were first mechanically disrupted followed by suspension in PBS and centrifuged. Lysis buffer was added to the pellet and the kit protocol was followed. Post-extraction, the RNA samples were stored at −20 °C. cDNA was prepared by following the cDNA synthesis kit (Thermo Fisher Scientific). For qPCR reactions, the cDNA sample was added along with TaqMan Fast Advanced Master Mix (Thermo Fisher Scientific), nuclease-free water (Invitrogen), and TaqMan assay primers and subjected to the reaction process in a Bio-Rad CFX96 Real-time PCR machine as per the manufacturer's protocol. The expression levels of the following genes were analyzed using commercially available TaqMan Gene Expression Assays (Thermo Fisher Scientific): TNF-α (Hs00174128), IL1-β (Hs01555410), IL10 (Hs00961622), IL1RN (Hs00893626), with β-Actin (Hs01060665) as a housekeeping gene.

Murine BMDM was differentiated into a resting phenotype in accordance with the culture conditions outlined above. Cells were then encapsulated in hydrogels at a concentration of 2×10^6 cell/mL and cultured for two weeks, after which gene expression analysis was performed. For the LPS stimulation experiments, the stimulated cells were then encapsulated in the hydrogels and cultured for 3 days, after which gene expression analysis was performed. In each setting RNA was extracted using a commercially available kit (RNeasy Mini kit, Qiagen). cDNA first strand was synthesized following the protocol from the iScript cDNA synthesis kit (BioRad). iQ SYBR Green Supermix was used to prepare the samples for qPCR on a CFX96 instrument from BioRad. The murine primers (sequences in SI) for the qPCR were obtained from Sigma Aldrich, Sweden.

The qPCR data were normalized and analyzed using a comparative quantitation method and data are presented as $\Delta\Delta$Ct method. To unequivocally quantify the immunological response of GA functionalization, we used the HA-HA gel (HA hydrogel without GA) as the normalizing variable. Reference housekeeping gene β-Actin (for the PCR with THP1 cells) and HPRT (for the murine BMDMs) were selected as an internal control for the normalization of qPCR data.

2.10. Multiplex bead-based immunoassays

Bead-based cytokine detection immunoassays from LEGENDplex (BioLegend) were used to identify secreted cytokines following in vitro cell culture. Cell culture supernatants were collected at the respective timepoints and stored at −80 °C before use. The Mouse Macrophage/Microglia Cytokine Panel (BioLegend) was used to detect secreted cytokines as per the manufacturer's instructions. Analyses were performed using LEGENDplex Data Analysis Software (BioLegend) and the cytokines were quantified by comparing samples to a set of standard curves prepared in parallel with supernatant samples.

2.11. In vivo recruitment of immune cells in C57BL/6 mice

Female mice (8–9 weeks old) were injected subcutaneously with 200 µL HA-GA and HA-HA gel on each side of the lower back area. Five days post injection the gels were recovered and digested in 500 µL PBS containing 0.4 mg/mL hyaluronidase (Sigma-Aldrich) and trypsin 1 g/mL (Gibco) for 50 min at 37 °C. The cell suspension was filtered using a 40 µm strainer and centrifuged at 350 g for 5 min at 4 °C. The pellet was resuspended in a cocktail of antibody solution (see below) for 30 min at 4 °C. After a wash with PBS, the cells were centrifuged as above and transferred to FACS tubes. The cells were analyzed using a BD LSR FORTESSA. The data was analyzed using the software Flowjo V 10.8.0. The antibody panel included CD45-PeCy7 1:100, CD11b-PercpCy5.5 1:100, CD36-Pe 1:100, CD86-APC 1:100, MHCII-A700 1:100, CD40-FITC 1:100, live dead marker – Near infrared 1:500). Ethical permission was obtained from the regional ethical committee, Stockholms djurförsöksetiska nämnd (Dnr 9328–2019).

2.12. Statistical analysis

The statistical measurements were achieved by comparing each experimental value with their respective controls (in our case HA-GA was compared with HA-HA). The assessments between the two groups were performed using the student's unpaired T-test and Mann Whitney test as indicated. These tests were performed using GraphPad Prism Software $P<0.05$ was the statistical significance for all tests.

3. Results and discussion

To design the bioactive 3D scaffold we utilized HA, an anionic non-sulfated glycosaminoglycan (GAG), as a base biopolymer. As an immunomodulatory agent we utilized gallic acid (GA), a low molecular weight polyphenol compound occurring naturally in various terrestrial plants including green tea. GA possesses diverse bioactivities such as anti-carcinogenic, anti-mutagenic, and anti-inflammatory properties [32]. We hypothesized that grafting of GA in a HA scaffold would provide antioxidant properties necessary to polarize macrophages into a tissue regenerative phenotype.

Conventionally, GA is conjugated to polysaccharides via ester linkages utilizing the aliphatic hydroxyls on the polymer or by carbodiimide coupling of amine-functionalized GA with the carboxylate residues of the polymer [33,34]. Both these approaches are inefficient, rendering a poor coupling yield. To circumvent this we modified the carboxylate residues of GA to a hydrazide derivative as they are known to undergo proficient EDC coupling owing to a lower pK_a of hydrazides over amines [35]. To achieve this we first transformed the carboxylate groups of GA to methyl ester followed by nucleophilic displacement with aqueous hydrazine (80% solution) to obtain GA-hydrazide in quantitative yields. The hydrazide derivative of GA was characterized by ^{1}H and ^{13}C NMR spectroscopy (Figure S2 and S3 in SI). We have recently shown that compared to hydrogels obtained by $NaIO_4$ oxidation of dopamine conjugated HA, the hydrogel obtained by GA functionalized HA displayed faster oxidation at physiological pH and possess higher tissue adhesive properties [35]. In this study, the GA functionalized HA was grafted with carbodihydrazide (CDH) groups as a biorthogonal moiety that facilitates covalent crosslinking reaction with aldehyde functionalized HA derivative. We have earlier reported that unlike other hydrazone bonds, which are labile, the CDH-derived hydrazones are exceptionally stable under physiological conditions due to their unique delocalized electronic structures [27].

Using this optimized protocol we developed hydrazone crosslinked HA-hydrogels grafted with the GA moiety, in which the degree of GA functionalization was 6% with respect to the disaccharide repeat units (Figure S5 and S6 in SI) and the degree of hydrazone crosslinking was fixed at 10%. For comparison, we used HA gels without GA by using the same hydrazone chemistry with similar levels of crosslinking density using 10 mol% modified HA-Aldehyde (Figure S7 and S8 in SI). A DPPH radical scavenging assay was used as a preliminary assessment of the changes in hydrogel antioxidant property upon the incorporation of gallol moieties. The DPPH reagent underwent a visual change in color from deep purple to deep orange in HA-GA, which is due to the antioxidant property imparted by GA. The UV–Vis spectroscopy measurement of 0.5 mg/mL HA-GA-CDH (75 μM GA grafted on HA-GA-CDH) in presence of DPPH displayed 50% reduction in absorption indicating potent antioxidant properties (Figure S12A in SI).

We performed the rheological evaluation of HA gels (HA-HA) and HA gels with 6% GA (HA-GA gels) by subjecting the gels to amplitude and frequency sweeps. The rheological analyses demonstrated that both HA-HA and HA-GA gels remained stable during the rheological testing and consistently yielded higher storage modulus (G′) values as compared to loss modulus (G′′) (Fig. 2A). For HA-HA gels, a storage modulus, G′, of 995 ± 4 Pa and a loss modulus G′′ of 7 ± 3 Pa was observed, while for HA-GA gels the G′ and G" values were 747 ± 57 and 4 ± 1 Pa, respectively. The tan δ value, which is the ratio between G′ and G′′, yielded significantly less values than 1 (0.0066 and 0.0057 for HA-HA and HA-GA gels, respectively), indicating that the gels were highly elastic in nature. The average mesh size (ξ), which represents the pore size of the gel by considering the distances between the two entanglement points, was calculated to be 16.05 nm and 17.70 nm, respectively, for HA-HA and HA-GA gels. The addition of GA moieties led to a decrease in the storage modulus values, indicating softer gels at the beginning. By using the modulus data, we also calculated the average critical molecular weight between the crosslinks (M_c) using rubber elastic theory that applies to highly elastic gels, which was evident from the tan δ values. M_c values were 39.11 kg mol^{-1} and 44.18 kg mol^{-1} for HA-HA and HA-GA gels, respectively, suggesting that HA-GA gels were softer than HA-HA gels with higher ξ (Table S1).

We next performed swelling studies to investigate the stability of these gels under physiological conditions (pH 7.4) and at acidic conditions (pH 5.0) where the hydrazone crosslinks are susceptible to degradation and at basic pH of 9.0 (Figure S9 in SI). Both HA-HA and HA-GA hydrogels showed rapid initial swelling followed by degradation in acidic buffer (pH 5.0), although the HA-GA gels displayed relatively lower swelling. However, under physiological conditions (pH 7.4) and at pH 9.0, both the gels remained stable.

We were intrigued by the fact that the GA functionalized HA gels did not show any significant swelling or degradation over the period of 25 days under basic or neutral conditions after the initial swelling within 5 days. This observation prompted us to investigate the viscoelastic properties of HA-HA and HA-GA gels at different time points at pH 7.4 to decipher the role of GA in inducing this characteristic. Fascinatingly, we observed matrix stiffening in HA-GA hydrogels at day 2 compared to day 0 when immersed in PBS at pH 7.4 (Fig. 2B). Thereafter, the HA-GA gels exhibited exceptionally stable storage modulus compared to HA-HA hydrogels until day 21, whose storage modulus slowly deteriorated until day 15 and then underwent rapid loss by day 21 (Fig. 2B). This clearly suggests that the grafting of GA in HA gels promote the formation of secondary network that stabilizes the gel and prevent excessive swelling (Table S2). We believe this is attributed to the unique capability of the gallol moiety to undergo oxidation that generates radicals and undergo intermolecular dimerization [35]. Such secondary stabilization decreases the segmental mobility of the polymer chains and reduces the pore size, favoring a stiffer and stable matrix formation.

To determine the injectability of these chemically cross-linked hydrogels we determined the flow behavior (viscosity) at room temperature (Figure S10) by continuously increasing the shear rate up to 10 s^{-1}. Both the HA-HA and HA-GA hydrogels displayed a rapid decline in the viscosity upon application of increasing shear rate (0.01 to 10 s^{-1}), suggesting their injectability. We further ascertained the shear-thinning characteristics of these gels by estimating the viscosity recovery by performing a dynamic experiment applying a periodic low (0.01 s^{-1}) and high shear rate (10 s^{-1}) to the hydrogel samples (seven cycles; Figure S11 in SI). Both the hydrogels recovered their initial viscosity when the shear rate was periodically lowered. We also tested the dynamic strain recovery properties of these hydrogels (Fig. 2C and 2D). At low strain (1%), both the hydrogels displayed higher storage modulus, and with increasing strain (100%) the storage modulus was reduced while loss modulus increased in HA-GA hydrogels, while they were similar in case of HA-HA gels. Upon withdrawal of the high strain both hydrogels recovered their initial storage modulus, suggesting the dynamic nature of the hydrogel chemistry.

We next performed tissue adhesion tack tests using a rheometer in order to investigate the tissue adhesive properties using porcine muscle tissue as a model. Notably, both HA-HA and HA-GA gels showed tissue-adhesive properties (Fig. 2E). However, HA-GA had significantly greater adhesion to the wet muscle tissue, as a greater negative force was required to induce cohesive failure between the top plate and the gel.

To further prove the gallol-mediated secondary network formation in the HA-GA hydrogels we performed an enzymatic degrada-

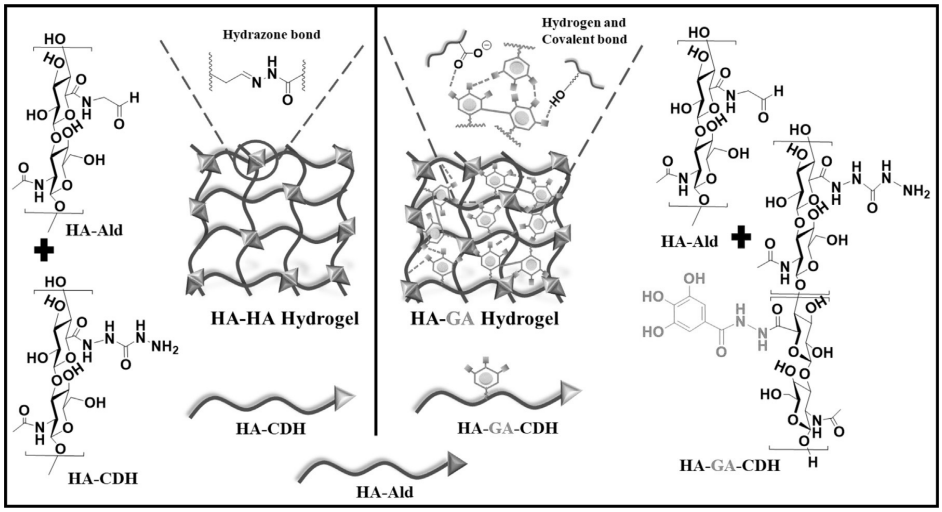

Fig. 1. Schematic representation of the formation of hydrazone crosslinked HA-HA and hydrazone and gallol crosslinked interpenetrating HA-GA hydrogel.

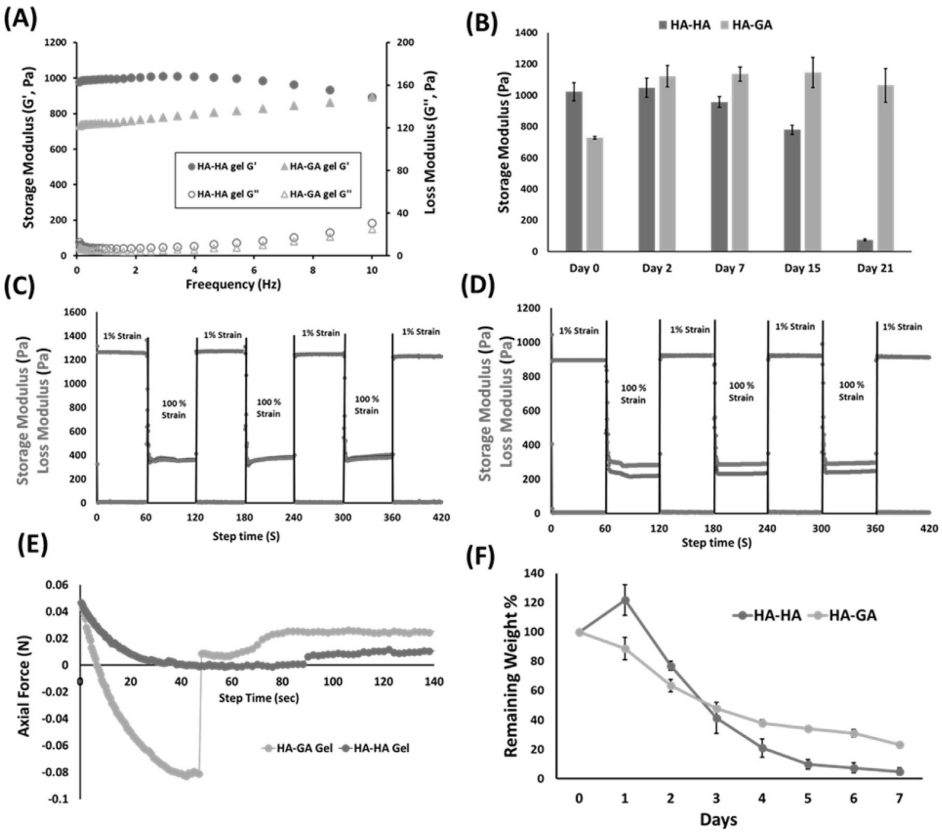

Fig. 2. (A) Rheological measurements obtained from frequency sweep for 250 μL HA-HA and HA-GA hydrogels ($n = 3$). (B) Rheological measurements of HA-HA and HA-GA hydrogels (250 μL, $n = 3$) immersed in PBS buffer (pH 7.40). Dynamic strain recovery of a (C) HA-HA, and (D) HA-GA hydrogel undergoing cyclic deformation of 1% (low) and 100% (high) strain at 1 Hz with G' (blue line) and G'' (red line). (E) Measurement of tissue adhesion force of the two hydrogels by rheological tack adhesion test (250 μL gels). (F) Degradation profiles of HA-HA and HA-GA hydrogels (250 μL, $n = 3$) in neutral PBS (pH 7.4) buffer containing 50 U/mL hyaluronidase. (For interpretation of the references to colour in this figure legend, the reader is referred to the web version of this article.)

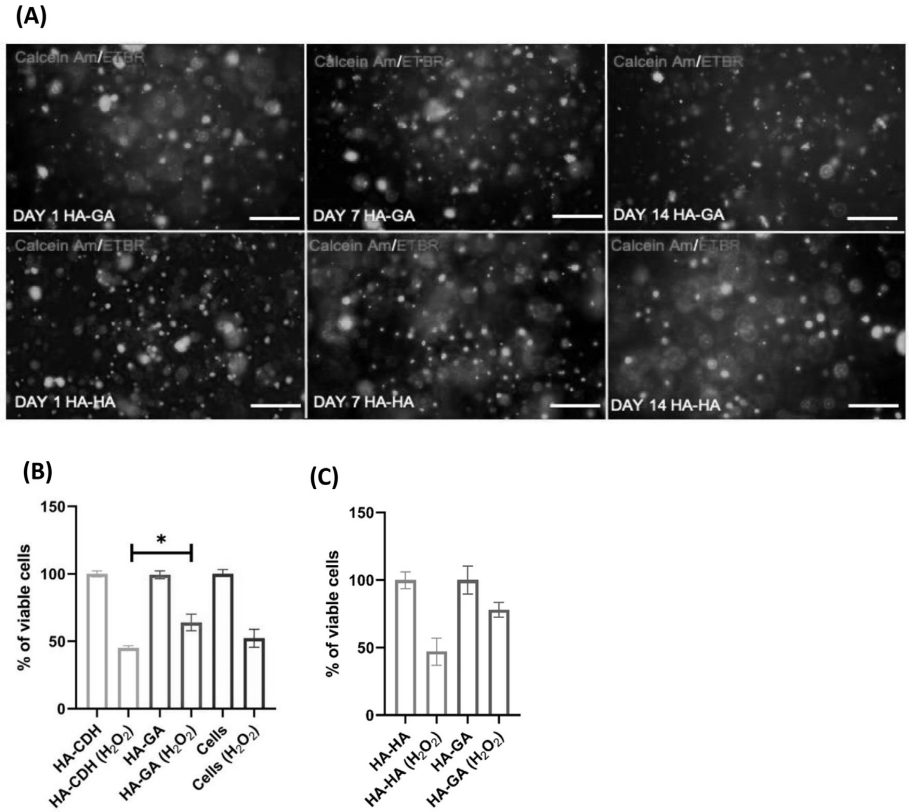

Fig. 3. (A) LIVE/DEAD staining of CRL2429 fibroblasts encapsulated inside hydrogels on 1, 7, and 14 days of culture. Cells stained in green (Calcein AM) represent live cells while cells stained in red (EtBr) represent dead cells. (Scale bar = 500 μm, Cell density = 2×10^6/mL). (B) 2D monolayer and (C) 3D encapsulated cells Presto Blue viability assays showing the antioxidant effect of GA moieties on CRL2429 cells during induced oxidative stress. HA-GA improves cell viability during oxidative stress in (B) monolayer and (C) 3D cultures. (Cell density = 5×10^4 cells/well for 2D ($n = 6$) and 2×10^6/mL for 3D cultures, ($n = 3$)). Statistical analysis used the Mann-Whitney Test $^*P<0.05$. (For interpretation of the references to colour in this figure legend, the reader is referred to the web version of this article.)

tion study in the presence of hyaluronidase in PBS at pH 7.4. Enzymatically, the HA-GA gels illustrated slower degradation in the presence of hyaluronidase than did the HA-HA gels, especially after day 2 (Fig. 2F). Conversely, the HA-HA gels initially swelled and then degraded at a faster rate than did HA-GA in the presence of hyaluronidase. The additional GA-mediated secondary crosslinking network along with the primary hydrazone network in the HA-GA hydrogel thus limits the hydrogel swelling and restricts the enzymatic degradation by bulk erosion, yet promotes degradation by surface erosion.

We next evaluated the biocompatibility of the materials using in vitro studies. We first encapsulated CRL2429 fibroblasts in both HA-HA and the HA-GA hydrogels and evaluated cell viability inside the hydrogels using live/dead staining. We observed that after 14 days in culture the CRL2429 fibroblasts were viable in both gels (Fig. 3A). To further confirm that primary cells are also viable in our hydrogels, we cultured the human bone marrow-derived mesenchymal stem cells (MSCs) and BMDMs (M0) in the two gels and performed live/dead staining. Interestingly, we did not observe significant cell death at the respective time points with both the cell types (Figure S13A & S13B in SI). To corroborate the viability and proliferation of cells (MSCs) in our hydrogels, we measured the DNA content of the cells from the respective hydrogels using the CyQuant cell proliferation kit at days 1,7,14 and 21, respectively. These experiments revealed that the cells were viable and proliferating from day 1 to day 21 in HA-HA gels. In the case of HA-GA hydrogels, we recorded limited cell proliferation between days 1 and 14 and a subsequent increase in the proliferation up to day 21 (Figure S13C in SI). The reduction of the cell proliferation could be attributed to the effect of the gallol on MSC proliferation [36].

To ascertain the antioxidant properties of the gallol-modified HA we first incubated the individual hydrogel components (HA-CDH and HA-GA-CDH) with the CRL2429 cells in the presence or absence of hydrogen peroxide (H_2O_2). Cells cultured in 2D without incubating with any hydrogel components (cultured in the presence or absence of H_2O_2) were used as a control group. As expected, we observed a reduction in cell viability (~50% reduction) when the cells were exposed to 200 μM H_2O_2. When HA-CDH (1 mg/mL) was added to the cells we observed a ~55% reduction of cell viability in the H_2O_2-treated cells compared to the untreated cells. Interestingly, when the cells were incubated within HA-GA (1 mg/mL), there was only ~36% reduction in the cell viability when exposed to 200 μM H_2O_2 (Fig. 3B). This clearly suggests that the GA moiety in the HA-GA polymer contributes to the radical scavenging property.

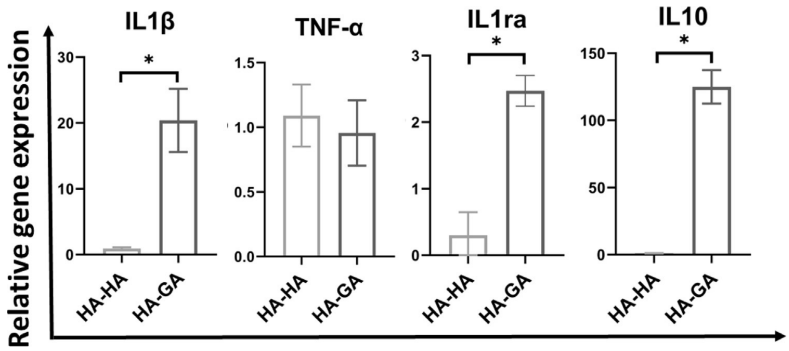

Fig. 4. Gene expression analysis of pro-inflammatory markers TNF-α and IL-1β and anti-inflammatory markers IL-10 and IL-1ra in THP-1 cells encapsulated in HA-GA hydrogels for 8 days in basal medium, as compared to HA-HA gels. Expression of anti-inflammatory markers was increased in HA-GA gels as compared to HA-HA gels, suggesting increased immunosuppressive polarization (200 µL gels. THP-1 density = 4×10^6/mL, $n = 6$). Statistics used Mann-Whitney Test $^*P<0.05$. (For interpretation of the references to colour in this figure legend, the reader is referred to the web version of this article.)

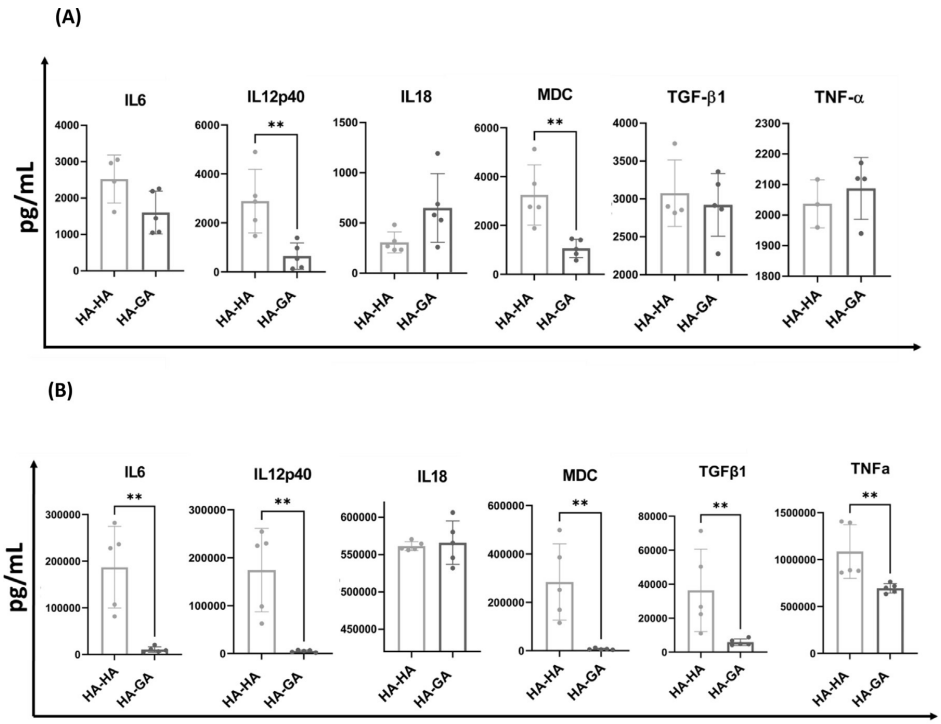

Fig. 5. Cytokine release in the medium by the primary murine BMDM cells analyzed by capture bead assay on (A) day 1 and (B) day 10. Statistical analysis done by Mann-Whitney Test using GraphPad Prism. $^{**}P<0.01$ (C) Cytokine mRNA levels produced by the BMDM cells as determined by qRT-PCR when encapsulated within HA-HA and HA-GA gels ($n = 5$) for 14 days. Statistical analysis using student T-test $^*P<0.05$.

To validate the antioxidant properties of the HA-GA hydrogels we performed 3D cellular oxidative stress measurement experiments. We encapsulated the CRL2429 fibroblasts in HA-HA and HA-GA gels and induced oxidative stress by exposing the system to 250 µM H_2O_2 for 48 h. The cells cultured in HA-HA gels displayed significant oxidative stress upon exposure to H_2O_2 and their viability was drastically reduced to 50% after 48 h in culture. As anticipated, the cells encapsulated in the HA-GA gels displayed higher cell viability (~78%) upon exposure to H_2O_2 (Fig. 3C and Figure S12B). These experiments suggest that the GA component in the hydrogel network shielded the encapsulated cells from oxidative stress by scavenging free radicals induced by the addition of H_2O_2.

As blood-derived monocytes are early responders to inflammation and injury that can differentiate into activated phenotypes we investigated if our HA-GA gels provided the necessary cues for the differentiation of monocytes to M1 or M2 macrophages, respec-

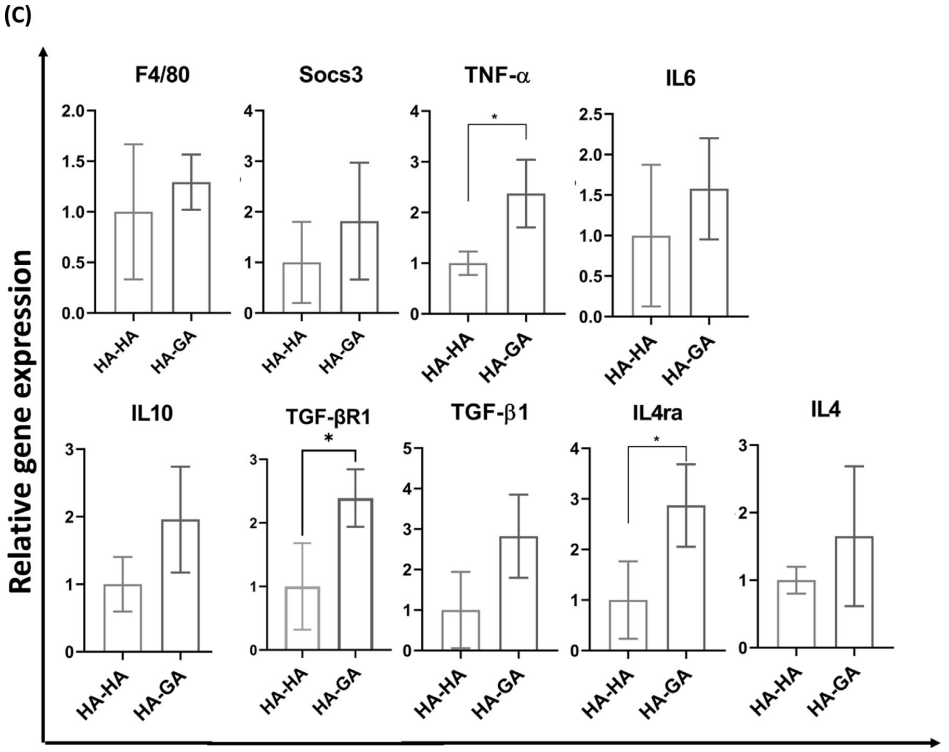

Fig. 5. Continued

tively (Fig. 4). For this purpose, we encapsulated human monocyte THP-1 cells in HA-HA and HA-GA gels without the addition of any immunomodulatory agents or differentiation factors. After 8 days in culture we observed that relative to the HA-HA gels, cells cultured in HA-GA gels exhibited ∼125-fold higher expression of IL-10 and ∼2.5-fold increase in IL-1ra as quantified by qRT-PCR. The higher expression of IL-10 and IL-1ra indicates that the macrophages had become preferably polarized towards an immunosuppressive M2 phenotype in HA-GA gels [37]. Interestingly, we also observed a ∼20-fold increase in IL-1β, a pro-inflammatory cytokine. It is important to consider that it is the net sum of inflammatory genes that determine the final macrophage activation phenotype, so the co-expression of both pro-inflammatory and immunosuppressive markers is expected. Immunosuppressive macrophages are known to mitigate tissue damage and to contribute to the recovery from conditions such as spinal cord injury and myocardial ischemia [38,39]. Furthermore, we believe that the substantial amount of IL-10 produced by these cells inhibits the differentiation of neighboring cells into pro-inflammatory activated macrophages by repressing the pro-inflammatory genes via the IL-10/STAT3 pathway [40] and thereby allowing the macrophage population to be self-regulating [41] which could be useful in reducing inflammation and could facilitate wound healing and tissue regeneration.

To further substantiate our observation that HA-GA gels polarize macrophages towards an immunosuppressive profile, we conducted further experiments by encapsulating murine bone marrow-derived primary macrophages (BMDM) in their resting state (M0 macrophage) within the HA-GA gels for 10 days. The BMDM cells used in this study were isolated and cultured following a standard protocol [42]. The conditioned media was collected on day 1 and day 10 and analyzed using a multiplex bead-based assay (LEGENDplex from Biolegend) (Fig. 5A>, 5B). We observed that at day 1 the cells cultured in the HA-GA gels produced lower levels of pro-inflammatory cytokines such as IL-6 (1.6 $\pm$ 0.5 ng/mL in HA-GA vs 2.5 $\pm$ 0.5 ng/mL in HA-HA), IL-12p40 (0.6 $\pm$ 0.4 ng/mL in HA-GA vs 3 $\pm$ 1 ng/mL in HA-HA) and MDC (1 $\pm$ 0.3 ng/mL in HA-GA vs 3 $\pm$ 1 ng/mL in HA-HA) when compared to the HA-HA gels. Interestingly, TGF-β (3 $\pm$ 0.3 ng/mL) and TNF-α (2 $\pm$ 1 ng/mL) cytokine release in the day 1 HA-GA gels were similar to that of the HA-HA gels (TGF-β – 3 $\pm$ 0.3 ng/mL; TNF-α – 2 $\pm$ 0.8 ng/mL). When the conditioned media obtained after 10 days of culture was analyzed, a similar trend was observed whereby the HA-GA gels had released significantly lower amounts of pro-inflammatory cytokines when compared to the HA-HA gels. Specifically, IL-6 (187 $\pm$ 28 ng/mL in HA-HA vs 104 $\pm$ 5 ng/mL in HA-GA), IL-12p40 (174 $\pm$ 78 ng/mL in HA-HA vs 5 $\pm$ 2 ng/mL in HA-GA), MDC (284 $\pm$ 140 ng/mL in HA-HA vs 7 $\pm$ 3 ng/mL in HA-GA) and TNF-α (1086 $\pm$ 257 ng/mL in HA-HA vs 695 $\pm$ 45 ng/mL in HA-GA) expression were significantly lower in the HA-GA gels, while IL-18 released by both the gels was at similar levels. Unexpectedly, TGF-β was less abundant in the HA-GA gels (6 $\pm$ 2 ng/mL) compared to the HA-HA gels (36 $\pm$ 22 ng/mL). These results indicate that HA-GA gels have the potential to drive BMDM towards a less inflammatory phenotype than do the HA-HA gels.

To further quantitatively assess the immunosuppressive characteristics, we analyzed mRNA expression of the pro-inflammatory and anti-inflammatory genes. For this purpose, BMDM cells (M0

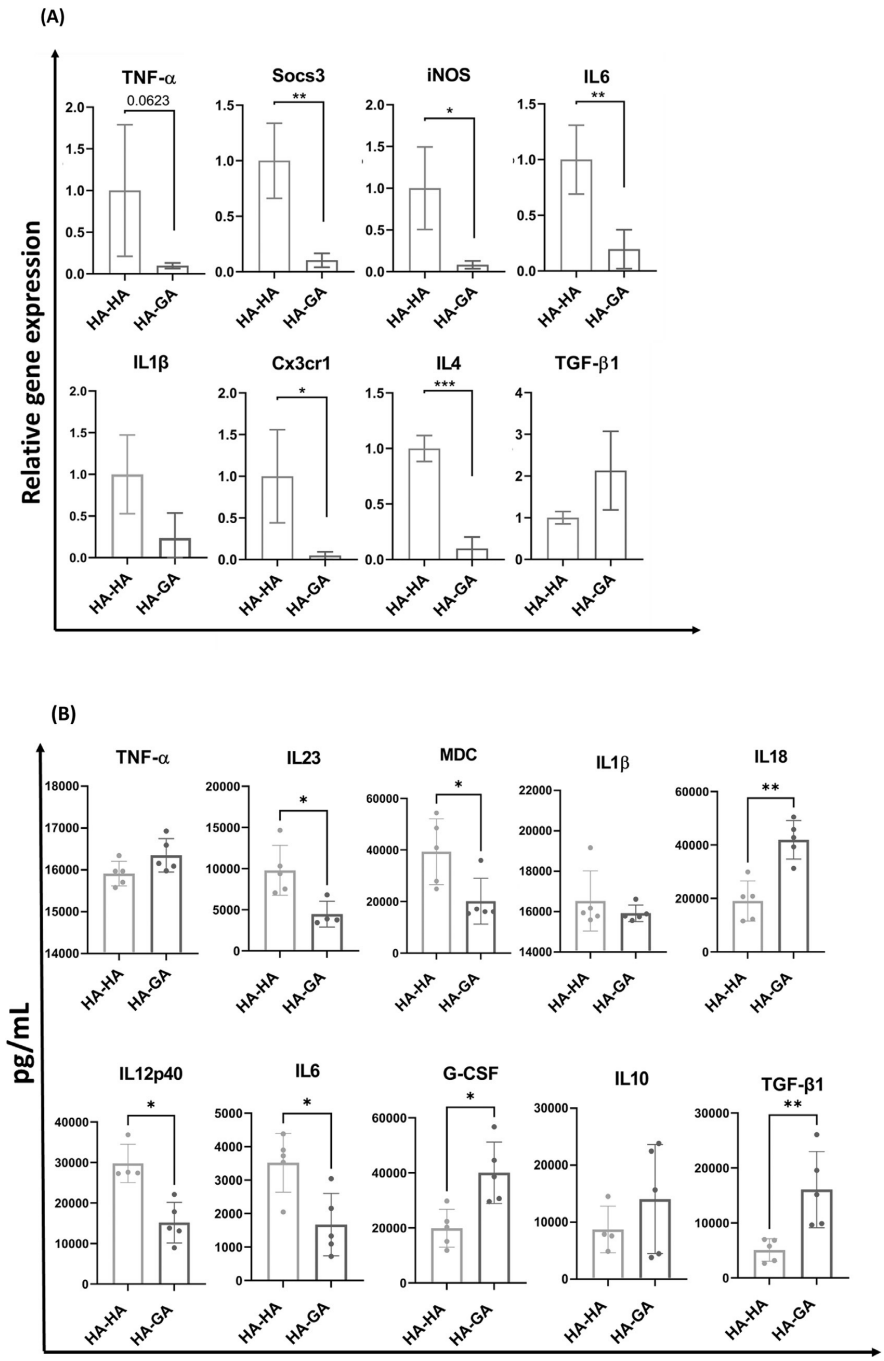

Fig. 6. (A) Primary murine BMDM cells were stimulated with LPS/IFNγ for 16 h and then encapsulated in HA-HA and HA-GA gels ($n = 4$) for 3 days. The expression of different inflammatory markers was determined by qRT-PCR. Statistics done by T-test using GraphPad Prism. $^{*}P<0.05$, $^{**}P<0.005$, $^{***}P<0.001$ (B) Cytokine present in the medium detected by multiplex bead-based assay after 3 days. Statistical analysis used Mann-Whitney Test. $^{*}P<0.05$, $^{**}P<0.01$.

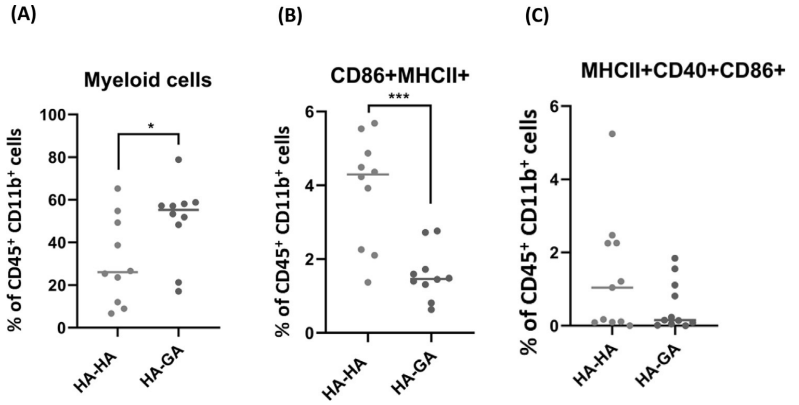

Fig. 7. Flow cytometric analysis of the cells recruited into the HA-HA and the HA-GA hydrogels when implanted subcutaneously in C57L/B6 mice. The hydrogels were excised and the cells recovered after dissolution of the hydrogels using hyaluronidase enzyme. The cells were then stained with CD86, MHCII, CD40 and CD45 antibodies and analyzed using flow cytometry. Statistics used student T-test. $^{*}P<0.05$, $^{**}P<0.005$, $^{***}P<0.0005$. (For interpretation of the references to colour in this figure legend, the reader is referred to the web version of this article.)

state) were encapsulated in the HA-HA and HA-GA hydrogels and cultured for 14 days. RNA was extracted from these gels and the expression of pro-and anti-inflammatory genes was quantified by qRT-PCR (Fig. 5C). We observed that the resting M0 macrophages differentiated into mature macrophages as evidenced by the expression of F4/80, a murine macrophage marker [43]. Interestingly, we observed an upregulation of anti-inflammatory genes, namely il10 (∼2-fold), tgfb-1 (∼3-fold), il4 (∼1.5-fold), il4ra (∼ 3-fold), and tgfb-r1 (∼2.5-fold), when compared to cells encapsulated in HA-HA gels (Fig. 6). Similar to the previous study with the THP1 cells, we also observed an upregulation of a few pro-inflammatory genes such as socs3 (∼2-fold), il6 (∼1.5-fold), and tnfa (∼2.5-fold) by the BMDM cells relative to cells encapsulated in the HA-HA gels. These results concord with our hypothesis that the covalent grafting of GA to the HA backbone acts as a cue to polarize macrophages towards an immunosuppressive phenotype [32]. The expression of the proinflammatory markers (SOCS3, IL6, and TNF-α) could be attributed to the flexible phenotypic paradigms of the macrophages [11]. There have also been reports suggesting that the temporality and responsiveness of macrophage functions necessitate this flexibility, with M2- activated macrophages being able to display M1-like features or to repolarize completely [44].

Although the results with the M0 macrophages indicated promising immunosuppression, the extent of this characteristic was not very clear. We therefore tested the immunosuppressive propensity of HA-GA gels by encapsulating proinflammatory BMDM cells (that were pre-stimulated with lipopolysaccharide (LPS) (10 ng/mL) and IFNγ (20 ng/mL) and estimated the gene expression after 3 days. As anticipated, we observed a significant decrease in expression of proinflammatory genes such as socs3, iNOS, and il6 (Fig. 6A), and a non-significant decrease in il-1β and tnf-α expression, which are hallmarks of pro-inflammatory M1 macrophages [16], in the HA-GA gels relative to the HA-HA gels. Interestingly, we also observed an increase in the expression of tgf-β1 in the HA-GA gels when compared to in HA-HA gels. However, we also observed a decrease in IL4 in the HA-GA gels with respect to the HA-HA gels. A significant decrease in expression levels of chemokine-derived cx3cr1 was also observed in the HA-GA gels. It has been reported that macrophages with low levels of cx3cr1 have the ability to express both pro-inflammatory and anti-inflammatory markers [45] and could be vital in the early and late stages of wound healing and repair in spinal cord injuries [46].

To further validate the immunosuppressive properties of the HA-GA gels, we estimated the amounts of the cytokines released by the pro-inflammatory BMDM cells upon encapsulation within the HA-HA or HA-GA gels after 3 days of culture following a multiplex bead-based assay (Fig. 6B). Interestingly, corroborating the qRT-PCR study we observed a significant reduction in most of the pro-inflammatory cytokines released by these cells in the HA-GA gels compared to in the HA-HA gels. Specifically, pro-inflammatory cytokines such as IL-23 (10 $\pm$ 3 ng/mL in HA-HA vs 4.5 $\pm$ 2 ng/mL in HA-GA), IL-6 (3.6 $\pm$ 1 ng/mL in HA-HA vs 1.7 $\pm$ 1 ng/mL in HA-GA), macrophage derived chemokine (MDC; 39 $\pm$ 12 ng/mL in HA-HA vs 20 $\pm$ 8 ng/mL in HA-GA) and IL-12p40 (30 $\pm$ 4 ng/mL in HA-HA vs 15 $\pm$ 4 ng/mL in HA-GA) were markedly decreased in the HA-GA gels compared to in the HA-HA gels. However, some pro-inflammatory cytokines such as TNF-α (16 $\pm$ 0.3 ng/mL in HA-HA vs 16 $\pm$ 0.4 ng/mL in HA-GA) and IL-18 (19 $\pm$ 7 ng/mL in HA-HA vs 42 $\pm$ 7 ng/mL in HA-GA) were upregulated in the HA-GA gels. Interestingly, we also observed that BMDM cells upregulated the production of anti-inflammatory cytokines when encapsulated in the HA-GA gels such as granulocyte colony stimulating factors (20 $\pm$ 7 ng/mL in HA-HA vs 40 $\pm$ 11 ng/mL in HA-GA), IL-10 (9 $\pm$ 4 ng/mL in HA-HA vs 14 $\pm$ 9 ng/mL in HA-GA) and TGF-β (5 $\pm$ 2 ng/mL in HA-HA vs 16 $\pm$ 7 ng/mL in HA-GA). The qRT-PCR together with the cytokine multiplex bead-based assay thus clearly suggest that the HA-GA gels predominantly possesses an immunosuppressive characteristic compared to the HA-HA gels.

Finally, to unequivocally validate the immunosuppressive characteristics of the HA-GA gels relative to the HA-HA gels we subcutaneously implanted the gels into healthy naive mice and evaluated the type of immune cells that infiltrated these gels after 5 days or 10 days of implantation. In order to minimize the variations between the groups, the HA-HA and HA-GA hydrogels were injected at two different subcutaneous sites in the same animals. Five days post implantation these hydrogels were recovered and the immune cells that infiltrated within the gels were harvested, stained with antibodies and analyzed by flow cytometry. Interestingly, we observed that the HA-GA cells attracted more myeloid cells ($CD45^{+}CD11^{+}$) relative to the HA-HA gels, clearly demonstrating differential properties (Fig. 7A and S14A in SI). However, when we examined the infiltrating cells for the pro-inflammatory markers CD86 and MHCII (Major Histocompatibility factor) [47] and CD40 [48,49] we noted that the percentage of cells

expressing $CD86^{+}MHCII^{+}$ was significantly higher in the HA-HA hydrogels compared to in the HA-GA hydrogels. (Fig. 7B and S14B in SI) Similar trends was observed for the $CD86^{+}MHCII^{+}CD40^{+}$ expressing myeloid cells (Fig. 7C) although the percentage of the myeloid cells remained the same in both groups. We believe that the lower expression of $CD86^{+}$ on cells in the HA-GA gels could be due to the intrinsic ability of the HA-GA gels to stimulate the infiltrating macrophages to secrete more IL-10, as we observed in the in vitro studies (Fig. 4, 5C & 6B). The presence of $CD40^{+}$cells in the HA-GA gels and the ability of the HA-GA gels to stimulate the cells to produce IL-10 could help in the reduction in the population of the proinflammatory $CD86^{+}$ $MHCII^{+}$cells [50]. Fascinatingly, when we analyzed the 10 days old implanted gels, we found that the HA-HA gels were intact, however, the HA-GA gels were completely resorbed. This unique degradation profile of HA-GA gels could be attributed to the higher number of M2 macrophages in the infiltrating myeloid cell population. Such fast degradation was observed after intradermal implantation of collagen matrix in mice that was attributed to the M2-like macrophages [51], which dramatically enhances the capacity to turnover extracellular matrix by an intracellular pathway. This was also confirmed by another study in which IL-4-containing implants display a distinct population of macrophages with an M2-like phenotype, yielding significant proteolytic activity, decreased fibrotic capsule deposition and improved peri–implant tissue quality [52]. These in-vitro and in-vivo results confirm our hypothesis that the HA-GA gels are more immunosuppressive when compared to the HA-HA gels and indicate that they could be utilized in the treatment of specific inflammatory diseases.

4. Conclusion

Undesired immune reaction to the implanted biomaterial is the major bottleneck for successful clinical translation of regenerative medicine and cell-based therapies. To address this, we have designed an innovative GA functionalized HA-based extracellular matrix mimetic (HA-GA) hydrogel that displays superior antioxidant and tissue-adhesive properties. The secondary network due to the presence of GA moiety in the HA-GA gels rendered an extremely stable hydrogel formation without excessive swelling. In addition, these scaffolds displayed a unique capability to differentiate monocytes to an immunosuppressive phenotype. Fibroblasts encapsulated inside these HA-GA gels were protected from oxidative stress. Our study clearly suggests that GA functionalized gels display radical scavenging activity and promote polarization of macrophages into an immunosuppressive phenotype have great potential to be used as scaffolds for cell-based therapies. The ability of the HA-GA gels to suppress the major pro-inflammatory genes and an increase in the TGF-β and IL-10 suggests that these hydrogels may be a valuable tool for tissue engineering applications, especially for wound healing during which suppression of inflammation is crucial [53] (Fig. 1).

Declaration of Competing Interest

The authors declare that they have no known competing financial interests or personal relationships that could have appeared to influence the work reported in this paper.

The authors declare no conflict of interest.

Acknowledgements

SS thanks the European Union's Horizon 2020 Marie Sklodowska-Curie Grant Program (Agreement No. 713645) for the financial support. The authors would also like to thank Dr. Irene Benito Cuesta from the Applied Immunology and Immunotherapy, Department of Clinical Neuroscience, Karolinska Institutet, Stockholm for assisting in the in vivo studies.

Supplementary materials

Supplementary material associated with this article can be found, in the online version, at doi:10.1016/j.actbio.2022.01.048.

References

[1] G.S. Hussey, J.L. Dziki, S.F. Badylak, Extracellular matrix-based materials for regenerative medicine, Nat. Rev. Mater. 3 (2018) 159–173, doi:10.1038/s41578-018-0023-x.
[2] J. Nicolas, S. Magli, L. Rabbachin, S. Sampaolesi, F. Nicotra, L. Russo, 3D Extracellular Matrix Mimics: fundamental Concepts and Role of Materials Chemistry to Influence Stem Cell Fate, Biomacromolecules 21 (2020) 1968–1994, doi:10.1021/acs.biomac.0c00045.
[3] S. Raveendran, A.K. Rochani, T. Maekawa, D.S. Kumar, Smart carriers and nanohealers: a nanomedical insight on natural polymers, Materials (Basel) 10 (2017), doi:10.3390/ma10080929.
[4] B.M. Holzapfel, J.C. Reichert, J.T. Schantz, U. Gbureck, L. Rackwitz, U. Nöth, F. Jakob, M. Rudert, J. Groll, D.W. Hutmacher, How smart do biomaterials need to be? A translational science and clinical point of view, Adv. Drug Deliv. Rev. 65 (2013) 581–603, doi:10.1016/j.addr.2012.07.009.
[5] C.E. Witherel, D. Abebayehu, T.H. Barker, K.L. Spiller, Macrophage and Fibroblast Interactions in Biomaterial-Mediated Fibrosis, Adv. Healthc. Mater. 8 (2019) 1–16, doi:10.1002/adhm.201801451.
[6] D.F. Williams, Biocompatibility pathways: biomaterials-induced sterile inflammation, mechanotransduction, and principles of biocompatibility control, ACS Biomater. Sci. Eng. 3 (2017) 2–35, doi:10.1021/acsbiomaterials.6b00607.
[7] I.M. Adjei, G. Plumton, B. Sharma, Oxidative Stress and Biomaterials: the Inflammatory Link, in: Oxidative Stress Biomater., Elsevier, 2016, pp. 89–115, doi:10.1016/B978-0-12-803269-5.00004-8.
[8] J. Lee, Y.S. Cho, H. Jung, I. Choi, Pharmacological regulation of oxidative stress in stem cells, Oxid. Med. Cell. Longev. (2018) 2018, doi:10.1155/2018/4081890.
[9] R. Sridharan, A.R. Cameron, D.J. Kelly, C.J. Kearney, F.J. O'Brien, Biomaterial based modulation of macrophage polarization: a review and suggested design principles, Mater. Today. 18 (2015) 313–325, doi:10.1016/j.mattod.2015.01.019.
[10] P. Italiani, D. Boraschi, From monocytes to M1/M2 macrophages: phenotypical vs. functional differentiation, Front. Immunol. 5 (2014) 514, doi:10.3389/fimmu.2014.00514.
[11] D.M. Mosser, J.P. Edwards, Exploring the full spectrum of macrophage activation, Nat. Rev. Immunol. 8 (2008) 958–969, doi:10.1038/nri2448.
[12] M.M. Alvarez, J.C. Liu, G. Trujillo-de Santiago, B.H. Cha, A. Vishwakarma, A.M. Ghaemmaghami, A. Khademhosseini, Delivery strategies to control inflammatory response: modulating M1–M2 polarization in tissue engineering applications, J. Control. Release. 240 (2016) 349–363, doi:10.1016/j.jconrel.2016.01.026.
[13] Z. Julier, A.J. Park, P.S. Briquez, M.M. Martino, Promoting tissue regeneration by modulating the immune system, Acta Biomater 53 (2017) 13–28, doi:10.1016/j.actbio.2017.01.056.
[14] R.A. Harris, Spatial, temporal, and functional aspects of macrophages during "The good, the bad, and the ugly" phases of inflammation, Front. Immunol. 5 (2014) 3–6, doi:10.3389/fimmu.2014.00612.
[15] R. Parsa, H. Lund, I. Tosevski, X.-.M. Zhang, U. Malipiero, J. Beckervordersandforth, D. Merkler, M. Prinz, A. Gyllenberg, T. James, A. Warnecke, J. Hillert, L. Alfredsson, I. Kockum, T. Olsson, A. Fontana, T. Suter, R.A. Harris, TGFβ regulates persistent neuroinflammation by controlling Th1 polarization and ROS production via monocyte-derived dendritic cells, Glia 64 (2016) 1925–1937, doi:10.1002/glia.23033.
[16] F.O. Martinez, S. Gordon, The M1 and M2 paradigm of macrophage activation: time for reassessment, F1000Prime Rep 6 (2014), doi:10.12703/P6-13.
[17] D.P. Vasconcelos, A.C. Fonseca, M. Costa, I.F. Amaral, M.A. Barbosa, A.P. Águas, J.N. Barbosa, Macrophage polarization following chitosan implantation, Biomaterials 34 (2013) 9952–9959, doi:10.1016/j.biomaterials.2013.09.012.
[18] D. Yang, K.S. Jones, Effect of alginate on innate immune activation of macrophages, J. Biomed. Mater. Res. - Part A. 90 (2009) 411–418, doi:10.1002/jbm.a.32096.
[19] B.N. Brown, R. Londono, S. Tottey, L. Zhang, K.A. Kukla, M.T. Wolf, K.A. Daly, J.E. Reing, S.F. Badylak, Macrophage phenotype as a predictor of constructive remodeling following the implantation of biologically derived surgical mesh materials, Acta Biomater 8 (2012) 978–987, doi:10.1016/j.actbio.2011.11.031.
[20] A. Vishwakarma, N.S. Bhise, M.B. Evangelista, J. Rouwkema, M.R. Dokmeci, A.M. Ghaemmaghami, N.E. Vrana, A. Khademhosseini, Engineering Immunomodulatory Biomaterials To Tune the Inflammatory Response, Trends Biotechnol 34 (2016) 470–482, doi:10.1016/j.tibtech.2016.03.009.
[21] J.E. Rayahin, J.S. Buhrman, Y. Zhang, T.J. Koh, R.A. Gemeinhart, High and Low Molecular Weight Hyaluronic Acid Differentially Influence Macrophage Activation, ACS Biomater. Sci. Eng. 1 (2015) 481–493, doi:10.1021/acsbiomaterials.5b00181.
[22] V.K. Rangasami, S. Samanta, V.S. Parihar, K. Asawa, K. Zhu, O.P. Varghese, Y. Teramura, B. Nilsson, J. Hilborn, R.A. Harris, O.P. Oommen, Harnessing hyaluronic

acid-based nanoparticles for combination therapy: a novel approach for suppressing systemic inflammation and to promote antitumor macrophage polarization, Carbohydr. Polym. 254 (2021) 117291, doi:10.1016/j.carbpol.2020.117291.

[23] V.Y. Kosovrasti, L.V. Nechev, M.M. Amiji, Peritoneal Macrophage-Specific TNF-α Gene Silencing in LPS-Induced Acute Inflammation Model Using CD44 Targeting Hyaluronic Acid Nanoparticles, Mol. Pharm. 13 (2016) 3404–3416, doi:10.1021/acs.molpharmaceut.6b00398.

[24] T.J. Beldman, M.L. Senders, A. Alaarg, C. Pérez-Medina, J. Tang, Y. Zhao, F. Fay, J. Deichmöller, B. Born, E. Desclos, N.N. Van Der Wel, R.A. Hoebe, F. Kohen, E. Kartvelishvily, M. Neeman, T. Reiner, C. Calcagno, Z.A. Fayad, M.P.J. De Winther, E. Lutgens, W.J.M. Mulder, E. Kluza, Hyaluronan Nanoparticles Selectively Target Plaque-Associated Macrophages and Improve Plaque Stability in Atherosclerosis, ACS Nano 11 (2017) 5785–5799, doi:10.1021/acsnano.7b01385.

[25] O.P. Oommen, J. Garousi, M. Sloff, O.P. Varghese, Tailored doxorubicin-hyaluronan conjugate as a potent anticancer glyco-drug: an alternative to prodrug approach, Macromol. Biosci. 14 (2014) 327–333, doi:10.1002/mabi.201300383.

[26] O.P. Oommen, C. Duehrkop, B. Nilsson, J. Hilborn, O.P. Varghese, Multifunctional Hyaluronic Acid and Chondroitin Sulfate Nanoparticles: impact of Glycosaminoglycan Presentation on Receptor Mediated Cellular Uptake and Immune Activation, ACS Appl. Mater. Interfaces. 8 (2016) 20614–20622, doi:10.1021/acsami.6b06823.

[27] O.P. Oommen, S. Wang, M. Kisiel, M. Sloff, J. Hilborn, O.P. Varghese, Smart Design of Stable Extracellular Matrix Mimetic Hydrogel: synthesis, Characterization, and In Vitro and In Vivo Evaluation for Tissue Engineering, Adv. Funct. Mater. 23 (2013) 1273–1280, doi:10.1002/adfm.201201698.

[28] D. Bermejo-Velasco, S. Kadekar, M.V. Tavares Da Costa, O.P. Oommen, K. Gamstedt, J. Hilborn, O.P. Varghese, First Aldol Cross-Linked Hyaluronic Acid Hydrogel: fast and Hydrolytically Stable Hydrogel with Tissue Adhesive Properties, ACS Appl. Mater. Interfaces 11 (2019) 38232–38239, doi:10.1021/acsami.9b10239.

[29] M. Paidikondala, V.K. Rangasami, G.N. Nawale, T. Casalini, G. Perale, S. Kadekar, G. Mohanty, T. Salminen, O.P. Oommen, O.P. Varghese, An Unexpected Role of Hyaluronic Acid in Trafficking siRNA Across the Cellular Barrier: the First Biomimetic, Anionic, Non-Viral Transfection Method, Angew. Chemie Int. Ed. 58 (2019) 2815–2819, doi:10.1002/anie.201900099.

[30] H.J. Yan, T. Casalini, G. Hulsart-Billström, S. Wang, O.P. Oommen, M. Salvalaglio, S. Larsson, J. Hilborn, O.P. Varghese, Synthetic design of growth factor sequestering extracellular matrix mimetic hydrogel for promoting in vivo bone formation, Biomaterials 161 (2018) 190–202, doi:10.1016/j.biomaterials.2018.01.041.

[31] J.Y. Lai, L.J. Luo, Antioxidant gallic acid-functionalized biodegradable in situ gelling copolymers for cytoprotective antiglaucoma drug delivery systems, Biomacromolecules 16 (2015) 2950–2963, doi:10.1021/acs.biomac.5b00854.

[32] B. Badhani, N. Sharma, R. Kakkar, Gallic acid: a versatile antioxidant with promising therapeutic and industrial applications, RSC Adv 5 (2015) 27540–27557, doi:10.1039/c5ra01911g.

[33] M.F. Queiroz, D.A. Sabry, G.L. Sassaki, H.A.O. Rocha, L.S. Costa, Gallic acid-dextran conjugate: green synthesis of a novel antioxidant molecule, Antioxidants 8 (2019), doi:10.3390/antiox8100478.

[34] M. Shin, H. Lee, Gallol-Rich Hyaluronic Acid Hydrogels: shear-Thinning, Protein Accumulation against Concentration Gradients, and Degradation-Resistant Properties, Chem. Mater. 29 (2017) 8211–8220, doi:10.1021/acs.chemmater.7b02267.

[35] S. Samanta, V.K. Rangasami, N.A. Murugan, V.S. Parihar, O.P. Varghese, O.P. Oommen, An unexpected role of an extra phenolic hydroxyl on the chemical reactivity and bioactivity of catechol or gallol modified hyaluronic acid hydrogels, Polym. Chem. 12 (2021) 2987–2991, doi:10.1039/d1py00013f.

[36] M.H. Abnosi, S. Yari, The toxic effect of gallic acid on biochemical factors, viability and proliferation of rat bone marrow mesenchymal stem cells was compensated by boric acid, J. Trace Elem. Med. Biol. 48 (2018) 246–253, doi:10.1016/j.jtemb.2018.04.016.

[37] Y. Bi, J. Chen, F. Hu, J. Liu, M. Li, L. Zhao, M2 Macrophages as a Potential Target for Antiatherosclerosis Treatment, Neural Plast (2019) 2019, doi:10.1155/2019/6724903.

[38] Y. Yue, X. Yang, K. Feng, L. Wang, J. Hou, B. Mei, H. Qin, M. Liang, G. Chen, Z. Wu, M2b macrophages reduce early reperfusion injury after myocardial ischemia in mice: a predominant role of inhibiting apoptosis via A20, Int. J. Cardiol. 245 (2017) 228–235, doi:10.1016/j.ijcard.2017.07.085.

[39] J.C. Gensel, B. Zhang, Macrophage activation and its role in repair and pathology after spinal cord injury, Brain Res 1619 (2015) 1–11, doi:10.1016/j.brainres.2014.12.045.

[40] A.P. Hutchins, D. Diez, D. Miranda-Saavedra, The IL-10/STAT3-mediated anti-inflammatory response: recent developments and future challenges, Brief. Funct. Genomics. 12 (2013) 489–498, doi:10.1093/bfgp/elt028.

[41] K.N. Couper, D.G. Blount, E.M. Riley, IL-10: the Master Regulator of Immunity to Infection, J. Immunol. 180 (2008) 5771–5777, doi:10.4049/jimmunol.180.9.5771.

[42] J. Weischenfeldt, B. Porse, Bone Marrow-Derived Macrophages (BMM): isolation and Applications, Cold Spring Harb. Protoc. (2008) 2008pdb.prot5080, doi:10.1101/PDB.PROT5080.

[43] A. dos, Anjos Cassado, F4/80 as a major macrophage marker: the case of the peritoneum and spleen, in: Results Probl. Cell Differ., Springer Verlag, 2017, pp. 161–179, doi:10.1007/978-3-319-54090-0_7.

[44] C. Atri, F. Guerfali, D. Laouini, Role of Human Macrophage Polarization in Inflammation during Infectious Diseases, Int. J. Mol. Sci. 19 (2018) 1801, doi:10.3390/ijms19061801.

[45] M. Burgess, K. Wicks, M. Gardasevic, K.A. Mace, Cx3CR1 Expression Identifies Distinct Macrophage Populations That Contribute Differentially to Inflammation and Repair, ImmunoHorizons 3 (2019) 262–273, doi:10.4049/immunohorizons.1900038.

[46] C.M. Freria, J.C.E. Hall, P. Wei, Z. Guan, D.M. McTigue, P.G. Popovich, Deletion of the fractalkine receptor, CX3CR1, improves endogenous repair, axon sprouting, and synaptogenesis after spinal cord injury in mice, J. Neurosci. 37 (2017) 3568–3587, doi:10.1523/JNEUROSCI.2841-16.2017.

[47] C. O'Carroll, A. Fagan, F. Shanahan, R.J. Carmody, Identification of a Unique Hybrid Macrophage-Polarization State following Recovery from Lipopolysaccharide Tolerance, J. Immunol. 192 (2014) 427–436, doi:10.4049/JIMMUNOL.1301722.

[48] G. Liu, X. Xia, S. Gong, Y. Zhao, The macrophage heterogeneity: difference between mouse peritoneal exudate and splenic F4/80+ macrophages, J. Cell. Physiol. 209 (2006) 341–352, doi:10.1002/JCP.20732.

[49] D.L. Morris, K.E. Oatmen, T.A. Mergian, K.W. Cho, J.L. DelProposto, K. Singer, C. Evans-Molina, R.W. O'Rourke, C.N. Lumeng, CD40 promotes MHC class II expression on adipose tissue macrophages and regulates adipose tissue CD4 + T cells with obesity, J. Leukoc. Biol. 99 (2016) 1107–1119, doi:10.1189/jlb.3a0115-009r.

[50] E. Nova-Lamperti, G. Fanelli, P.D. Becker, P. Chana, R. Elgueta, P.C. Dodd, G.M. Lord, G. Lombardi, M.P. Hernandez-Fuentes, IL-10-produced by human transitional B-cells down-regulates CD86 expression on B-cells leading to inhibition of CD4+T-cell responses, Sci. Reports 6 (2016) 1–8 2016 61, doi:10.1038/srep20044.

[51] D.H. Madsen, D. Leonard, A. Masedunskas, A. Moyer, H.J. Jürgensen, D.E. Peters, P. Amornphimoltham, A. Selvaraj, S.S. Yamada, D.A. Brenner, S. Burgdorf, L.H. Engelholm, N. Behrendt, K. Holmbeck, R. Weigert, T.H. Bugge, M2-like macrophages are responsible for collagen degradation through a mannose receptor-mediated pathway, J. Cell Biol. 202 (2013) 951–966, doi:10.1083/jcb.201301081.

[52] D. Hachim, S.T. Lopresti, R.D. Rege, Y. Umeda, A. Iftikhar, A.L. Nolfi, C.D. Skillen, B.N. Brown, Distinct macrophage populations and phenotypes associated with IL-4 mediated immunomodulation at the host implant interface, Biomater. Sci. 8 (2020) 5751–5762, doi:10.1039/D0BM00568A.

[53] R.G. Rosique, M.J. Rosique, J.A. Farina Junior, Curbing inflammation in skin wound healing: a review, Int. J. Inflam. (2015) 2015, doi:10.1155/2015/316235.